AD-A138 808 STUDY AND DESIGN OF A CYLINDRICAL LENS ARRAY ANTENNA FOR WIDEBAND ELECTRONIC SCANNING(U) HAZELTINE CORP GREENLAWN NY P W HANNAN ET AL. DEC 83 RADC-TR-83-128 1/2

UNCLASSIFIED F19628-80-C-0110 F/G 9/5 NL

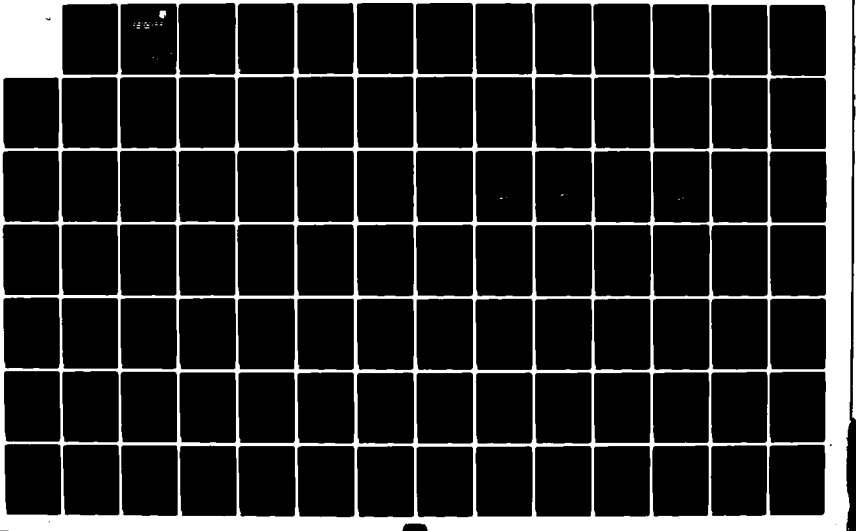

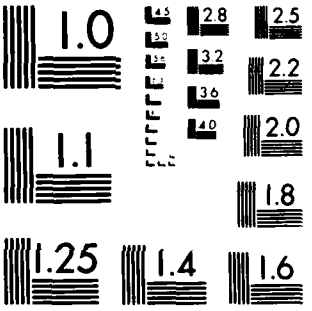

MICROCOPY RESOLUTION TEST CHART
NATIONAL BUREAU OF STANDARDS-1963-A

(12)

RADC-TR-83-128
Interim Report
December 1983

STUDY AND DESIGN OF A CYLINDRICAL LENS ARRAY ANTENNA FOR WIDEBAND ELECTRONIC SCANNING

Hazeltine Corporation

Peter W. Hannan
Edward M. Newman

ROME AIR DEVELOPMENT CENTER
Air Force Systems Command
Griffiss Air Force Base, NY 13441

This report has been reviewed by the RADC Public Affairs Office (PA) and is releasable to the National Technical Information Service (NTIS). At NTIS it will be releasable to the general public, including foreign nations.

RADC-TR-83-128 has been reviewed and is approved for publication.

APPROVED: Peter R. Franchi

PETER R. FRANCHI
Project Engineer

APPROVED: Allan C. Schell

ALLAN C. SCHELL, Chief
Electromagnetic Sciences Division

FOR THE COMMANDER: John P. Huss

JOHN P. HUSS
Acting Chief, Plans Office

If your address has changed or if you wish to be removed from the RADC mailing list, or if the addressee is no longer employed by your organization, please notify RADC (EEAA), Hanscom AFB MA 01731. This will assist us in maintaining a current mailing list.

Do not return copies of this report unless contractual obligations or notices on a specific document requires that it be returned.

UNCLASSIFIED

SECURITY CLASSIFICATION OF THIS PAGE (When Data Entered)

REPORT DOCUMENTATION PAGE

READ INSTRUCTIONS BEFORE COMPLETING FORM

1. REPORT NUMBER: RADC-TR-83-128	2. GOVT ACCESSION NO.: AD-A138 806
3. RECIPIENT'S CATALOG NUMBER:	
4. TITLE (and Subtitle): STUDY AND DESIGN OF A CYLINDRICAL LENS ARRAY ANTENNA FOR WIDEBAND ELECTRONIC SCANNING	5. TYPE OF REPORT & PERIOD COVERED: Interim Report October 1980 - April 1982
	6. PERFORMING ORG. REPORT NUMBER: N/A
7. AUTHOR(s): Peter W. Hannan, Edward M. Newman	8. CONTRACT OR GRANT NUMBER(s): F19628-80-C-0110
9. PERFORMING ORGANIZATION NAME AND ADDRESS: Hazeltine Corporation, Pulaski Road, Greenlawn NY 11740	10. PROGRAM ELEMENT, PROJECT, TASK AREA & WORK UNIT NUMBERS: 62702F, 46001458
11. CONTROLLING OFFICE NAME AND ADDRESS: Rome Air Development Center (EEAA), Hanscom AFB MA 01731	12. REPORT DATE: December 1983
	13. NUMBER OF PAGES: 196
14. MONITORING AGENCY NAME & ADDRESS(if different from Controlling Office): Same	15. SECURITY CLASS. (of this report): UNCLASSIFIED
	15a. DECLASSIFICATION/DOWNGRADING SCHEDULE: N/A

16. DISTRIBUTION STATEMENT (of this Report)

Approved for public release; distribution unlimited.

17. DISTRIBUTION STATEMENT (of the abstract entered in Block 20, if different from Report)

Same

18. SUPPLEMENTARY NOTES

RADC Project Engineer: Peter R. Franchi (RADC/EEAA)

19. KEY WORDS (Continue on reverse side if necessary and identify by block number)

Phased-Array Antenna
Lens Antenna
Wideband Antennas
Electronic Scanning

20. ABSTRACT (Continue on reverse side if necessary and identify by block number)

This Interim Report presents the results of studies leading to the design of a cylindrical lens-array antenna for two-dimensional electronic scanning when the signal has a wide instantaneous bandwidth.

The constant-path cylindrical lens defined by Rotman and Franchi is studied for contours, phase aberrations, amplitude distortions, and surface incidence angles. One form of this lens is the R-2R lens, which is chosen for this project.

DD FORM 1 JAN 73 1473 EDITION OF 1 NOV 65 IS OBSOLETE

UNCLASSIFIED

SECURITY CLASSIFICATION OF THIS PAGE (When Data Entered)

Design of the antenna for low sidelobes is considered. In azimuth, when the beam is scanned off the antenna axis the sidelobes are affected by the curvature of the lens outer surface. In elevation, the sidelobes are affected by feed/lens diffraction.

Performance of the electronic-scan antenna with a wideband signal is a function of the number of line feeds that are used to illuminate the cylindrical lens. For a $\pm$ 45° by $\pm$ 25° scan coverage with a 40 by 35 wavelength antenna aperture, and with a 400 MHz wide rectangular spectrum assumed for the wideband signal, 6 or 8 line feeds appear to be an appropriate choice. The electronic phase shifters in the cylindrical lens should provide essentially constant phase over the 400 MHz spectrum, in order to preserve low sidelobes.

Internal reflections in the constant-path cylindrical lens can create a spurious-beam sidelobe that scans away from the main beam when the phase shifters electronically scan the main beam. This effect can be reduced by reducing the variation of impedance with incidence angle of the array elements at both lens surfaces. Computations indicate that a bent-dipole array has the potential for exceptionally constant impedance in the E plane of incidence from 0° to over 60°. Patterns computed for a cylindrical lens using bent dipoles show a major reduction of this spurious-beam sidelobe, as compared with ordinary dipoles.

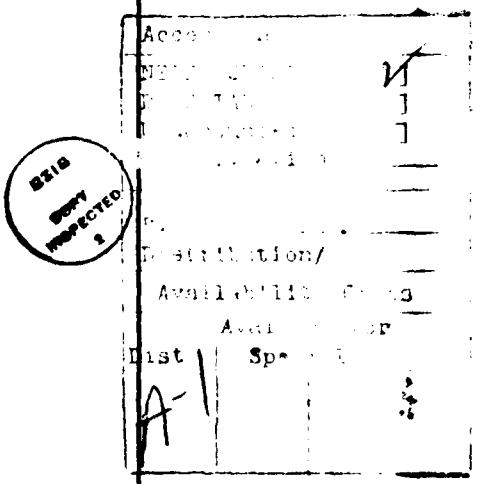

CONTENTS

ILLUSTRATIONS

ILLUSTRATIONS (Cont)

ILLUSTRATIONS (Cont)

ILLUSTRATIONS (Cont)

ILLUSTRATIONS (Cont)

TABLES

SECTION I

INTRODUCTION

A cylindrical-lens phased-array antenna offers the capability for electronically scanning a narrow pencil beam over wide angles in two dimensions, and for handling wide signal bandwidths without using variable time-delay devices.

An investigation of such a lens-array antenna is being conducted by Hazeltine for RADC/EEA. The first part of the program involves study of the antenna and design of a specific configuration. The second part of the program will include the fabrication and test of a lens-array antenna having an aperture of at least 40 x 30 wavelengths.

This interim report presents the results obtained in the first part of the program. The basic features of the lens-array antenna are first reviewed (Section II), and the objectives and problem areas of the program are outlined (Section III). Then the characteristics of the lens itself are described, including its contours, aberrations, and incidence angles (Section IV).

The basic design of the antenna is then discussed with regard to four properties: azimuth patterns, elevation patterns, directive gain, and signal bandwidth (Section V). The significant problem of lens internal reflections is considered and an array element offering remarkably low reflection over a wide range of incidence angles is discussed (Section VI). Finally, some conclusions are drawn from this first part of the program (Section VII).

SECTION II

THE CYLINDRICAL LENS-ARRAY ANTENNA

2.1 THE BASIC ANTENNA

A fundamental approach for a constrained cylindrical-lens antenna has been derived by Rotman and Franchi (refs 1, 2, 3). The three-dimensional cylindrical lens comprises a stacked set of identical two-dimensional lenses. Each two-dimensional lens consists of two arrays of radiators interconnected by transmission lines. This configuration is shown in figure 2-1.

There are four degrees of freedom in the design of such a lens: the inner contour, the outer contour, the relative location of the inner and outer array elements, and the lengths of the interconnecting transmission lines. Rotman and Franchi (refs 1, 2, 3) derive a lens design in which the first three of these degrees of freedom are used to provide three points of perfect focusing in the azimuth plane. At azimuth angles between these three directions the focusing may be imperfect but may still be quite satisfactory.

Ref 1- W. Rotman and P. Franchi, "Cylindrical Microwave Lens Antenna for Wideband Scanning Applications", Exhibit A in ESD RFP F19628-80-R-0077; November 1979.

Ref 2- P. Franchi, N. Kernweis, W. Rotman, "Wideband Microwave Lens Antenna for Tactical Radar Applications", Proceedings of 1980 Antenna Applications Symposium, Allerton Park, Illinois; September 1980.

Ref 3- W.Rotman et al, "Cylindrical Microwave Lens Antenna for Wideband Scanning Applications", AD-D008526; February 1981.

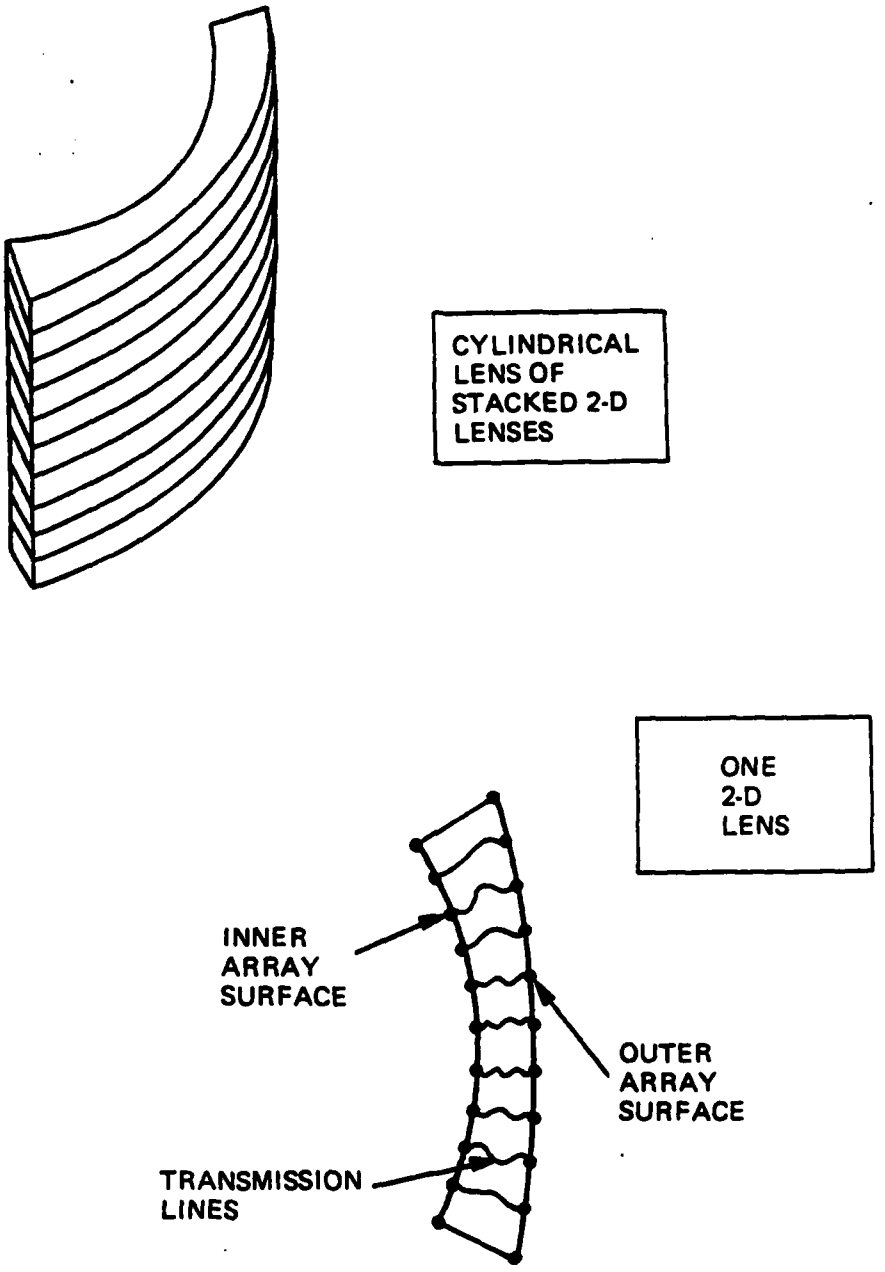

Figure 2-1. Cylindrical Lens Configuration

The fourth degree of freedom, namely, the lengths of the interconnecting transmission lines, is used to control the change of azimuth focusing that may occur with the three-dimensional lens when elevation angle is varied. In particular, Rotman and Franchi show that if the lengths of the interconnecting transmission lines are constant throughout the lens, the three points of perfect azimuth focusing are retained independent of elevation angle. Furthermore, at intermediate azimuth angles the azimuth aberration at any elevation angle is no greater than the azimuth aberration of the two-dimensional lens.

The significance of this result is that a cylindrical lens designed in this way can, when combined with an appropriate line-feed system, provide wide-angle scanning of a narrow pencil beam in both azimuth and elevation. For azimuth scanning the line feed is displaced in azimuth, while for elevation scanning the line feed aperture is phase steered. This is illustrated in figure 2-2.

The ability of this constant-line-length cylindrical lens to permit elevation scanning without aberration is analogous to the similar ability of the widely used cylindrical reflector. However the azimuth-scanning capability of the cylindrical reflector is severely limited by its coma aberration and by the aperture-blocking effect of any centrally-located feed system. The cylindrical lens avoids these limitations.

2.2 APPLICATION TO WIDEBAND ELECTRONIC SCANNING

A phased-array antenna that is electronically scanned can rapidly steer a narrow pencil beam over wide angles. However, if the signal bandwidth (instantaneous bandwidth) is so wide that the correlation distance or equivalent pulse length is not large compared with the antenna aperture, then a phased-array antenna can degrade the signal when the array scans over wide angles. One approach to this problem employs variable time-delay devices in the antenna, but these have some disadvantages. An alternate approach (refs 1, 2, 3) employs the cylindrical-lens antenna as the feeding system for a standard electronically scanned phased array, as will be described.

Suppose that the scan coverage of an antenna is $\pm \sin\theta_h$ horizontally and $\pm \sin\theta_v$ vertically. This coverage can be divided into M by N equal-size sub-regions, so that each sub-region covers only $\pm (1/M) \sin\theta_h$ by $\pm (1/N) \sin\theta_v$ as indicated in figure 2-3. If the feeding system for the phased-array antenna can provide a wideband beam that can be

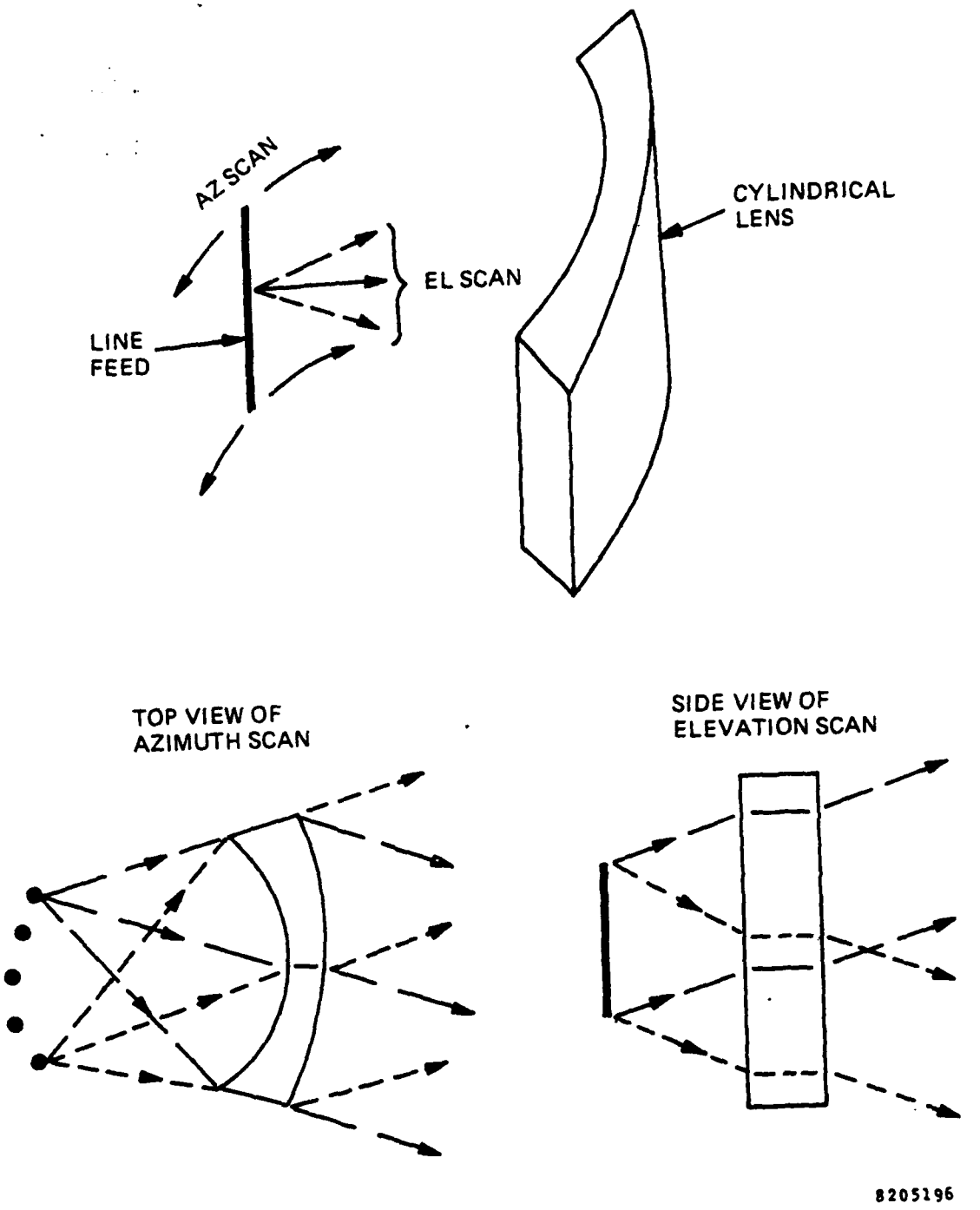

Figure 2-2. Scanning with a Cylindrical Lens Antenna

ANTENNA SCAN COVERAGE:

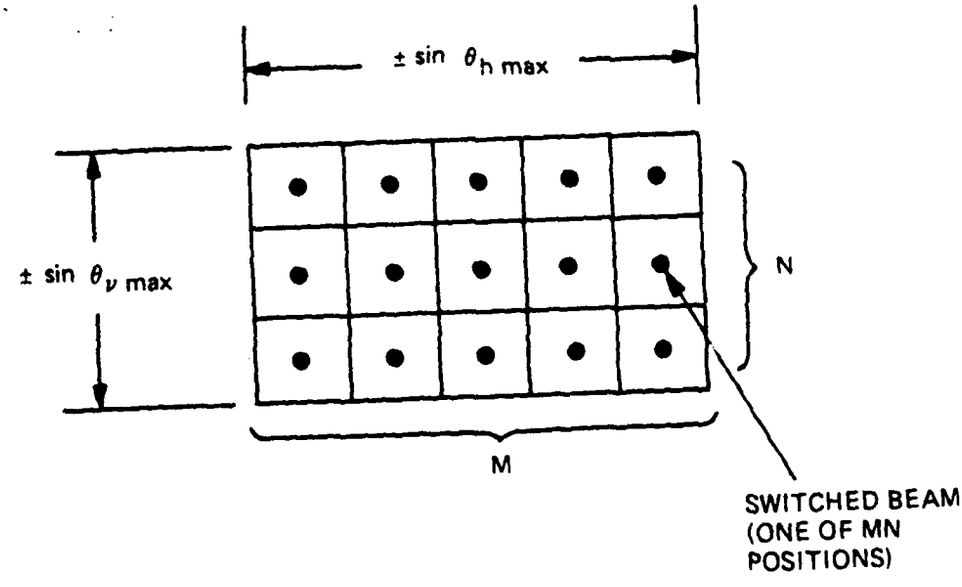

PHASED-ARRAY COVERAGE:

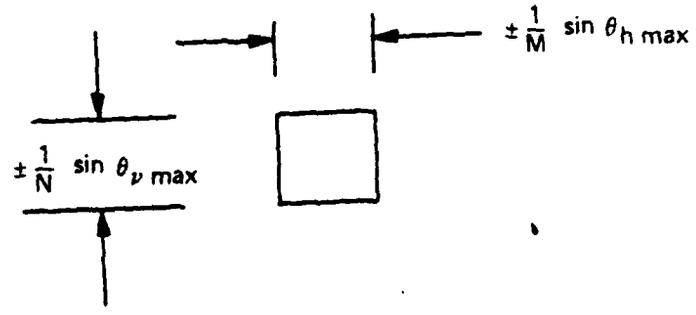

8205195

Figure 2-3. Approach for Wideband Wide-Angle Electronic Scanning

electronically switched from the center of one sub-region to another, then the phased array needs to scan over only the relatively small sub-region rather than over the full coverage of the antenna. This will permit a much wider signal bandwidth to be handled without substantial degradation of the signal.

The cylindrical lens antenna has the capability for providing a wideband beam at the center of each sub-region. Each beam in a different azimuth direction requires a line feed that is appropriately displaced in azimuth, as indicated in figure 2-4(a). Each beam in a different elevation direction requires a line feed having collimated radiation that is steered by fixed time delays to the appropriate elevation angle, as indicated in figure 2-4(b). An electronic switch connects in sequence to each of the M x N line feeds, to provide the coarse steering from one sub-region to another. Electronic phase shifters located in the cylindrical lens provide the fine steering over each sub-region.

Each coarse beam position provides wide signal bandwidth because the lens antenna with multiple line feeds provides true time-delay steering and focusing. The phased array located in the lens uses simple phase shifters for fine-steering the beam, but achieves wide signal bandwidth because of the relatively small size of the sub-region compared with the full scan coverage of the antenna.

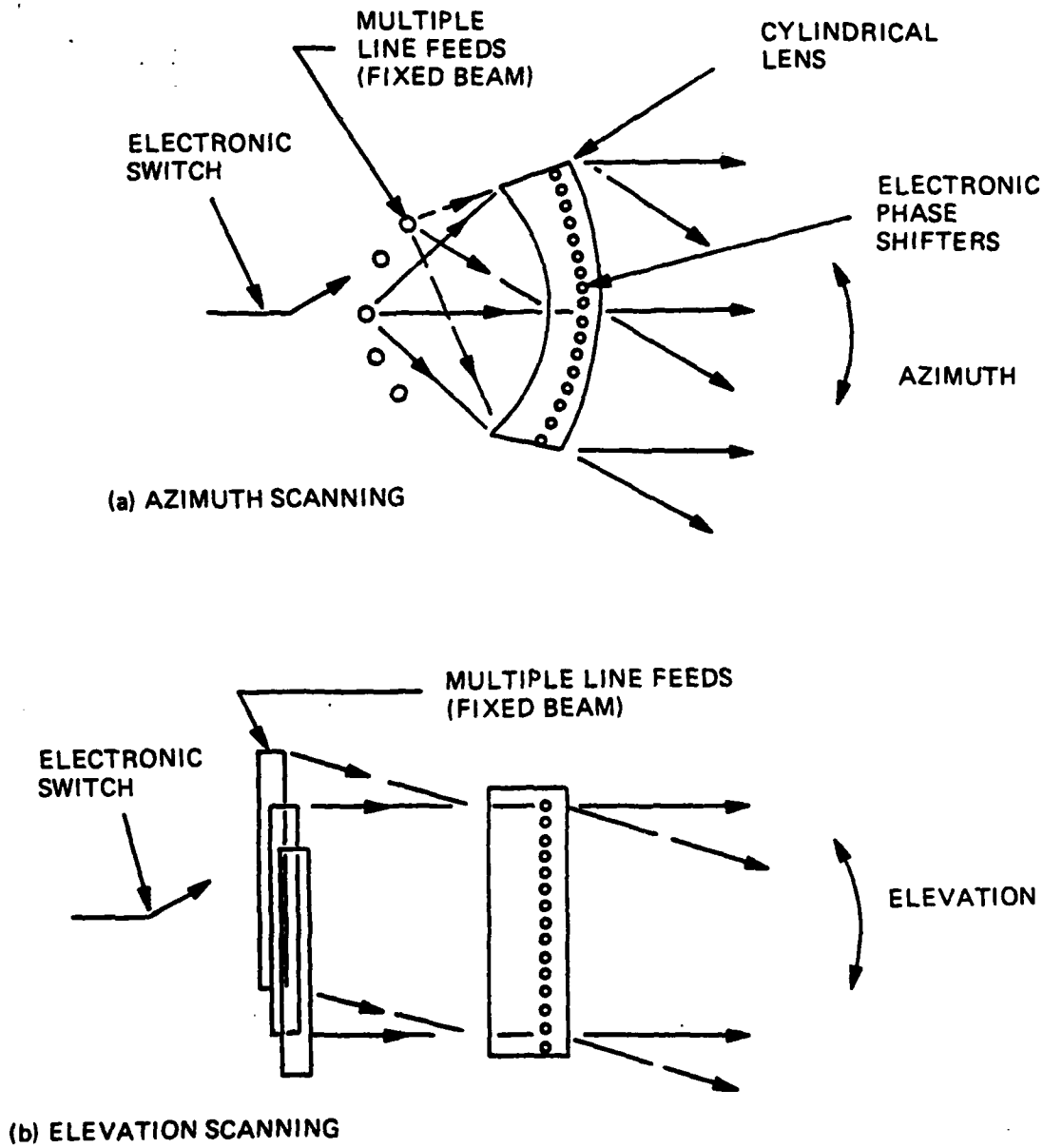

Figure 2-4. Cylindrical Lens Antenna for Wideband Wide-Angle Electronic Scanning

SECTION III

PROGRAM OBJECTIVES AND PROBLEM AREAS

3.1 OBJECTIVES OF PROGRAM

The general objective of this program is to determine the theoretical and practical feasibility of achieving wide-angle scanning with a wide signal bandwidth, using a phased array in combination with a cylindrical lens antenna.

A more specific objective is to be addressed in which the azimuth scan coverage is $\pm 45^{\circ}$ and the elevation scan coverage is $\pm 25^{\circ}$. The signal bandwidth should be 400 MHz in a tunable band from 5.0 to 5.6 GHz. The antenna aperture should be at least 40 x 30 wavelengths and the directive gain should be at least 38 dB. Low azimuth sidelobes are desired: better than -32 dB first sidelobe, decaying to better than -50 dB beyond the third sidelobe. Low elevation sidelobes are also desired. The antenna is to be linearly polarized.

The first part of the program includes conceptual design, analysis, and theoretical performance predictions. The results of this investigation are covered in this interim report.

In the second part of the program an antenna designed in accordance with the above objectives will be constructed and tested. The cylindrical lens that is built will not include the electronic phase shifters, nor will the line-feed system include the electronic switch; these well-understood components would add unnecessary cost to the program. The line feed will be built to demonstrate two coarse-steering angles in elevation, and the location of the line feed will be varied to demonstrate a range of coarse-steering angles in azimuth. The results of this hardware part of the program will appear in the final report.

3.2 PROBLEM AREAS NEEDING STUDY

In this first part of the program there are several areas in which study is needed for more complete understanding of the basic cylindrical lens-array antenna, as well as for design information directed toward the specific objectives outlined above. These study areas are:

a. The basic lens design, including its surface contours and array element locations

b. The lens phase aberrations, amplitude distortions, and angles of incidence

c. The design of the line feed for low sidelobes in the azimuth antenna pattern

d. The effect of a curved lens surface on the azimuth antenna pattern

e. The effect of feed/lens diffraction on sidelobes in the elevation antenna pattern

f. The effect of lens internal reflections on the sidelobes of the antenna patterns

g. The identification of an array element that minimizes the lens internal reflections

h. Specific relationships between signal bandwidth and the number of line feeds, the scan coverage, the antenna beamwidth, and the signal loss. Also, the effect of signal bandwidth on antenna pattern sidelobes.

SECTION IV

THE CONSTANT-W LENS

As mentioned earlier, a constrained cylindrical lens in which the length (W) of the transmission lines is the same throughout the lens has been shown by Rotman and Franchi to retain its azimuth focusing properties when the line feed is phase-scanned in elevation. Such a "constant-W" design is therefore appropriate for the present application in which a cylindrical lens antenna system is to provide wideband coarse-steered beams covering a substantial range of angles in elevation as well as in azimuth. This constant-W lens design is considered in the following discussion.

4.1 CONTOURS OF THE LENS

Rotman and Franchi have derived an equation for the outer surface of the constant-W lens that has three points of perfect focus in azimuth. The equation appears in formula 32 of ref. 1 and formula 36 of ref. 3. The equation is as follows:

$$p^2\xi^4 + 4p\xi^3 + 4\left[\left\{\cos^2\alpha_o - \tfrac{1}{2}p^2\right\}\eta^2 + pg\right]\xi^2 \qquad (1)$$

$$+ 4(2\cos\alpha_o - p)\eta^2\,\xi + 4(1 - pg)\,\eta^2 + p^2\eta^2 = 0$$

where $$p = \frac{\sin^2\alpha_o}{g - \cos\alpha_o}$$

and g = a parameter discussed below.

In this equation, η and ξ are the coordinates of the outer surface of the two-dimensional slice of the cylindrical lens, and α_o is the angle between the axial point of perfect focus and either of the other two points of perfect focus. The geometry is shown in figure 4-1.

The parameter g is the ratio of the central focal length to the outer focal length, as shown in figure 4-1. This parameter determines the arc on which the feeds should be located. It also affects the contour of the lens, as will be seen.

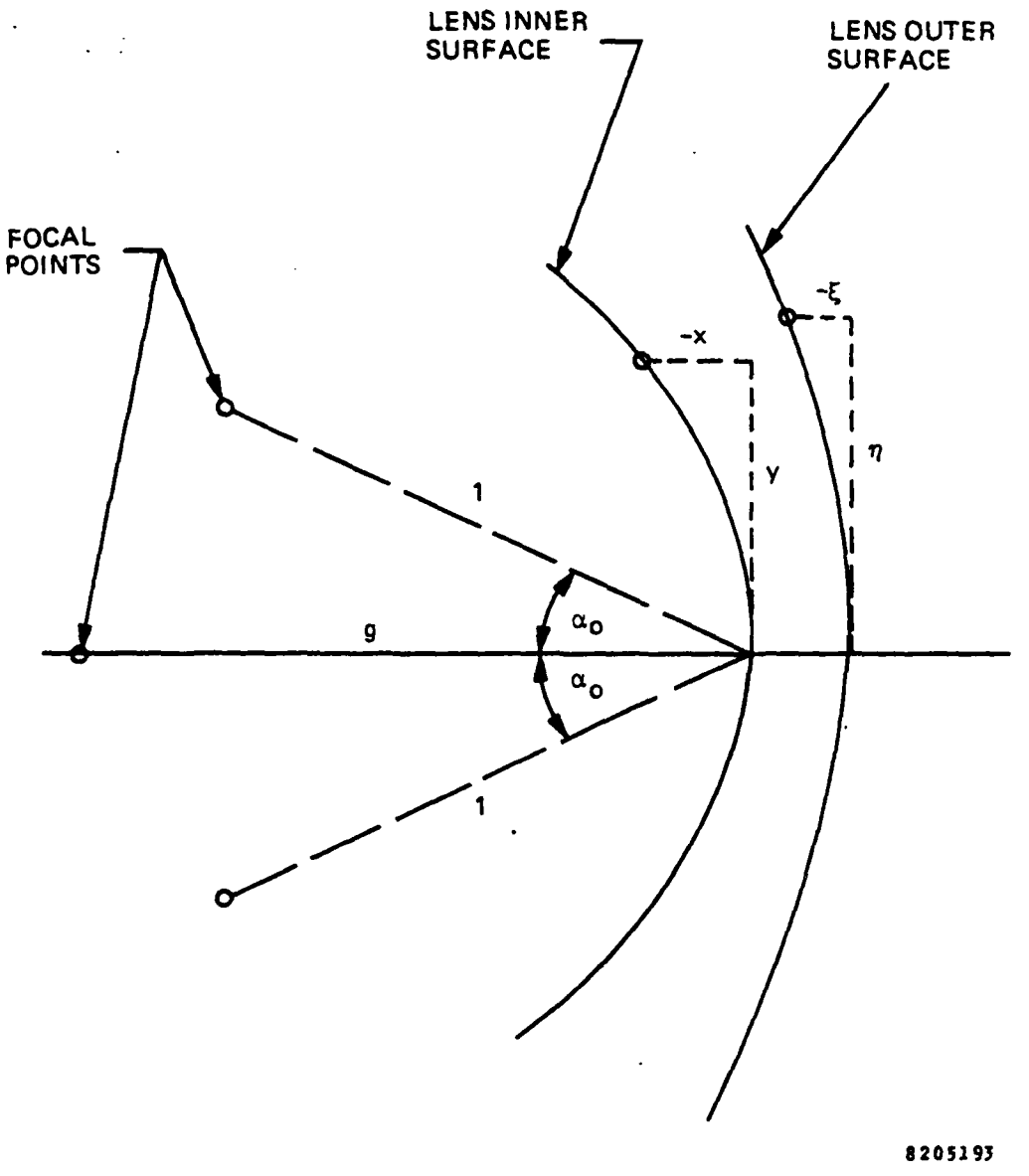

Figure 4-1. Lens Geometry

The equations for the inner surface of the lens appear in formulas 27 and 30 of ref. 1 or formulas 31 and 34 of ref. 3. These equations are:

$$y = \eta (1 + \xi \cos \alpha_o)$$

$$x = \frac{(\xi^2 - \eta^2) \sin^2 \alpha_o}{2(g - \cos \alpha_o)} \qquad (2)$$

In these equations, y and x are the coordinates of the inner surface as shown in figure 4-1. For any point η, ξ on the outer surface, a corresponding point y, x may be found on the inner surface from these equations. The two points are connected to the same transmission line.

In order to determine the lens contours it is necessary to solve the equation for the outer surface given in (1). This quartic equation was solved by a computer-aided procedure that yielded two useful roots. Thus there are two possible contours for the lens.

a. <u>The Two Contours for the Lens</u>.

Figure 4-2 shows one such lens contour, for $\alpha_o = 35^o$ and $g = 1.187$. Both the outer and inner surfaces are shown (the two surfaces are arbitrarily shown coincident at the lens vertex, since their displacement is of no theoretical significance). Also shown, by means of straight lines connecting the two surfaces, are some of the corresponding elements on the two surfaces. Note that both surfaces come to a point at the vertex.

Figure 4-3 shows the other lens contour for the same values of α_o and g. Note that in this case both surfaces have an inverse point, or a dimple, at the vertex.

The angular discontinuity at the vertex has the same magnitude for the pointed lens and the dimpled lens. Therefore, half of one lens can be combined with the opposite half of the other lens, yielding a smooth but unsymmetrical lens. Figure 4-4 shows this "hybrid" lens.

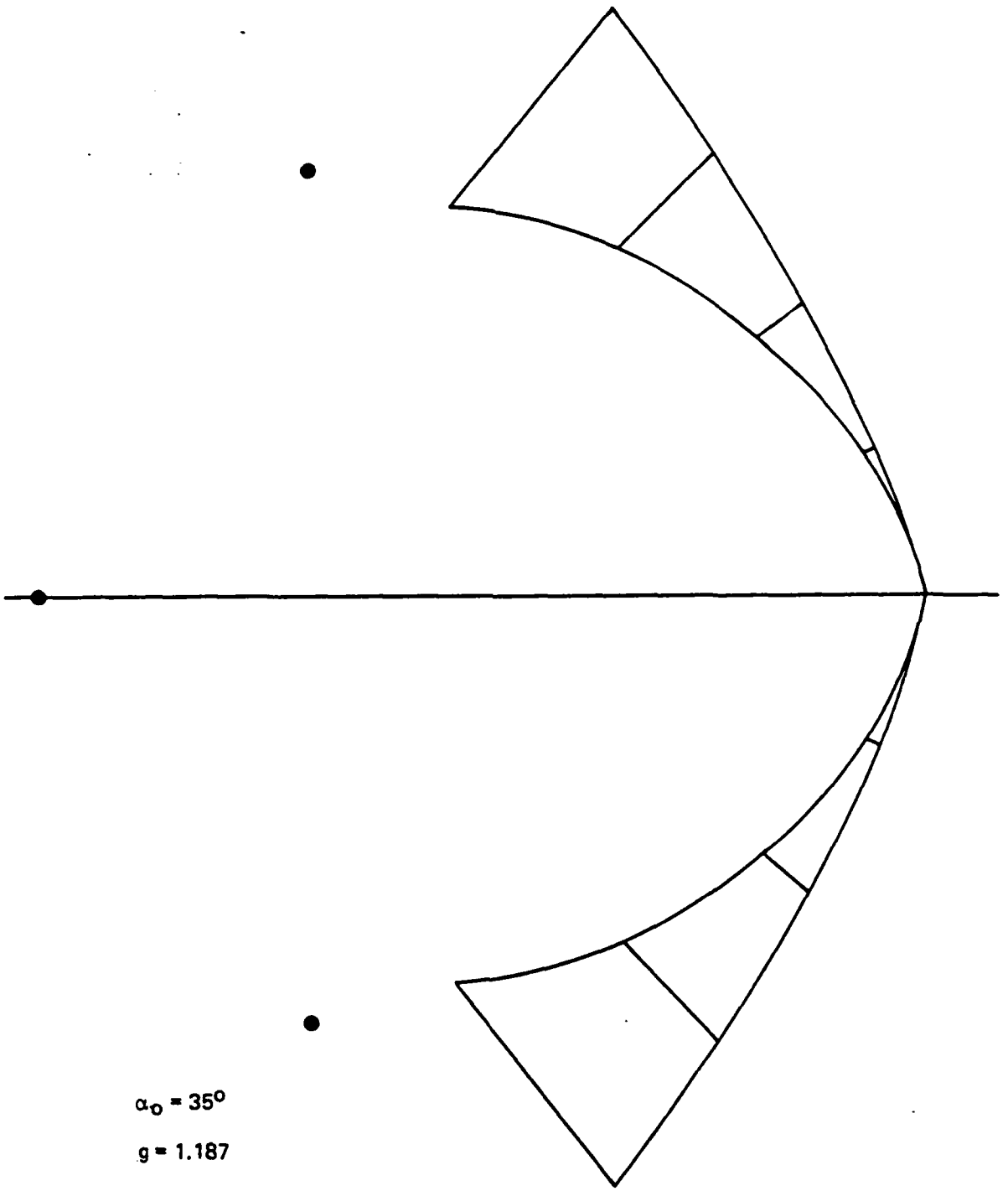

Figure 4-2. Pointed Lens Contours

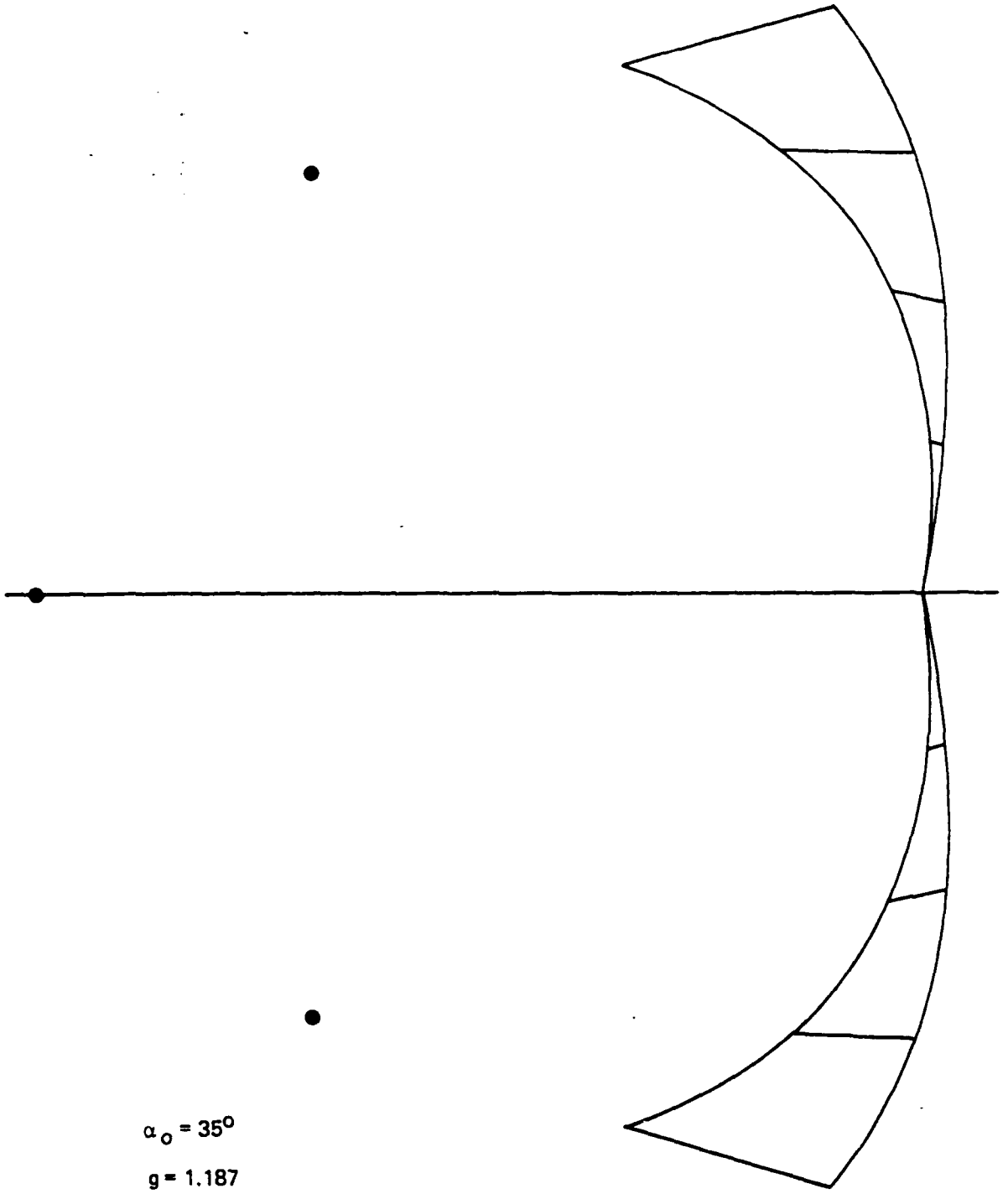

Figure 4-3. Dimpled Lens Contours

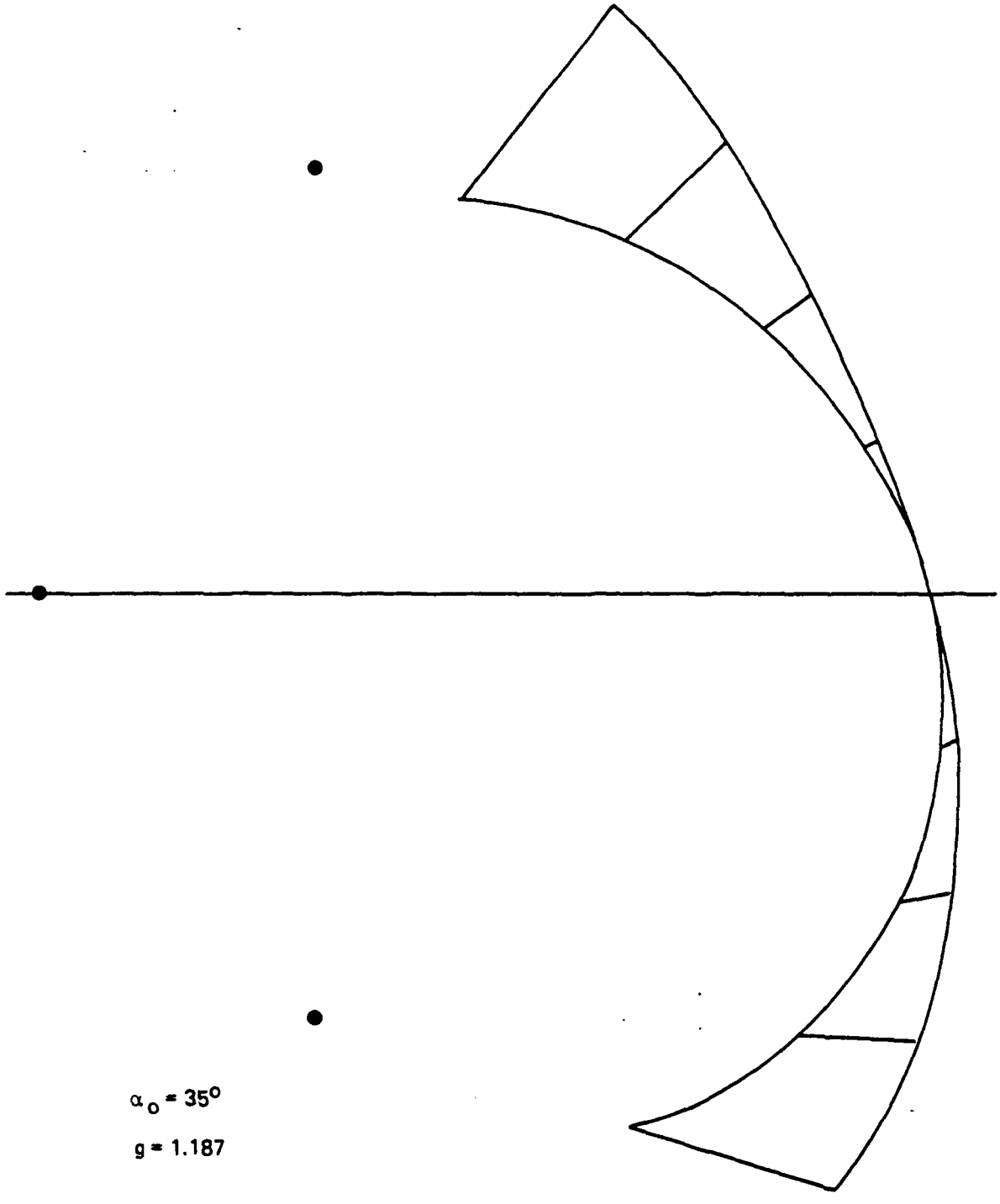

Figure 4-4. Hybrid Lens Contours

b. Parametric Control of the Angular Discontinuity.

The value of g = 1.187 used for the previous examples was obtained from the relation $g = 1 + \alpha_o^2/2$ that is suggested in ref. 1 and ref. 3. It is found, however, that by choosing other values for g, we can control the sharpness of the points and the dimples in the two symmetrical lenses. Suppose that we define g in terms of α_o as follows:

$$g = \frac{k}{\cos \alpha_o} \tag{3}$$

where k is a constant that will be specified. Then consideration of (1) yields a relation between k and the angular discontinuity τ of the symmetrical lens surface at the vertex:

$$\tau = 2 \arctan\left[\sqrt{\frac{1 - k}{k}} \operatorname{ctn} \alpha_o\right] \tag{4}$$

This result for the angular discontinuity τ applies to both the outer and inner surfaces, and to both the pointed and dimpled symmetrical lenses. For g = 1.187 and $\alpha_o = 35^o$, the value of k is 0.9723. This yields from (4) an angular discontinuity τ of 27.1^o. An inspection of figures 4-2 and 4-3 confirms this value for the angular discontinuity.

c. Elimination of the Angular Discontinuity.

It is seen from (4) that when k is less than one τ has a real value, but when k is greater than one τ becomes imaginary. (We also found that the roots of equation (1) for the outer surface are not real numbers when k is greater than one.) When k is exactly one, the angular discontinuity τ is zero and the symmetrical lens becomes smooth at the vertex. For this case $g = 1/\cos \alpha_o$.

Substituting this special value for g into equation (1) yields the following relatively simple equation for the outer surface:

$$\left[\xi + \frac{1}{p}\right]^2 + \eta^2 = \frac{1}{p^2} \tag{5}$$

where $p = \cos \alpha_o$

This is the equation of a circle having radius 1/p and displacement 1/p.

Similar substitutions into equations (2) for the inner surface yields:

$$\left[x + \frac{1}{2p}\right]^2 + y^2 = \left[\frac{1}{2p}\right]^2 \qquad (6)$$

which is also the equation of a circle, but having half the radius and displacement of the first circle.

Further study of this special case yields two additional results. First, the three points of perfect focus lie on the small circle given by (6). Second, corresponding points on the inner and outer surfaces (ie, points connected to the same transmission line) lie on a straight line passing through the axial focal point.

All these characteristics of this special case are identical with those of the R-2R lens (ref 4), which also is a constant-W lens. Therefore we conclude that this special case is an R-2R lens.

d. The R-2R Case.

An R-2R lens provides wide-angle scanning by motion of a feed around the smaller circle. It can be shown that there is no phase aberration with an R-2R lens for any location of the feed on the smaller circle (see Appendix A). Therefore the special case provides perfect focusing not only at the three specified points, but also for any other point on the small circle.

Figure 4-5 shows the lens contours for the R-2R case. The feed locus lies on the same circle as the inner lens surface. Also shown, by means of straight lines connecting the two surfaces, are some of the corresponding elements on the two surfaces. All these straight lines pass through the axial feed point, and the spacing between the elements along the outer surface is the same as the spacing along the inner surface. The coordinate h in the figure is normalized to the axial focal length (2R), rather than to an off-axis focal length, because there is no particular off-axis angle α_o that has special significance with the R-2R lens.

Ref 4- H.B. DeVore and H.Iams, "Microwave Optics Between Parallel Conducting Sheets", RCA Review, pp. 721-732; December 1948.

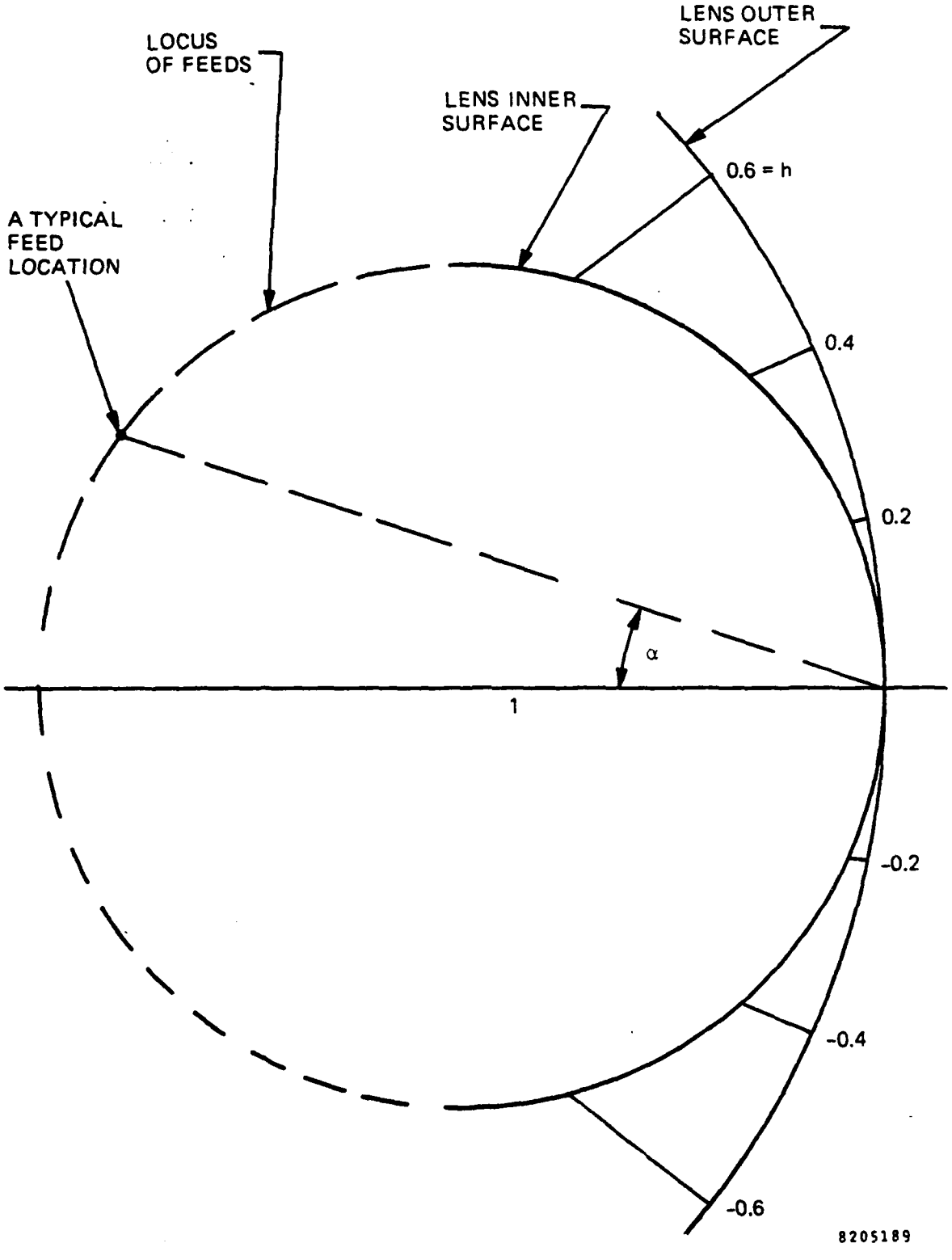

Figure 4-5. R-2R Lens Contours

4.2 APERTURE PHASE AND AMPLITUDE ERRORS

Except for the special R-2R case, the lenses have phase aberrations when the feed is not located at 0 or $\pm \alpha_o$. Also, all the lenses create an amplitude distortion across the antenna aperture. These two effects are examined below.

a. Phase Aberration.

For the pointed and dimpled lenses of figures 4-2 and 4-3, the phase aberration was computed for feed locations on a circular arc through the three focal points. The angle α between the feed and the lens axis was varied in 5^o intervals from 0^o to 45^o. Figures 4-6 and 4-7 show the results for the two lenses. The horizontal coordinate is the normalized aperture variable η from 0 to $\pm$ 1.0. The vertical coordinate is the aberration, given in terms of path-length error as defined in refs. 1 and 3, and also normalized to the off-axis focal length. The value of 0.001 for this coordinate corresponds to a phase error of roughly 10^o for a lens 40 wavelengths across and with an F/D of about 0.7.

The results for the pointed lens in figure 4-6 show substantial coma aberration consisting mainly of cubic and higher order terms. The quadratic component is not large, indicating that refocusing the feed to a location off the assumed circular feed locus would not yield a major benefit. Note that the cubic component reverses when the feed is scanned past the off-axis focal point at 35^o.

Inspection of figure 4-6 indicates that for scan from 0^o to somewhat beyond 35^o, the aberration may be tolerable out to an η of about 0.6 for a 40 wavelength lens. This assumes that a linear component of error can be subtracted because it represents only a beam displacement.

The results for the dimpled lens in figure 4-7 again show coma aberration, but less than for the pointed lens. Inspection of the results indicates that for scan from 0^o to about 40^o, the aberration may be tolerable out to an η of about 0.7 for a 40 wavelength lens.

The "hybrid" lens of figure 4-4 would have aberration characteristics that are partly those of the pointed lens and partly those of the dimpled lens. The R-2R lens of figure 4-5 has no phase aberration.

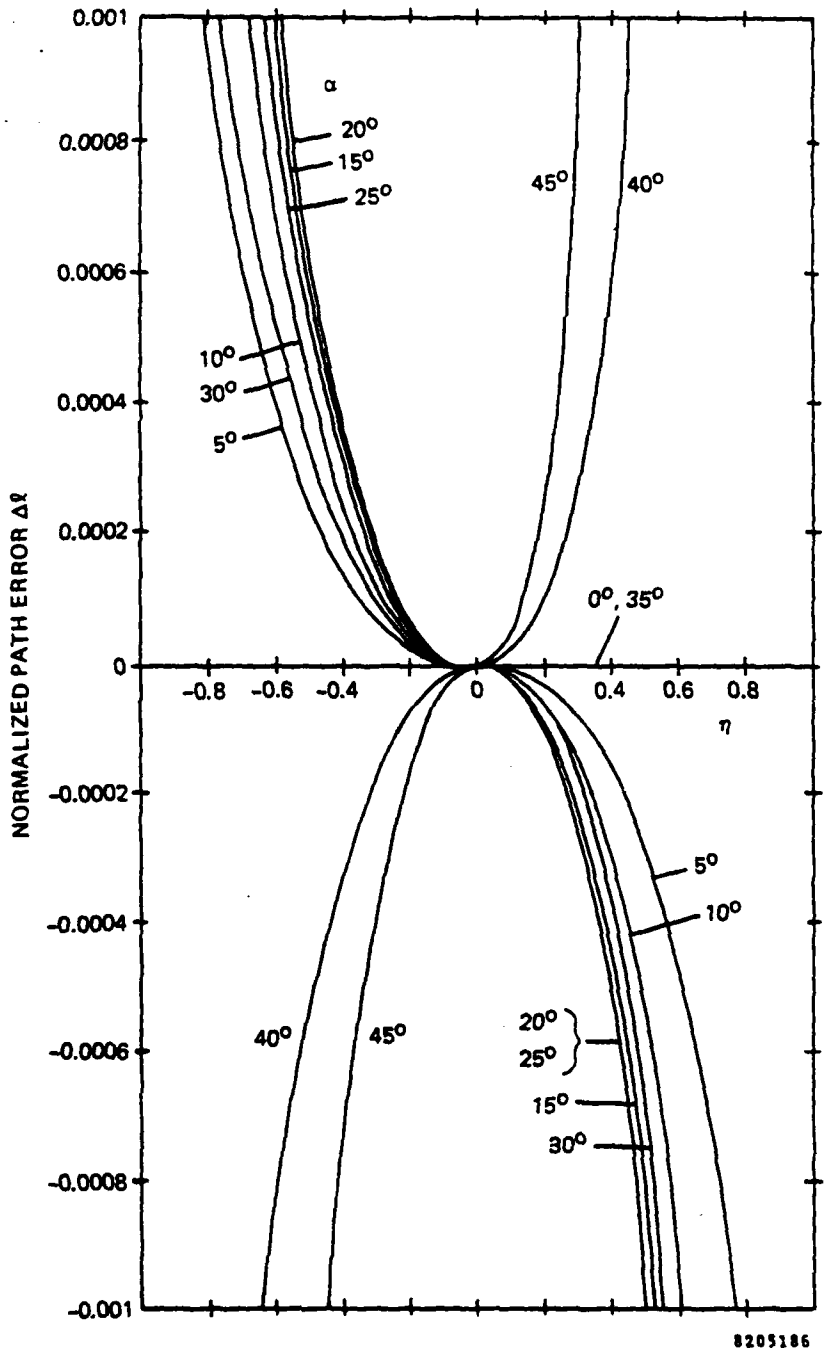

Figure 4-6. Phase Aberration of Pointed Lens

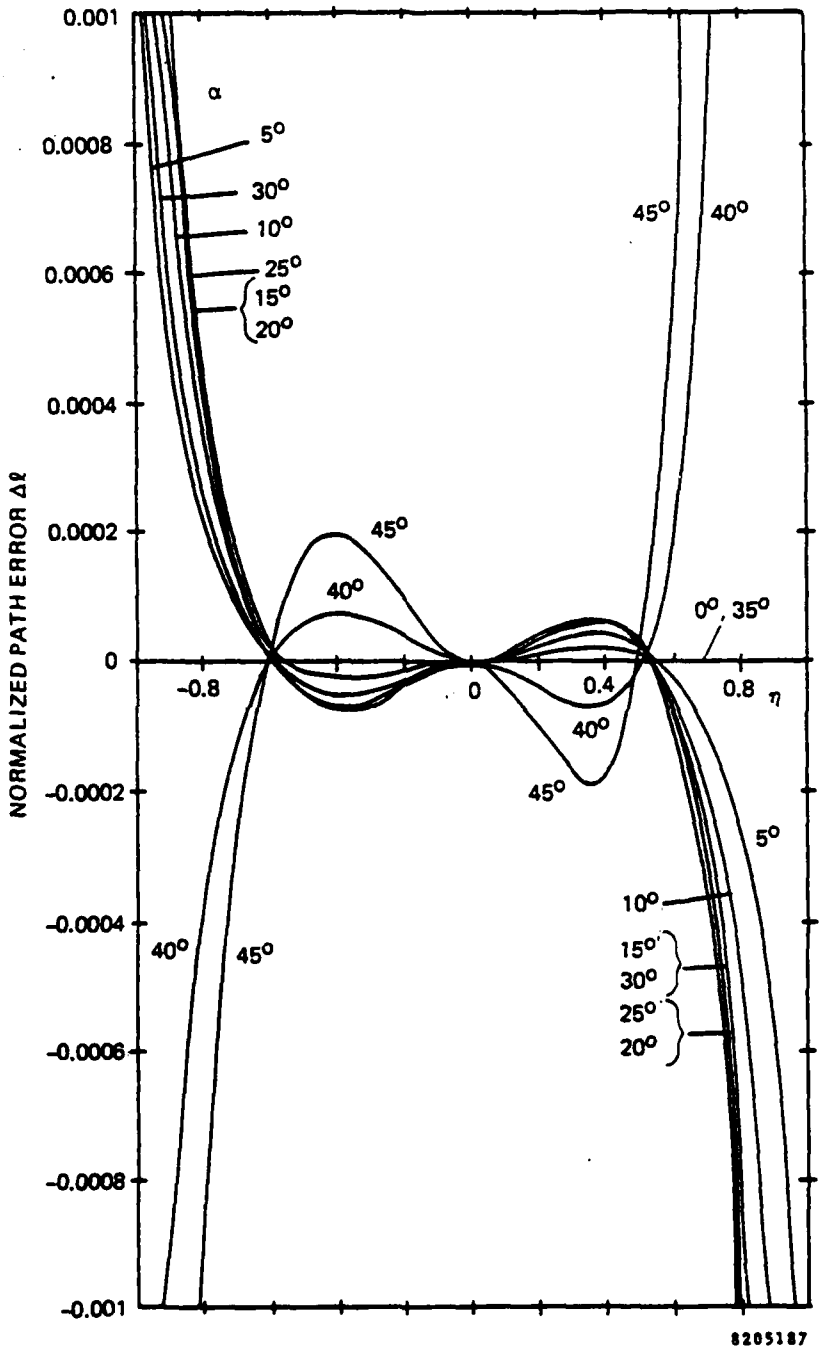

Figure 4-7. Phase Aberration of Dimpled Lens

b. Amplitude Distortion.

The highly curved contours of the lenses, together with their internal path displacement, introduce a distortion of the amplitude distribution that is provided by the line feed. This effect becomes exaggerated and unsymmetrical when the feed is displaced from the antenna axis. Figures 4-8 and 4-9 show the results for the pointed and dimpled lenses of figures 4-2 and 4-3. The vertical coordinate is the amplitude obtained across the planar effective aperture, which is perpendicular to the central ray. The amplitude shown is normalized to the amplitude at the center of the aperture. An omnidirectional pattern is assumed for the line feed. Also, it is assumed that the lens surfaces are perfectly matched to waves incident at any angle.

The results in figure 4-8 for the pointed lens show that for the 0° feed location there is a symmetrical inverse-tapering effect. This is typical of focusing devices that provide small phase aberrations over wide scan angles.

As the feed is scanned in 5° intervals out to 45°, the amplitude distortion in figure 4-8 becomes unsymmetrical. Furthermore, a discontinuity in the slope of the curves at the center of the aperture becomes evident. This is caused by the angular discontinuity of the lens surfaces at the center. For 35°, 40°, and 45° scans, an anomolous effect is observed for η near +0.6 where the inner surface of the lens goes through tangency with the rays from the nearby feed. Beyond this point the curves do not represent the physical lens.

The results in figure 4-9 for the dimpled lens show a similar inverse taper for 0° scan. Also, the unsymmetrical tapering and the central discontinuity, both increasing with scan, are evident. The anomolous effect is not seen here because this flatter lens does not reach the tangency condition.

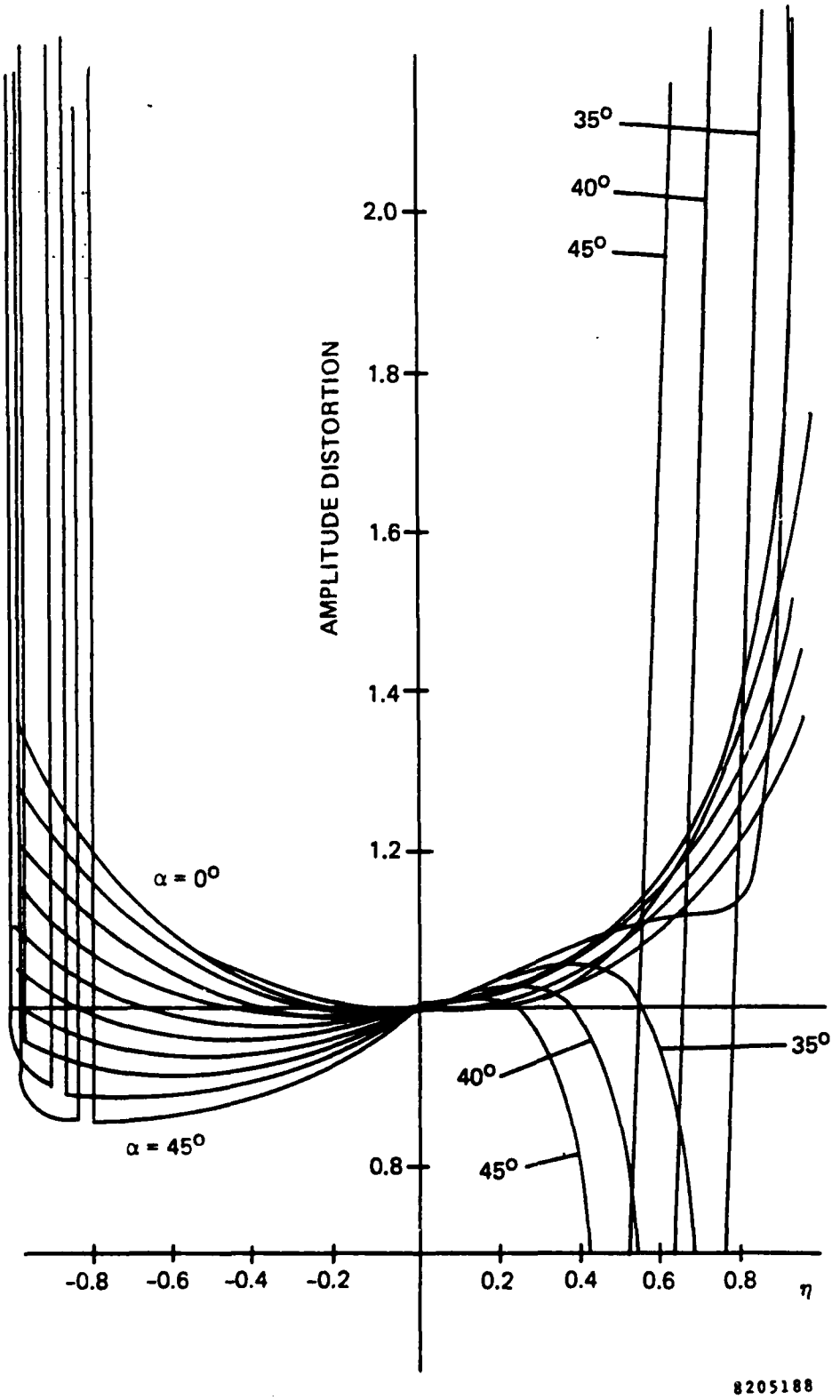

Figure 4-8. Amplitude Distortion of Pointed Lens

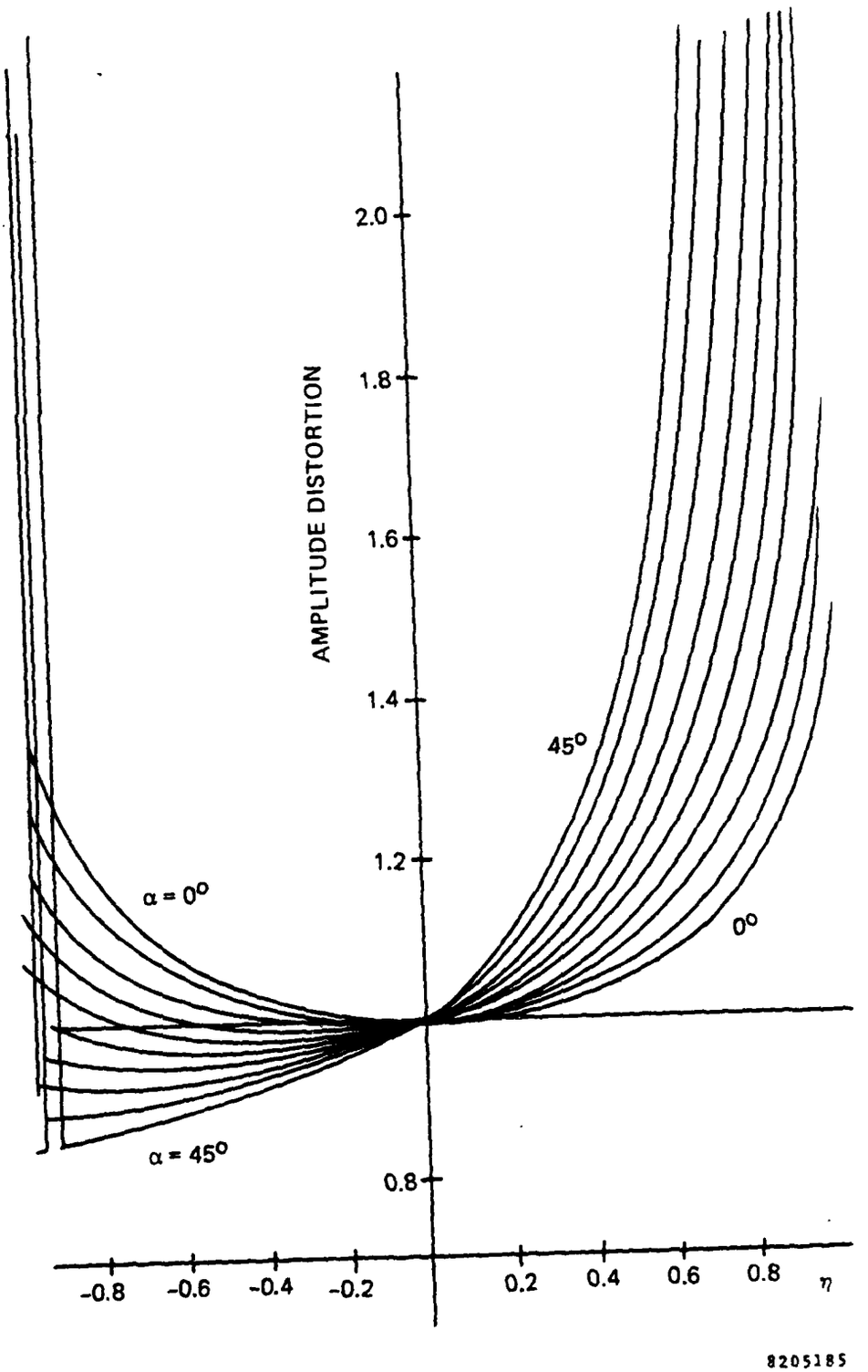

Figure 4-9. Amplitude Distortion of Dimpled Lens

Figure 4-10 shows the amplitude distortion for a lens that approximates the special R-2R case. As would be expected, the central discontinuity is no longer evident. There remains, of course, the symmetrical inverse tapering for the 0^{o} feed location, and the unsymmetrical tapering for feeds scanned away from 0^{o}.

A simple relation exists for the amplitude distortion of the R-2R case. Figure 4-11 shows an R-2R lens that is scanned off its axis by the angle α. An effective aperture plane is defined tilted by α and tangent to the outer circle as shown. From the center of this circle two lines are drawn: one to the tangency point A and the other to any specified point B on the outer circle. The angle between these two lines is ψ. The amplitude distortion is then given by:

$$\frac{E(B)}{E(C)} = \sqrt{\frac{\cos \alpha}{\cos \psi}} \qquad (7)$$

where E(B) and E(C) are the field amplitudes on the aperture plane corresponding to rays from the specified point B and the axial point C. It is assumed that the lens surfaces are perfectly matched to waves incident at any angle. The feed pattern is considered to be omnidirectional.

The amplitude distortion given by (7) becomes $\sqrt{\sec \psi}$ when referenced to point A instead of C. It is interesting to note that exactly the same result exists for the Luneburg lens. Both the Luneburg and the R-2R lenses provide scanning free of phase aberration. Therefore both lenses are free of coma aberration and both obey the Abbe sine condition (ref 5). This condition yields the amplitude distortion described above.

The viewpoint of amplitude across an effective planar aperture is a useful one. However for a more accurate computation of the radiation patterns, it is preferable to use the amplitude of excitation of the actual radiating elements across the actual curved array. It can be shown

---

Ref 5- F.A. Jenkins and H.E. White, "Fundamentals of Optics", McGraw-Hill Book Co., pp. 120, 135; 1950.

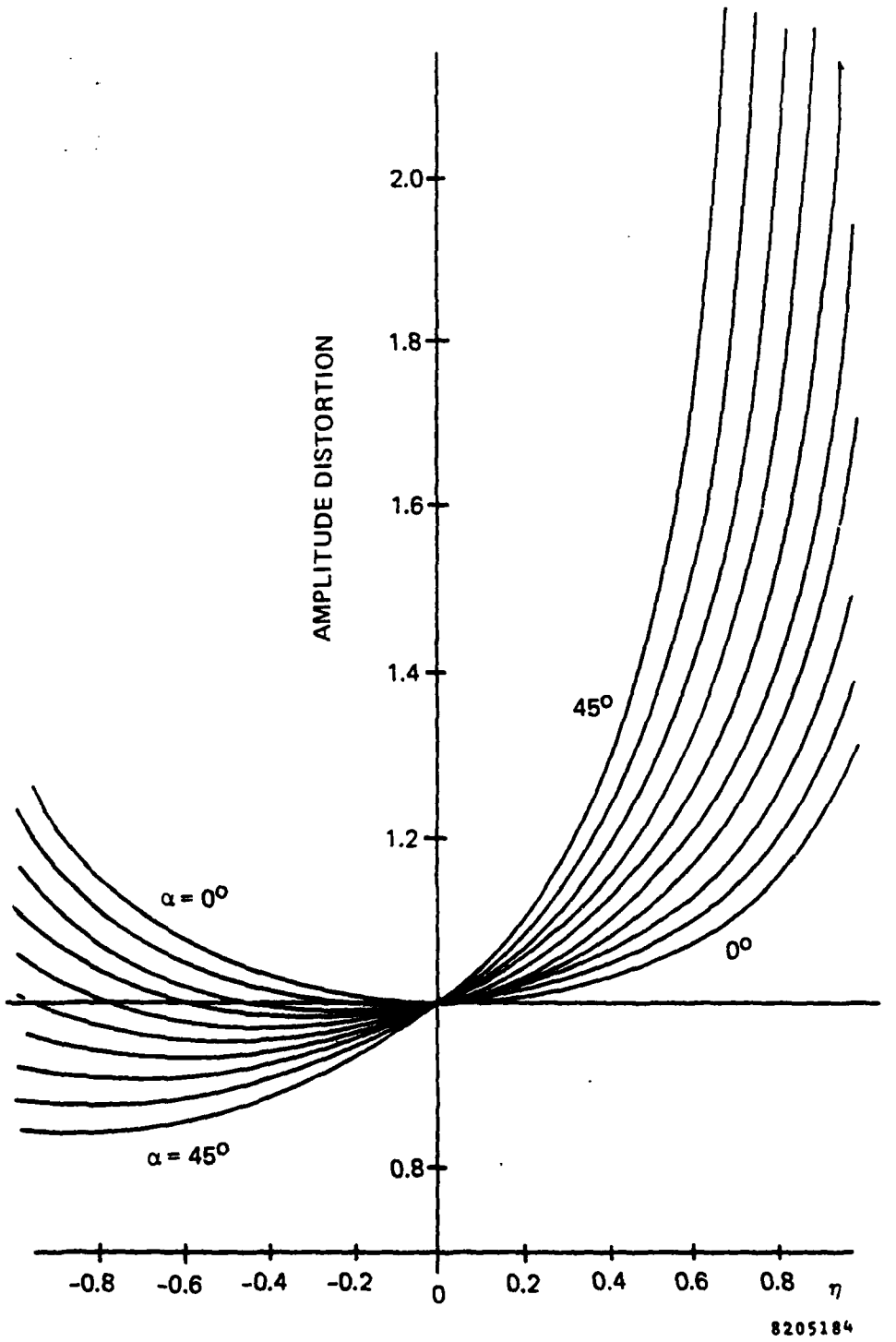

Figure 4-10. Amplitude Distortion of R-2R Lens

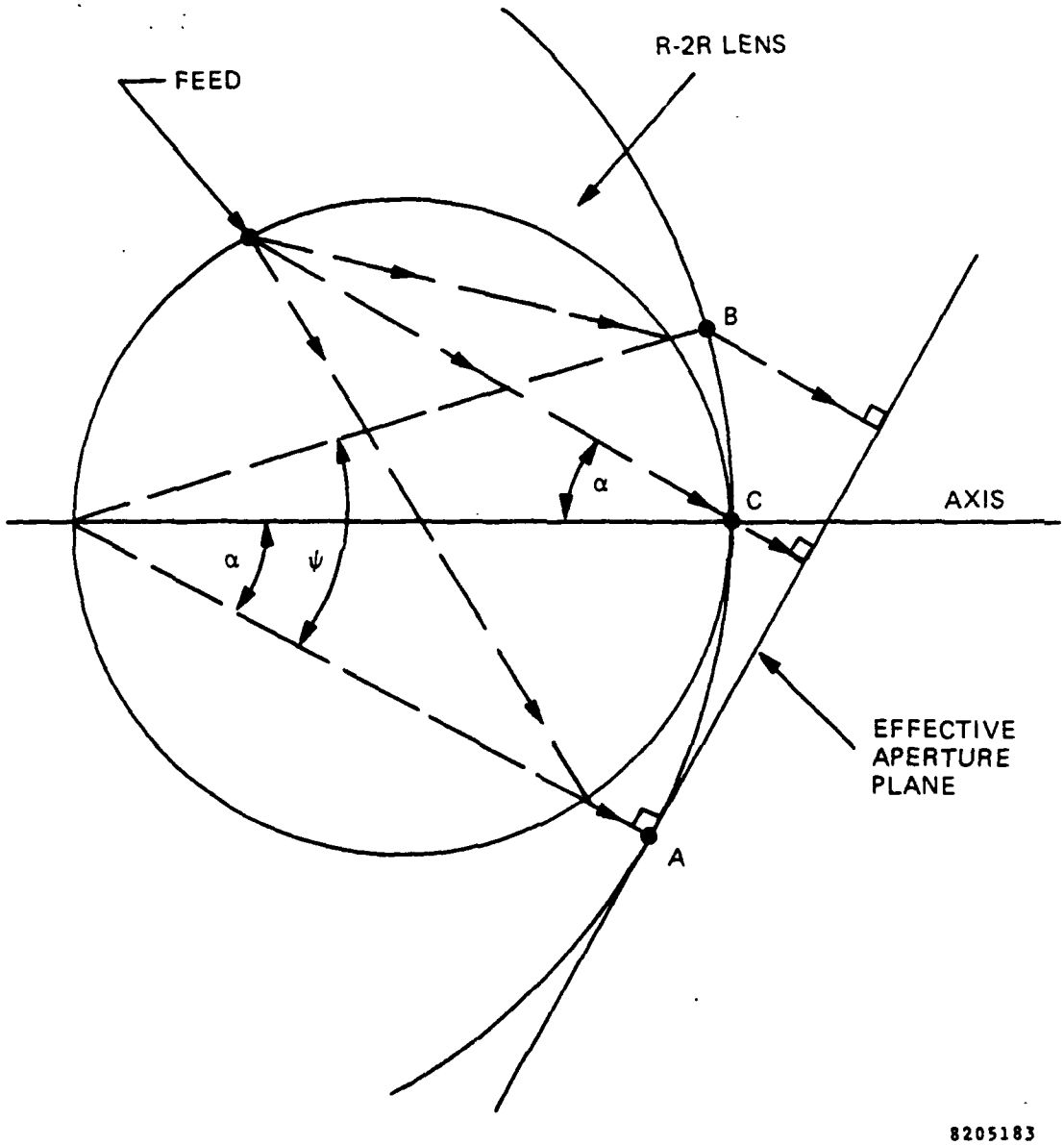

Figure 4-11. Ray Geometry for R-2R Lens

that for elements that are equispaced along the curved surface of the R-2R lens, an omnidirectional feed will produce equal amplitude of excitation in all the elements on the outer surface. This assumes a very large or infinite size array in wavelengths, and assumes unidirectional array elements that are perfectly matched at all incidence angles in the array. These ideal elements then radiate with essentially a cosine power pattern (ref 6), assuming they are spaced close enough to avoid grating-lobe radiation.

4.3 INCIDENCE ANGLES OVER LENS SURFACE

In addition to possible phase and amplitude errors, lenses have a problem of reflection at their surfaces. This reflection problem is compounded by the variation of incidence angles that may be encountered over the lens surface. It is therefore important to ascertain how the incidence angle varies for the constant-W lenses being investigated.

a. Incidence Angles for Pointed, Dimpled, and Hybrid Lenses.

Figure 4-12 shows the angle of incidence on the outer surface of the pointed lens of figure 4-2, as a function of the aperture coordinate η. Three curves are shown corresponding to feed locations for $+35^{\circ}$, 0°, and -35° scan. It can be seen that each curve has a large step discontinuity at the middle of the lens where the lens surface is discontinuous. The value for the step in incidence angle is equal to the angular discontinuity τ defined previously (see formula 4).

Also evident in figure 4-12 is a substantial variation of incidence angle over each half of the lens. This variation is caused by the substantial curvature of the lens surface.

Figure 4-13 shows a similar set of curves for the outer surface of the dimpled lens of figure 4-3. Again, the central discontinuity and the substantial variation in each half are evident.

With the unsymmetrical "hybrid" lens of figure 4-4, half of the curves of figure 4-12 are combined with the other half of the curves of figure 4-13. This yields a set of curves (not shown) having no central discontinuity, but exhibiting an unsymmetrical character.

Ref 6- P.W.Hannan, "The Element-Gain Paradox for a Phased-Array Antenna", IEEE Trans. Antennas and Propagation, pp. 423-433; July 1964.

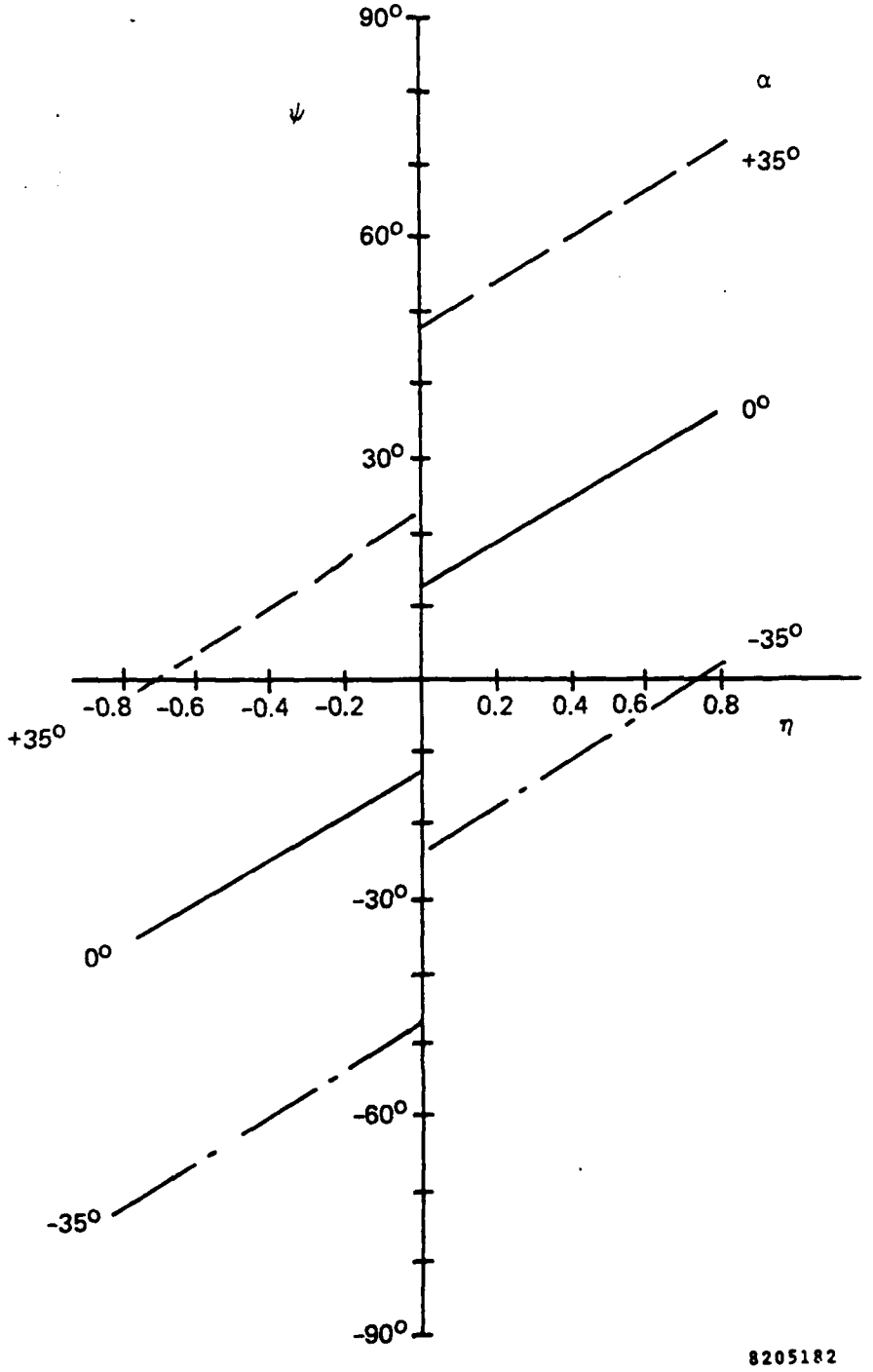

Figure 4-12. Incidence Angles for Outer Surface of Pointed Lens

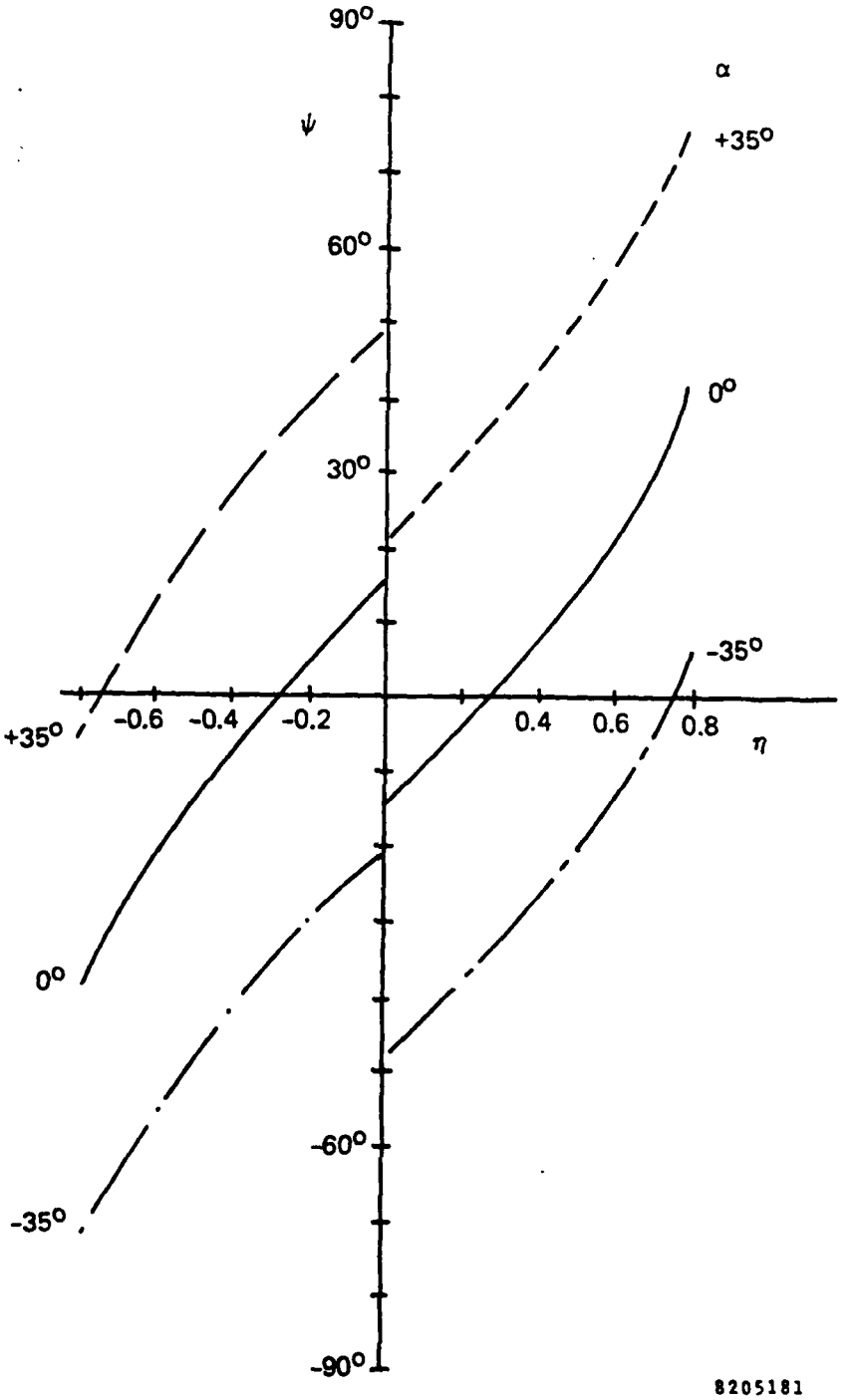

Figure 4-13. Incidence Angles for Outer Surface of Dimpled Lens

b. Incidence Angles for R-2R Lens.

Referring to figure 4-11, it can be seen that the angle ψ is the angle of incidence of a ray at the general point B on the outer surface of the R-2R lens. It can also be seen that for any particular ray, the incidence angle ψ is the same at the inner and outer surfaces. From the figure, the following simple formula can be derived for ψ :

$$\sin(\psi - \alpha) = h \qquad (8)$$

where α is the scan angle as determined by the feed location, and h is the vertical coordinate of point B normalized to the axial focal length (2R).

Figure 4-14 shows three curves of ψ versus h for $\alpha = -30^{\circ}$, 0°, and $+30^{\circ}$. There is, of course, no central discontinuity in these curves because the R-2R special case has no angular discontinuity in its lens surfaces. There remains a continuous variation of incidence angle over the lens surface that is substantial, because of the substantial curvature of the lens surface.

c. Effect of F/D on Incidence Angles.

In any optical type of microwave antenna (lens or reflector), the ratio of its focal length F to its aperture diameter D is a significant parameter. A small F/D is desirable to conserve physical space, but a larger F/D may be needed to avoid degradation of performance.

Let us consider the focal length of the constant-W lens to be the distance from the axial feed to the center of the inner lens surface, neglecting any lens thickness that would be needed at the center in practice. Also, let us take the lens aperture diameter as the diameter of the outer lens surface. Then:

$$\frac{F}{D} \approx \frac{q}{2\eta_{max}} \approx \frac{1}{2h_{max}} \qquad (9)$$

where the first relation applies to the pointed or dimpled lenses, and the second relation is convenient for the R-2R case. For a compact antenna having a small F/D, we would need a large η_{max} or a large h_{max}.

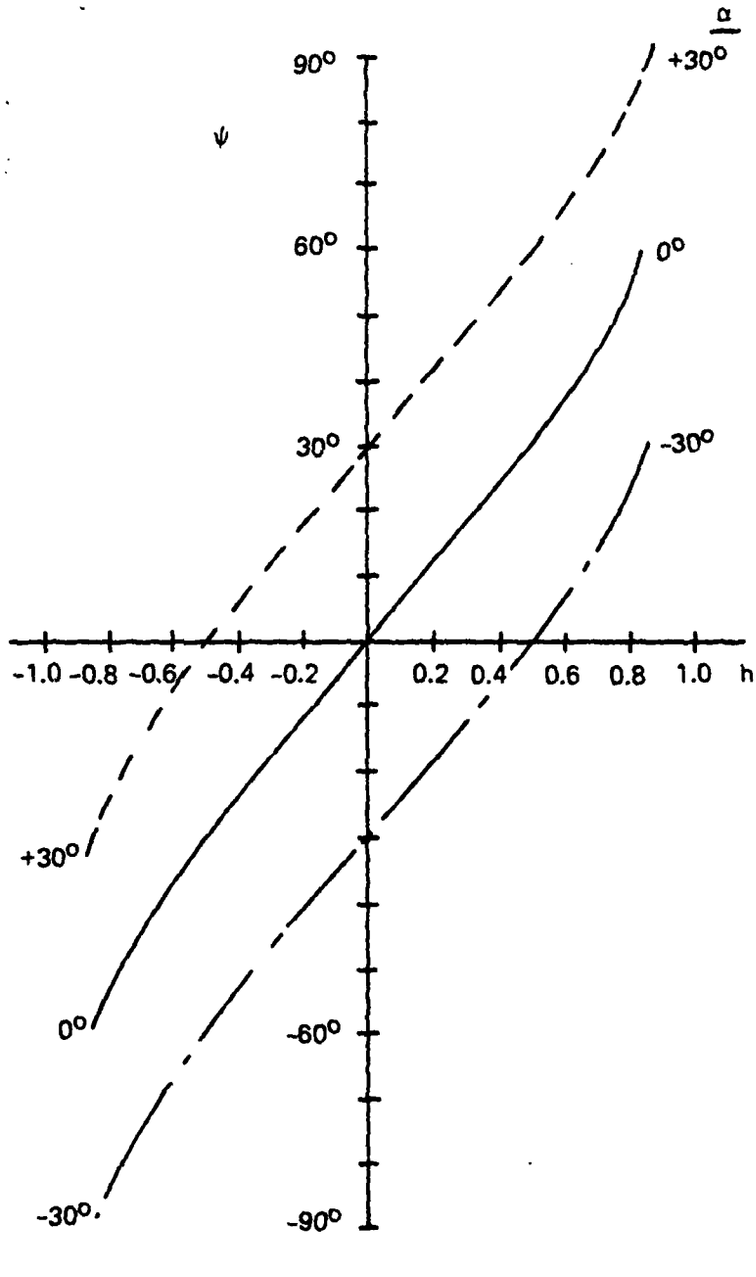

Figure 4-14. Incidence Angles for R-2R Lens

It is apparent from figures 4-12, 4-13, and 4-14 that a large value for η_{max} or h_{max} will result in a large value for the maximum incidence angle. Unfortunately, the impedance match of the lens surface array degrades as the incidence angle becomes large. Therefore the value of η_{max} or h_{max} cannot be chosen arbitrarily large. If a 60^{o} incidence angle is assumed to be about the largest incidence angle that would yield acceptable performance, and the feed is scanned to about 30^{o} off axis, then a value of η_{max} or h_{max} in the vicinity of 0.6 or 0.5 is the largest that should be used. This corresponds to an F/D of about one as the smallest acceptable value.

The discussion above has considered the incidence angle resulting only from the basic passive lens-feed system. However it is intended that the lens will ultimately include electronic phase shifters for fine steering. Suppose that the basic lens-feed system covers $\pm 30^{o}$ in azimuth, and that the electronic phase shifters add $\pm 15^{o}$ of fine steering to yield a total azimuth scan coverage of $\pm 45^{o}$. Then the incidence angle at the outer surface of the lens will have approximately an additional $\pm 15^{o}$ beyond the angles shown in figures 4-12, 4-13, and 4-14, or in equation (8). Thus the maximum incidence angle with an F/D of one is no longer about 60^{o} but is now about 75^{o}.

If it was necessary to keep the maximum incidence angle within 60^{o} in order to preserve acceptable performance, then an F/D greater than one would have to be used, yielding a bulkier antenna. Alternatively, if the F/D is restricted to one, then the outer surface array design should be such that array scan angles (incidence angles) out to 75^{o} off broadside can be tolerated. The latter approach is more difficult but would lead to a more compact antenna. We have chosen this approach. Further discussion of the incidence-angle problem, lens internal reflections, and array element design appears in Section VI of this report.

4.4 CHOICE OF LENS

In the second part of the program a lens antenna is to be designed, constructed, and tested. A selection of one among the four types (pointed, dimpled, hybrid, or R-2R) must be made for this program.

Two of the types, the pointed and dimpled lenses, have a discontinuity right down the center of the cylindrical antenna aperture. It is expected that this discontinuity would degrade the azimuth sidelobes, both by its effect on the basic aperture field and also by its effect on the angle of incidence and hence array impedance. The pointed or dimpled shape has no particular advantage for this program.

The other two types, the hybrid and R-2R lenses, have no central discontinuities. The hybrid lens is unsymmetrical while the R-2R lens is symmetrical. An unsymmetrical shape has no advantage for this program, and it introduces complexities of both construction and performance. The R-2R lens, therefore, appears to be best suited for development in this program, and it has been selected for this purpose.

SECTION V

THE LENS ANTENNA BASIC DESIGN

In this section is described the basic electrical design of the lens antenna. First, the configuration of the line feed for low azimuth sidelobes is discussed, and some azimuth patterns are presented. Then the line-feed configuration for low elevation sidelobes is considered, and some elevation patterns are shown. Next, the antenna directive gain is discussed. Finally, the signal bandwidth/scan performance is considered, including the tradeoff between number of feeds and signal loss, and also the potential effect on sidelobes.

Figure 5-1 shows the basic antenna configuration comprising the cylindrical lens and its on-axis line feed. An h_{max} of 0.52 has been selected, corresponding to an F/D = 0.96. The horizontal aperture dimension D has been chosen as 40 wavelengths at 5.3 GHz, or about 7.4 feet. The vertical length of the line feed L_f is about 35 wavelengths or 6.5 feet, and the lens vertical dimension is somewhat larger.

5.1 LINE FEED AND AZIMUTH PATTERNS

In order to obtain low-sidelobe antenna azimuth patterns, the line feed must provide a horizontal illumination of the lens that is well tapered at the edges of the lens. The feed radiation, therefore, must be confined within the sector $\pm\phi_f$ where ϕ_f is the half-angle subtended by the vertex and the edge of the lens. With an R-2R lens, it can be shown that:

$$\phi_f = \arcsin h_{max} \qquad (10)$$

It can also be shown that with an R-2R lens, this half-angle remains invariant as the feed is moved around its feed arc. The geometry is shown in figure 5-2.

For $h_{max} = 0.52$, the feed half-angle ϕ_f is 31.3^{o}. To provide well-tapered illumination, then, the effective horizontal aperture of the feed should be about two wavelengths. As will be discussed, the actual feed aperture should be considerably larger.

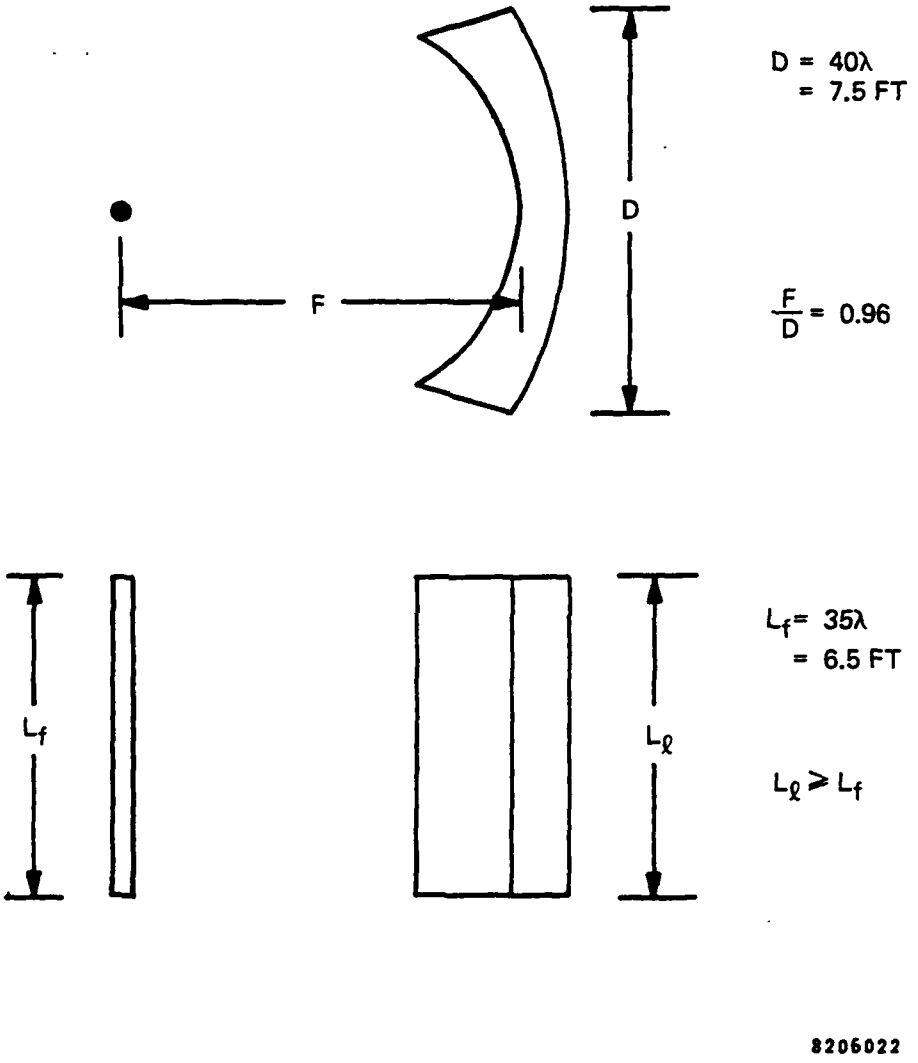

Figure 5-1. Basic Antenna Configuration

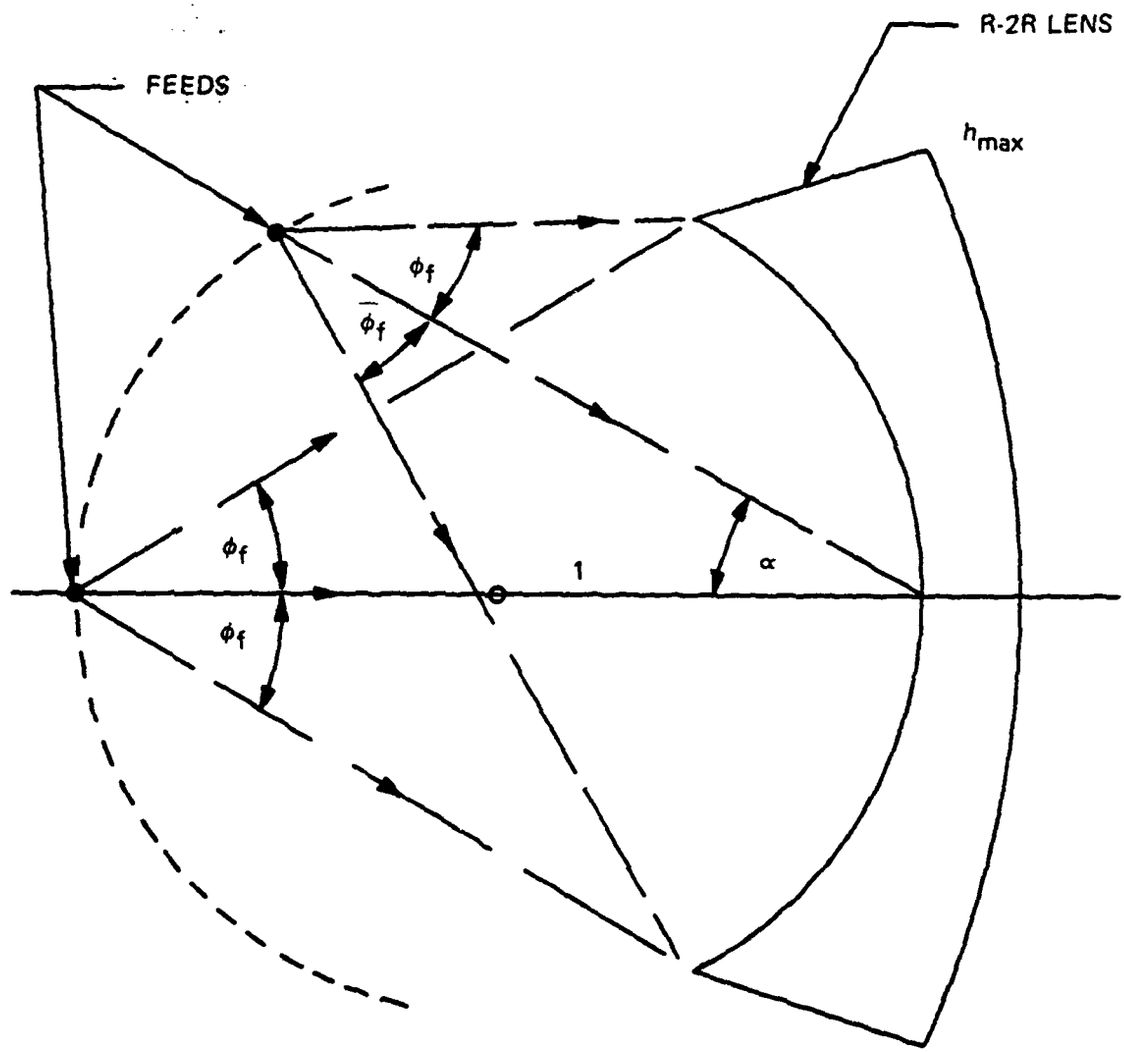

$$h_{max} = \frac{D}{2F} = 0.52$$

$\phi_f = 31.3°$

8206021

Figure 5-2. Feed-Lens Geometry

To obtain low azimuth sidelobes in the antenna pattern it is necessary to have not only a well-tapered illumination, but also a particular shape of the illumination amplitude distribution. It happens that this illumination shape is provided by a feed aperture excitation that is tapered, rather than uniform. Therefore, the actual feed aperture should be substantially larger than its effective aperture size.

a. Design for On-Axis Beam.

The feed design for low azimuth sidelobes is first considered for the case where the feed is on the antenna axis and there is no fine steering. There are various approaches for arriving at a specific excitation of the feed aperture. We have used the approach described by Fante, Franchi, Kernweis, and Dennett (ref 7). The feed aperture is assumed to contain two waveguide modes: a one-mode (half cosine) and a three-mode (1.5 cosine). The mode ratio and the feed aperture dimension are then varied until the best antenna sidelobe response is obtained without an excessive increase of beamwidth. The best sidelobe response is considered to be one having the greatest margin below the -32 to -50 dB azimuth sidelobe envelope defined by RADC.

Various physical realizations of this feed excitation were considered. One type, an actual multimode horn system, would have been acceptable but, because its aperture dimension is 4.8 wavelengths, would be susceptible to many undesired higher modes. A system of about eight exciter elements could be used to avoid the higher modes. Another type of feed, an array of radiating elements, needs about the same number (eight) of elements across the aperture to avoid grating lobes. Since this type provides similar pattern performance without the additional horn structure, it was selected.

Ref 7- R.L.Fante, P.R.Franchi, N.R.Kernweis, L.F.Dennett, "A Parabolic Cylinder Antenna with Very Low Sidelobes", IEEE Trans. Antennas and Propagation, pp. 53-59; January 1980.

Figure 5-3 shows the configuration of the feed array, consisting of strip dipoles. The dipoles are horizontally oriented because horizontal polarization has been selected for the antenna (discussed in a later section). Each horizontal row of dipoles is excited from an integral microstrip network, as indicated.

The distribution of excitation currents across the dipole feed is shown in figure 5-4. This excitation provides the computed feed pattern shown in figure 5-5. At the feed half-angle of 31.3° the feed pattern is quite weak, yielding an illumination of the lens that is almost completely tapered at the sides. The sidelobes of the computed feed pattern are low enough that their contribution to antenna pattern sidelobes is not substantial. It is possible that the actual feed to be constructed will have sidelobes sufficiently higher that they would degrade the sidelobe performance of the antenna; if this occurs, an absorbing enclosure can prevent the radiation of these sidelobes.

Computation of the antenna azimuth pattern is based on the approach given at the end of section 4.2. The feed pattern amplitude transfers directly into the excitation amplitude of the array elements in the outer lens surface. These elements are assumed to radiate with a cosine power pattern out to 85° from the local normal. Beyond 85°, the element pattern is assumed to decay linearly in dB; this is not an unreasonable assumption for a large circular array. The cosine power pattern assumed from 0° to 85° is based on a lens surface array that is perfectly matched for all incidence angles, and which has a very large or infinite size and employs closely-spaced unidirectional elements. The case in which the lens surface array is not perfectly matched at all incidence angles is considered in section VI of this report.

A computed on-axis antenna azimuth pattern is shown for 5.3 GHz (midband) in figure 5-6. The sidelobes are at least 10 dB below the sidelobe envelope defined by RADC, leaving a reasonable margin for errors. The beamwidth is 2.3° and is comparable with that of a cosine-squared illumination taper.

The computed effects of operation at the ends of the 5.0 to 5.6 GHz frequency band are shown in figures 5-7 and 5-8. It is assumed that the feed excitation (figure 5-4) remains constant across the band. The beamwidth of the feed pattern changes with frequency but, because of the highly tapered lens illumination, this change has little effect on the azimuth sidelobes of the antenna.

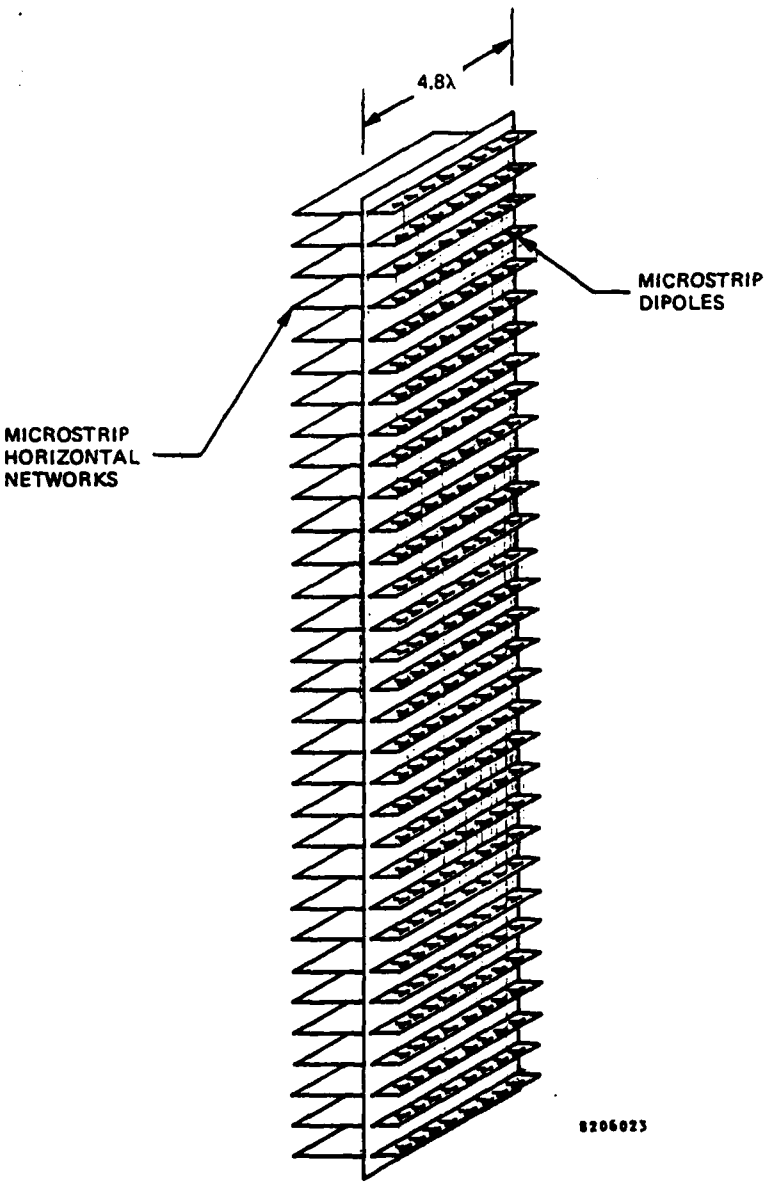

Figure 5-3. Line Feed Array Configuration

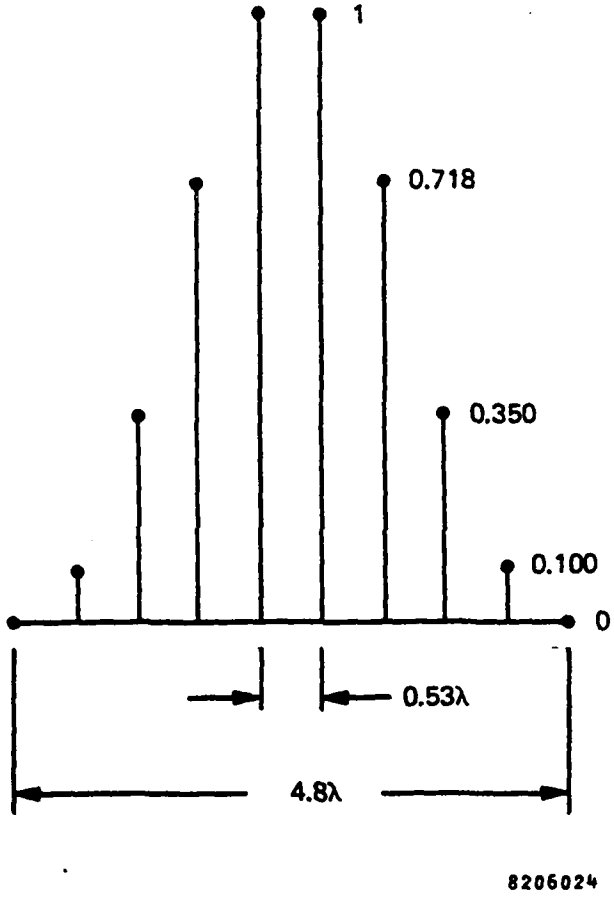

Figure 5-4. Current Distribution Across Dipole Feed

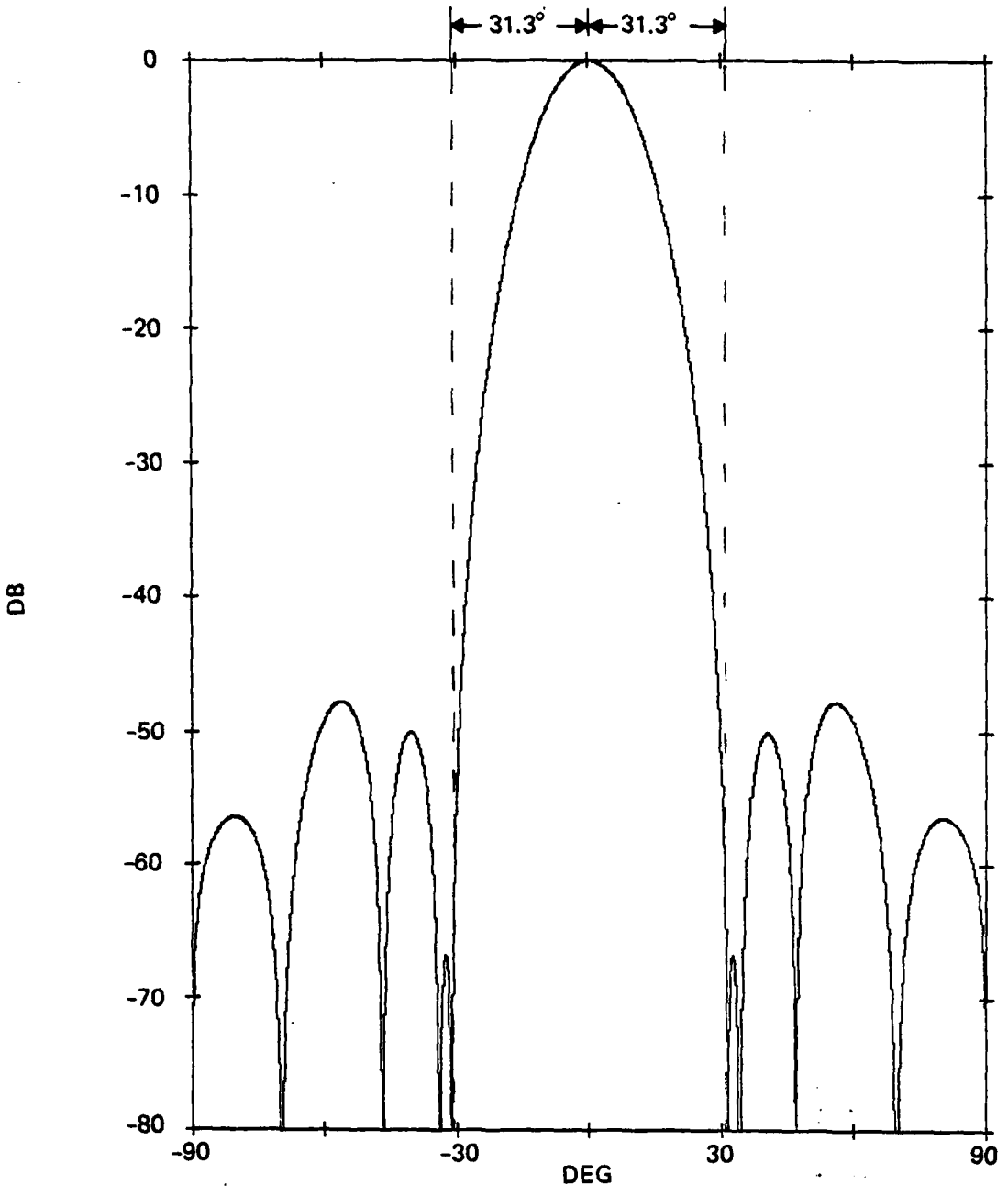

Figure 5-5. Line Feed Azimuth Pattern

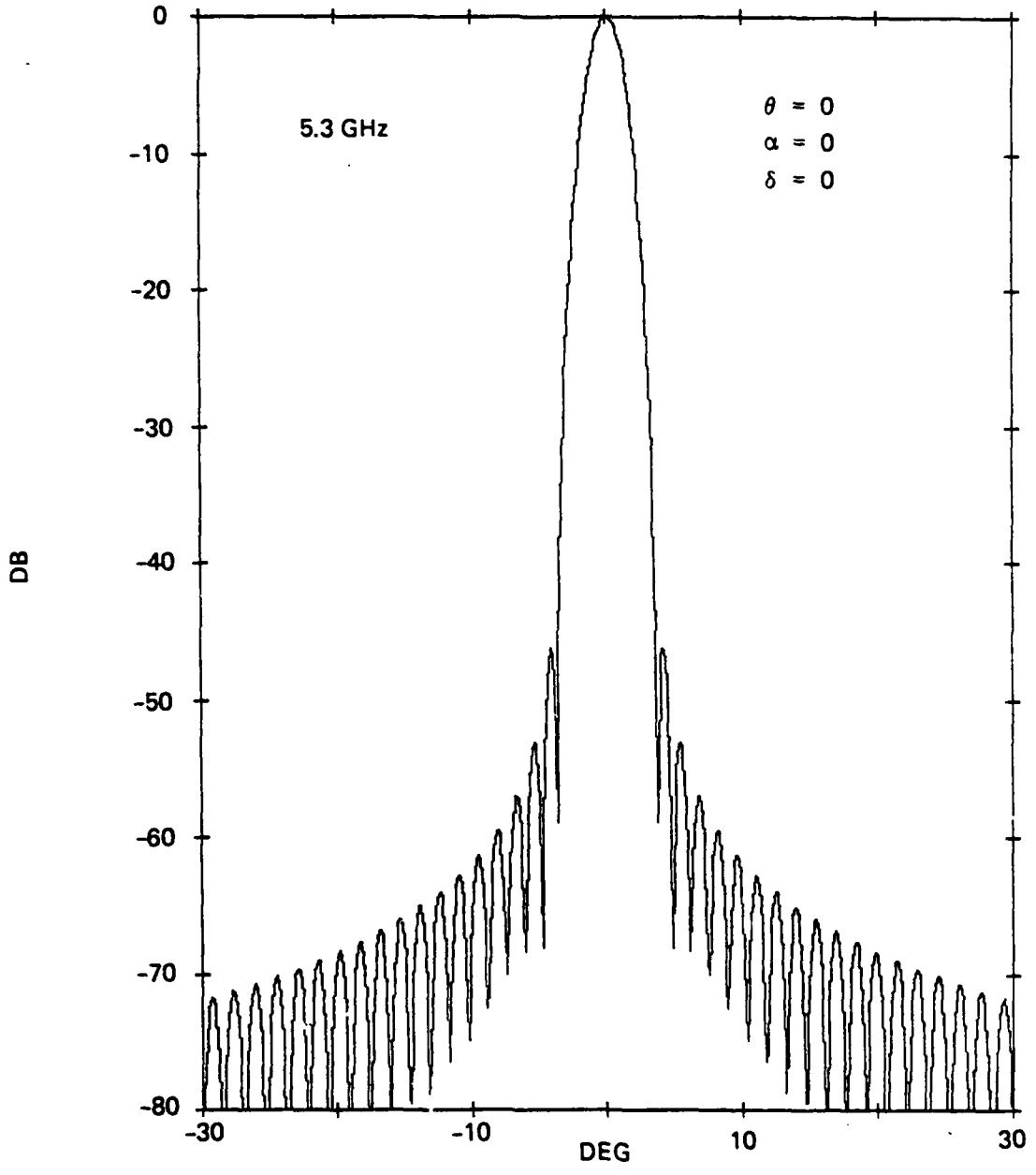

Figure 5-6. Azimuth Pattern of Antenna at 5.3 GHz for $\theta = 0$

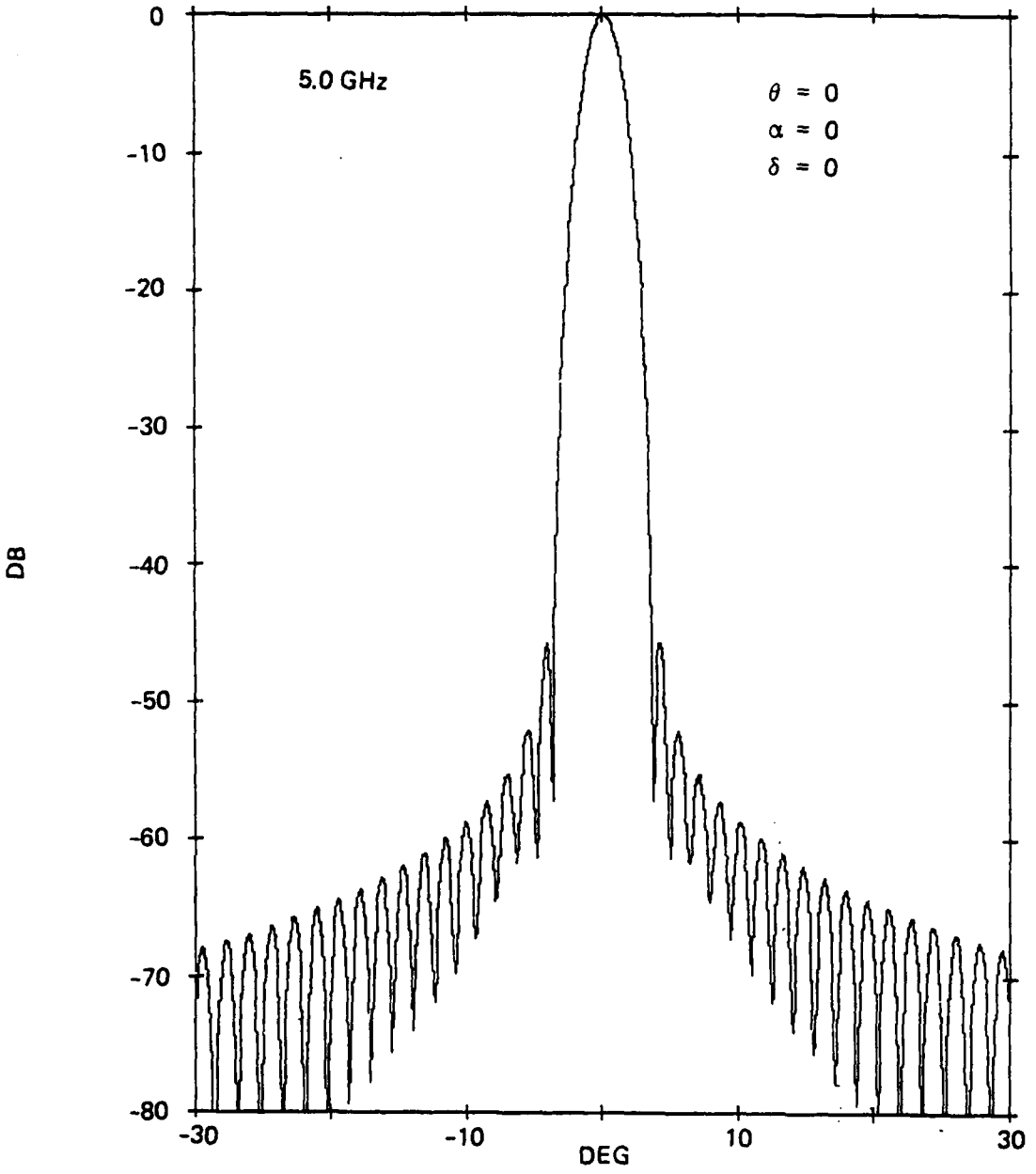

Figure 5-7. Azimuth Pattern of Antenna at 5.0 GHz for $\theta = 0$

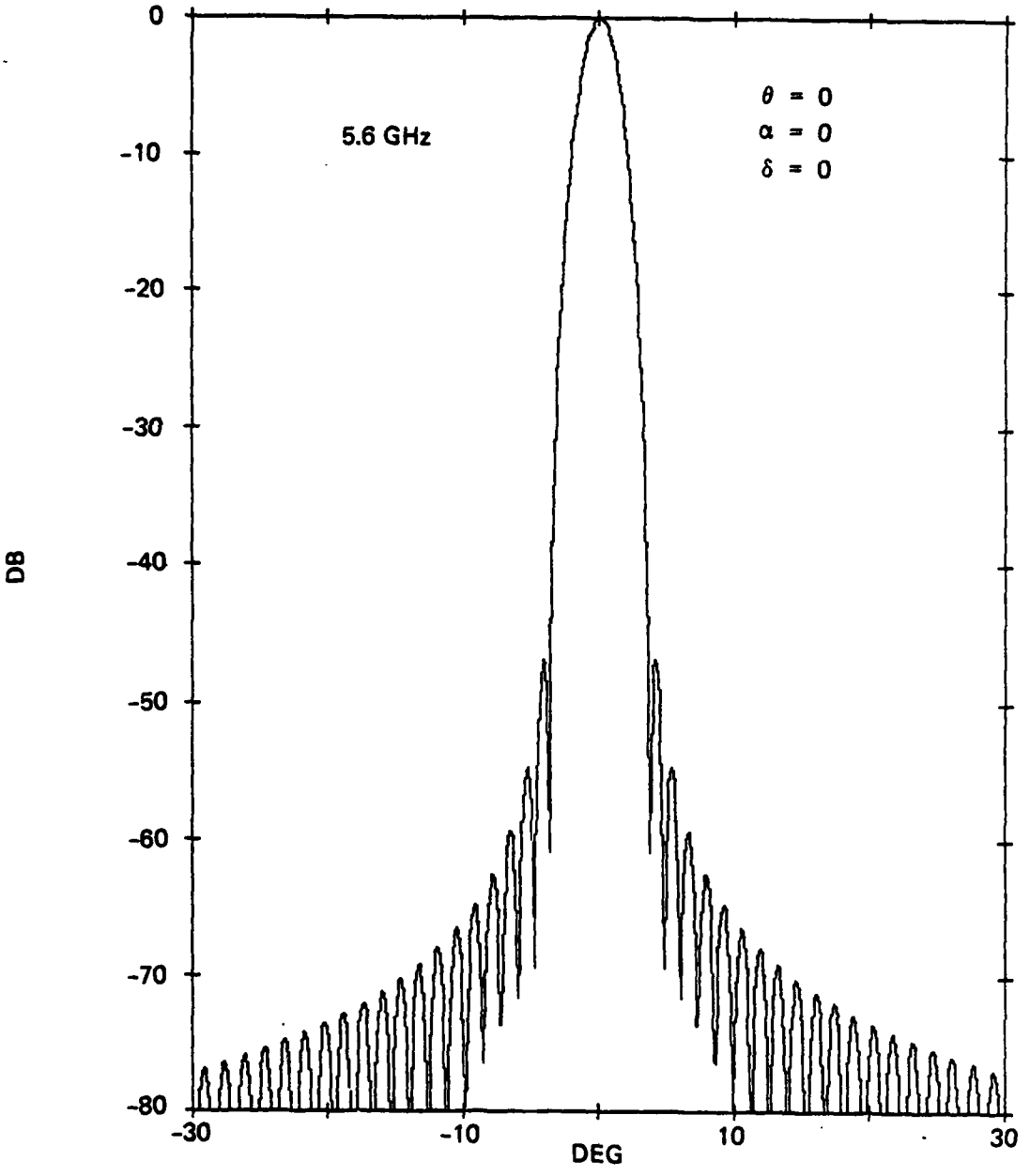

Figure 5-8. Azimuth Pattern of Antenna at 5.6 GHz for $\theta = 0$

The computed wide-angle sidelobe response in azimuth at midband is shown in figure 5-9. The wide-angle response is dependent on the element pattern and the spacing between elements. For the element pattern assumed (discussed previously) and for the 0.4 wavelength horizontal spacing between elements that is chosen (discussed in section VI) the wide-angle sidelobe response is seen to be satisfactory. Computed wide-angle patterns at 5.0 and 5.6 GHz yield similar satisfactory results.

b. Design for Off-Axis Beams.

When the feed is moved off the axis of the lens for coarse steering, or when the phase shifters provide fine steering of the beam off the lens axis, a significant effect on the azimuth patterns occurs. Figure 5-10 shows the beam-steering geometry in which θ is the beam direction relative to the lens axis, α is the coarse-steering angle, and δ is the fine-steering angle.

The azimuth pattern for a beam direction θ of 15° is shown at midband in figure 5-11. It is seen that there is some deterioration of the sidelobe response. An identical pattern is obtained regardless of what combination of coarse steering and fine steering provides the 15° beam direction.

The azimuth pattern for a 30° beam direction at midband is shown in figure 5-12. Here the deterioration of the sidelobe response is greater. Again, the same pattern is obtained for any combination of coarse steering and fine steering that yields the 30° beam direction.

The azimuth pattern for a 45° beam direction at midband is shown in figure 5-13. The deterioration of the sidelobe response is seen to be still greater.

The R-2R lens provides perfect collimation for any coarse-steering angle, and the phase shifters are set to provide perfect collimation for any fine-steering angle. Therefore the sidelobe deterioration cannot be ascribed to any defect in the lens focusing or phase-shifter settings. Rather, the effect is related to the fact that the radiating aperture of the antenna is curved. The following discussion is intended to provide some insight into this effect.

Curved Aperture Effect. Figure 5-14 shows a curved aperture radiating a collimated beam at an angle θ to the axis of symmetry of the aperture. The pattern angle γ is defined as the angle away from the main beam, giving the direction of interest in the sidelobe region. The transverse aperture

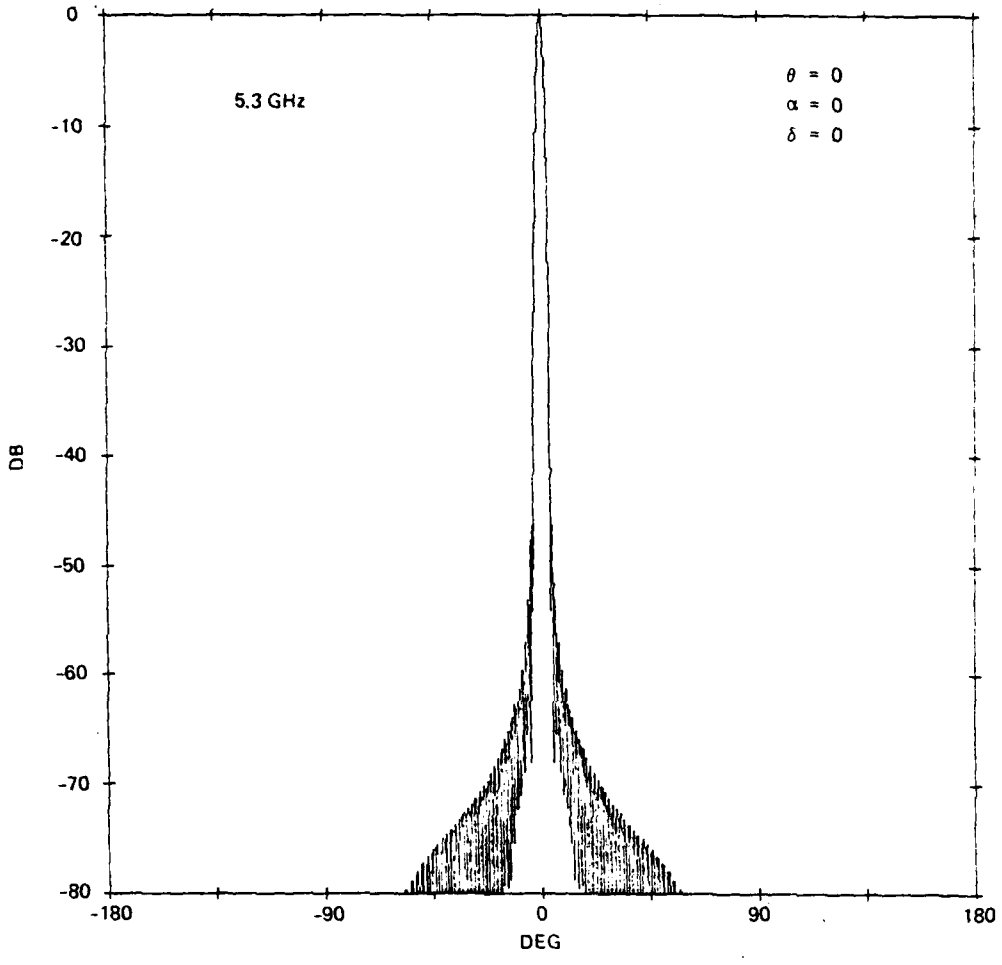

Figure 5-9. Wide-Angle Azimuth Pattern of Antenna at 5.3 GHz for $\theta = 0$

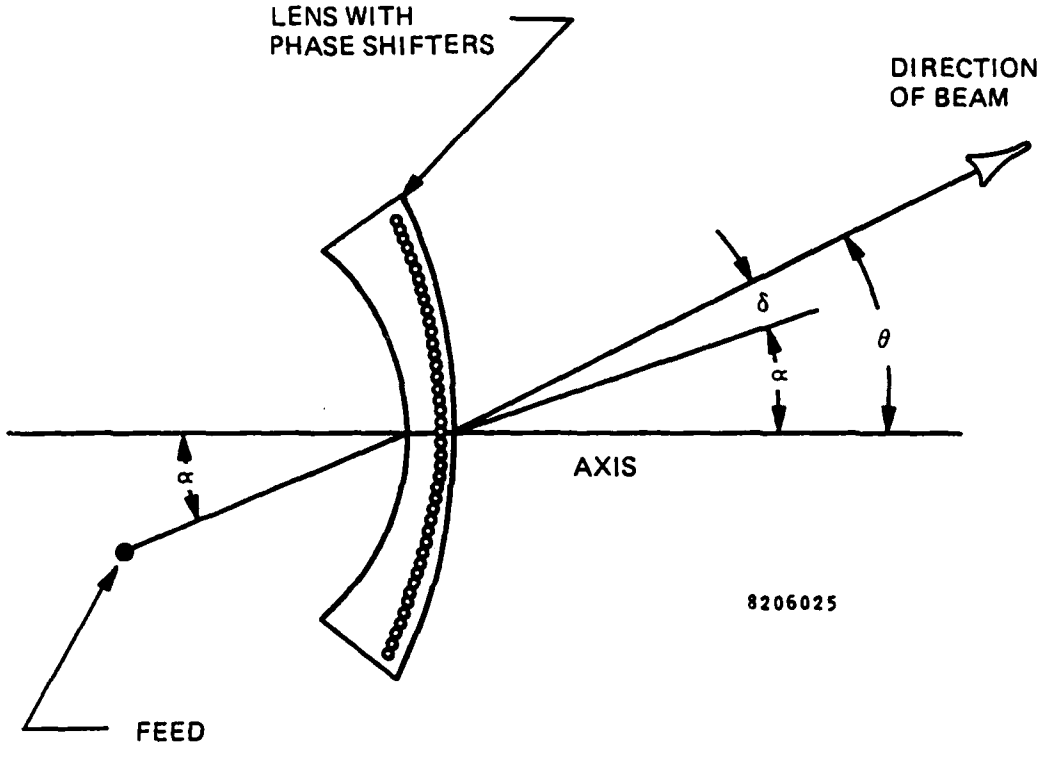

Figure 5-10. Definition of Beam-Steering Angles

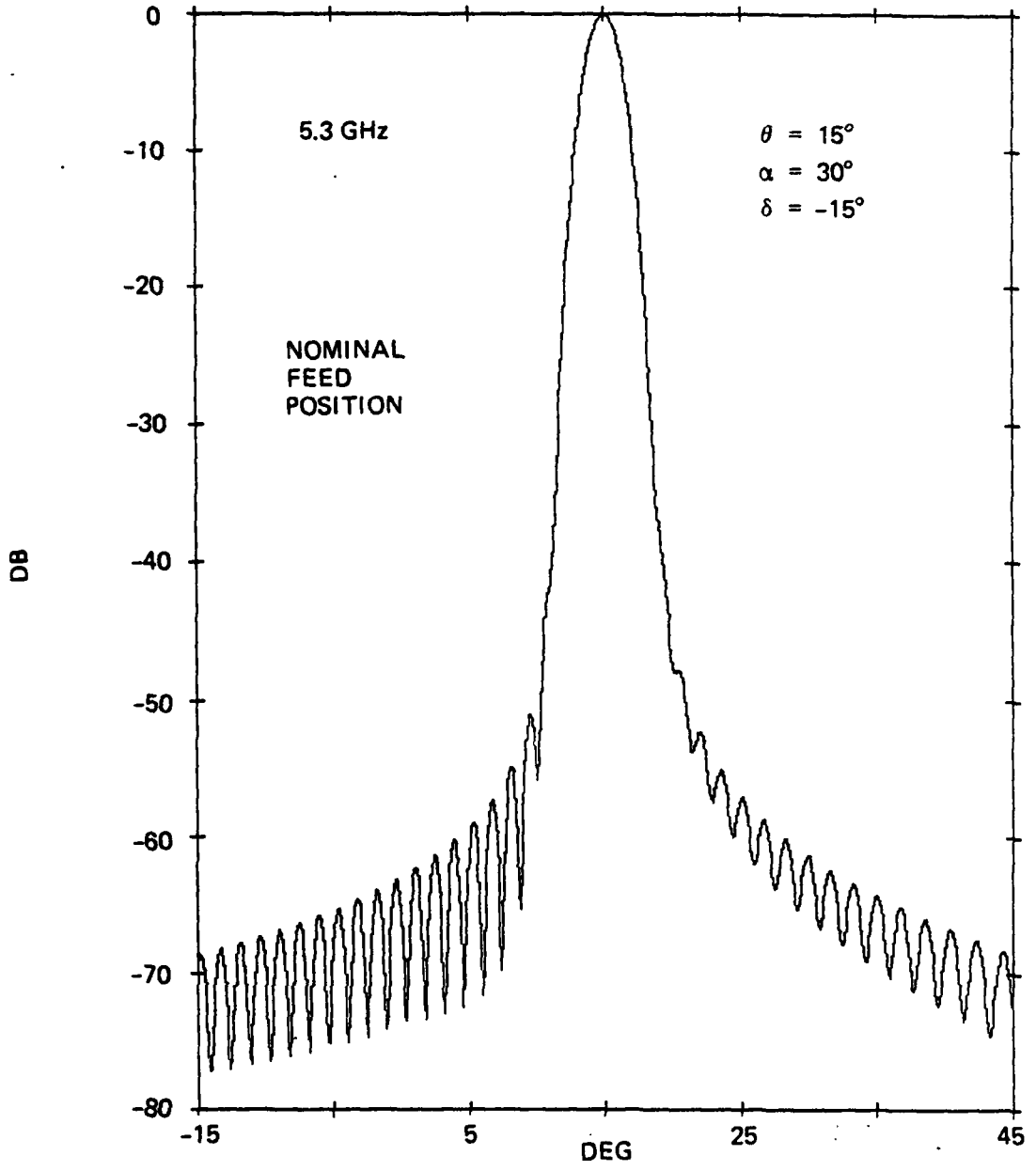

Figure 5-11. Azimuth Pattern of Antenna with Nominal Feed Position for $\alpha = 30^{\circ}$ and $\theta = 15^{\circ}$

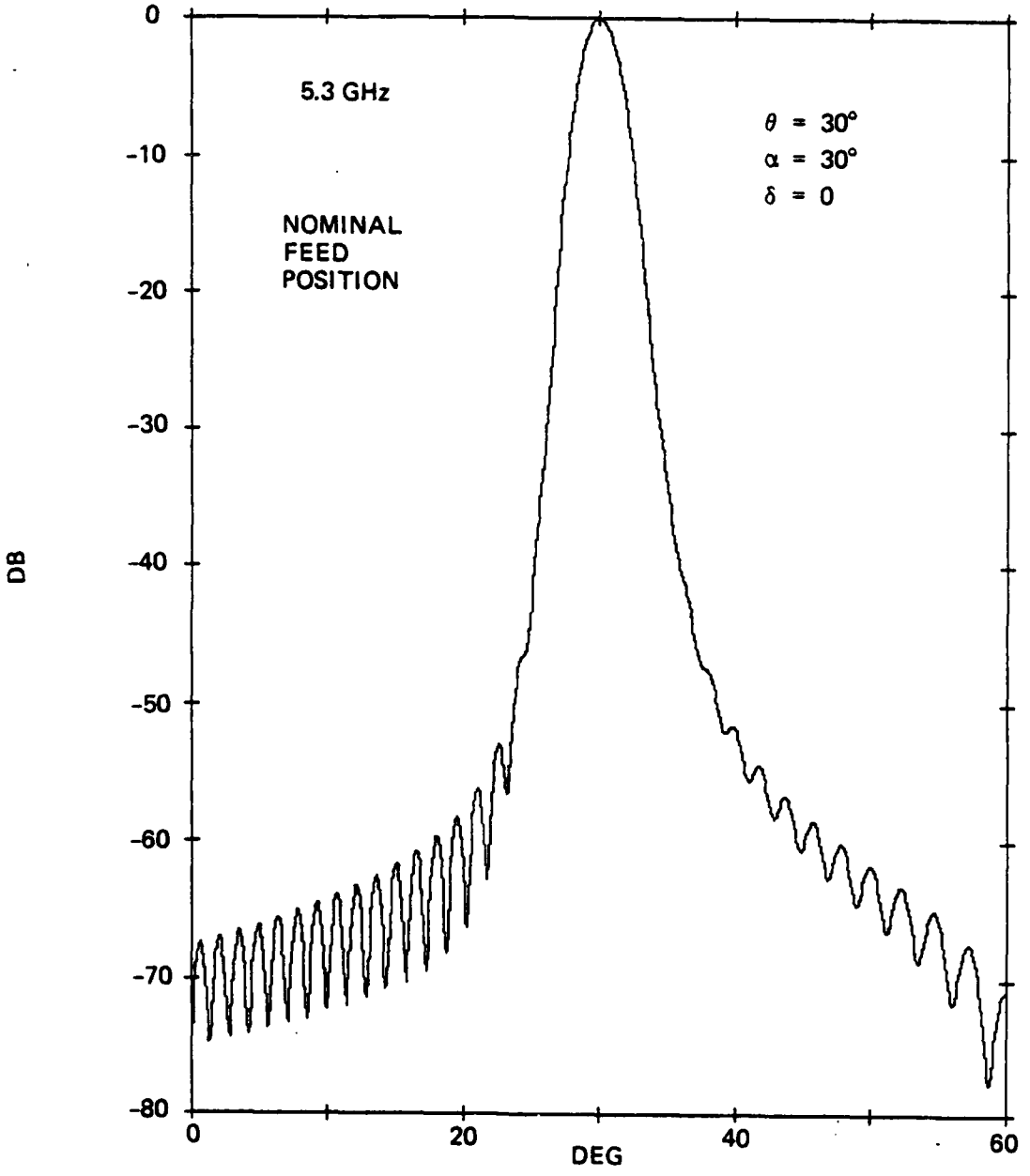

Figure 5-12. Azimuth Pattern of Antenna with Nominal Feed Position for $\alpha = 30^{\circ}$ and $\theta = 30^{\circ}$

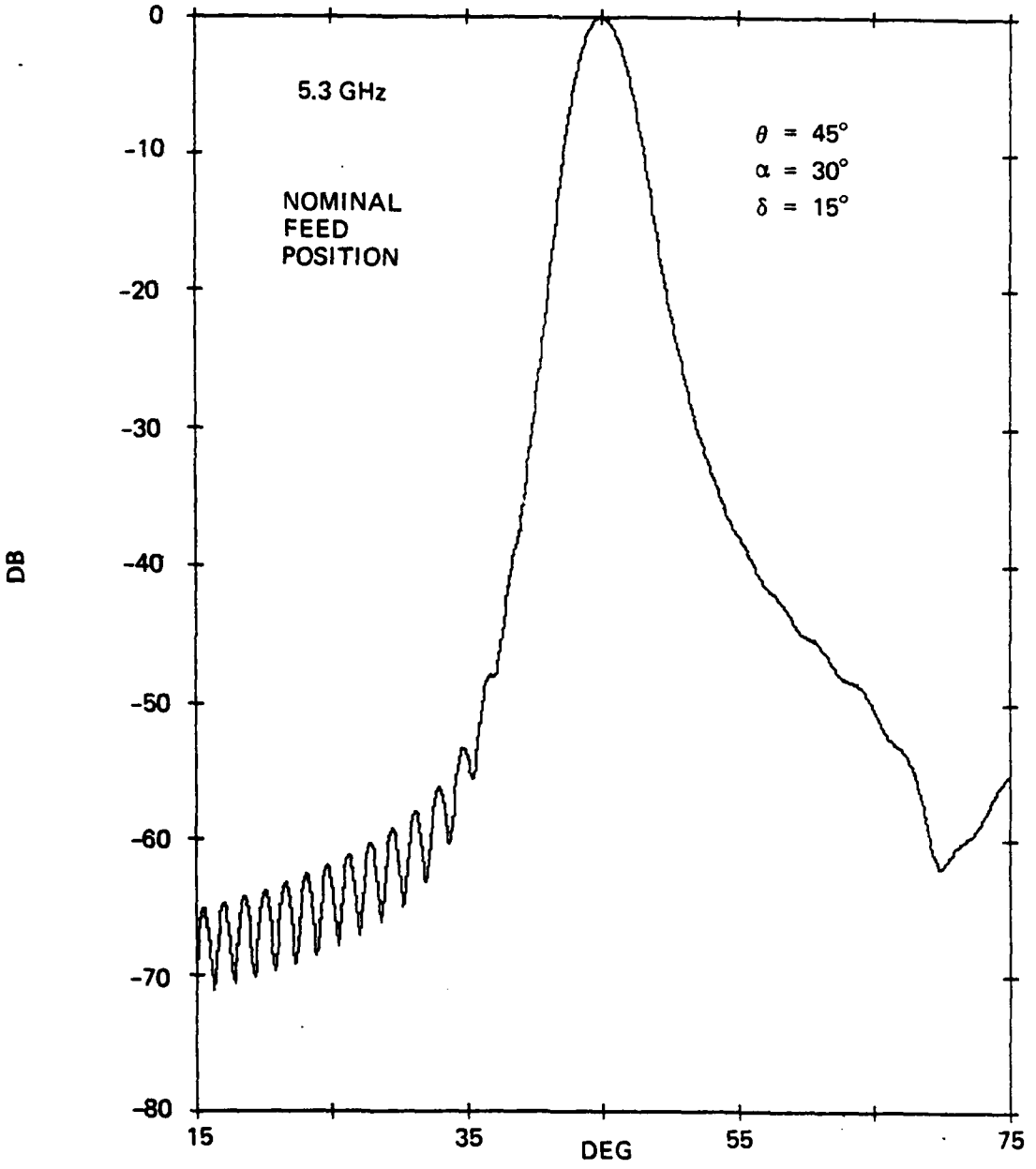

Figure 5-13. Azimuth Pattern of Antenna with Nominal Feed Position for $\alpha = 30^{\circ}$ and $\theta = 45^{\circ}$

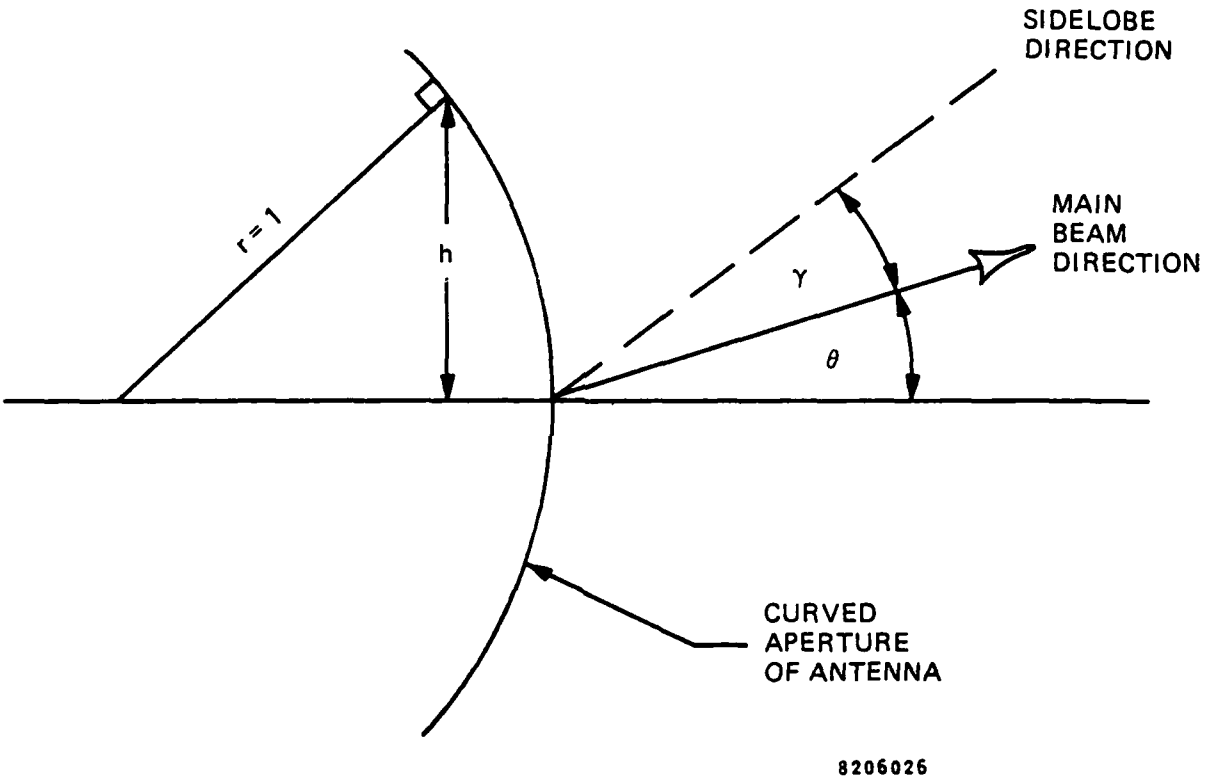

Figure 5-14. Coordinates for Radiation from Curved Antenna Aperture

coordinate normalized to the radius of curvature is h and the radius of curvature of the aperture is r. For the sidelobe direction (γ) the phase error (ϕ) across the aperture when $\theta = 0$ is:

$$\frac{\phi \lambda}{2 \pi r} = h \sin\gamma - \left[\sqrt{1 - h^2} - 1\right] \sin^2 \frac{\gamma}{2} \qquad (11)$$

The first term is linear in h, the same as with a straight aperture. The second term is approximately quadratic in h but is very small for small γ. Therefore only a very small effect on the sidelobes should occur because of the curved aperture for this $\theta = 0$ case.

When θ is not zero the phase error (ϕ) for the sidelobe direction (γ) is:

$$\frac{\phi\lambda}{2 \pi r} = h \left(\sin\gamma \cos\theta + \sin^2 \frac{\gamma}{2} \sin\theta \right) + \left[\sqrt{1 - h^2} - 1\right] \left(\sin\gamma \sin\theta - \sin^2 \frac{\gamma}{2} \cos\theta \right) \qquad (12)$$

Here the first two terms are linear in h, and the fourth term is very small for small γ. However the third term, which is approximately quadratic in h, is not very small when θ is substantial. Thus, in the sidelobe direction there can be a substantial phase-error term that is approximately quadratic across the aperture, although the aperture is perfectly collimated in the main-beam direction. This quadratic phase error is not constant, but is proportional to sin γ as well as to sin θ.

For $h = 0.5$, $\theta = 30^\circ$, and $\gamma = 10^\circ$, the quadratic phase error would be about 150° for a 40 wavelength aperture. Such a large phase error, increasing with γ and θ, can account for the effect on sidelobes that is shown in figures 5-12 and 5-13. Since the phase error varies with γ, it cannot be usefully compensated by simply refocusing the antenna.

At this point, the question arises: is there any simple method for improving the azimuth sidelobes of the antenna when the beam is scanned far off the axis of the curved aperture? Of course, a feed with a much larger horizontal dimension could be designed to cancel each individual sidelobe in one particular antenna pattern, but a feed size even larger than the feed shown in figure 5-3 would be unattractive. Furthermore, different feed designs for different coarse-steering angles would probably be needed. A simpler approach would be preferable.

Referring to figure 4-10 in section 4.2, it is recalled that when the rays emanating from the curved aperture are projected onto a fictitious planar aperture, there appears to be an inverse tapering effect. Furthermore, when the beam is scanned off the axis of the antenna, the tapering becomes unsymmetrical. This suggests that a lateral distortion of the aperture illumination may be involved in the sidelobe deterioration when the beam is scanned off the antenna axis.

Another viewpoint leads to a similar conclusion, as indicated in figure 5-15. Suppose that a straight array radiating a low-sidelobe pattern is scanned off axis. Suppose further that a curved array is located just in front of the straight array, where it samples the near field of the straight array. If the curved array now re-radiates in accordance with this sampled field, a low-sidelobe pattern should be obtained from the curved array.

The desired excitation amplitude of the curved array (the sampled field) will be similar to that of the straight array but will be laterally distorted, as can be seen by considering the rays emanating from the straight array. A more exact computation of the near field of the straight array shows that there should also be a phase distortion involving linear, quadratic, and higher-order components. The amplitude distortion is, however, more obvious and more substantial.

Pattern Improvement by Feed Positioning. A simple way to approximate this desired lateral distortion of the excitation amplitude on the lens aperture is to tilt the feed. The direction of feed tilt should be in the direction of beam scan, as indicated in figure 5-16. The quadratic component of the desired phase distortion can also be approximated by refocusing (moving) the feed slightly toward the lens.

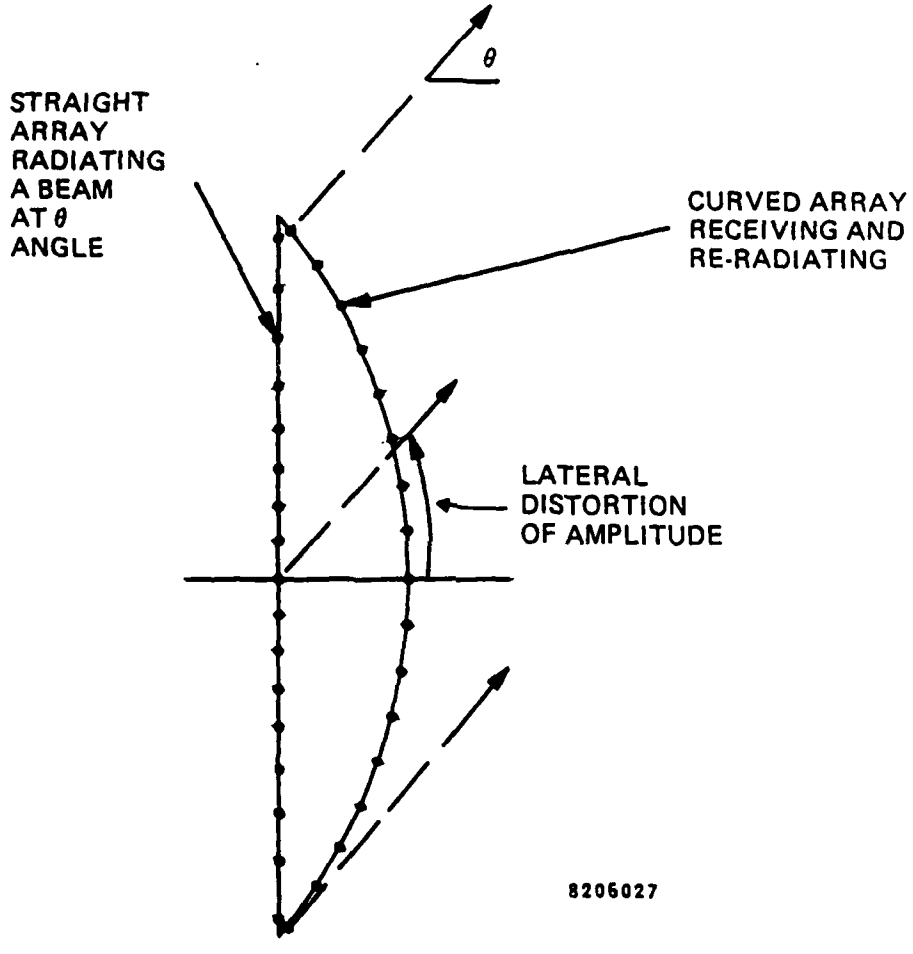

Figure 5-15. Viewpoint Leading to Ideal Patterns from Curved Array

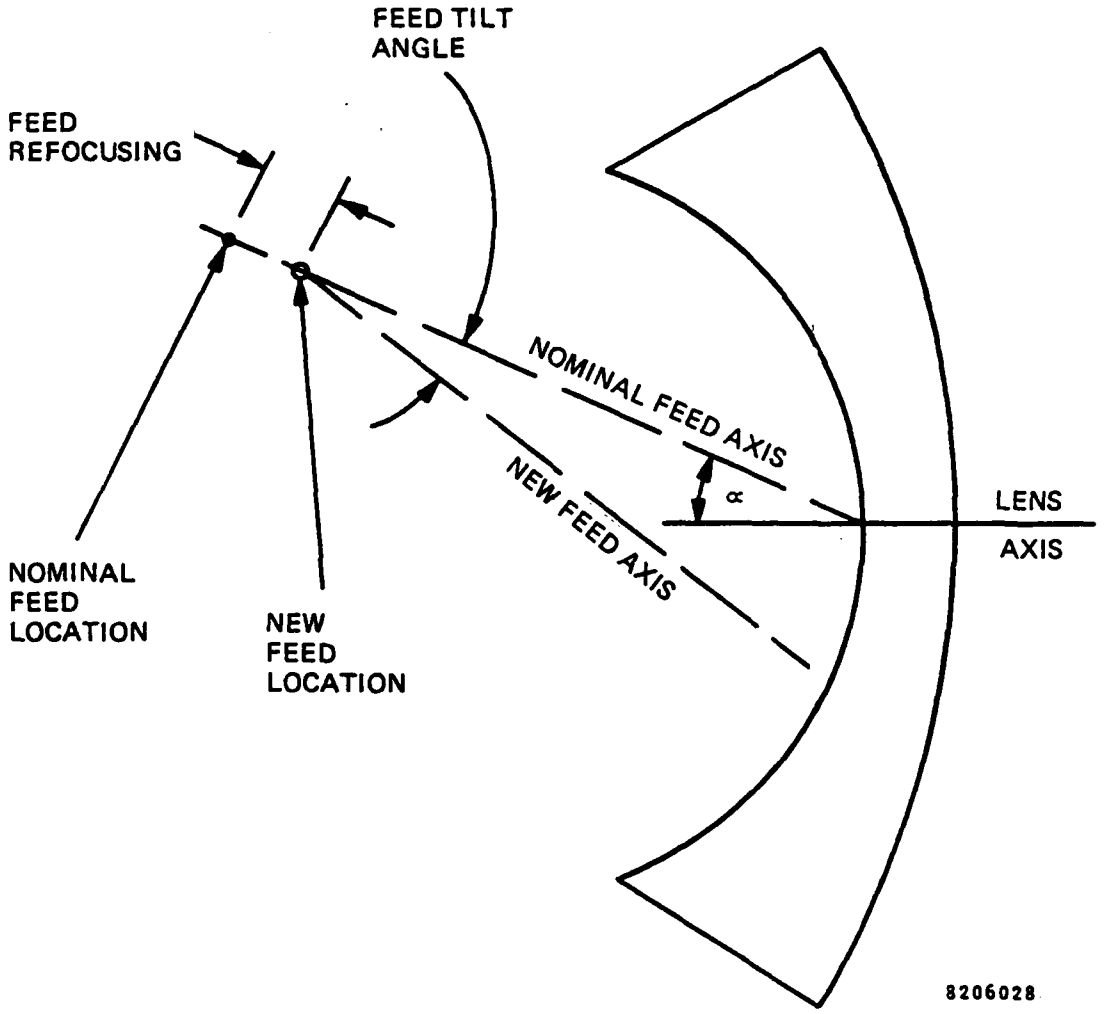

Figure 5-16. New Position for Off-Axis Feed

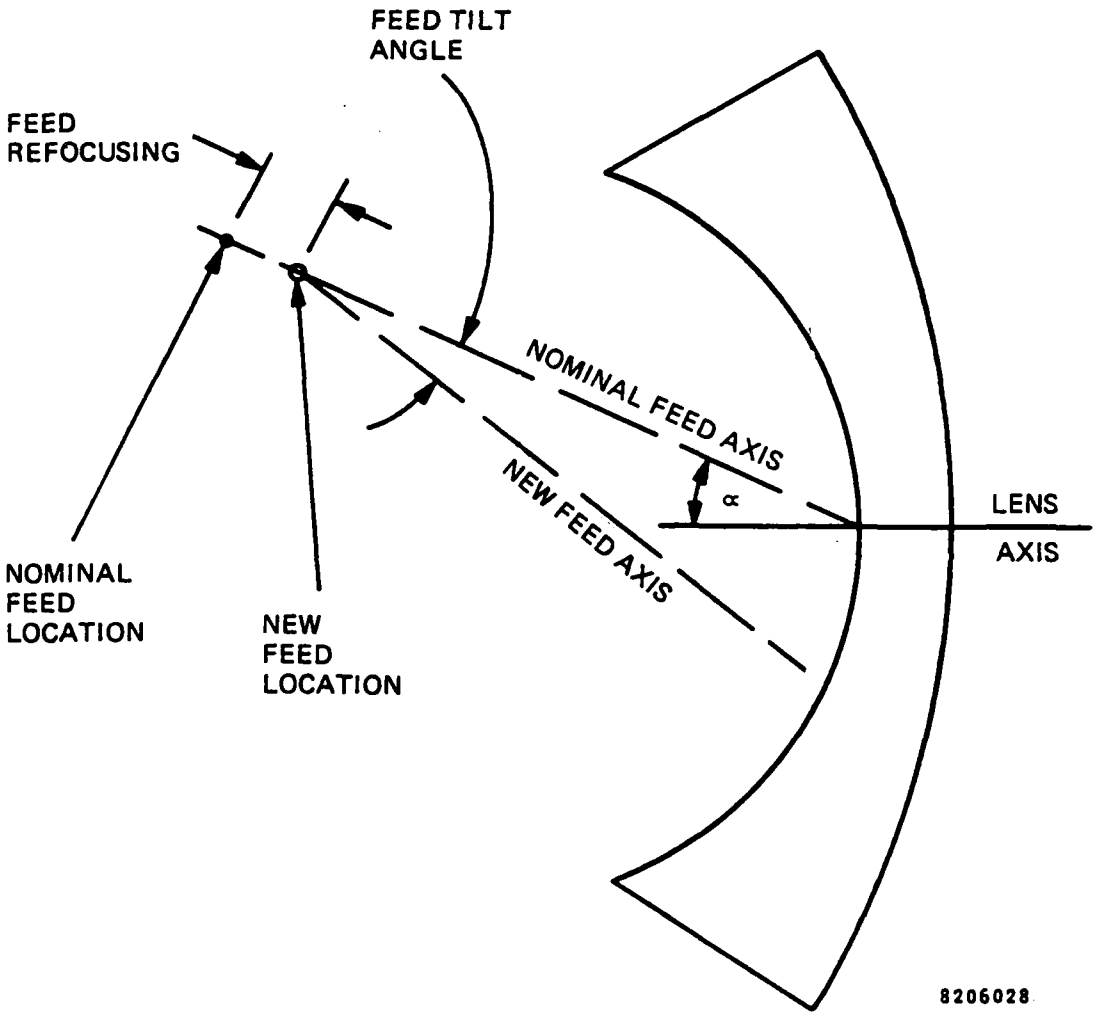

Figure 5-16. New Position for Off-Axis Feed

To determine the value of this approach, various feed tilts and refocusings were tried at midband until the best improved azimuth pattern was obtained for a 30^{o} coarse-steering angle plus a 15^{o} fine-steering angle. (The best tilt angle and refocusing distance found by this process were 5^{o} toward the scan direction and 0.8 wavelengths toward the lens, respectively). Then the fine steering was changed to 0^{o} and to -15^{o} to see whether the azimuth patterns remained at least as good as the original ones.

Figure 5-17 shows the resulting azimuth pattern for $\alpha = 30^{o}$ and $\delta = -15^{o}$, yielding $\theta = 15^{o}$. Comparison of this pattern with the original given in figure 5-11 shows that the optimization for $\theta = 45^{o}$ did not seriously degrade the $\theta = 15^{o}$ pattern, and perhaps improved it a little.

Figure 5-18 shows the azimuth pattern for $\alpha = 30^{o}$ and $\delta = 0$, yielding $\theta = 30^{o}$. Comparison of this pattern with the original given in figure 5-12 again shows that the optimization for $\theta = 45^{o}$ did not seriously degrade the $\theta = 30^{o}$ pattern, and, on balance, improved it somewhat.

Figure 5-19 shows the azimuth pattern for $\alpha = 30^{o}$ and $\delta = 15^{o}$, yielding $\theta = 45^{o}$. This is the case for which the optimization of feed tilting and refocusing was performed. Comparison of this pattern with the original one given in figure 5-13 shows a significant improvement.

To summarize the above results, a combination of tilting and refocusing the feed gives a significant improvement in the most distorted azimuth pattern (45^{o}) without seriously degrading the less distorted patterns (15^{o}, 30^{o}). While the resulting patterns are clearly not ideal they appear to be the best that can be obtained by simple means. We propose to use this approach for the lens antenna to be developed.

The effects of operation at the ends of the 5.0 to 5.6 GHz frequency band are shown in figures 5-20 through 5-25 for $\theta = 15^{o}$, 30^{o}, 45^{o} for the antenna with a tilted/refocused feed. In general, the sidelobes are higher at 5.0 GHz and are lower at 5.6 GHz. This is probably the result of the normal variation of feed beamwidth with frequency, combined with the increased illumination at one side of the lens aperture caused by the feed tilt.

The computed wide-angle sidelobe response in azimuth at midband is shown for $\theta = 15^{o}$, 30^{o}, 45^{o} in figures 5-26 through 5-28. For the element pattern assumed (discussed previously) and for the 0.4 wavelength horizontal spacing

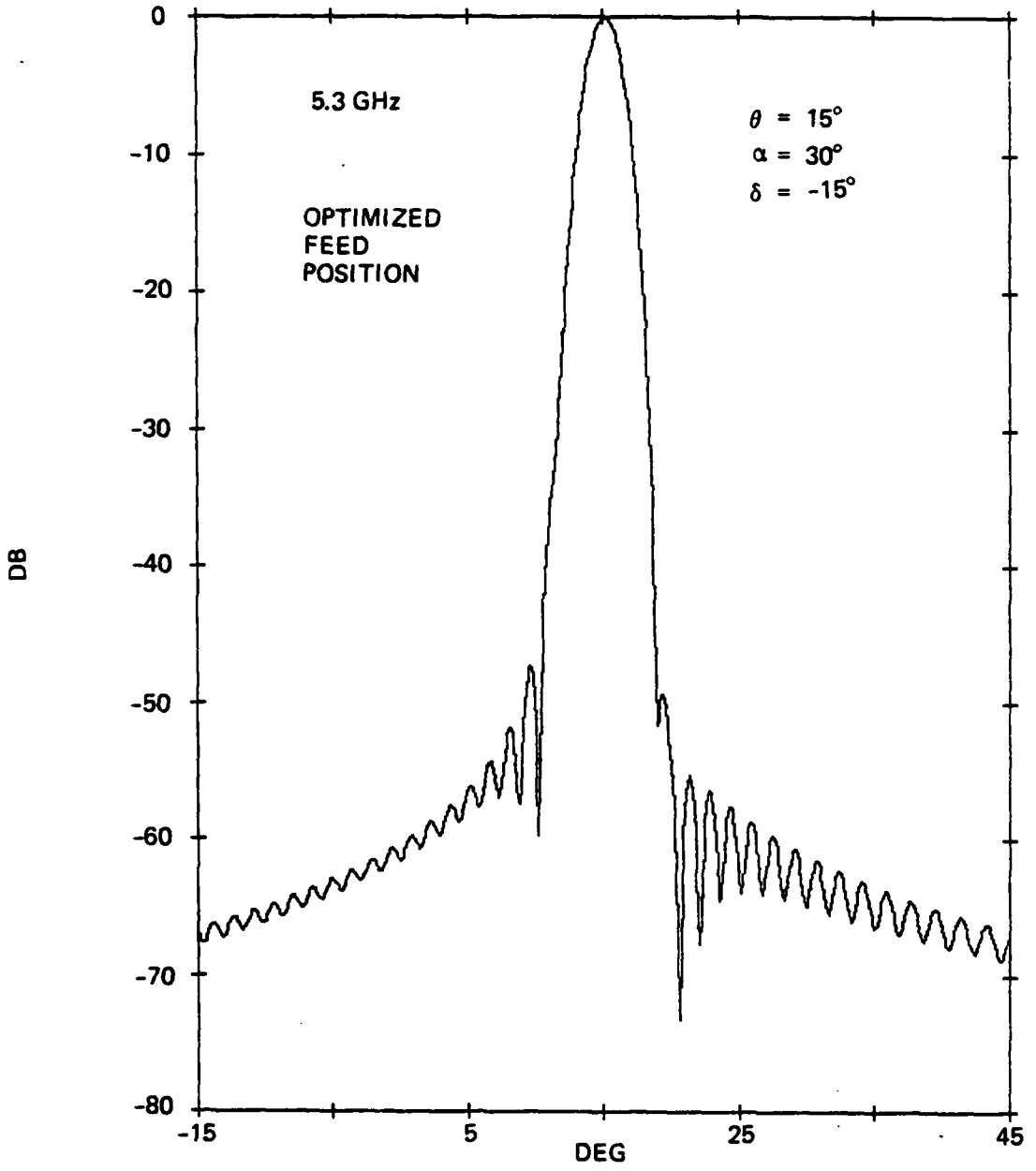

Figure 5-17. Azimuth Pattern of Antenna with Optimized Feed Position, $\theta = 15^{\circ}$

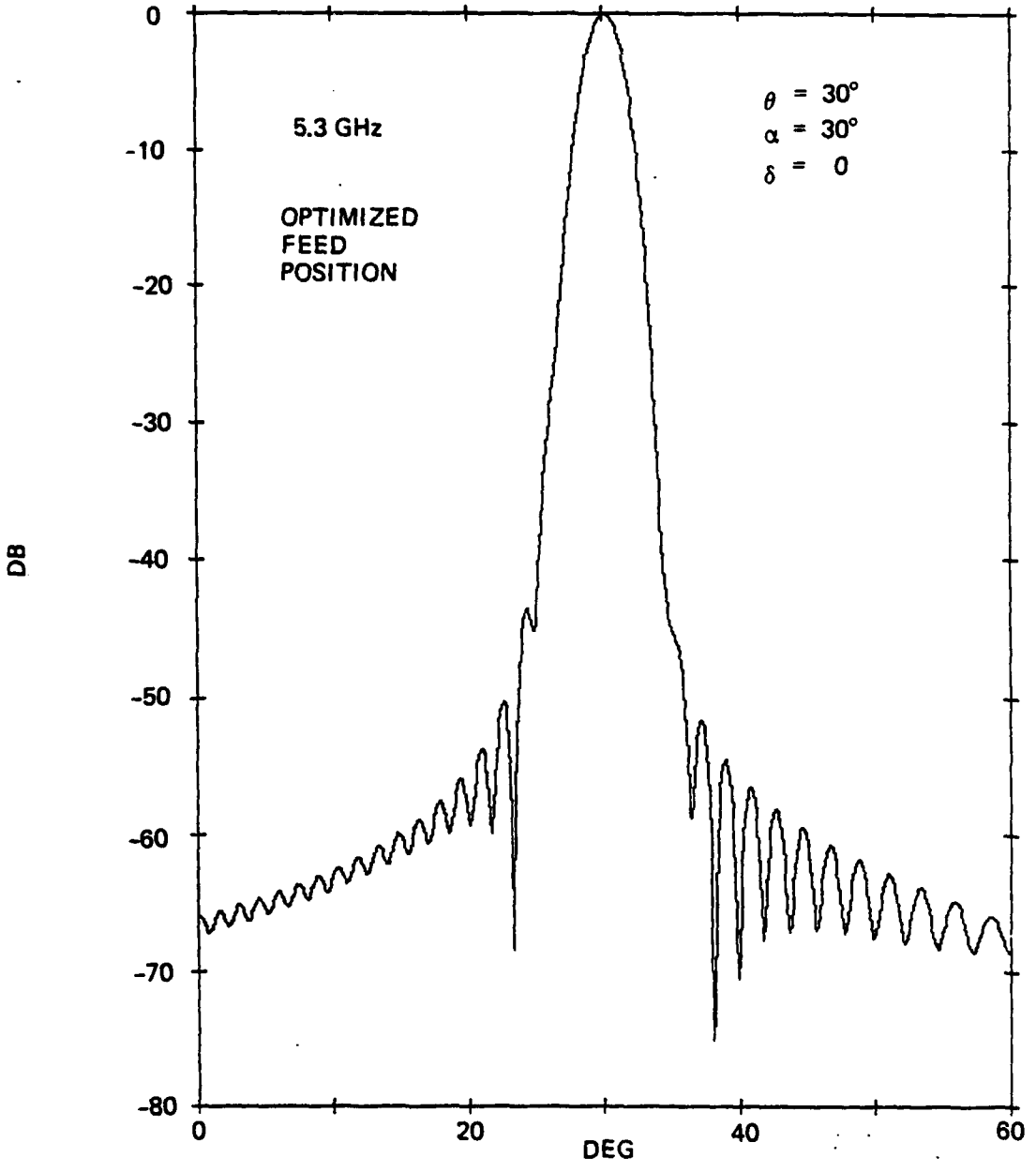

Figure 5-18. Azimuth Pattern of Antenna with Optimized Feed Position, $\theta = 30^{\circ}$

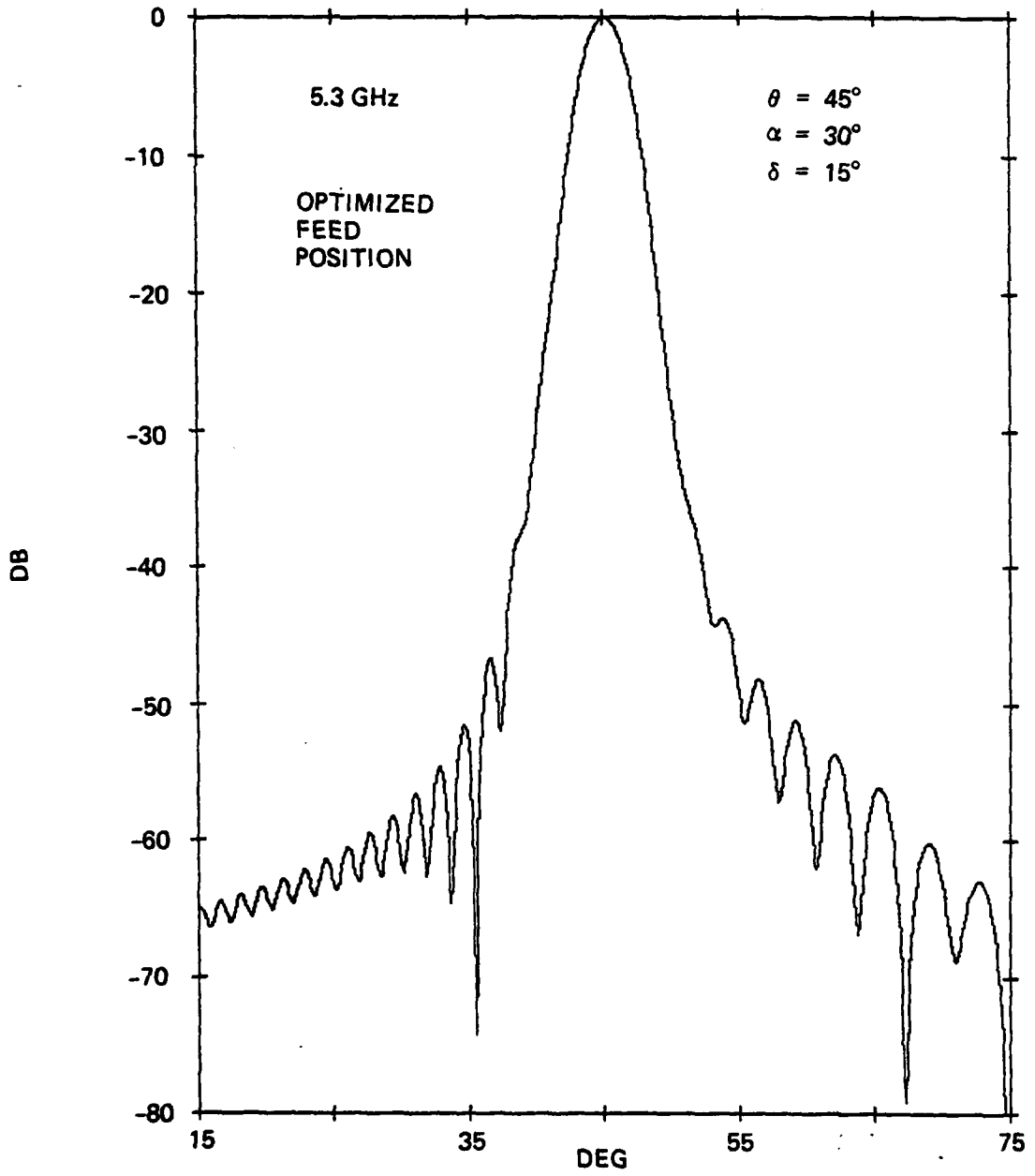

Figure 5-19. Azimuth Pattern of Antenna with Optimized Feed Position, $\theta = 45^{\circ}$

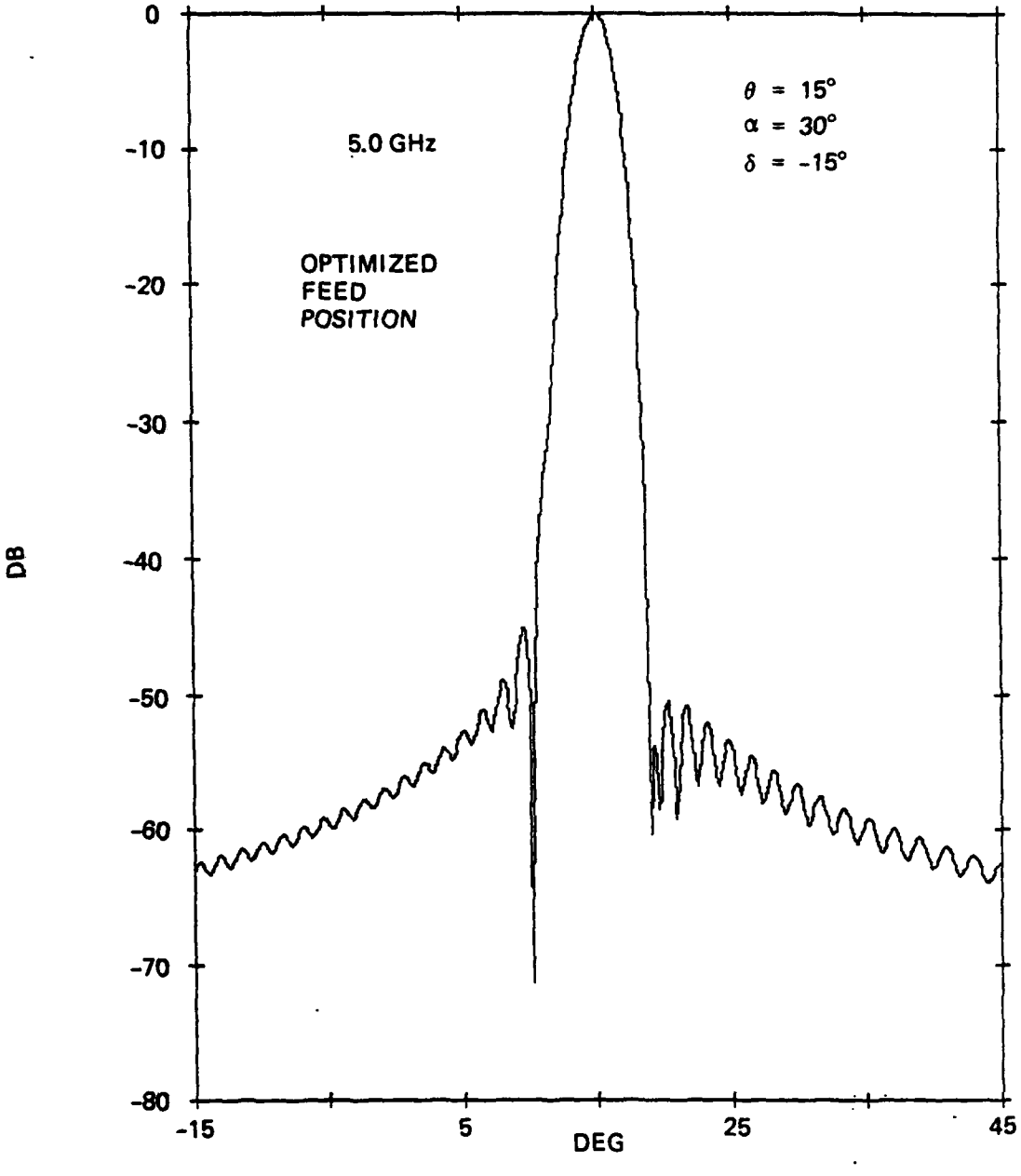

Figure 5-20. Azimuth Pattern of Antenna at 5.0 GHz with Optimized Feed Position, $\theta = 15^{\circ}$

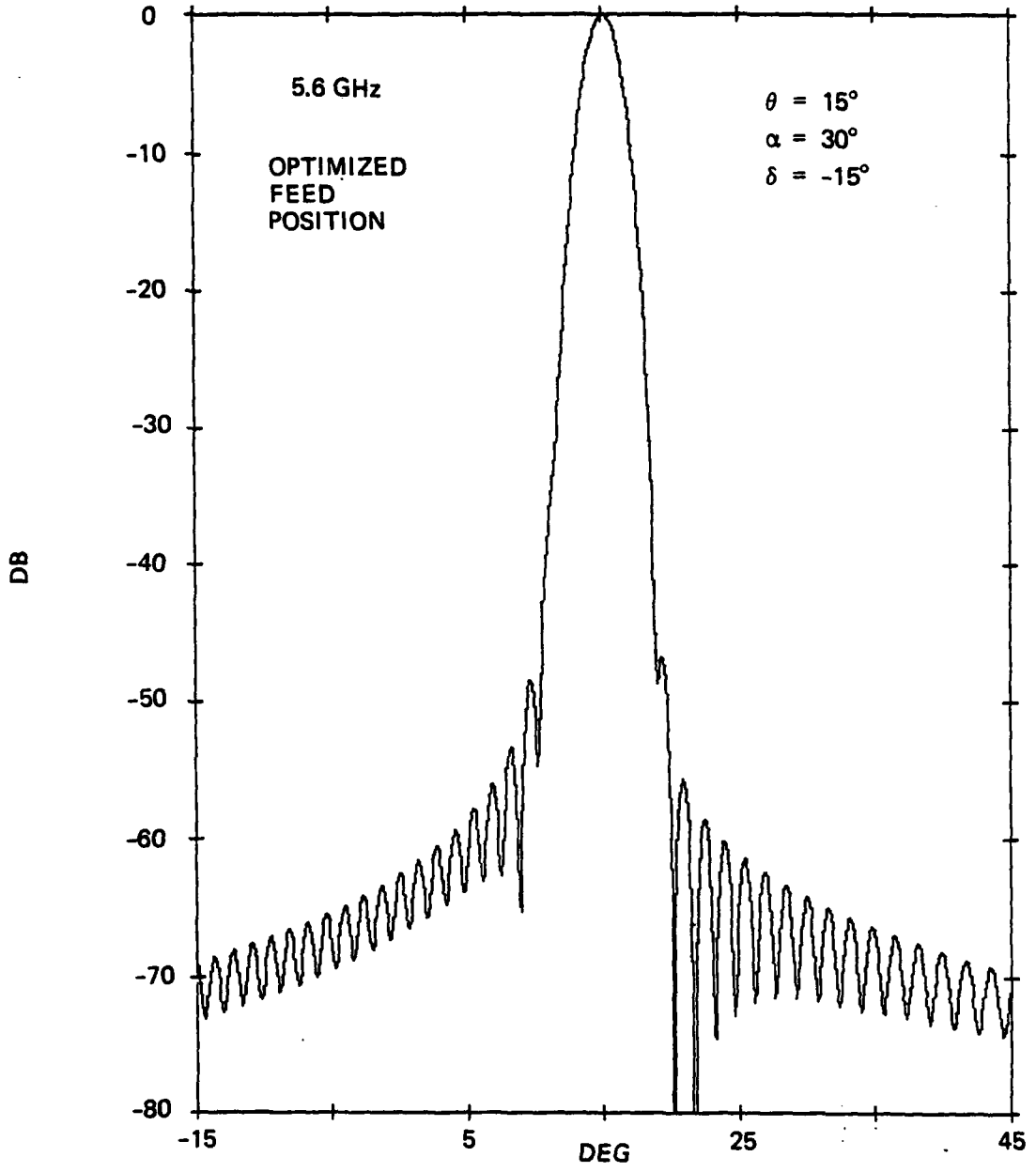

Figure 5-21. Azimuth Pattern of Antenna at 5.6 GHz with Optimized Feed Position, $\theta = 15^{o}$

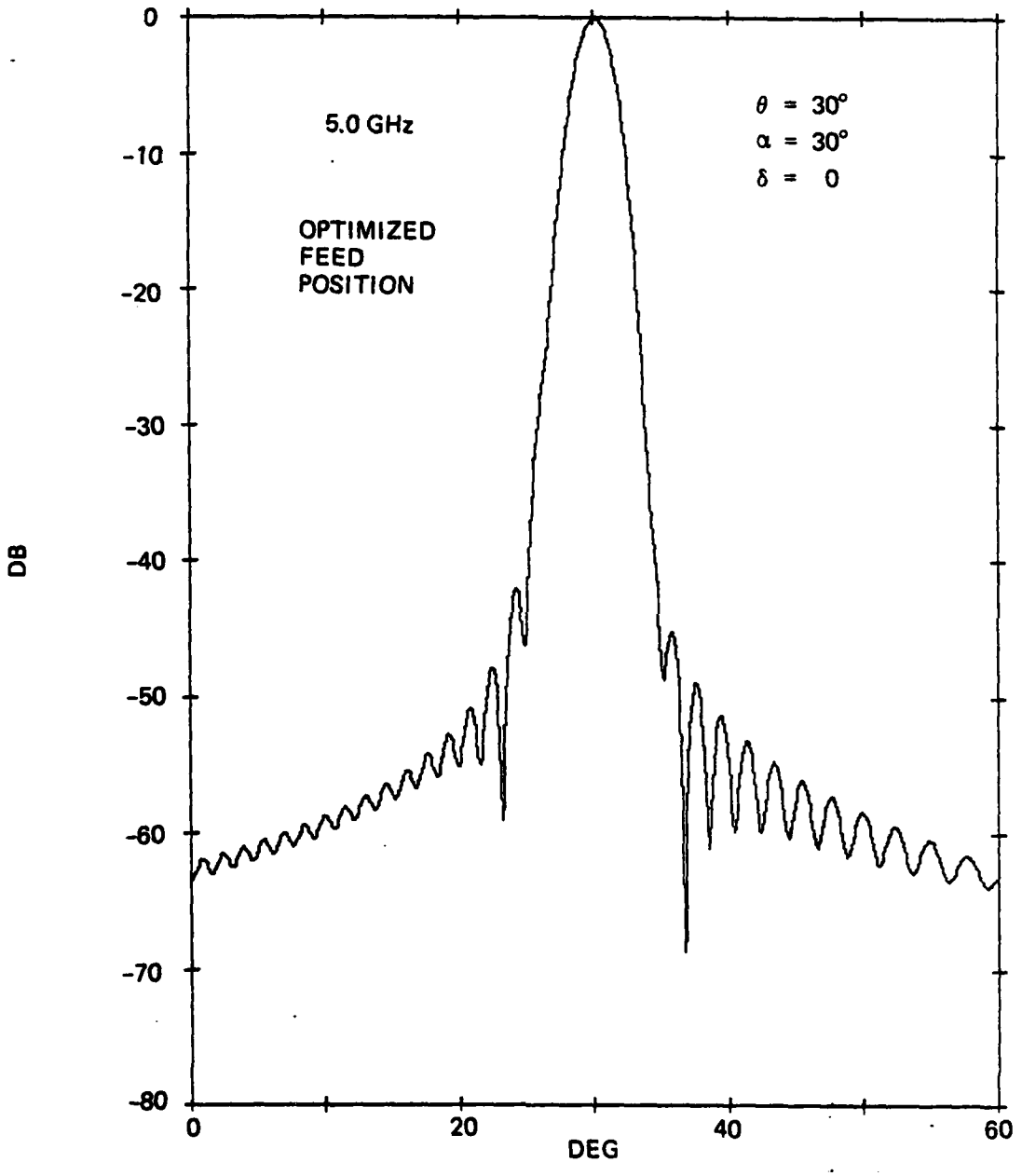

Figure 5-22. Azimuth Pattern of Antenna at 5.0 GHz with Optimized Feed Position, $\theta = 30^{o}$

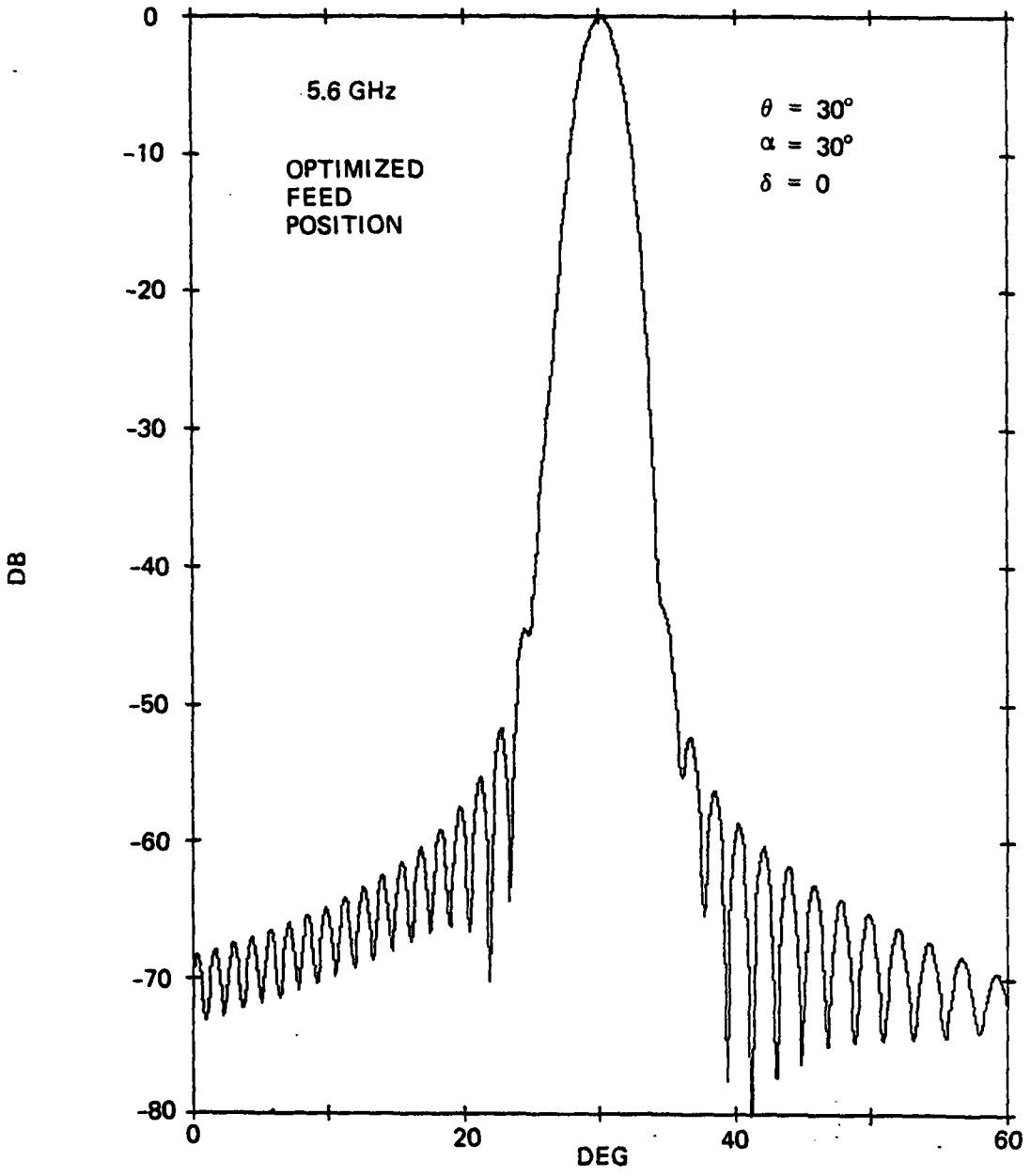

Figure 5-23. Azimuth Pattern of Antenna at 5.6 GHz with Optimized Feed Position, $\theta = 30^{\circ}$

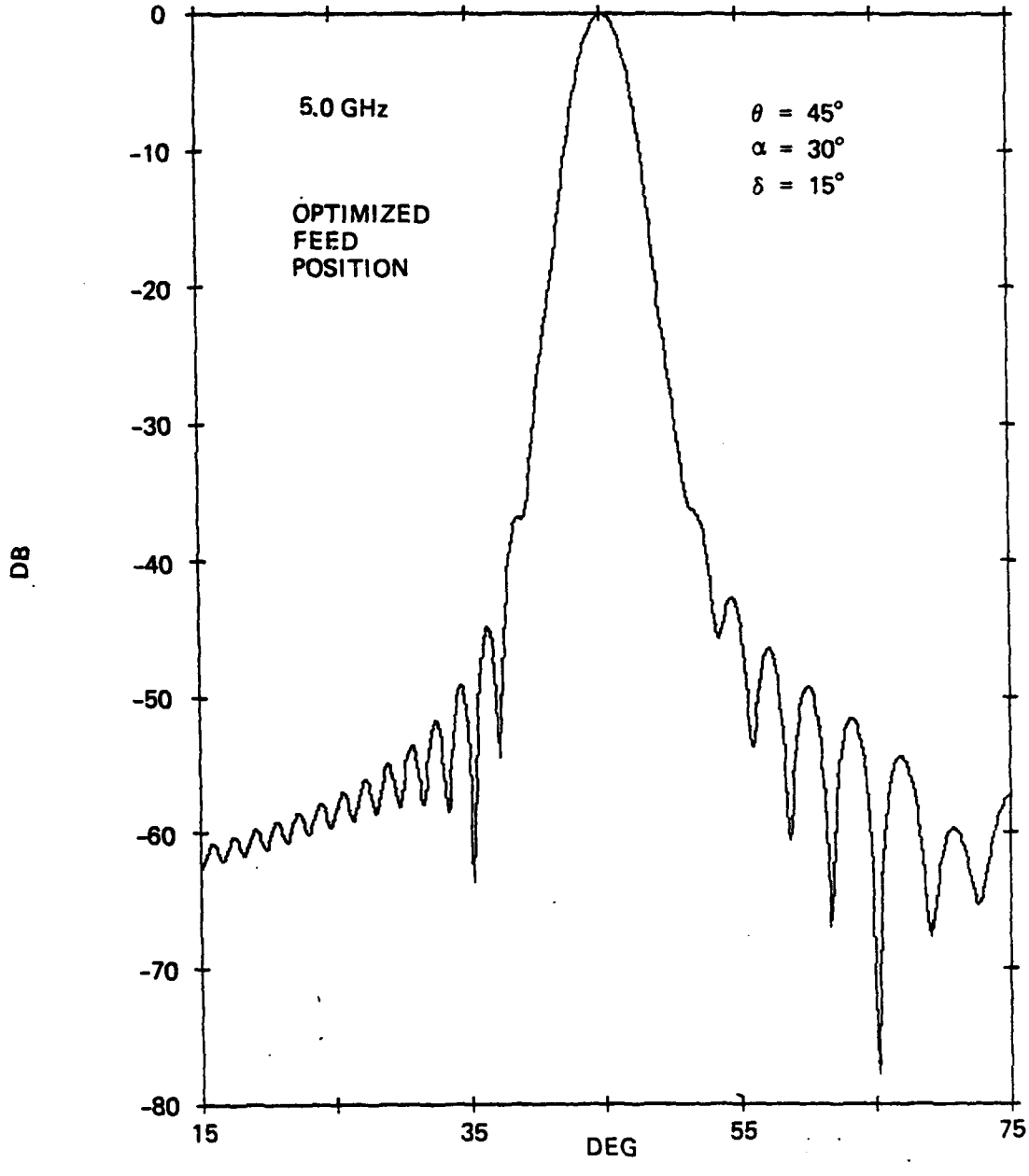

Figure 5-24. Azimuth Pattern of Antenna at 5.0 GHz with Optimized Feed Position, $\theta = 45^{o}$

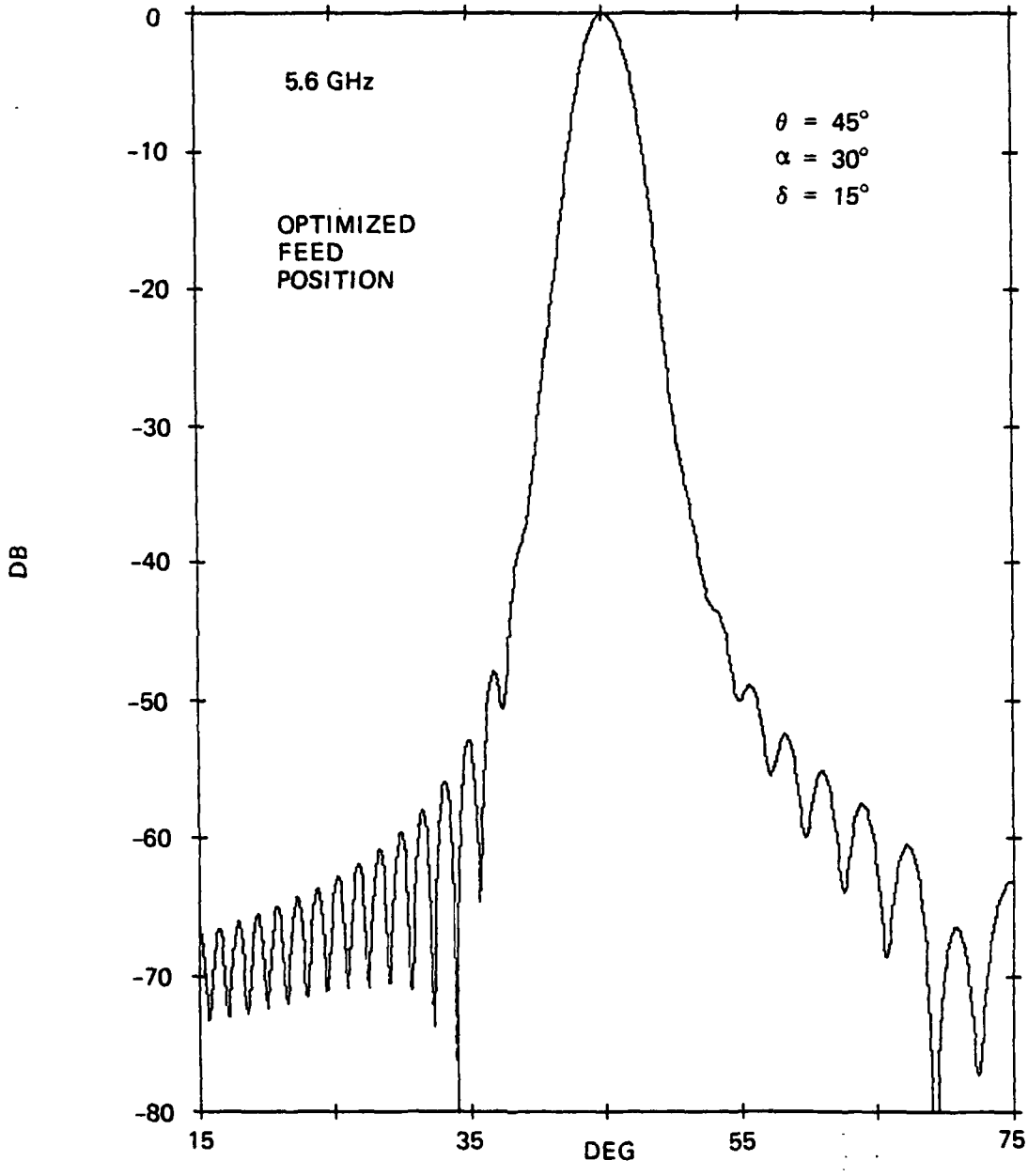

Figure 5-25. Azimuth Pattern of Antenna at 5.6 GHz with Optimized Feed Position, θ = 45°

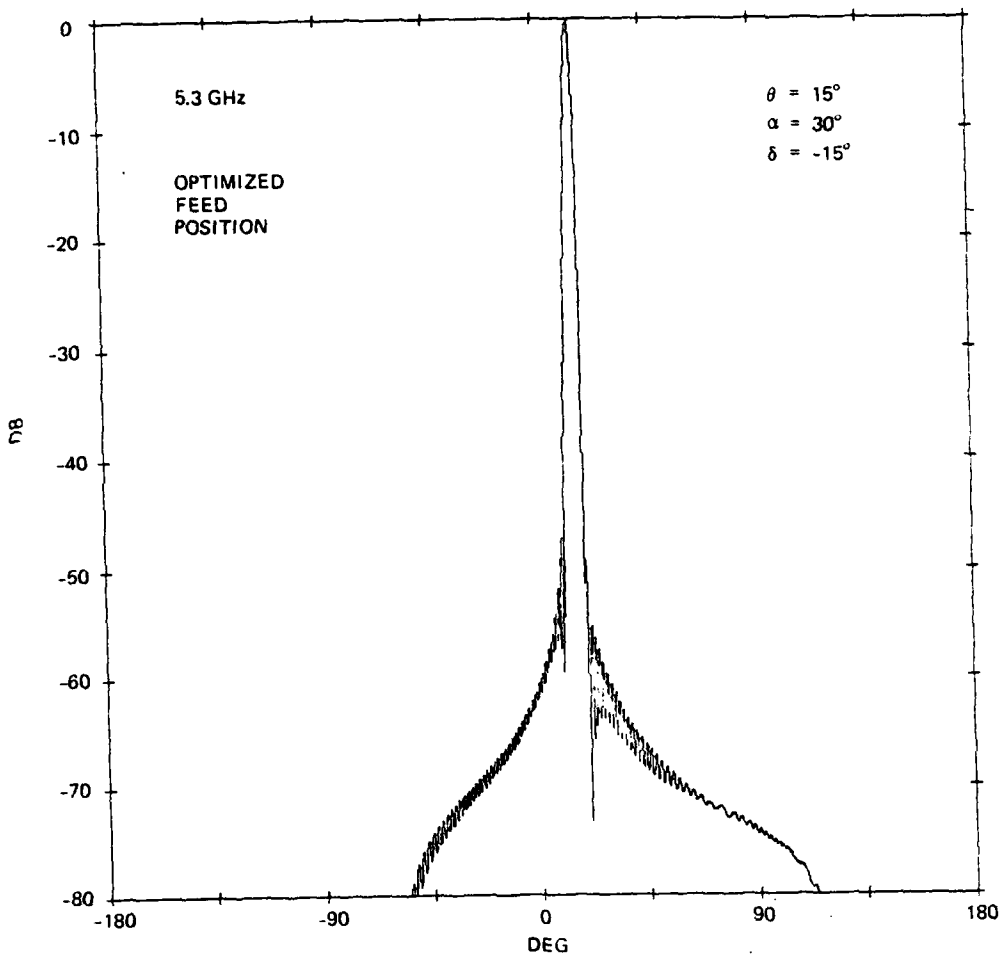

Figure 5-26. Wide-Angle Azimuth Pattern of Antenna at 5.3 GHz with Optimized Feed Position, $\theta = 15^{o}$

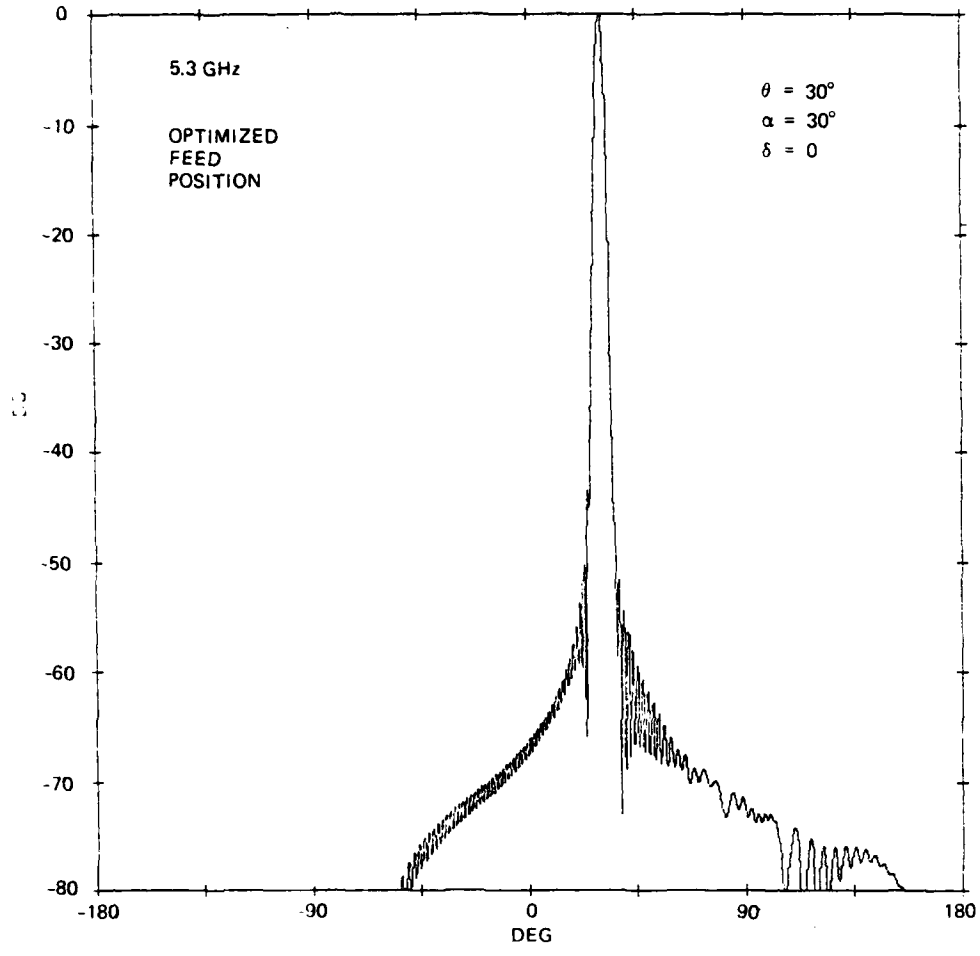

Figure 5-27. Wide-Angle Azimuth Pattern of Antenna at 5.3 GHz with Optimized Feed Position, $\theta = 30^{\circ}$

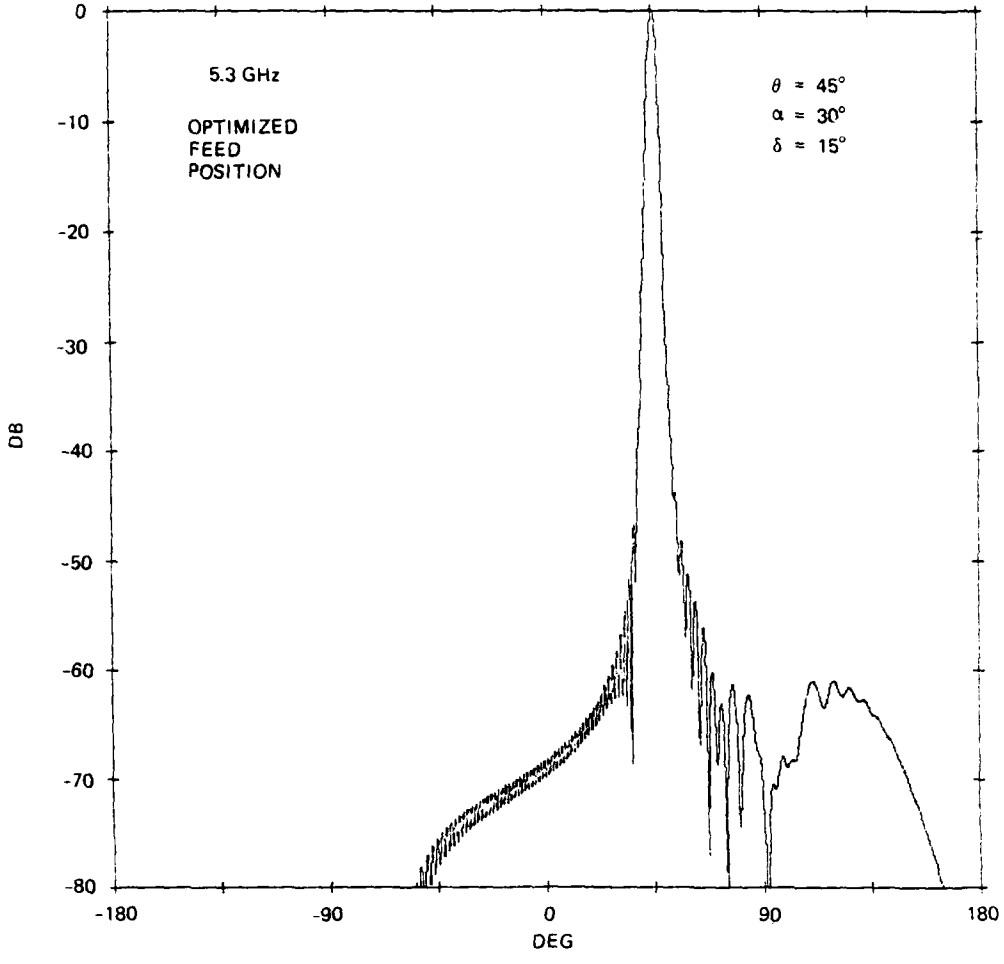

Figure 5-28. Wide-Angle Azimuth Pattern of Antenna at 5.3 GHz with Optimized Feed Position, $\theta = 45^{\circ}$

between elements that is chosen, the wide-angle sidelobe response appears to be satisfactory. Computed wide-angle patterns at 5.0 and 5.6 GHz yield similar results.

Pattern Improvement by Feed Difference Mode. Another way to approximate the desired lateral distortion of the illumination amplitude on the lens aperture is by the addition of a difference mode of excitation to the feed array. If this difference-mode component of excitation is in phase quadrature with the original excitation component at the feed array, then at the lens aperture it will have $0/180^{\circ}$ phase relative to the original illumination and will laterally distort the amplitude. This method differs from the feed-tilt method because it steers primarily the central part of the lens illumination, while the feed-tilt method steers the whole illumination. Figure 5-29 indicates the concept.

To explore the value of this approach, various sizes and amplitudes of the difference mode at the feed aperture have been combined with the original feed excitation, and antenna azimuth patterns have been computed for $\alpha = 30^{\circ}$. Feed tilt and refocusing are included as optimization variables. One favorable set of patterns is shown in figures 5-30, 31 and 32 for $\theta = 15^{\circ}$, 30° and 45°. Comparison of these patterns with the feed-repositioning-only patterns of figures 5-17, 18 and 19 indicates that a significant improvement is obtained at $\theta = 45^{\circ}$, but some degradation is obtained at $\theta = 15^{\circ}$. Overall, it appears that the difference-mode method provides better results.

As indicated in figure 5-29, the better antenna patterns are obtained when the size of the difference-mode feed excitation is larger than the original size. Therefore, the feed size would have to be increased. Furthermore, this feed for $\alpha = 30^{\circ}$ would have an excitation different from that of the feed for $\alpha = 0$ (which should be the original feed), so that two different feed designs would be needed. Compared with the simple feed-repositioning approach discussed earlier, the moderate improvement of patterns obtained with the difference-mode approach is not considered to be worth the extra size and complexity that would be involved on this project. Therefore the feed-repositioning approach is selected rather than the difference-mode approach.

c. Summary of Line Feed/Azimuth Patterns.

For the on-axis beam, a line feed comprising an array of dipoles can provide a lens illumination yielding antenna

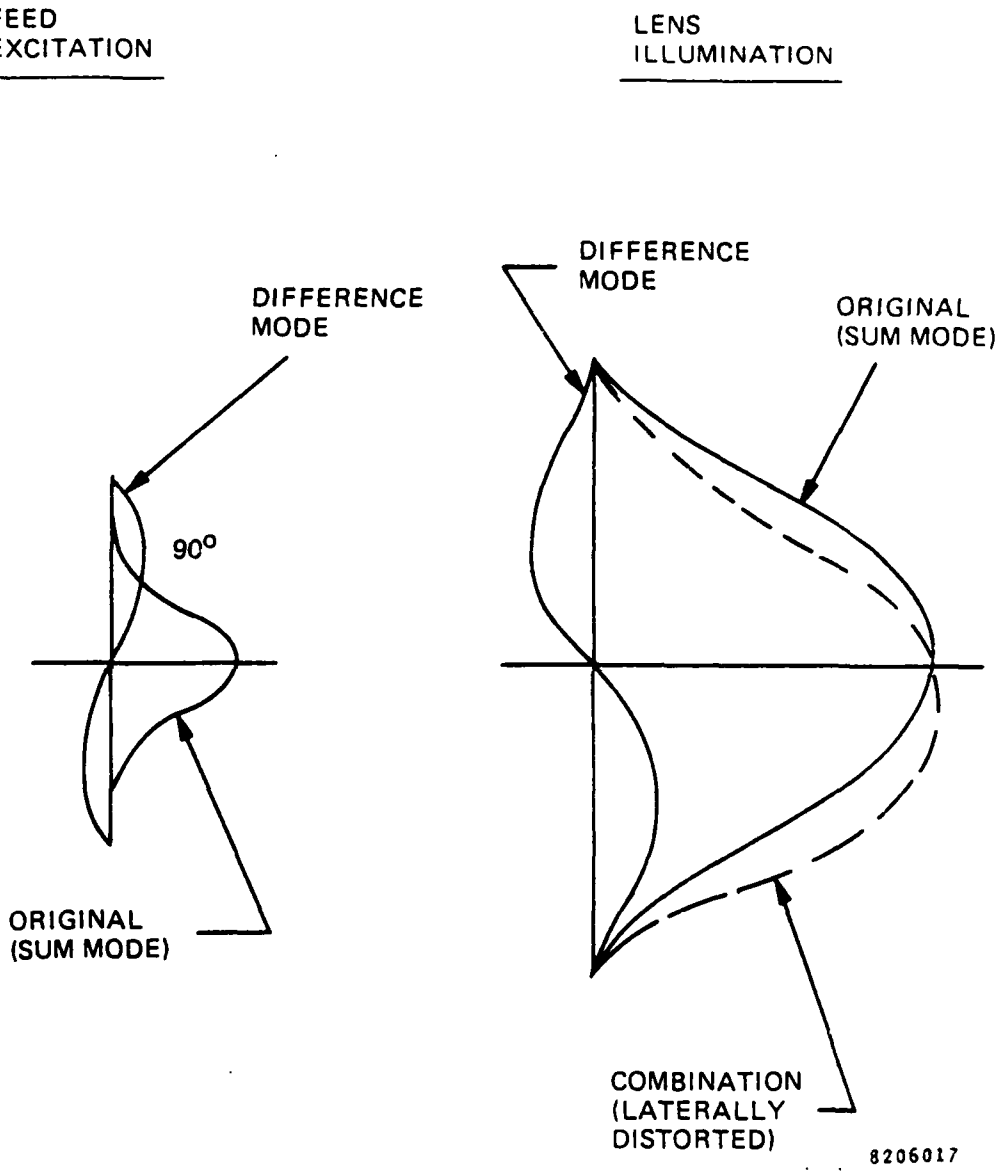

Figure 5-29. Difference Mode Added to Feed Excitation

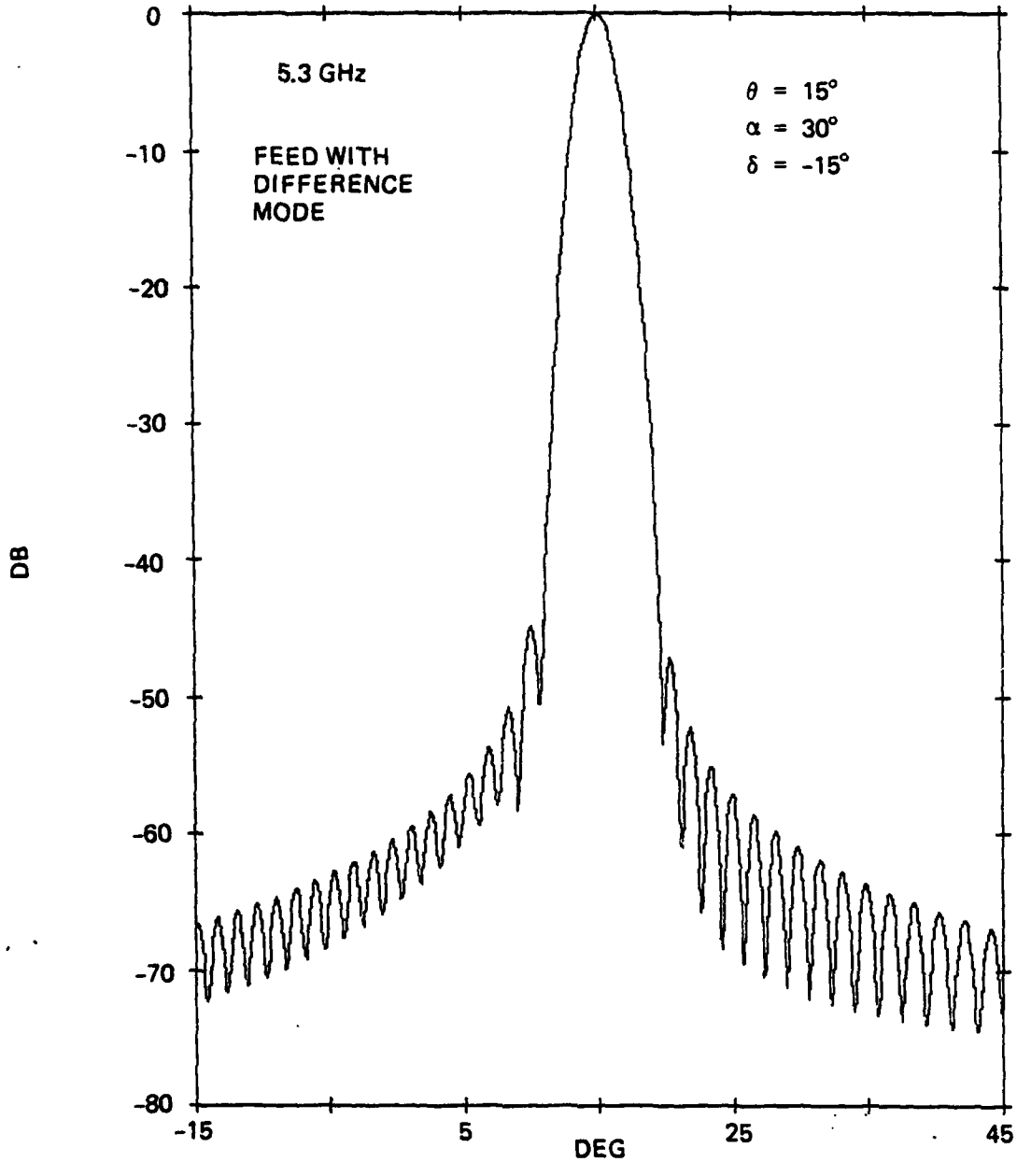

Figure 5-30. Azimuth Pattern of Antenna with Feed Difference Mode, $\theta = 15^{\circ}$

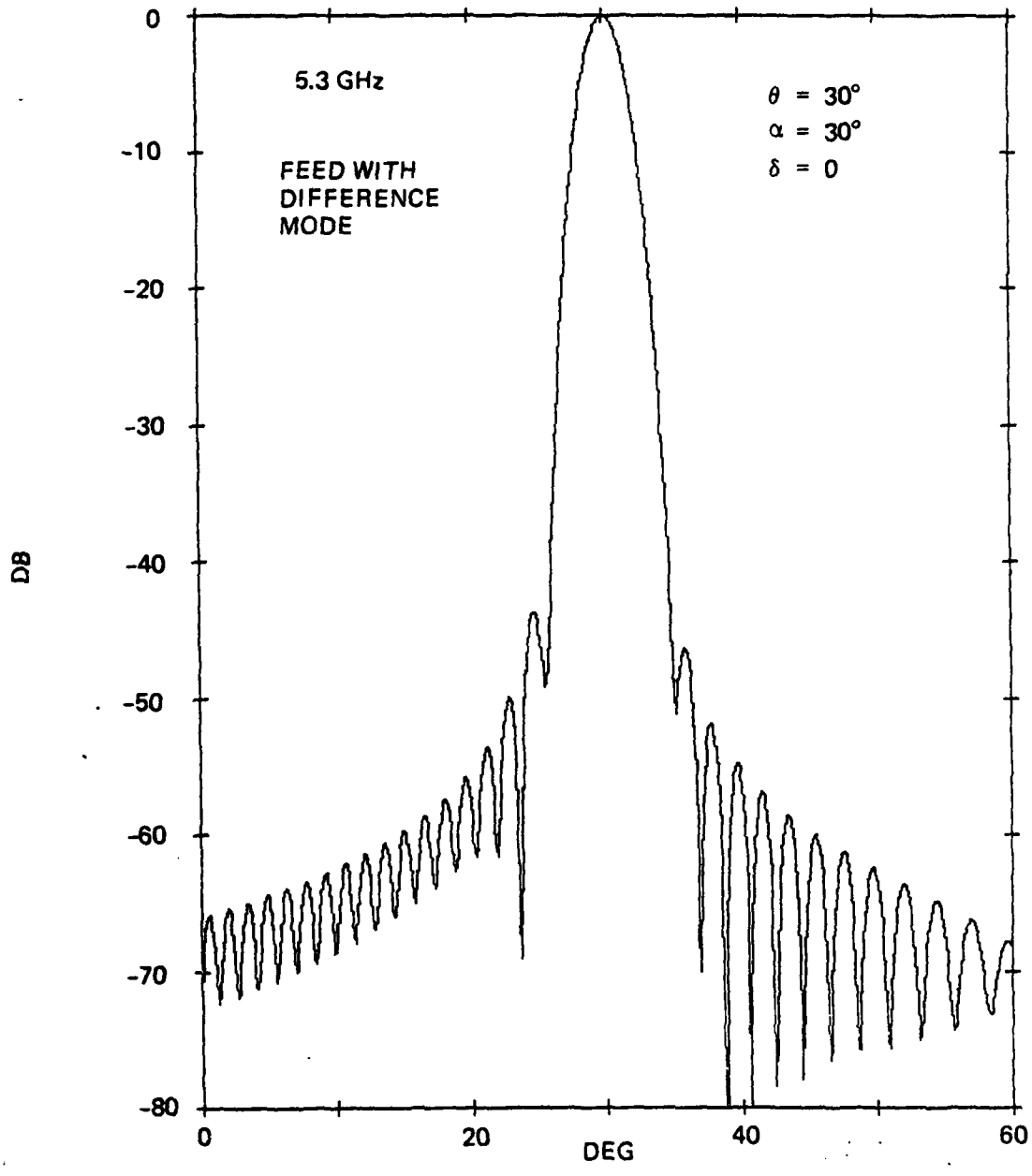

Figure 5-31. Azimuth Pattern of Antenna with Feed Difference Mode, $\theta = 30^{O}$

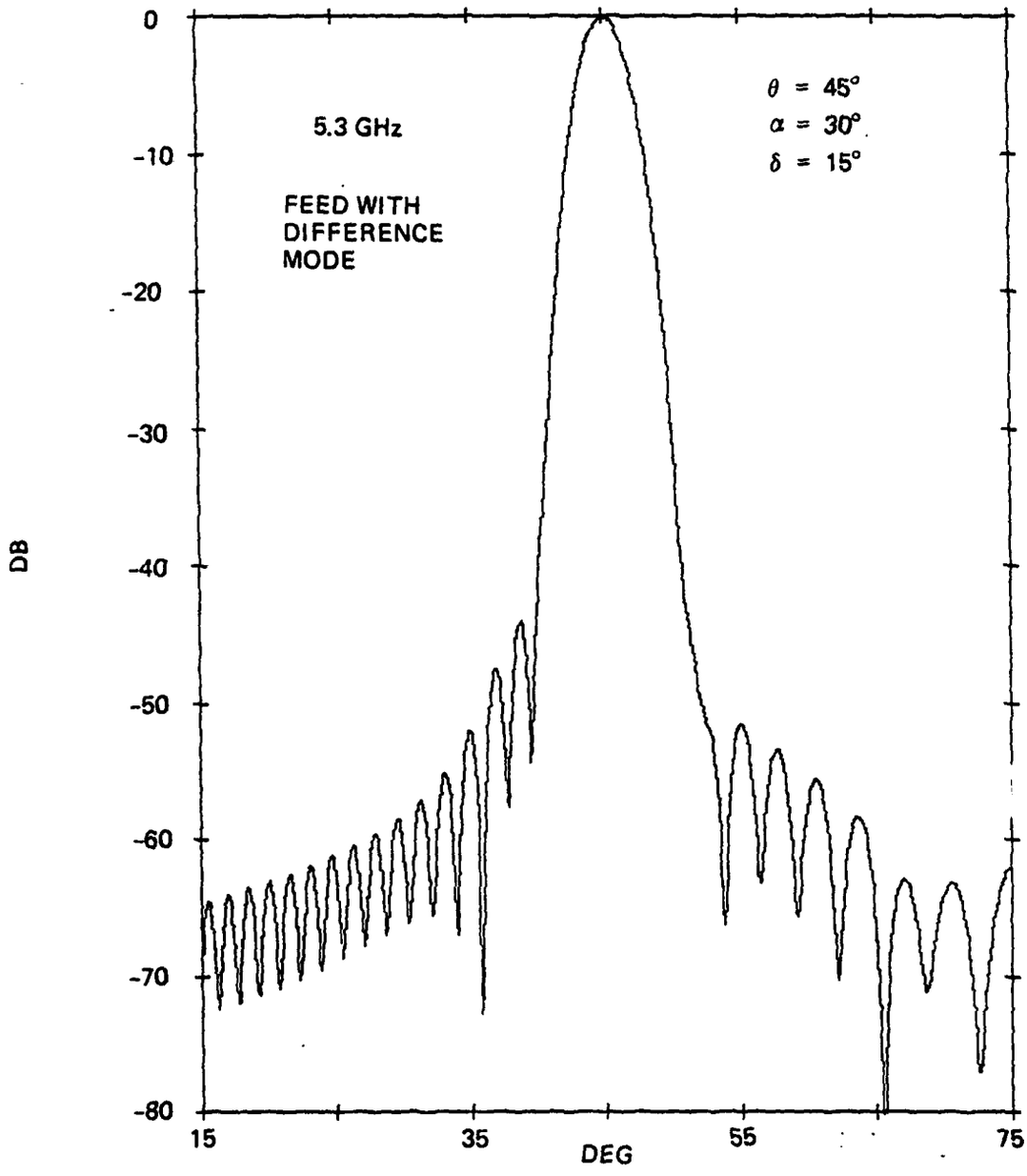

Figure 5-32. Azimuth Pattern of Antenna with Feed Difference Mode, $\theta = 45^{o}$

azimuth patterns having the desired low sidelobes. With a lens F/D of approximately one, the horizontal dimension of the line-feed array is approximately five wavelengths.

For the off-axis beams, the curvature of the cylindrical lens aperture creates a distortion of the azimuth patterns that increases with scan (θ) off the lens axis. This is a basic problem of low-sidelobe conformal arrays that are scanned only by aperture phase shift, without any aperture amplitude change.

For the multibeam lens antenna, a different feed design for each coarse-steered beam position could yield nearly ideal azimuth patterns if a much larger horizontal feed dimension were used; this is clearly unattractive. A smaller, simpler version of this approach involves a feed having a difference-mode excitation component; improved azimuth patterns are obtained but different feed designs are still needed. The most practical approach for this lens-antenna project is a combination of feed tilt and feed refocusing, which yields improved azimuth patterns with a single feed design having the original five-wavelength horizontal dimension.

5.2 LINE FEED AND ELEVATION PATTERNS

The elevation pattern of the cylindrical lens antenna is similar to the elevation pattern of the line feed. Therefore the line feed should be designed to radiate a low-sidelobe, far-field elevation pattern. However an additional factor affecting the antenna elevation pattern is the diffraction caused by the top and bottom edge of the cylindrical lens.

This diffraction effect could be made small by having a lens vertical dimension much larger than the line-feed vertical dimension. The diffraction effect can also be reduced by using a well-tapered vertical excitation of the line feed. We have chosen the modified sin u/u distribution (refs 8, 9) for the line feed because it is well tapered and can provide low sidelobes. The lens is then made only a little larger than the line feed.

Ref 8- H.Jasik, "Antenna Engineering Handbook", McGraw-Hill, pp. 2.27-2.28; 1961.

Ref 9- R.C. Hansen, "Microwave Scanning Antennas", Academic Press, Vol. 1, pp. 58-60; 1964.

Figure 5-33 shows the nominal vertical-excitation amplitude of the line feed, chosen for a nominal first-sidelobe level of -45 dB. The vertical excitation is to be provided by a microstrip power-divider network (discussed in a later section) and a set of interconnecting cables. The cable lengths are to be chosen so as to provide constant path length to the elements of the line feed for radiation at 0^{o} elevation. A second set of cables will provide a time-delay-steered elevation angle of radiation.

The line-feed array was previously shown in figure 5-3. There are 58 elements along the 35 wavelength line feed, giving a vertical spacing between elements of about 0.6 wavelengths. The computed elevation pattern of this line feed array, excited with the nominal distribution given in figure 5-33, is shown in figure 5-34 for a beam at 0^{o} elevation. The computed pattern of the line feed array when steered 15^{o} off broadside is shown in figure 5-35.

Elevation Patterns Including Diffraction

In order to determine the effect of lens diffraction on the elevation pattern sidelobes, a pattern computation was performed that included the truncation by the lens of the near-field radiation of the line feed. Figure 5-36 shows the line feed and the inner surface of the lens. Also indicated are rays emanating from the top and bottom of the line feed; the intersection of these rays with the inner surface of the lens is shown by lines drawn across the inner surface. For this case of no elevation scan, these "ray illumination boundary" lines are straight. Of course, the actual illumination of the lens surface is given by the near-field radiation of the line feed, which is only approximated by the ray viewpoint.

Figure 5-37 shows the antenna elevation pattern computed from the actual lens illumination, ie, the near field of the line feed, when the vertical dimension of the lens is 37 wavelengths. Comparison with figure 5-34 shows that the sidelobes are slightly affected by the lens truncation action. Figure 5-38 shows the pattern when the lens dimension is 35 wavelengths, the same as the feed dimension. Here a greater effect can be seen.

When the line feed is steered in elevation, the ray illumination boundary lines become curved as indicated in figure 5-39. It is assumed here that the line feed is diplaced vertically so as to center on the lens surface that part of the ray boundary that is in the middle of the lens where the horizontal illumination distribution is strongest.

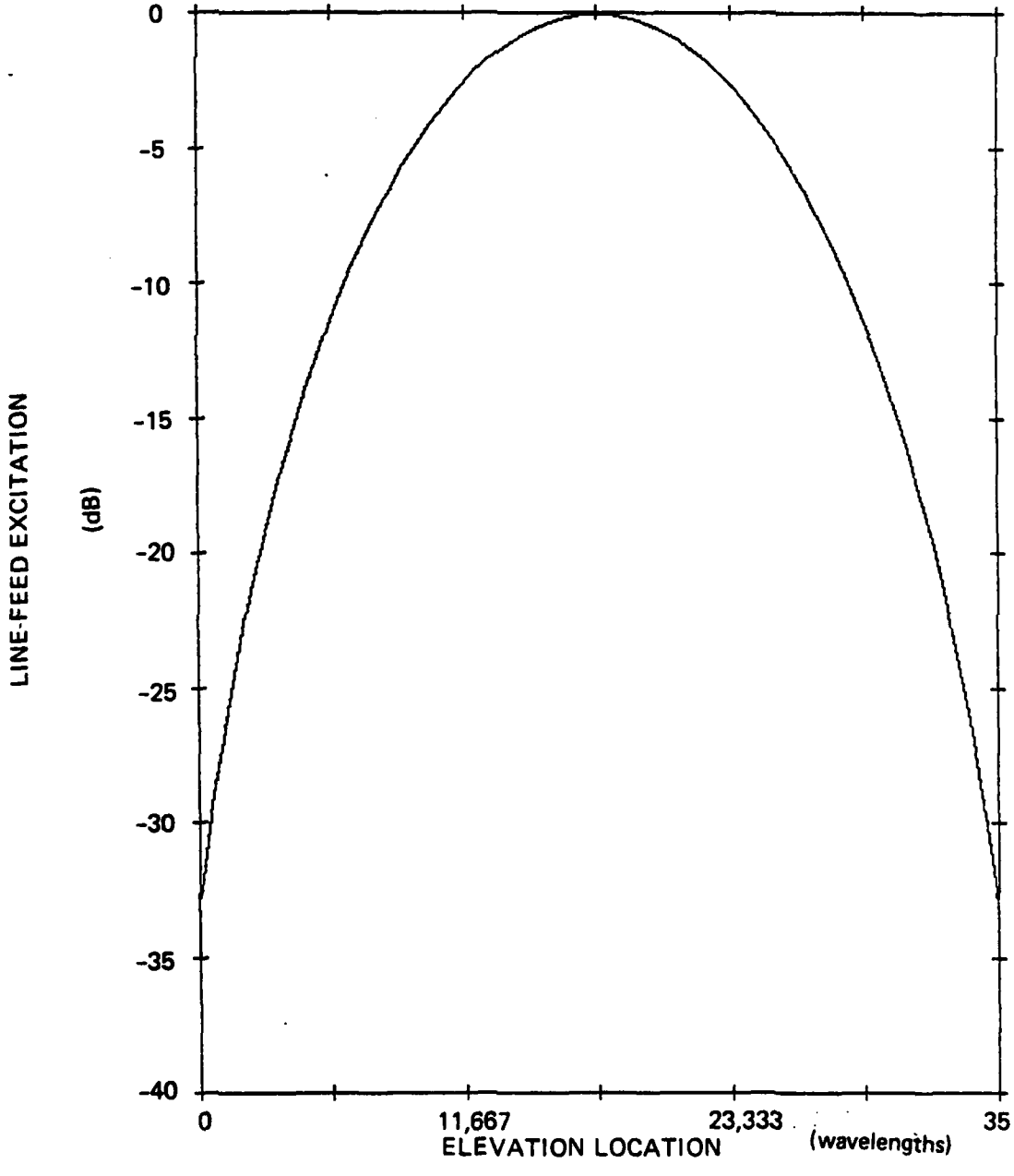

Figure 5-33. Vertical Distribution of Line-Feed Excitation

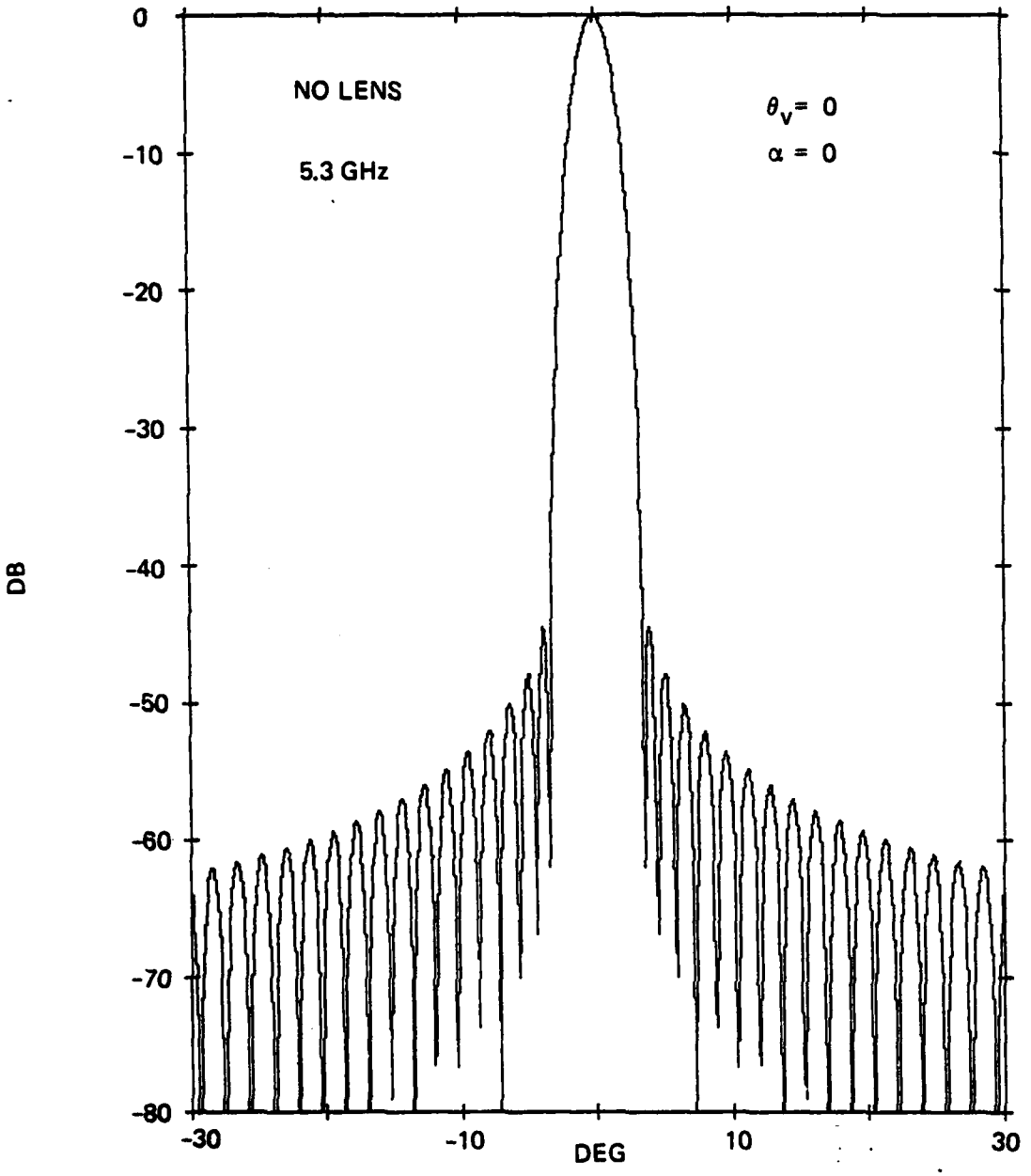

Figure 5-34. Elevation Pattern of Line Feed, θ_V = 0

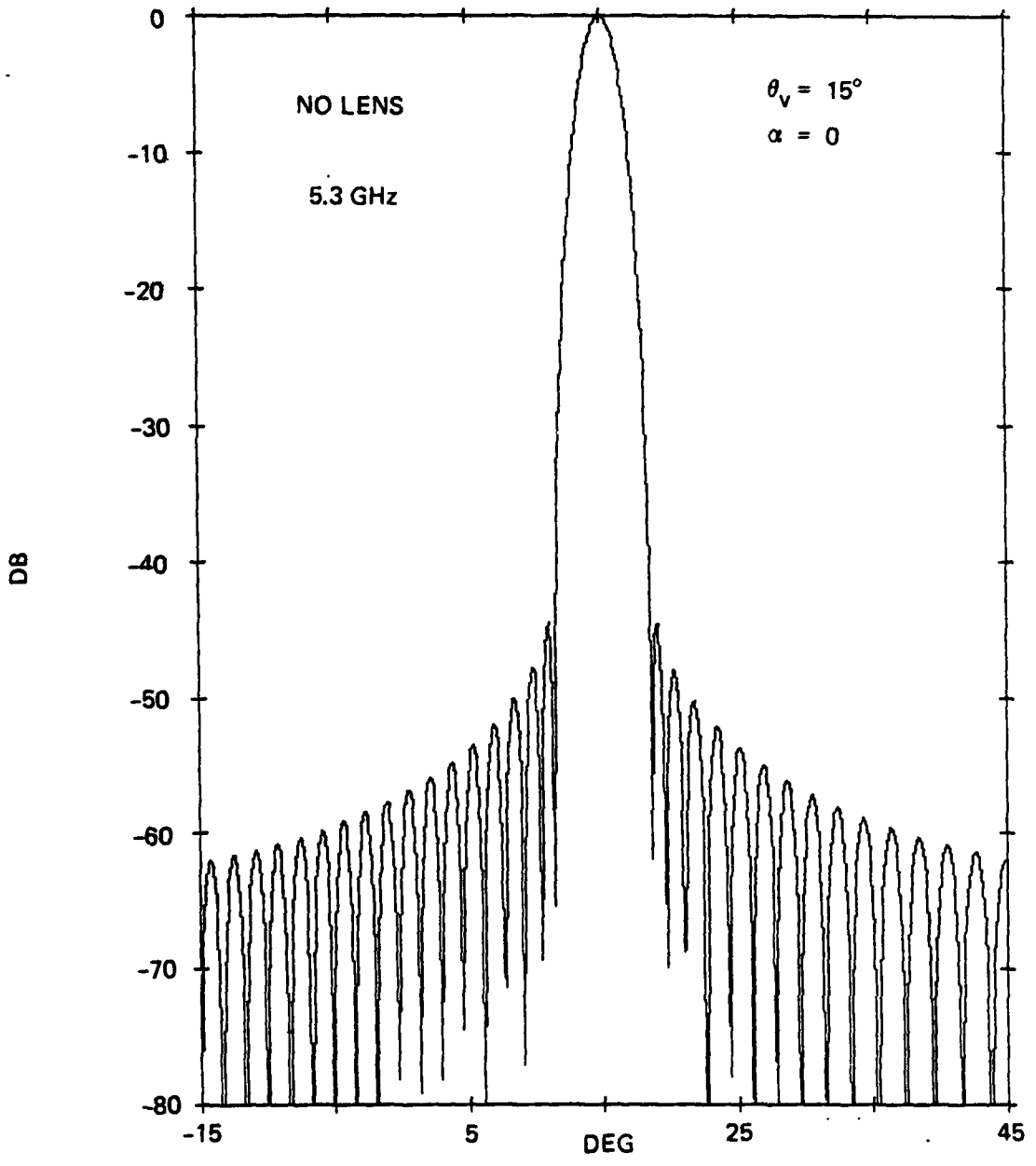

Figure 5-35. Elevation Pattern of Line Feed, $\theta_v = 15^o$

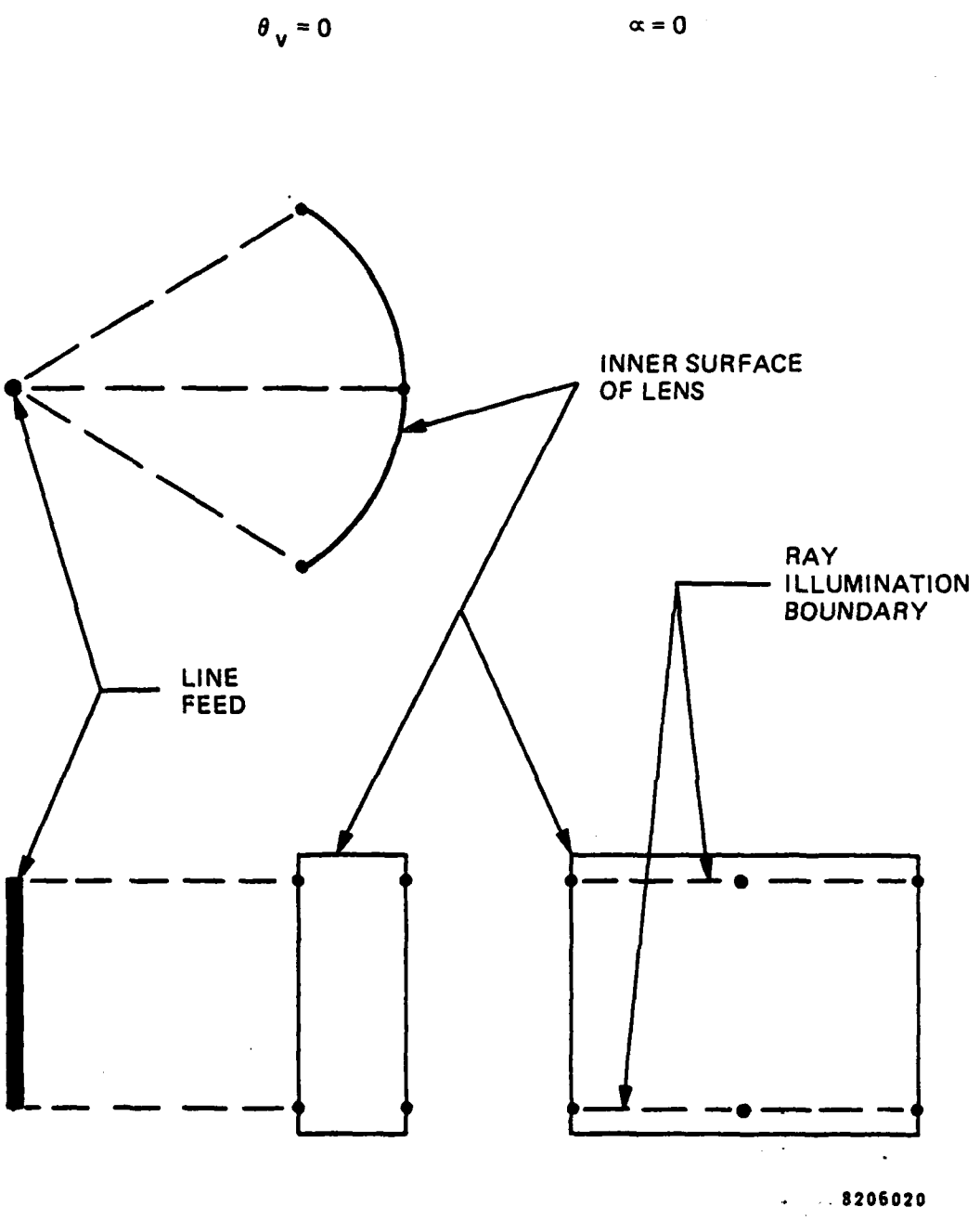

Figure 5-36. Ray Illumination of Lens, $\theta_v = 0$

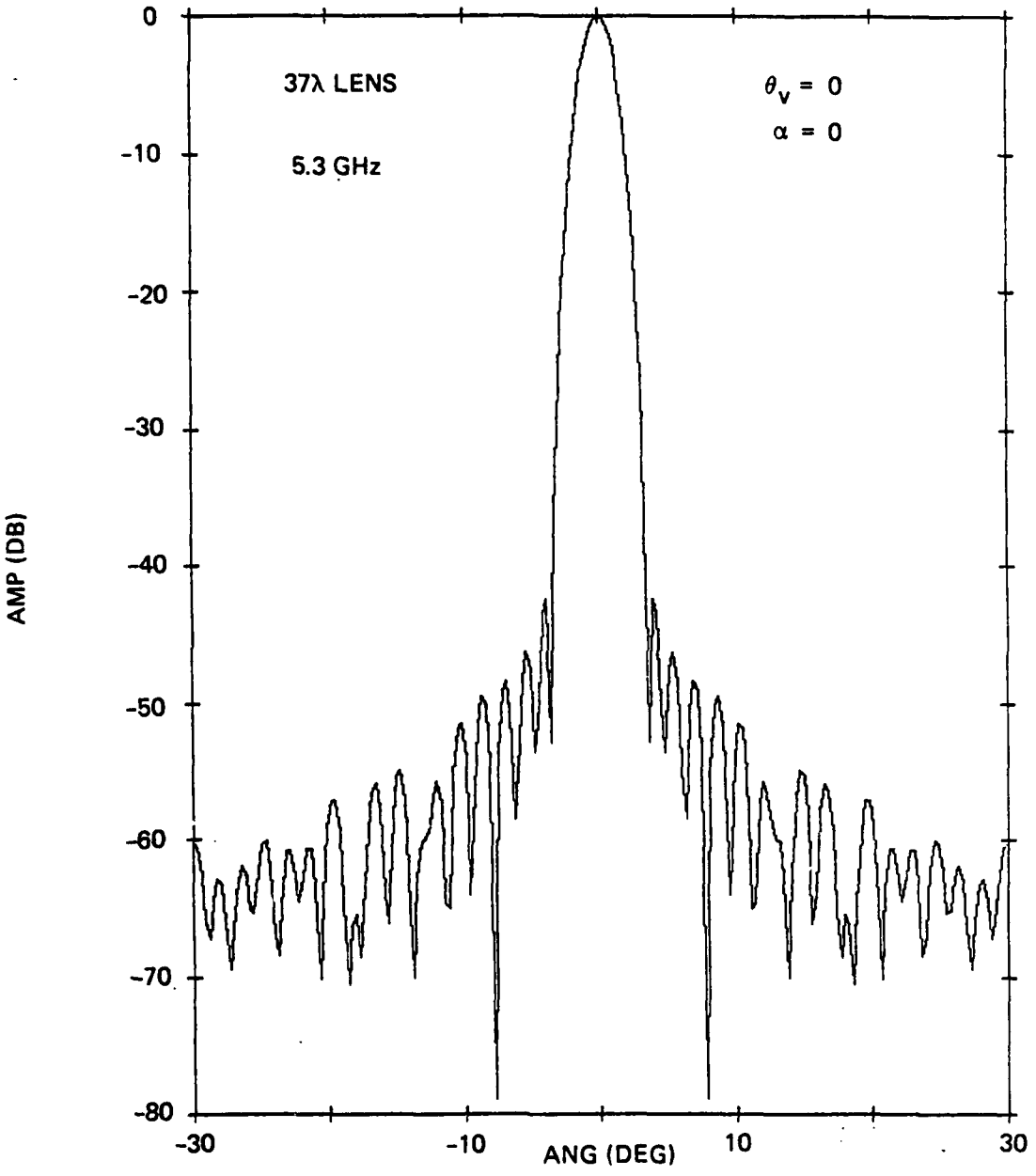

Figure 5-37. Elevation Pattern of Antenna, $\theta_v = 0$, 37 λ Lens

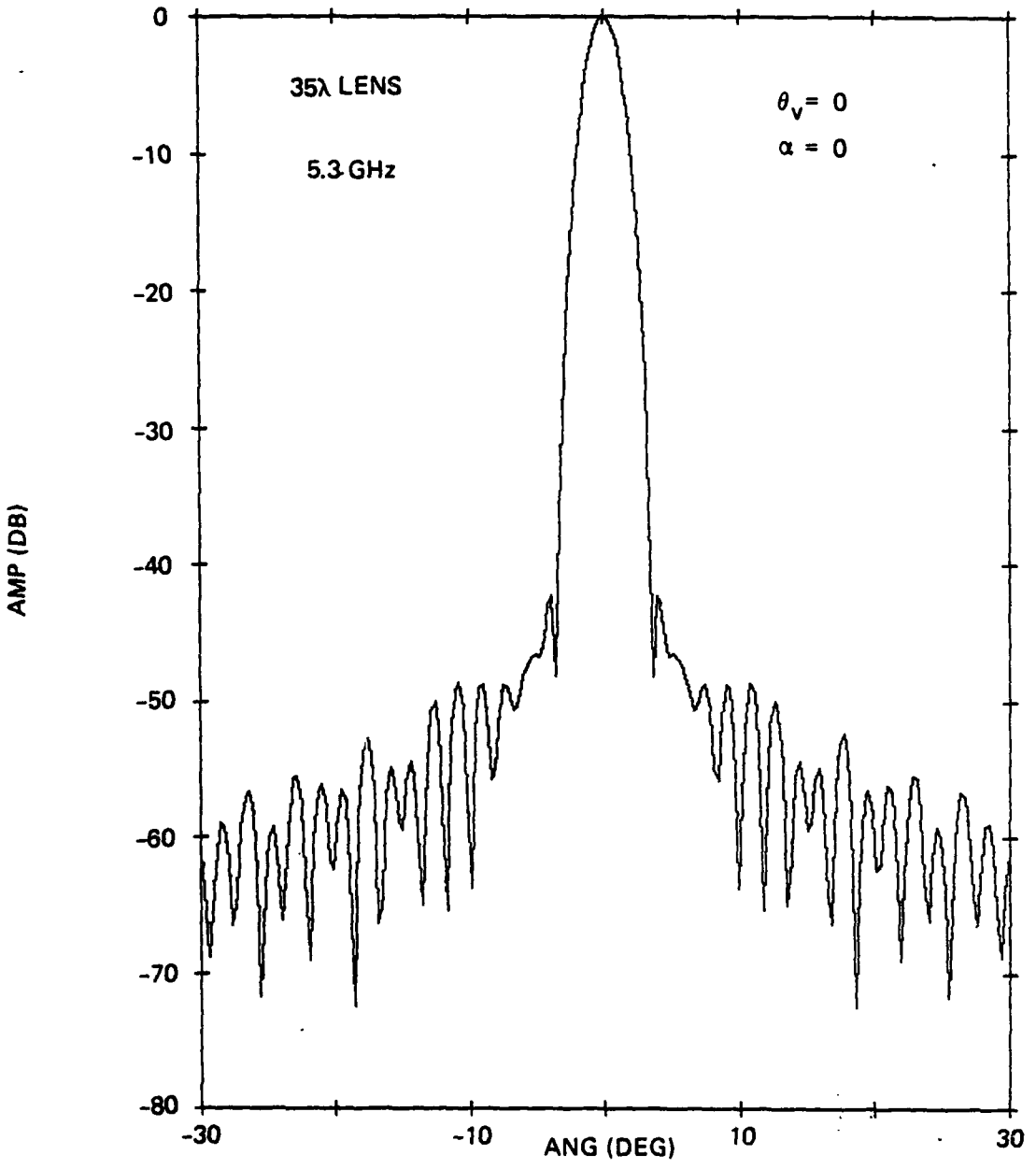

Figure 5-38. Elevation Pattern of Antenna, θ_V = 0, 35 λ Lens

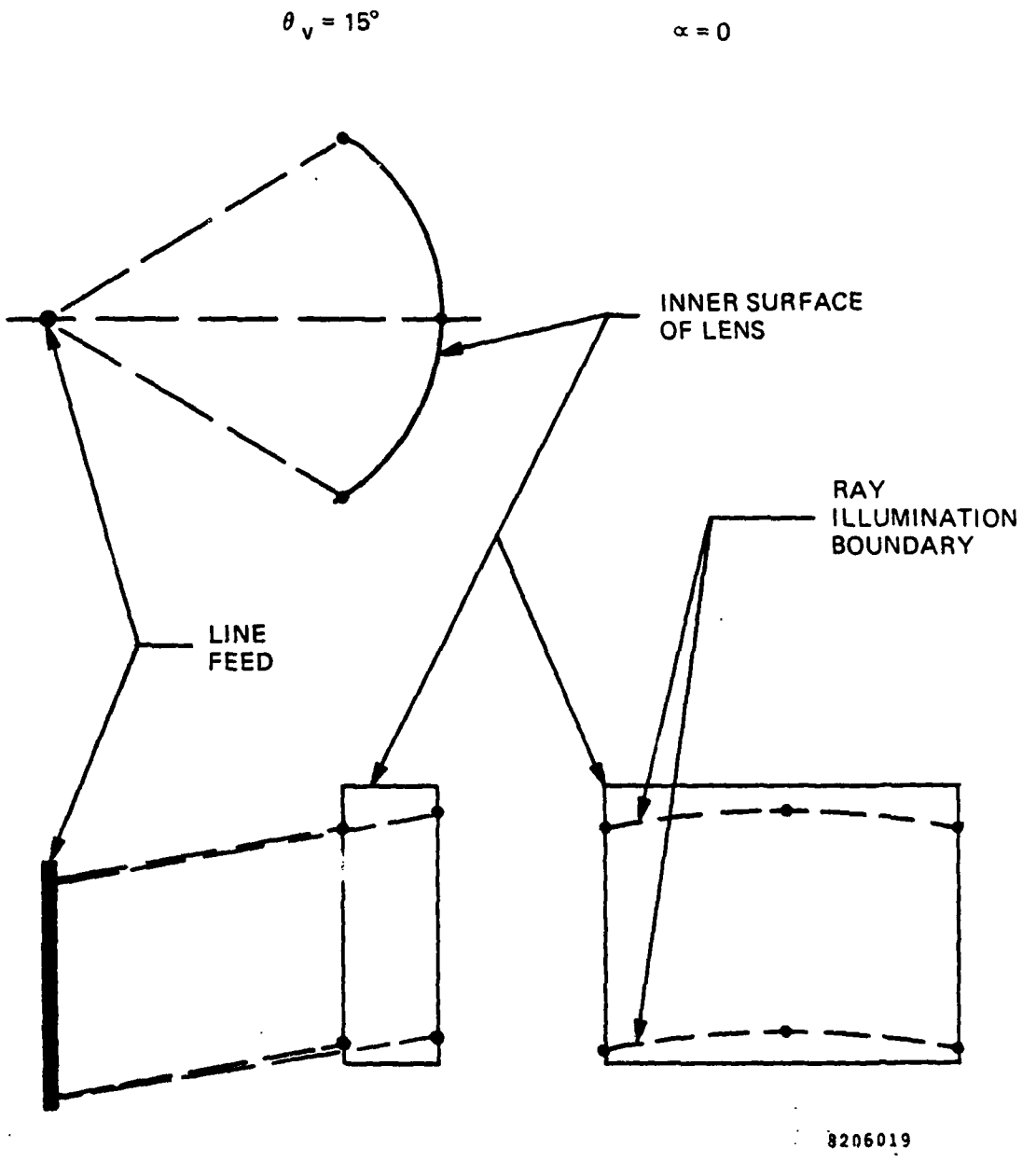

Figure 5-39. Ray Illumination of Lens, $\theta_v = 15°$

AD-A138 808 STUDY AND DESIGN OF A CYLINDRICAL LENS ARRAY ANTENNA FOR WIDEBAND ELECTRONIC SCANNING(U) HAZELTINE CORP GREENLAWN NY P W HANNAN ET AL. DEC 83 RADC-TR-83-128 2/2

UNCLASSIFIED F19628-80-C-0110 F/G 9/5 NL

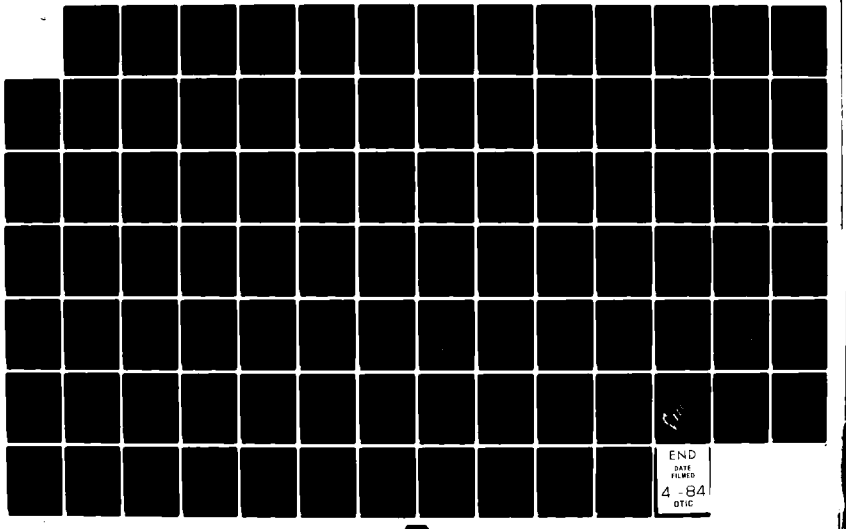

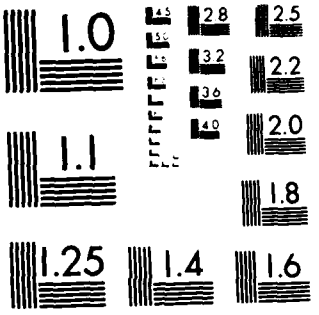

Figure 5-40 shows the antenna pattern computed for this case, when the lens dimension is 37 wavelengths. Figure 5-41 shows the pattern computed for a 35 wavelength lens. As before, the larger lens produces only a slight effect on the sidelobes, and the smaller lens has a greater effect.

When the line feed is not only steered in elevation but is also horizontally displaced to provide coarse steering in azimuth, the curved boundary lines are also displaced, as indicated in figure 5-42. Again, it is assumed that the line feed is displaced vertically so as to center on the lens surface that part of the ray boundary that is in the middle of the lens surface. However, because of the horizonal displacement, one side of the boundary lines show a relatively large deviation from the centered condition.

Figure 5-43 shows the antenna pattern computed for this case, when the lens dimension is 37 wavelengths. Figure 5-44 shows the pattern computed for a 35 wavelength lens. A substantial amount of asymmetry can be seen in these patterns, particularly for the smaller lens.

None of the elevation patterns that have been computed have shown a serious degradation of the sidelobes. This is believed to be a result of the well-tapered illumination used in elevation and also in azimuth. Since the 37 wavelength lens vertical dimension gives better sidelobe chracteristics than the 35 wavelength dimension, while requiring only a small increase of antenna size, it has been selected.

5.3 ANTENNA DIRECTIVE GAIN

The directivity of the cylindrical lens antenna has been estimated by first calculating the directivity of a uniformly illuminated planar aperture with area equal to the projected area of the lens, and then computing the reduction of directivity caused by the horizontally and vertically tapered aperture illumination. This reduction for taper is called the aperture efficiency. An additional reduction factor for spillover power would ordinarily be needed; however the spillover power is negligible in this antenna because of the well-tapered aperture illumination and the low sidelobes of the feed pattern.

The lens aperture is 40 wavelengths wide at midband, corresponding to a width of 90 inches. The height of the lens is 83 inches. Thus, the projected area of the lens in

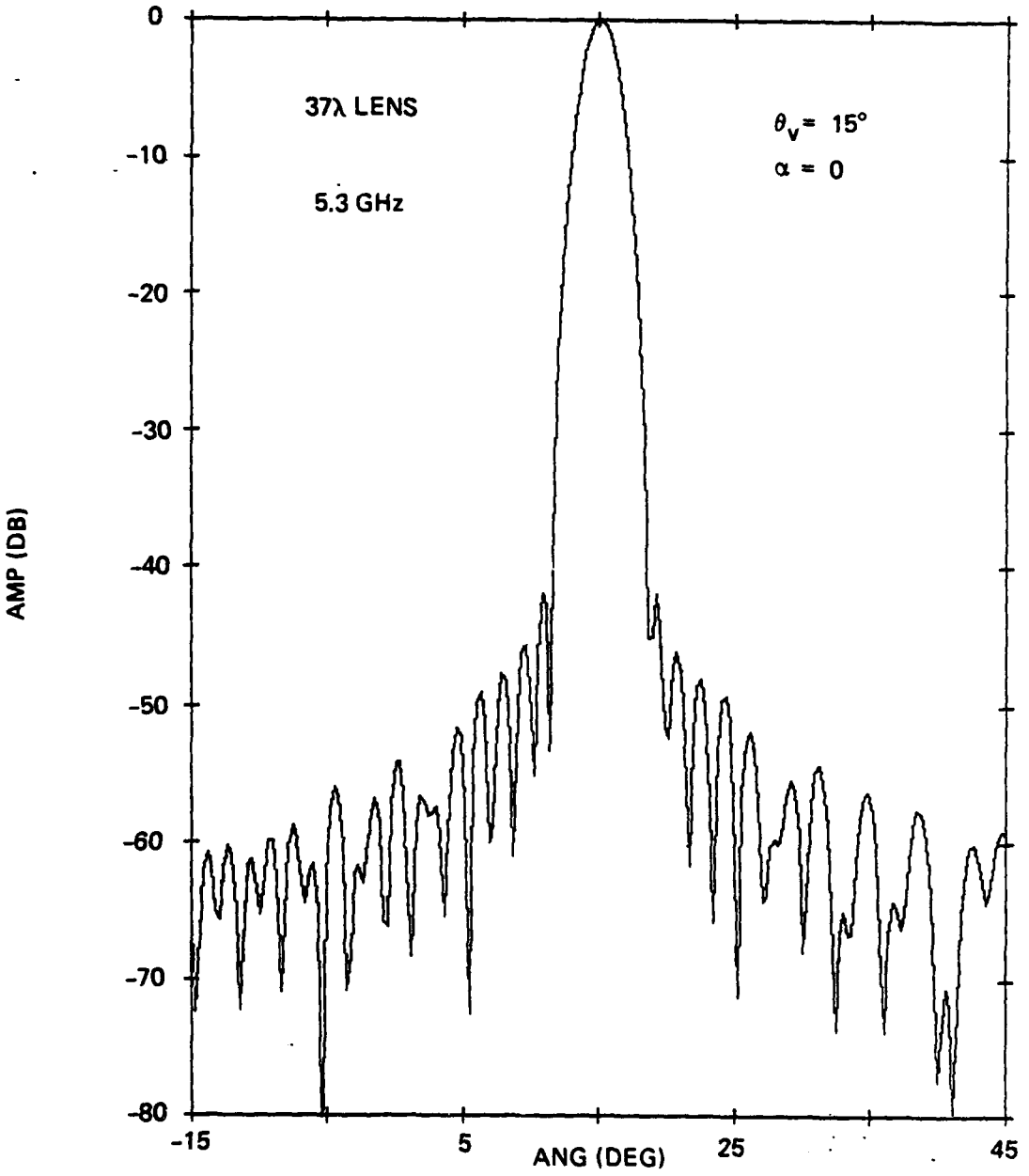

Figure 5-40. Elevation Pattern of Antenna, $\theta_V = 15^O$, 37 λ Lens

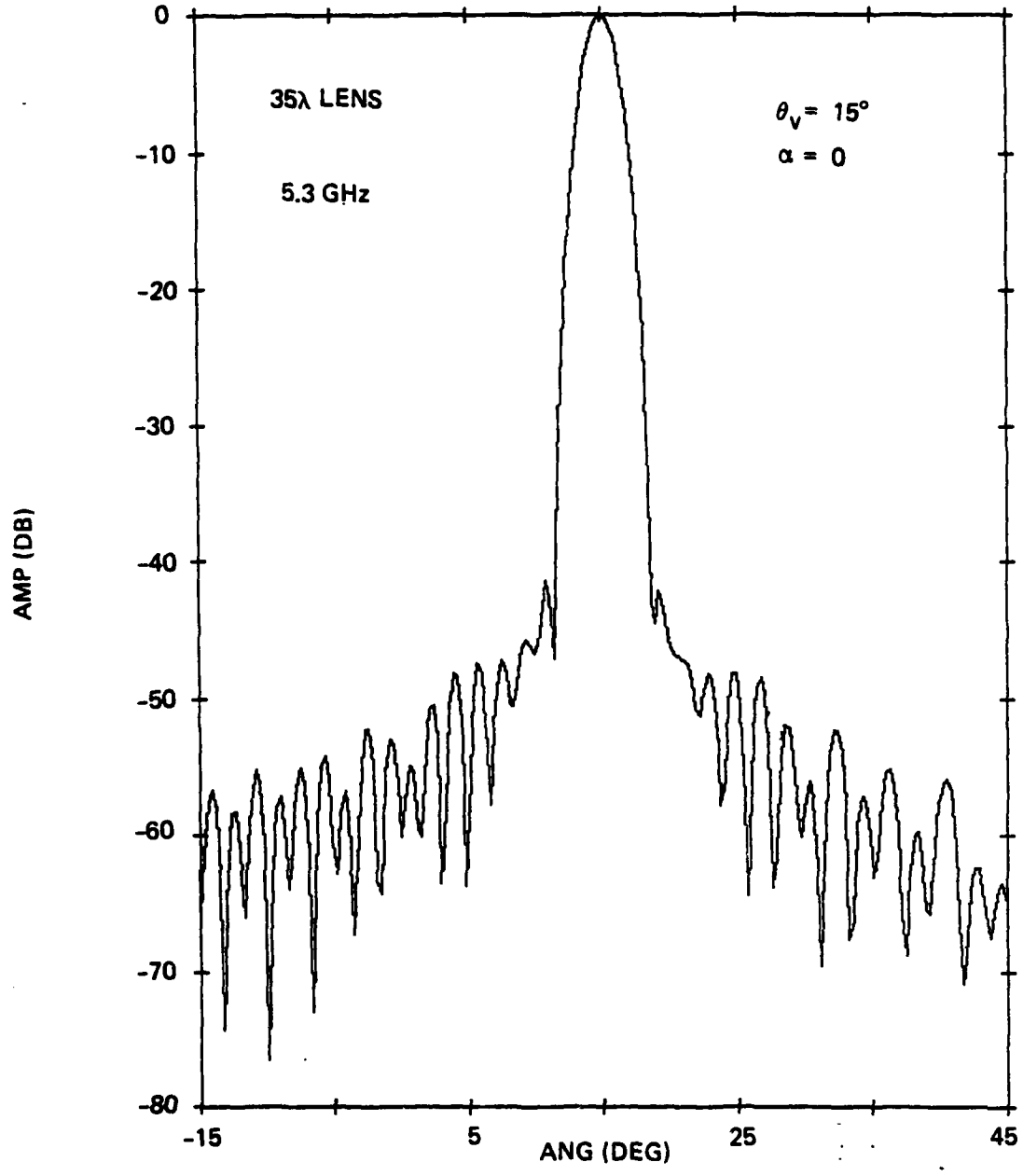

Figure 5-41. Elevation Pattern of Antenna, $\theta_V = 15^O$, 35 λ Lens

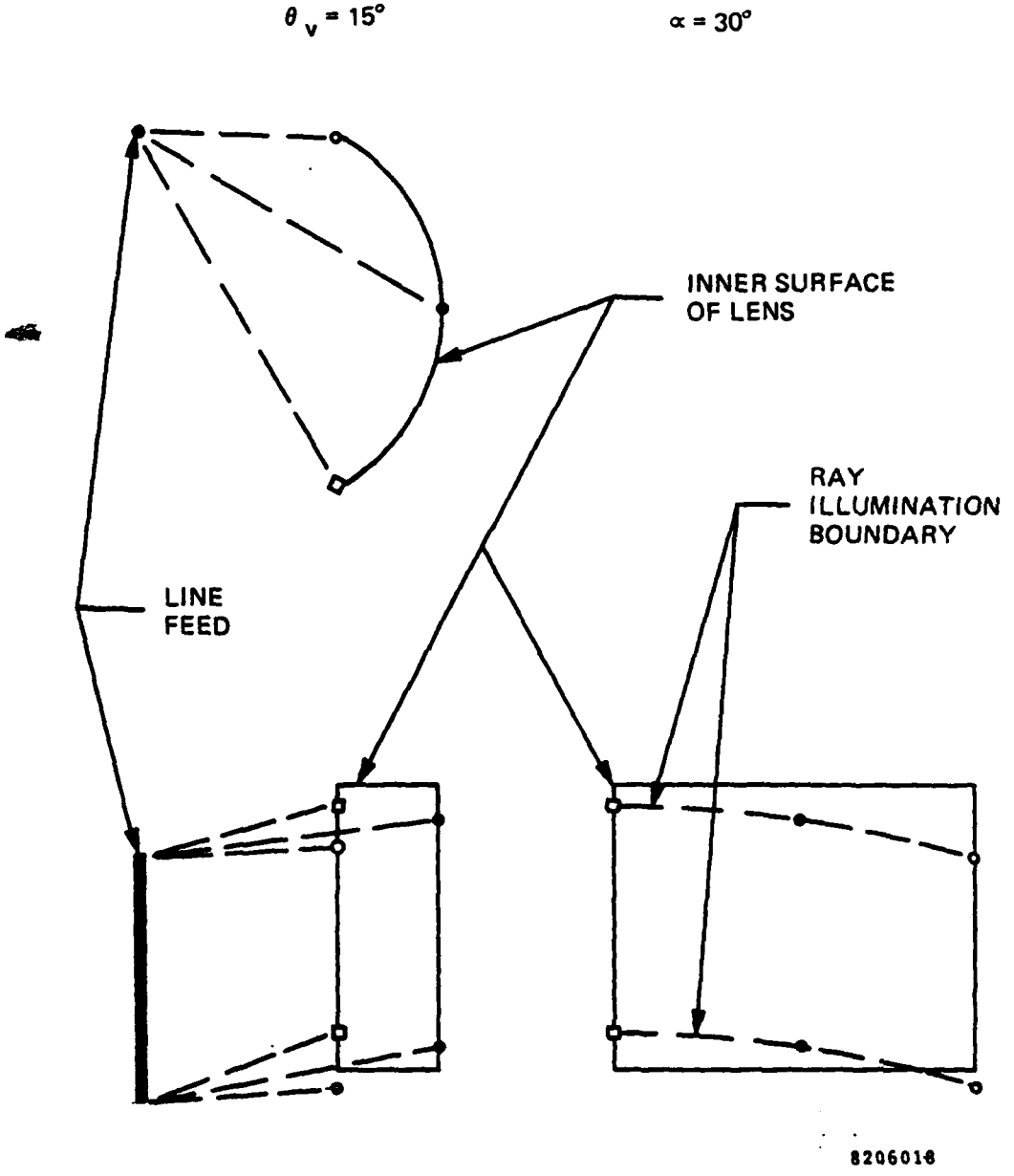

Figure 5-42. Ray Illumination of Lens, $\theta_v = 15°$, $\alpha = 30°$

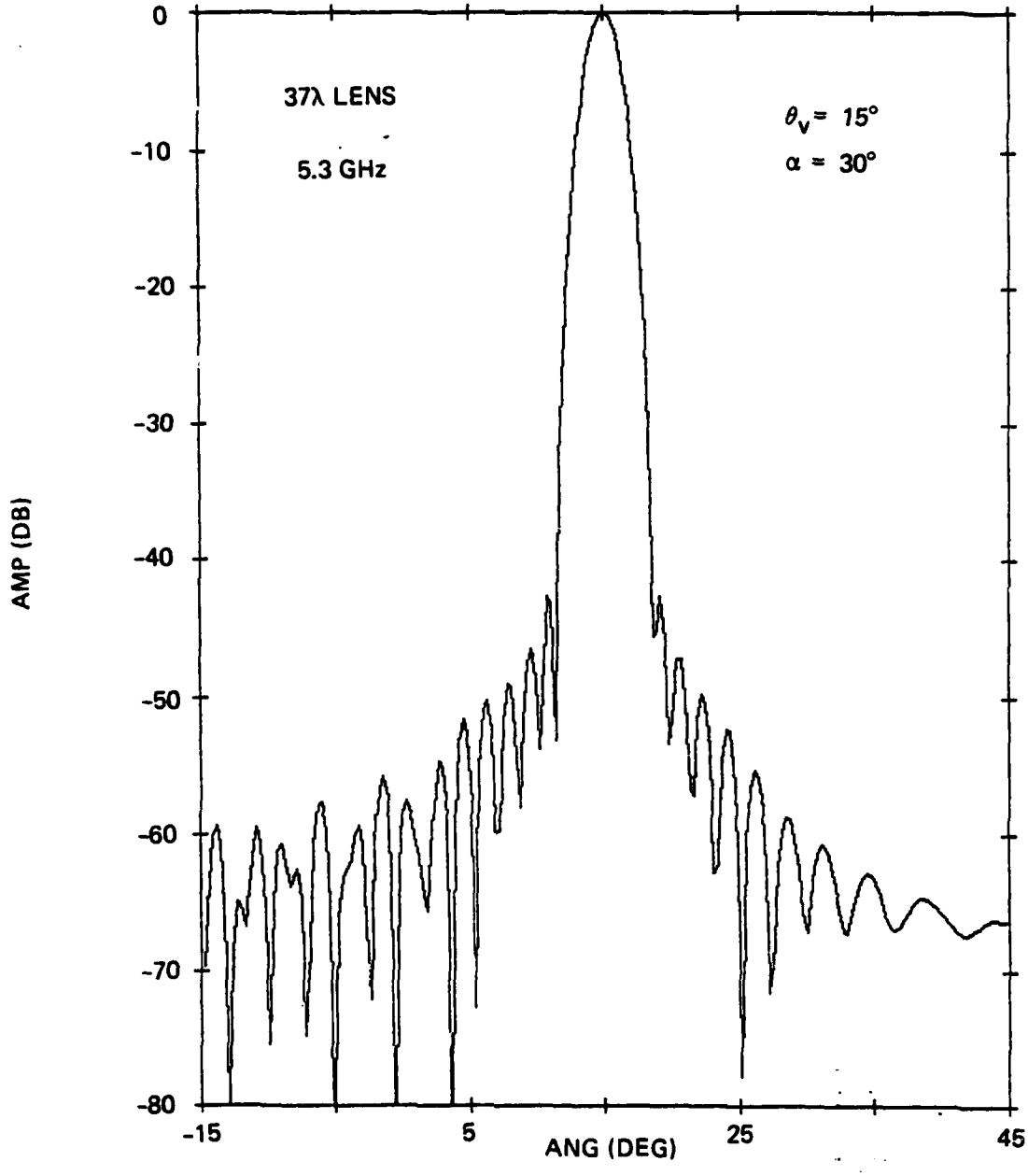

Figure 5-43. Elevation Pattern of Antenna
$\theta_V = 15^O$, $\alpha = 30^O$, 37 λ Lens

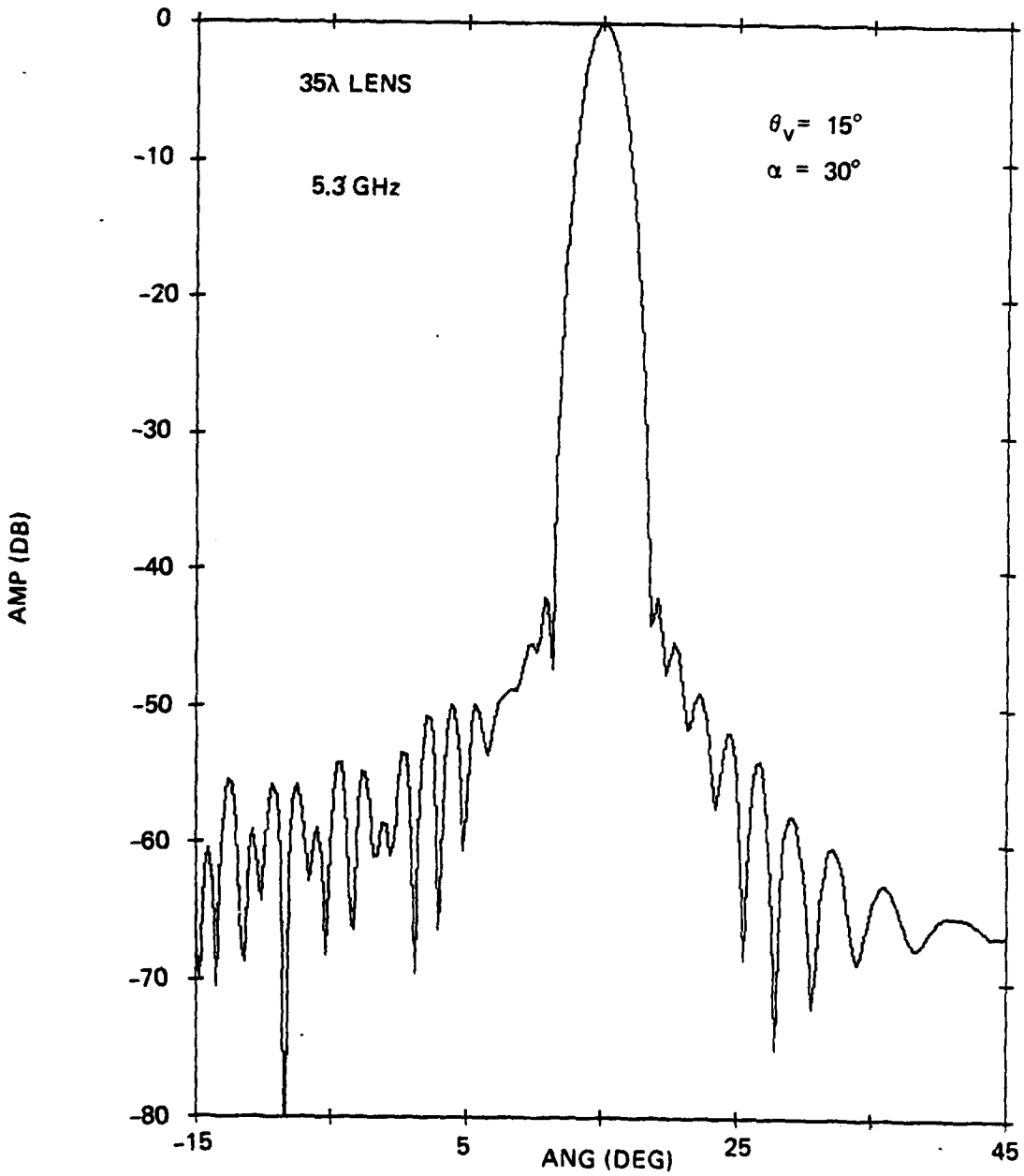

Figure 5-44. Elevation Pattern of Antenna, $\theta_V = 15^O$, $\alpha = 30^O$, 35 λ Lens

the boresight direction is 7450 square inches. The directivity of a uniformly-illuminated planar aperture of this area is:

$$D(\text{area}) = 10 \log \left[4\pi(7450)/(2.23)^2\right] = 42.8 \text{ dBi}$$

The aperture efficiency of the curved lens array is determined from a viewpoint that includes the varying element-pattern directions over the curved array (ref 10). When referenced to a uniformly illuminated planar array, this curved-array aperture efficiency is:

$$\text{aperture efficiency} = \frac{\left[\Sigma V_n \, e_n(\psi)\right]^2}{\left[\Sigma V_n^2\right]\left[\Sigma e_{on}^2(\psi)\right]} \qquad (13)$$

where V_n is the relative amplitude of excitation of the nth element, $e_n(\psi)$ is the element pattern amplitude in a direction ψ toward the antenna pattern peak for a beam in the θ direction, and $e_{on}(\psi)$ is the element pattern amplitude in a direction ψ toward the antenna pattern peak for a 0^o beam direction.

The aperture efficiency is calculated by the computer as part of the antenna pattern computation. The element pattern used in all the calculations is $\sqrt{\cos\psi}$ out to 85 degrees.

The area directivity, aperture efficiency, and antenna directivity are tabulated in table 5-1 below for three frequencies across the operating band.

Ref 10- J.C.Sureau, A. Hessel, "On the Realized Gain of Arrays", IEEE Trans. Antennas and Propagation, pp. 122-124; January 1971.

Table 5-1. Antenna Directivity

Frequency (GHz)	5.0	5.3	5.6
D(area) (dBi)	42.3	42.8	43.2
Aperture Efficiency (dB)	-4.3	-4.6	-4.8
Antenna Directivity (dBi)	38.0	38.2	38.4

It is interesting to note that the 0.5 dB decrease of aperture efficiency with increasing frequency is caused by the change of azimuth feed pattern beamwidth with frequency. This efficiency decrease partially compensates for the normal increase of D(area) with frequency, to yield a computed antenna directivity that varies by only 0.4 dB over the 11% operating frequency band.

It should be recognized, however, that lens internal reflections are likely to introduce an oscillatory variation of realized antenna gain with frequency; this will be discussed in section VI. In addition, there is a scan-dependent wideband effect that will be discussed in paragraph 5.4.

The aperture efficiency of the antenna is also affected by scanning the antenna beam away from the antenna axis. For the 25° elevation scan, the aperture efficiency is reduced by 0.4 dB in accordance with the natural decrease of projected aperture area. For the 45° azimuth scan, the natural decrease of projected area of a planar aperture would give a 1.5 dB reduction of aperture efficiency. The computer calculation with formula 13 yields this 1.5 dB reduction for the curved lens array when the line feed is in its nominal position for 30° coarse steering with 15° fine steering. However, when the line feed is tilted and refocused for improved azimuth patterns (see paragraph 5.1), the aperture efficiency increases by about 0.3 dB, yielding an efficiency that is only 1.2 dB below the unscanned value. This result is consistent with the improved beam shape and lower sidelobes that are obtained when the off-axis line feed is repositioned.

5.4 SIGNAL BANDWIDTH/SCAN PERFORMANCE

The multibeam lens antenna has the capability for wide signal bandwidth (instantaneous bandwidth) and wide-angle electronic scanning, with only a nominal degradation of performance. Increasing the number of feeds reduces the size of the fine-steered sub regions of scan, and therefore improves the wideband performance. In the following discussion, the tradeoff between performance and number of feeds is examined. Additionally, the effect of the electronic phase-shifter design on wideband sidelobe level is discussed. The analysis is based on the material given in refs 1, 2, 3, 11, 12.

a. Beam Motion Over Signal Band

Fine steering with phase shifters causes the scan angle of the beam to change with frequency according to:

$$\partial\theta = \pm \frac{\Delta f}{2f} \tan\theta \qquad (14)$$

where $\partial\theta$ is half of the total change of scan angle, Δf is the total bandwidth, f is the center frequency, and θ is the nominal scan angle. The half-power beamwidth of the array is approximately:

$$BW = k \frac{\lambda}{L \cos\theta} \qquad (15)$$

Ref 11- J.Frank, "Bandwidth Criteria for Phased-Array Antennas", Proceedings of the 1970 Phased Array Antenna Symposium, edited by Oliner and Knittel, Artech House, pp.243-253; 1972.

Ref 12- T.C.Cheston and J.Frank, Chapter 11.6 of Radar Handbook, edited by M.I.Skolnik, McGraw-Hill, pp. 11-43 to 11-50; 1970.

where L is the aperture dimension and k is a beamwidth constant depending on the effective aperture amplitude distribution. Combining these two relations gives:

$$\frac{\partial\theta}{BW} = \pm \frac{\Delta f}{2f} \frac{L}{\lambda k} \sin\theta \qquad (16)$$

Now dividing the total scan coverage of $\pm\theta_{max}$ into M sub-regions, and assuming the beam is at the edge of the fine-steered sub-region, this becomes:

$$\text{edge } \frac{\partial\theta}{BW} = \pm \frac{\Delta f}{2f} \frac{L}{\lambda k} \frac{\sin\theta_{max}}{M} \qquad (17)$$

as was derived in ref 1.

b. Loss Caused By Beam Motion

The principal effect of the $\pm\partial\theta$ motion of the beam over the frequency band Δf is to cause a loss, because the beam peak is not pointed in the desired direction near the ends of the band. The loss in dB when a beam is displaced by the small angle $\partial\theta$ is approximately:

$$\text{loss (dB)} \approx 12 \left(\frac{\partial\theta}{BW}\right)^2 \qquad (18)$$

Therefore the loss at the ends of the frequency band Δf is approximately:

$$\text{max CW edge loss (dB)} \approx 3\left(\frac{\Delta f}{f}\right)^2 \left(\frac{L}{\lambda k} \frac{\sin\theta_{max}}{M}\right)^2 \qquad (19)$$

This loss at the ends of the frequency band is applicable to the case of a narrowband signal (much narrower than Δf), ie, a signal that is essentially CW.

For a signal having an instantaneous bandwidth (pulse bandwidth or information bandwidth) that is equal to Δf, an integration or weighted averaging over the signal frequency spectrum is necessary. If the wideband signal is assumed to have a spectrum with power that is uniformly distributed over the frequency band Δf and is zero outside of the Δf band (a rectangular spectrum), then the effective loss over the Δf band is approximately 1/3 of the maximum loss:

$$\text{wideband effective edge loss (dB)} \approx \left(\frac{\Delta f}{f}\right)^2 \left(\frac{L}{\lambda k} \frac{\sin \theta_{max}}{M}\right)^2 \quad (20)$$

It should be noted that with a frequency spectrum that is not zero outside of a band Δf because of frequency skirts and sidelobes, differing estimates of loss can occur (see ref 11) depending on whether the frequency skirts and sidelobes are utilized or are filtered out in the actual system. A frequency spectrum having non-uniform power also can yield differing loss estimates depending on whether a flat filter response or a matched filter response is used.

c. Two-Dimensional Scanning Loss

The lens antenna discussed in this report scans electronically in two dimensions: a horizontal scan (θ_h) and a vertical scan (θ_v). Figure 5-45 shows the total electronic scan coverage and the division into M x N fine-steered sub regions. The relation for $\partial\theta/BW$ now becomes two relations:

$$\text{edge} \quad \frac{\partial\theta_h}{BW_h} = \pm \frac{\Delta f}{2f} \frac{L_h}{\lambda k_h} \frac{\sin \theta_{h\,max}}{M}$$

$$\text{edge} \quad \frac{\partial\theta_v}{BW_v} = \pm \frac{\Delta f}{2f} \frac{L_v}{\lambda k_v} \frac{\sin \theta_{v\,max}}{N} \quad (21)$$

TOTAL SCAN COVERAGE:

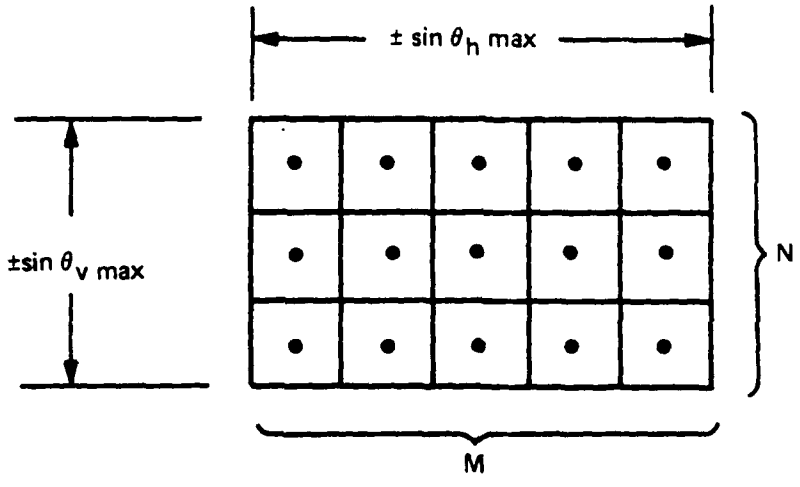

FINE-STEERING SUB-REGION:

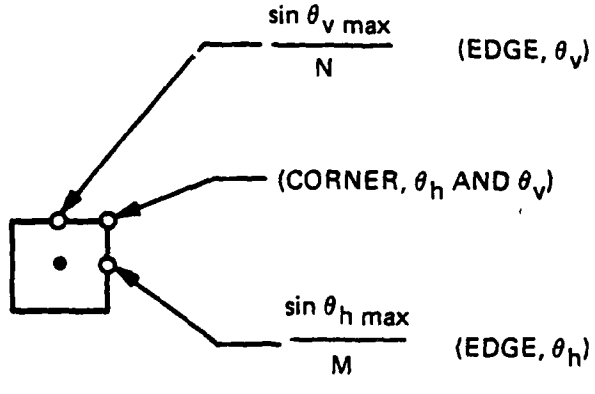

8206039

Figure 5-45. Electronic Scan Regions for Cylindrical Lens Antenna

This cylindrical lens antenna has pattern characteristics that are essentially separable into horizontal and vertical components whose product is the actual pattern. Therefore, the loss at the corners of the fine-steering sub-regions is approximately:

$$\text{loss (dB)} \approx 12 \left[\left(\frac{\partial \theta_h}{BW_h} \right)^2 + \left(\frac{\partial \theta_v}{BW_v} \right)^2 \right] \qquad (22)$$

Therefore, the CW loss at the ends of the frequency band Δf is approximately:

$$\text{max CW corner loss (dB)} \approx$$

$$3 \left(\frac{\Delta f}{f} \right)^2 \left[\left(\frac{L_h}{\lambda k_h} \frac{\sin \theta_{h\ max}}{M} \right)^2 + \left(\frac{L_v}{\lambda k_v} \frac{\sin \theta_{v\ max}}{N} \right)^2 \right] \qquad (23)$$

As before, the wideband effective loss over a rectangular spectrum Δf wide is about 1/3 of the maximum loss:

$$\text{wideband effective corner loss (dB)} \approx \qquad (24)$$

$$\left(\frac{\Delta f}{f} \right)^2 \left[\left(\frac{L_h}{\lambda k_h} \frac{\sin \theta_{h\ max}}{M} \right)^2 + \left(\frac{L_v}{\lambda k_v} \frac{\sin \theta_{v\ max}}{N} \right)^2 \right]$$

d. Cylindrical Lens Loss Tradeoff

The specific parameters of the cylindrical lens antenna to be developed in this program can be substituted in equations 23 and 24. These parameters are:

$$\frac{\Delta f}{f} = \frac{400}{5300} = 0.076$$

$\theta_{h\ max}$ = 45° (or 40°, see below) (25)

$\theta_{v\ max}$ = 25°

$L_h = 40\lambda$ $k_h = 1.7$

$L_v = 35\lambda$ $k_v = 1.6$

The resulting CW loss at the ends of the frequency band and at the corners of the fine-steering sub-regions is approximately:

$$\text{max CW corner loss (dB)} \approx \frac{4.8}{M^2} + \frac{1.5}{N^2} \quad (26)$$

If M = 3 and N = 2, then:

$$\text{max CW corner loss (dB)} \approx 0.5 + 0.4 \approx 0.9 \quad (27)$$

Actually this CW corner loss would be somewhat less because the angle $\theta_{h\ max}$ is only about 40° when the azimuth angle ϕ is 45° and the elevation angle θ_v is 25°. The two edge losses, however, remain 0.5 and 0.4 dB, respectively, for azimuth or elevation scan.

The wideband effective loss over a rectangular spectrum Δf wide for M = 3 and N = 2 is approximately:

wideband effective corner loss (dB) (28)

$\approx$ 1/3 max CW corner loss

$\approx$ 0.2 + 0.1 $\approx$ 0.3

A range of values for M and N can be considered for the antenna. Table 5-2 shows five possible sets of values, and the various losses that can be calculated for them. It is seen that if the antenna has less than 3 x 2 feeds, the losses are rather large. Either 4 x 2 or 5 x 3 feeds yields losses that are rather small. Since 8 feeds are less expensive than 15, the 4 x 2 set would probably be preferred over the 5 x 3 set from a cost-effectiveness viewpoint.

The 3 x 2 set with only 6 feeds has only a moderate loss, and may be the most cost-effective choice.

Table 5-2

Antenna Wideband Losses vs Number of Feeds

M x N	1 x 1*	2 x 1	3 x 2	4 x 2	5 x 3
max CW[1] (h)	4.8	1.2	0.5	0.3	0.2
edge loss (v)	1.5	1.5	0.4	0.4	0.2
max CW[1] corner loss	6.3	2.7	0.9	0.7	0.4
wideband[2] effective (h)	1.6	0.4	0.2	0.1	0.05
edge loss (v)	0.5	0.5	0.1	0.1	0.05
wideband[2] effective corner loss	2.1	0.9	0.3	0.2	0.1

*values in this column are rough approximations

(1) max CW loss = one-way loss in dB for a CW signal at ends of an operating band f wide

(2) wideband effective loss = one-way average loss in dB for a wideband signal with rectangular spectrum f wide

It should be noted that the losses shown in table 5-2 and in the formulas occur at the edges or the corners of the fine-steered sub-regions. There is no such loss at the center of each sub-region. Thus the average loss over all scan angles is substantially less than the edge or corner loss. It should also be noted that all of the losses discussed here are one-way losses as opposed to radar round-trip losses.

For the experimental antenna to be developed in this program, there is no need to select a particular set of M x N feeds. The line feed can be moved to many locations in azimuth, and therefore can simulate any reasonable choice of M. Similarly, the radiation of the line feed can be steered to any angle in elevation that represents a reasonable choice of N. Thus a single line feed will provide experimental data that is representative of any likely choice that might be made for the M x N feed system in an operational antenna.

e. Discussion of Possible Wideband Sidelobe Effects

When a phase-scanned array is steered off broadside, the potential exists for a degradation of the wideband sidelobes. An example of such a sidelobe degradation has been described for a series-end-fed linear array having a complete cosine illumination taper, connected to a transmitter providing a short rectangular pulse (refs 13 and 14). In that case, it was assumed that all the sidelobes of the transmitter frequency spectrum contributed to the radiated signal. Those CW frequency components corresponding to the spectrum sidelobes, although weak, can be so different from the center frequency as to steer the antenna main beam well into the pattern sidelobe region, hence raising the effective sidelobe level.

If, on the other hand, we assume a frequency spectrum that has a definite width Δf with no substantial power outside of the Δf band, then there is an opportunity to design the

Ref 13- M.S. Wheeler and D.K. Alexander, "Short Pulse Effects in Traveling-Wave Antennas", Eighth Annual Radar Symposium Record, AD-331299, pp. 293-304; June 1962.

Ref 14- I.W.Hammer, "Frequency-Scanned Arrays", Chapter 13 in the Radar Handbook, edited by M.I.Skolnik, McGraw-Hill Book Co., pp. 13-21 to 13-23; 1970.

antenna so as to avoid steering the main beam much into the sidelobe region for any CW frequency given by the spectrum. (Most transmitting or receiving systems have some form of filtering, either unintended or specifically designed, that limits the bandwidth of a signal). The rectangular spectrum is a simplified example of such a band-limited spectrum. The improvement of antenna pattern characteristics with band limiting has been recognized (refs 11, 15, 16).

With the multibeam wideband antenna proposed by Rotman and Franchi (refs 1, 2, 3), the motion of the main beam over a specified band Δf can be limited to a small fraction of the beamwidth by using a sufficient number of feeds. This small beam motion will lower the wideband effective gain and, correspondingly, widen the wideband effective beamwidth. However the small beam motion will not significantly degrade the wideband sidelobes provided that at any CW frequency within the Δf band the antenna yields its normal low sidelobes.

The most likely source of sidelobe degradation at any CW frequency in the Δf band is the phase shifters in the cylindrical lens. Consideration of the manner in which the phase shifters operate in a phased array leads to the conclusion that if the phase-shifter design is such that its phase shift is constant over the Δf band, then the normal low sidelobes will be preserved for all CW frequencies within this band. Typical ferrite phase shifters tend to have such a constant phase versus frequency characteristic, although exact constancy may not be practical. Typical diode phase shifters do not have constant phase shift with frequency because they typically employ short lengths of switched transmission line, or an equivalent mechanism. However diode phase shifters can be designed to have nearly constant phase over a frequency band, if this is needed.

Ref 15 -W.B.Adams, "Phased-Array Performance with Wideband Signals", Supplement to IEEE Trans. Aerospace and Electronic Systems, Vol. AES-3, No.6, pp. 257-271; November 1967.

Ref 16- M.S.Wheeler, "Pulse Excitation of a Traveling-Wave Array", IEEE Trans. Antennas and Propagation, Vol. AP-20, No.3, pp. 239-244; May 1972.

Suppose that diode switched-line phase shifters having phase shift proportional to frequency are used. Then, for an array that is fine-steered, there will be a sawtooth phase error across the antenna aperture at CW frequencies off the center frequency where presumably the phase setting has been computed. At the ends of the frequency band Δf the magnitude of the sawtooth phase step would be approximately:

$$\Delta \text{phase} \approx \pi \frac{\Delta f}{f} \tag{29}$$

This would result in pairs of sidelobes, the strongest pair having a level of approximately:

$$\frac{\text{amplitude CW sidelobe}}{\text{amplitude CW mainlobe}} \approx \frac{1}{2} \frac{\Delta f}{f} \tag{30}$$

for a CW signal at the ends of a frequency band Δf. For a 400 MHz band at 5.3 GHz, this sidelobe level would be about -34dB. The sidelobe locations off the main beam would, of course, be a function of the fine-steering angle.

It should be noted that, because of the curvature of the outer surface of the cylindrical lens, the period of the sawtooth phase error is only approximately constant across the aperture. Therefore the sidelobe amplitude can be somewhat lower than the value given in (30), particularly for large amounts of fine steering. It should also be noted that the essentially constant periodicity of the sawtooth error exists because, with the true time-delay focusing provided by the cylindrical lens, the phase shifters do not provide collimation of the beam. If the feature of time-delay focusing were sacrificed so that the phase shifters provided collimation (focusing) as well as fine steering, then the sawtooth periodicity would vary across the aperture and the sidelobes would be much lower.

For a wideband signal having an instantaneous bandwidth Δf, the situation is more complex, because the signal waveform and the signal-processing characteristics of the complete system are involved. Assuming a signal having a rectangular spectrum amplitude and a linear spectrum phase, the main-beam signal would have approximately the well-known waveform:

$$\text{mainlobe } E(t) \sim \frac{\sin(\pi \Delta f\, t)}{(\pi \Delta f\, t)} \tag{31}$$

However the sidelobe caused by the sawtooth phase-shifter error would have approximately the following waveform:

$$\text{sidelobe } E(t) \sim \frac{(\pi \Delta f\, t)\cos(\pi \Delta f\, t) - \sin(\pi \Delta f\, t)}{(\pi \Delta f\, t)^2} \tag{32}$$

which has odd symmetry about $t = 0$ where it is zero. The two waveforms are indicated in figure 5-46, together with the CW sawtooth aperture phase error, the resulting CW antenna pattern, and the assumed rectangular spectrum. The reason for the odd symmetry of the wideband sidelobe waveform is the reversal of polarity of the sawtooth phase step with positive or negative frequency deviation from midband.

The effect of this wideband sidelobe waveform on system performance depends on how the signal is processed in a particular system, and on the nature of the target or interfering source in the direction of the sidelobe. One relatively simply but important example is an interfering source radiating noise power. In this case, the energy in the wideband sidelobe waveform, rather than its shape, is most significant. For the case of the assumed rectangular spectrum, this wideband sidelobe energy relative to the

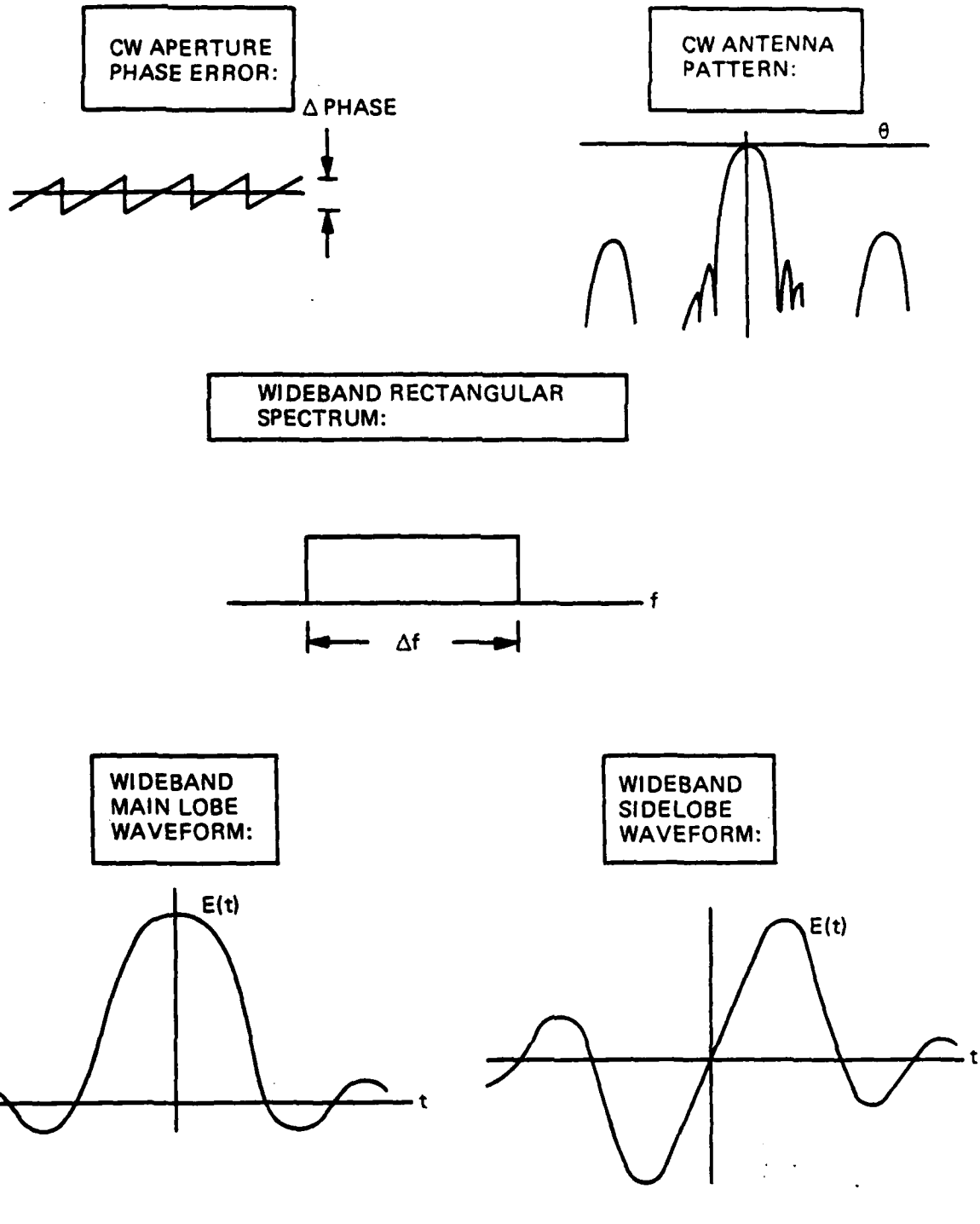

Figure 5-46. Comparison of Theoretical Waveforms for Mainlobe and Wideband Sidelobes Caused by Switched-Line Phase Shifters

mainlobe energy is approximately 1/3 of the energy ratio for the CW end-of-band case previously given. Thus:

$$\frac{\text{energy (wideband effective sidelobe)}}{\text{energy (wideband effective mainlobe)}} \approx \frac{1}{12}\left(\frac{\Delta f}{f}\right)^2 \qquad (33)$$

For the 400 MHz band at 5.3 GHz, this ratio would be about -39dB.

The cylindrical lens antenna has an objective of -50dB for all azimuth sidelobes except those close to the main beam. A -39dB effective level for the wideband sidelobe pair is therefore undesirable. This implies that fine steering in the wideband cylindrical lens antenna should be obtained with phase shifters that provide phase shift that is essentially invariant with frequency. This would avoid the sawtooth phase error and its resulting pairs of wideband sidelobes.

f. Summary

This section has described the factors involved in obtaining good performance from the multibeam cylindrical lens antenna over wide electronic scan angles with wide signal bandwidths.

An effective wideband scanning loss has been determined for the case of a wide rectangular frequency spectrum. This loss has been defined for both 1-dimensional and 2-dimensional scan. For the cylindrical lens antenna being designed in this program, the tradeoff between number of feeds and various scanning losses has been determined for a signal having a 400 MHz wide rectangular spectrum. Either 3 x 2 or 4 x 2 feeds appears to be a reasonable choice for such an antenna.

The potential creation of effective wideband sidelobes caused by fine steering with switched-line phase shifters has been described. For a signal having a 400 MHz wide rectangular spectrum, these effective sidelobes have significant levels. Therefore phase shifters designed for invariant phase versus frequency would be more appropriate for use in this low side-lobe wideband scanning antenna.

SECTION VI

LENS INTERNAL REFLECTIONS

A basic problem of lens antennas is the reflection that occurs at the lens surfaces. As discussed in section IV, the surfaces of the cylindrical lens to be developed will encounter a wide range of incidence angles as well as a range of frequencies. Therefore, a significant reflection can be expected at these surfaces. With the constant-W lens the reflections create specific performance problems, as will be described.

6.1 EFFECT OF LENS REFLECTIONS

When the antenna is transmitting, the reflection at the outer surface returns to the inner surface where there is another reflection. This doubly-reflected wave now radiates through the outer surface of the lens, and adds an undesired component to the radiation pattern of the antenna.

a. Without Fine Steering

When the constant-W lens is operating without fine steering, all of the paths in the lens have the same electrical length. Therefore the doubly-reflected wave is collimated toward essentially the same far-field direction as is the desired wave. Figure 6-1 shows this case, and indicates the relative strength of the doubly-reflected wave in terms of the effective values of the two reflection coefficients involved.

If the surface reflection coefficients were constant over the lens surface, the only effect of the doubly-reflected wave on antenna performance would be to cause a periodic variation of antenna gain with frequency, as indicated in figure 6-1. The peak-to-peak variation of gain in dB is approximately:

$$\Delta \text{Gain (dB)} \approx 17.4\ \rho_i\ \rho_o \qquad (34)$$

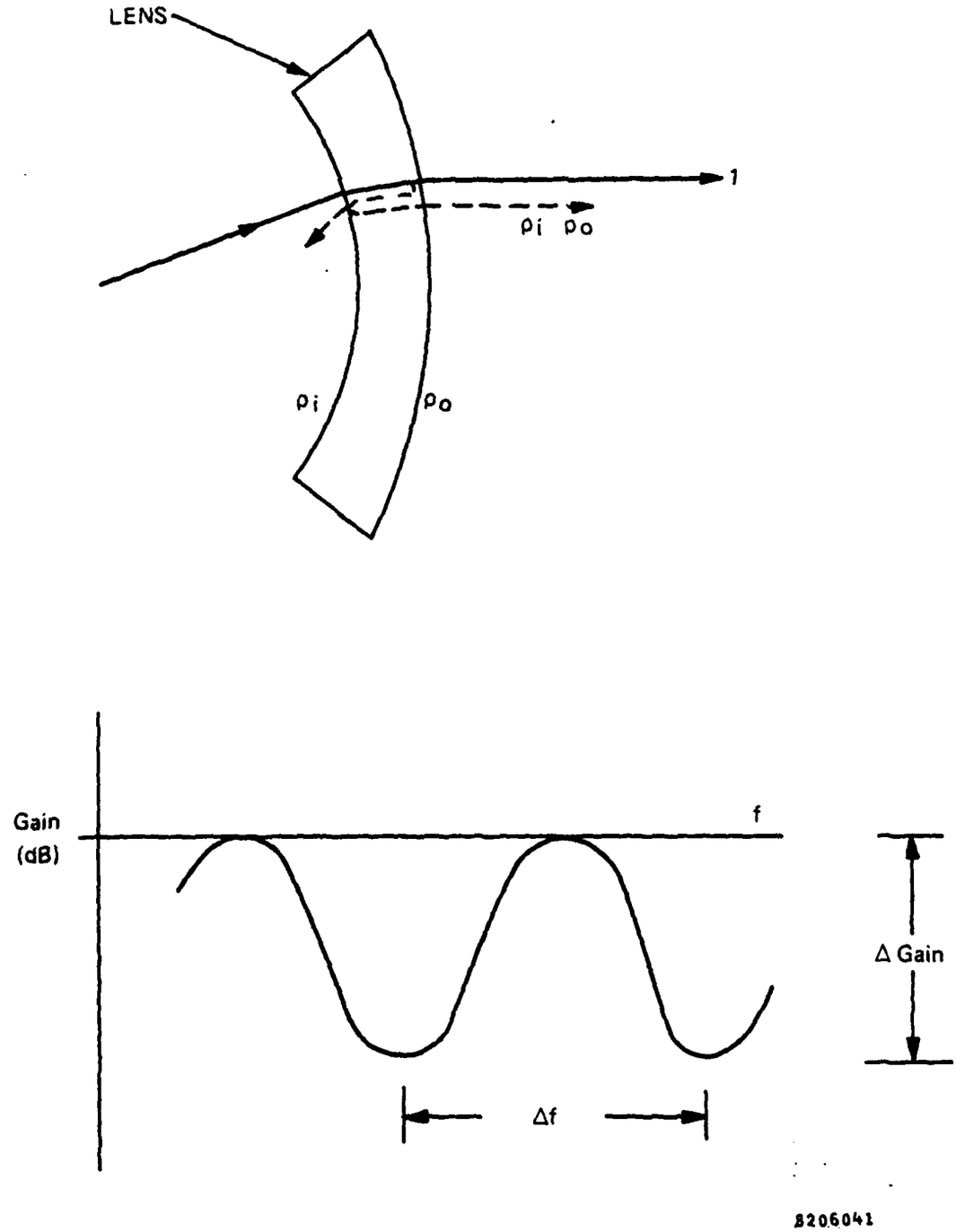

Figure 6-1. Effect of Lens Internal Reflections Without Fine Steering

where ρ_i and ρ_o are the effective reflection coefficient magnitudes of the inner and outer surfaces, respectively, and are assumed to be small. When the two lens surfaces have the same reflection coefficients, the value of gain at the upper peaks of the periodic curve is equal to the gain that would exist if the lens surfaces were perfectly matched, and ΔGain represents the loss at the lower peaks of the curve. The periodicity of the gain variation is approximately:

$$\Delta f \approx \frac{c}{2W} \approx f \frac{\lambda}{2W} \qquad (35)$$

where W is the electrical path length in the lens and c is the velocity of light in free space. As an example, if $\rho_i = \rho_o = 0.2$ then ΔGain is about 0.7 dB. If W = 2 feet then Δf is about 250 MHz.

It should be noted that the multiple reflection within the lens could also affect the temporal performance of the system, which has an instantaneous bandwidth of 400 MHz. The first echo from the multiple reflection would be delayed about 4ns if W = 2 feet, which is in the time-sidelobe region of a narrow compressed pulse that corresponds to an assumed 400 MHz rectangular frequency spectrum. This subject is beyond the scope of our investigation.

So far in this discussion, it has been assumed that the reflection coefficients are essentially constant over the lens surfaces. Actually, the reflection coefficients vary because of the variation of incidence angle over the surface (see figure 4-14). As a result, the far-field pattern of the doubly-reflected wave is not identical to the pattern of the desired wave. Therefore the double reflection may cause some increase of antenna pattern sidelobes. In addition, even the directly transmitted wave undergoes some amplitude and phase distortion over the lens aperture because of the array impedance variation with incidence angle. These effects will be analyzed later.

b. With Fine Steering

When the constant-W lens is operating with fine steering, the paths in the lens have a progressive increase of electrical length across the lens aperture because of the action of the phase shifters in the lens. Assuming that

these phase shifters are reciprocal devices (using PIN diodes rather than ferrites), the doubly-reflected wave encounters three times the electrical length as does the desired wave. Consequently, the doubly-reflected wave is fine-steered by about three times the angle that the desired wave is steered. This is indicated in figure 6-2.

The result is the creation of a new sidelobe component at an angle 2δ from the main beam, where δ is the main-beam fine-steering angle. The amplitude of this sidelobe component relative to the main-lobe peak is approximately:

$$\frac{E \text{ (sidelobe)}}{E \text{ (main lobe)}} \approx \rho_i \rho_o \qquad (36)$$

This approximate relation assumes that the reflection coefficients are small and that the fine-steering angle δ is small. It also assumes that the reflection coefficients are constant over the lens aperture, creating a beam sidelobe that is as narrow as the main lobe. As an example of equation 36, if $\rho_i = \rho_o = 0.2$, the resulting sidelobe component would be approximately -28 dB relative to the main-beam peak.

The values for ρ_i and ρ_o are effective values representing a weighted average over the lens aperture; these values may be difficult to determine accurately. Also, when the reflection coefficients are not constant over the lens aperture, the sidelobe beamwidth is broadened and its gain may be reduced. Further, when the reflection coefficients are not small, higher-order multiple reflections will create additional sidelobe components at 4δ, 6δ, etc, away from the main beam that may have significant levels. An additional factor that is not covered by equation 36 is the defocusing of the spurious beams by the curved lens surface when δ is not small. All of these factors are included in the analysis given in the next section.

6.2 ANALYSIS OF LENS REFLECTION EFFECTS

In the preceeding discussion, an approximate viewpoint was given for the effect of lens internal reflections, both with and without fine steering. Now an analysis will be given that permits a more accurate computation of the sidelobes that are obtained with the lens antenna when the lens surface impedance is known.

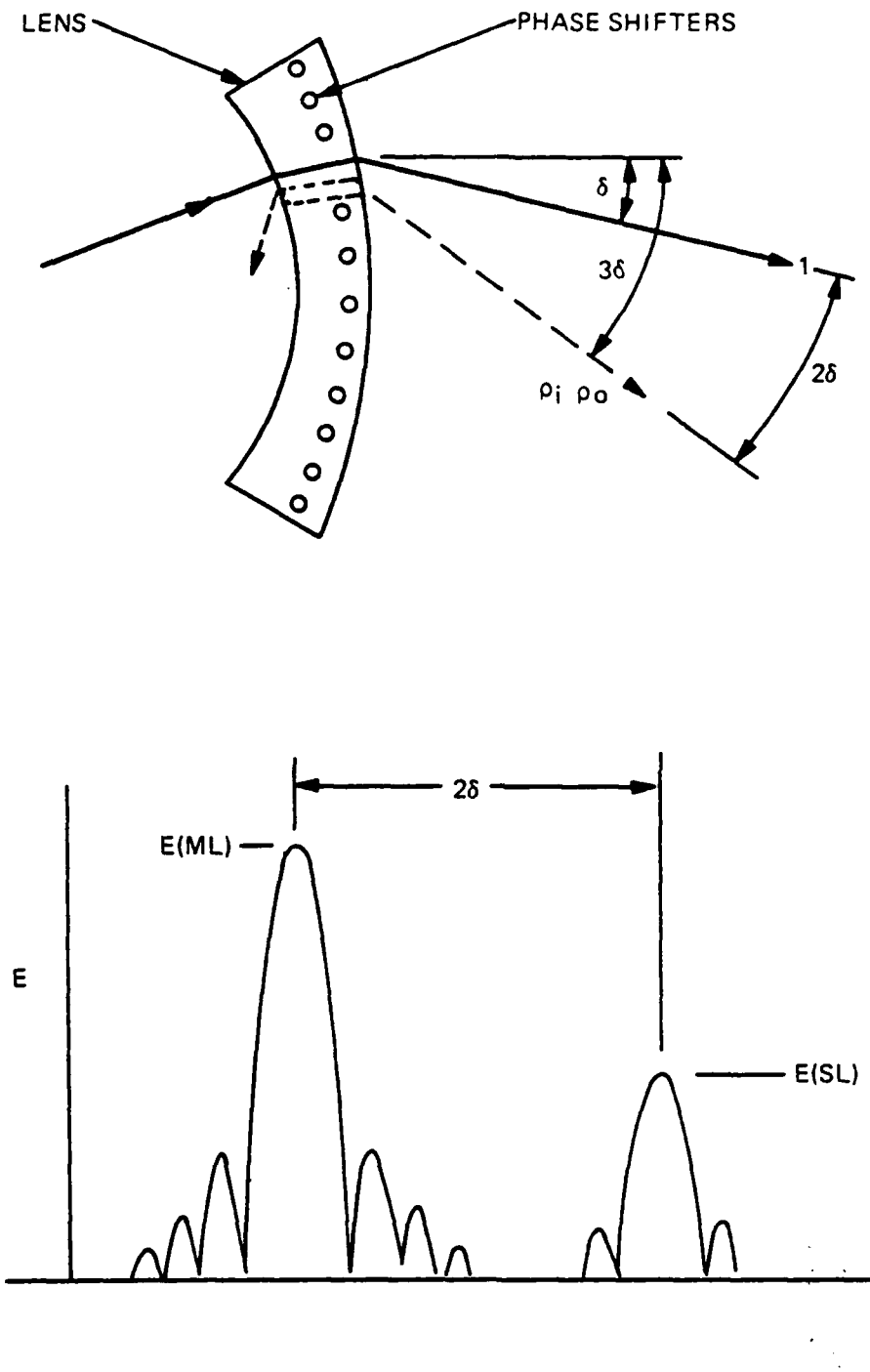

Figure 6-2. Effect of Lens Internal Reflections With Fine Steering

a. Inclusion of Lens Impedance in Pattern Computation

Computation of the far-field patterns of the R-2R cylindrical lens antenna is performed in accordance with the viewpoint given at the end of paragraph 4.2. The radiation pattern amplitude of the line feed is applied directly to the excitation amplitude of the appropriate array elements in the outer surface of the lens, which ideally radiate with essentially a cosine power pattern. A computer sums the contribution from all the elements in the proper amplitude and phase to obtain the far-field antenna pattern.

When the impedance of the lens surface arrays is not perfectly matched, both the amplitude and the phase of the excitation amplitude is modified for each element in the surface array. This modification factor will be designated T because it can be regarded as an overall transmission coefficient for each path in the lens. The following relationship has been derived for T:

$$T = \frac{4R\left[\frac{1 + R - jX}{(1 + R)^2 + X^2}\right]^2}{1 - \left[\frac{R - 1 + jX}{R + 1 + jX}\right]^2 \exp\frac{-j4\pi W}{\lambda}} \qquad (37)$$

where R and X are the resistance and the reactance of the array element relative to the resistance of the lens transmission line, and W is the electrical length of the lens transmission line. Both R and X are a function of the incidence angle ψ, which varies across the curved surface of the lens as was given in equation 8 and was shown in figure 4-14. The formula assumes that the impedance is the same for the inner and outer surface elements. This implies that the same elements are used for the inner and outer surface arrays, and that ψ is the same for corresponding

elements on the inner and outer surface. The latter condition is exactly correct for an R-2R lens with no fine steering. The formula includes the effect of all multiple reflections inside the lens, as well as the direct amplitude and phase distortion caused by the array impedance variation.

The electrical length W of the lens transmission lines in formula 37 is the sum of the constant length W_o plus a variable length ΔW that is equivalent to that of the phase shifter for fine steering. This can be expressed by the following formula:

$$W = W_o + \Delta W$$

$$\Delta W = Fh\left(\sin\delta\cos\alpha + \sin^2\frac{\delta}{2}\sin\alpha\right) \qquad (38)$$

$$+ F\left(\sqrt{1 - h^2} - 1\right)\left(\sin\delta\sin\alpha - \sin^2\frac{\delta}{2}\cos\alpha\right)$$

where h is the normalized vertical coordinate of an outer-surface array element, F is the lens focal length (to which h is normalized), δ is the fine-steering angle, and α is the coarse-steering angle.

The inclusion of formulas 37 and 38 into the computation of the far-field patterns of the lens antenna permits an evaluation of the pattern sidelobe degradation that would be caused by the lens internal reflections, either with or without fine steering. To accomplish this, it is necessary to know the resistance (R) and the reactance (X) of the surface array elements as a function of the incidence angle (ψ). This is discussed in the following paragaphs.

b. Impedance of Typical Elements for Lens Surface

It is intended to use strip transmission line for the lens medium. A convenient type of array element is a strip dipole, because it can be printed together with the strip transmission line without requiring connections. Since the antenna polarization can be either vertical or horizontal, the dipole orientation can be vertical or horizontal. A vertical orientation would use vertically-oriented stripline boards, each board having a different width in the cylindrical lens. A horizontal orientation would use horizontally-oriented stripline boards, all essentially identical in the cylindrical lens.

Vertical Dipoles. Figures 6-3 and 6-4 show the variation of resistance and reactance with incidence angle in the H plane, for dipoles a quarter wavelength over a ground plane in a large, closely spaced array. The resistance is normalized to its value at normal incidence, and the reactance is tuned out at normal incidence as well as normalized to the resistance at normal incidence. Thus the array is assumed to be impedance matched at normal incidence.

The impedance variation shown in the figure illustrates the well-known result that the resistance variation is small, but the reactance variation is large in the H plane. A vertically oriented dipole on the lens surface could encounter incidence angles out to at least 60^{o} (75^{o} with fine steering) in the H plane, as was shown in figure 4-14.

Horizontal Dipoles. Figures 6-5 and 6-6 show the variation of resistance and reactance in the E plane for a similar array of dipoles a quarter wavelength over a ground plane. Here also is seen the well-known result, that the resistance variation is large in the E plane. The reactance variation, which is somewhat dependent on the element spacing chosen in the E plane, is fairly small. A horizontally oriented dipole on the lens surface could encounter incidence angles out to at least 60^{o} (or 75^{o}) in the E plane, as shown in figure 4-14.

The reflection coefficient for either of these orientations is approximately 0.2 at 30^{o} incidence, and is greater than 0.5 at 60^{o} incidence. Also, for the vertical orientation there is a substantial transmission-phase distortion caused by the reactance variation. Thus it would be anticipated from the discussion in paragraph 6.1 that a significant degradation of sidelobe performance would occur because of the wide-angle reflection of the array.

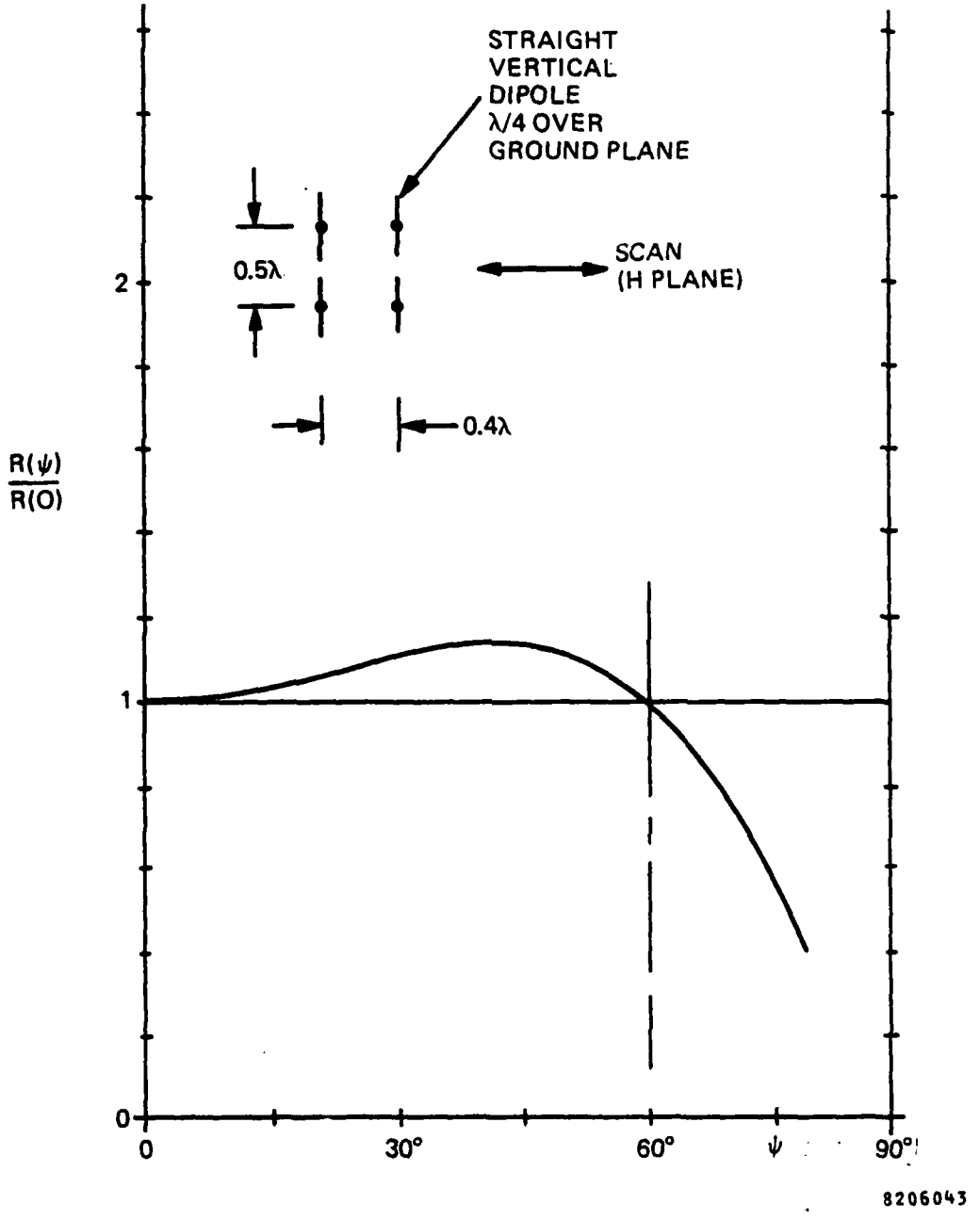

Figure 6-3. Typical Array Resistance vs Angle for Straight Dipole in H Plane

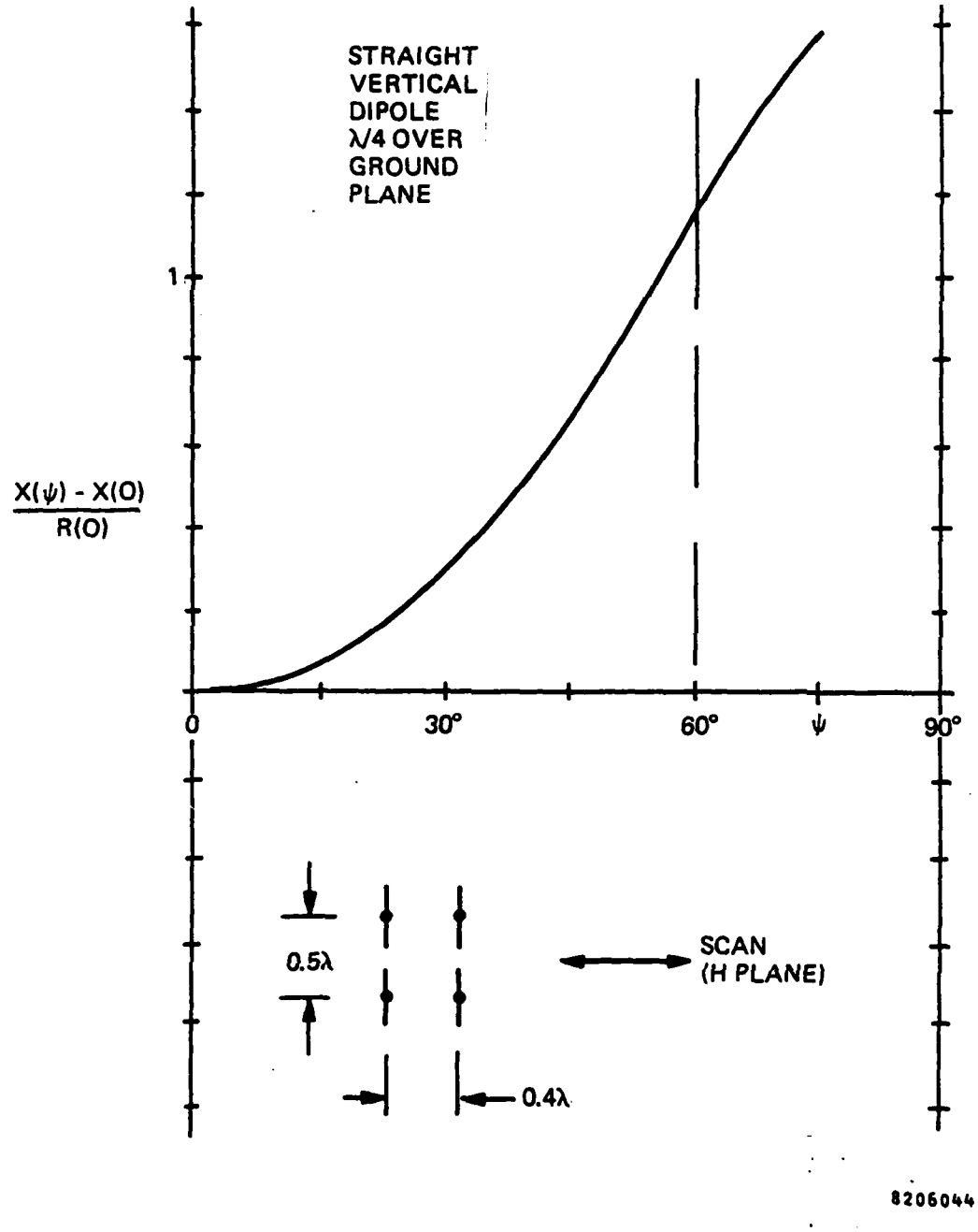

Figure 6-4. Typical Array Reactance vs Angle for Straight Dipole in H Plane

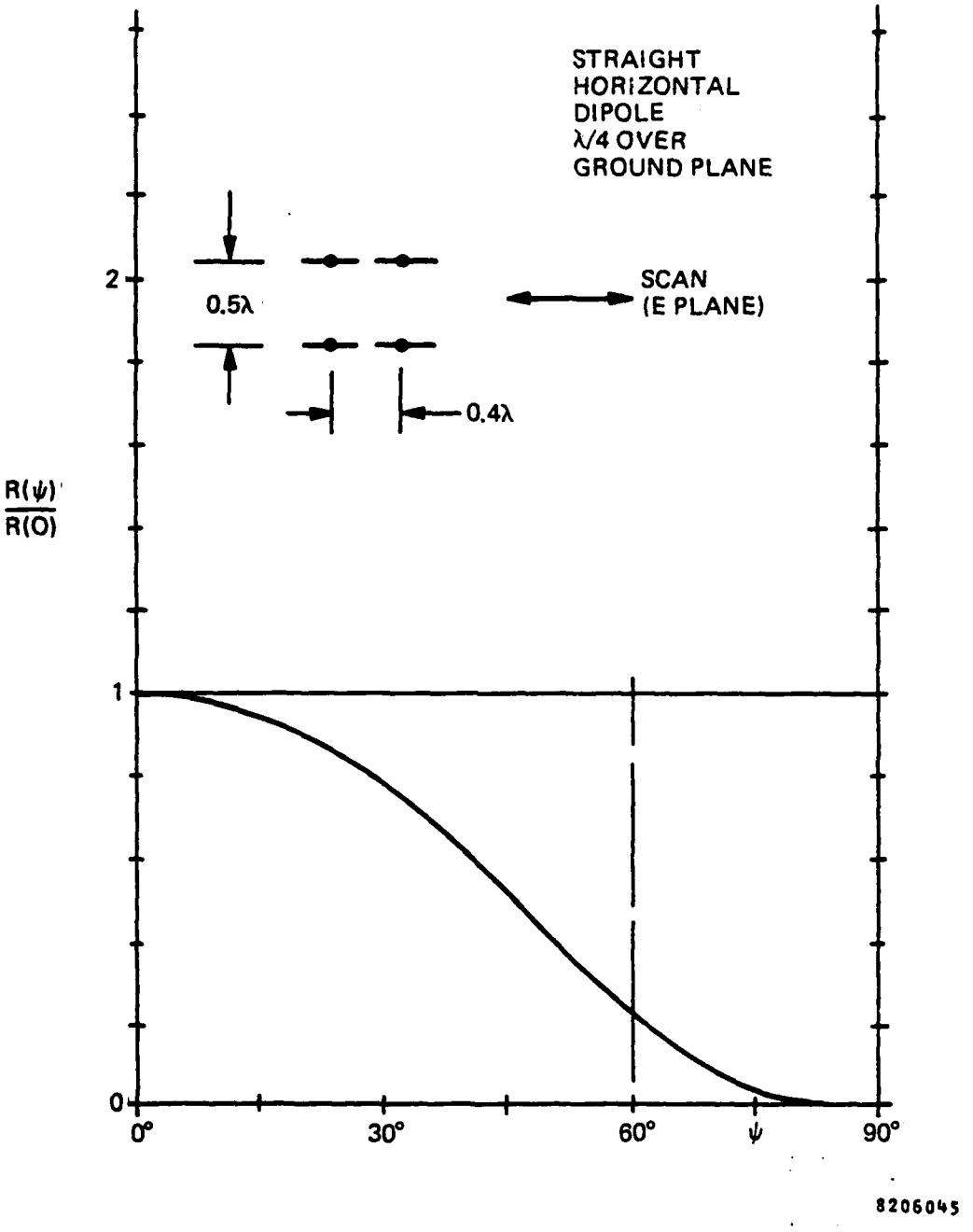

Figure 6-5. Typical Array Resistance vs Angle for Straight Dipole in E Plane

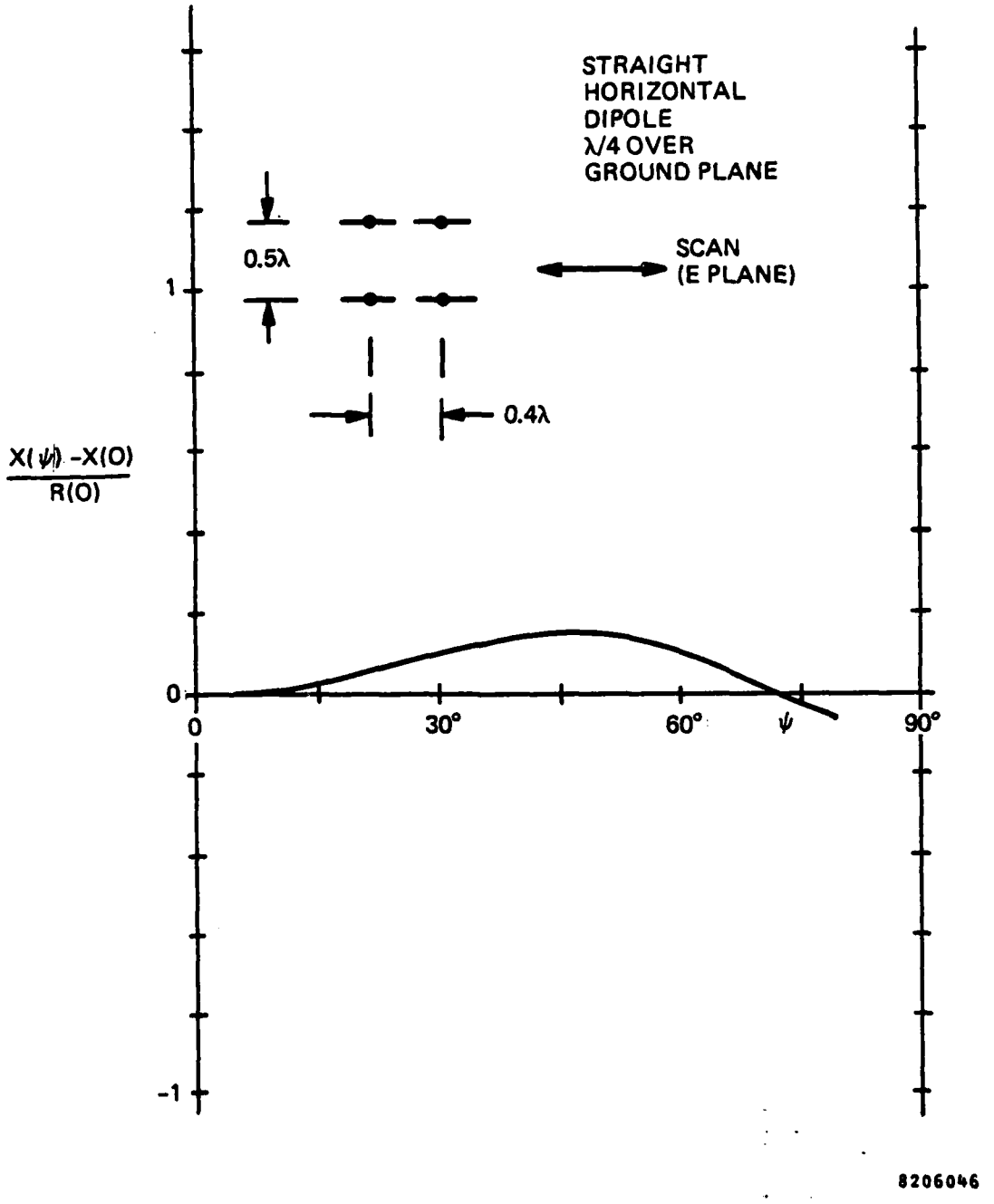

Figure 6-6. Typical Array Reactance vs Angle for Straight Dipole in E Plane

In addition to the impedance variation with incidence angle, the array elements will also have an impedance variation with frequency. Over the 5.0 to 5.6 GHz operating band, a typical VSWR at normal incidence for a wideband-matched dipole might be 1.5, corresponding to a 0.2 reflection coefficient. Therefore, the wideband reflection of the array may also contribute to degradation of the sidelobe performance. Furthermore, it often happens that when an array is operating at an incidence angle where its wide-angle match is not good, its wideband match is considerably poorer than it is at normal incidence.

c. Computed Effect of Typical Elements on Sidelobes

The basic patterns of the antenna without lens-surface-array reflections were given in paragraph 5.1. Now these patterns can be recomputed to include the effect of the impedance variation of typical array elements at the lens surfaces. Equations 37 and 38 are employed, together with the appropriate array impedance variations, to yield a new set of antenna patterns.

Without Fine Steering. First the case of a beam with no fine steering and no coarse steering is examined. The previously computed variations of impedance with incidence angle are used for both a vertical-dipole and a horizontal-dipole lens array, as were shown in figures 6-3 through 6-6. Also included is a broadside reflection coefficient of 0.2 to represent a typical wideband impedance.

The azimuth patterns with these two lens-array elements are shown in figures 6-7 and 6-8. Comparison of these patterns with the pattern of figure 5-6 shows only a slight distortion from the lens internal-reflection effect for this case having no fine or coarse steering.

With Fine Steering. Now some cases that include fine steering are examined for a coarse-steering angle of 30°, giving substantial reflection in the center of the lens. The broadside reflection coefficient of the array element is assumed to be zero, in order to clearly show the effect of the wide-angle array mismatch.

Figures 6-9 and 6-10 show the azimuth patterns for a fine-steering angle (δ) of -5° and $+5^{\circ}$, and with the vertical-dipole array element. Figures 6-11 and 6-12 show the same two cases with the horizontal-dipole element. In all these patterns a strong sidelobe is seen at approximately 2δ away from the main lobe. This is the spurious beam caused by the

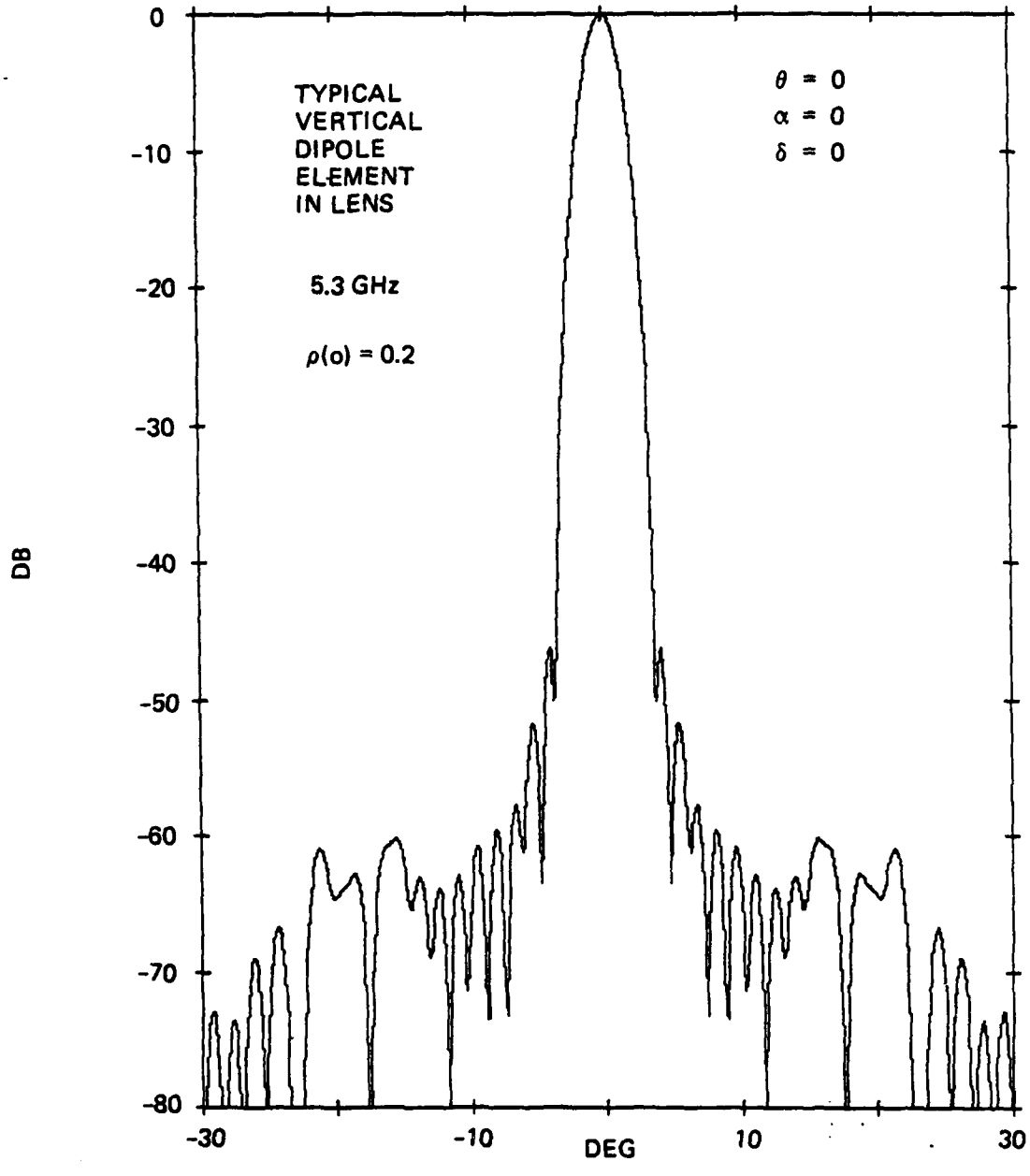

Figure 6-7. Azimuth Pattern of Antenna with Typical Vertical-Dipole Element, $\theta = 0$

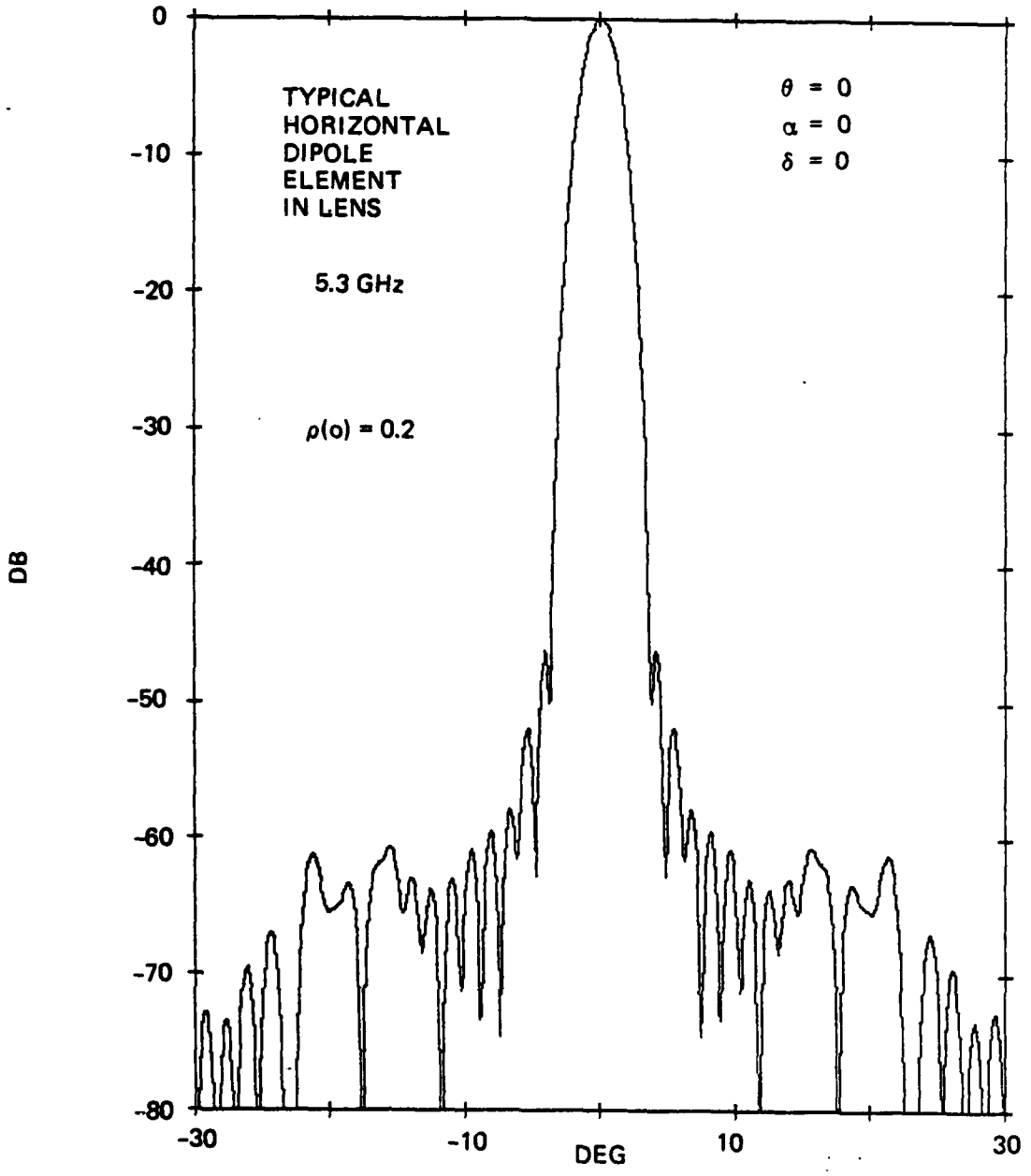

Figure 6-8. Azimuth Pattern of Antenna with Typical Horizontal-Dipole Element, $\theta = 0$

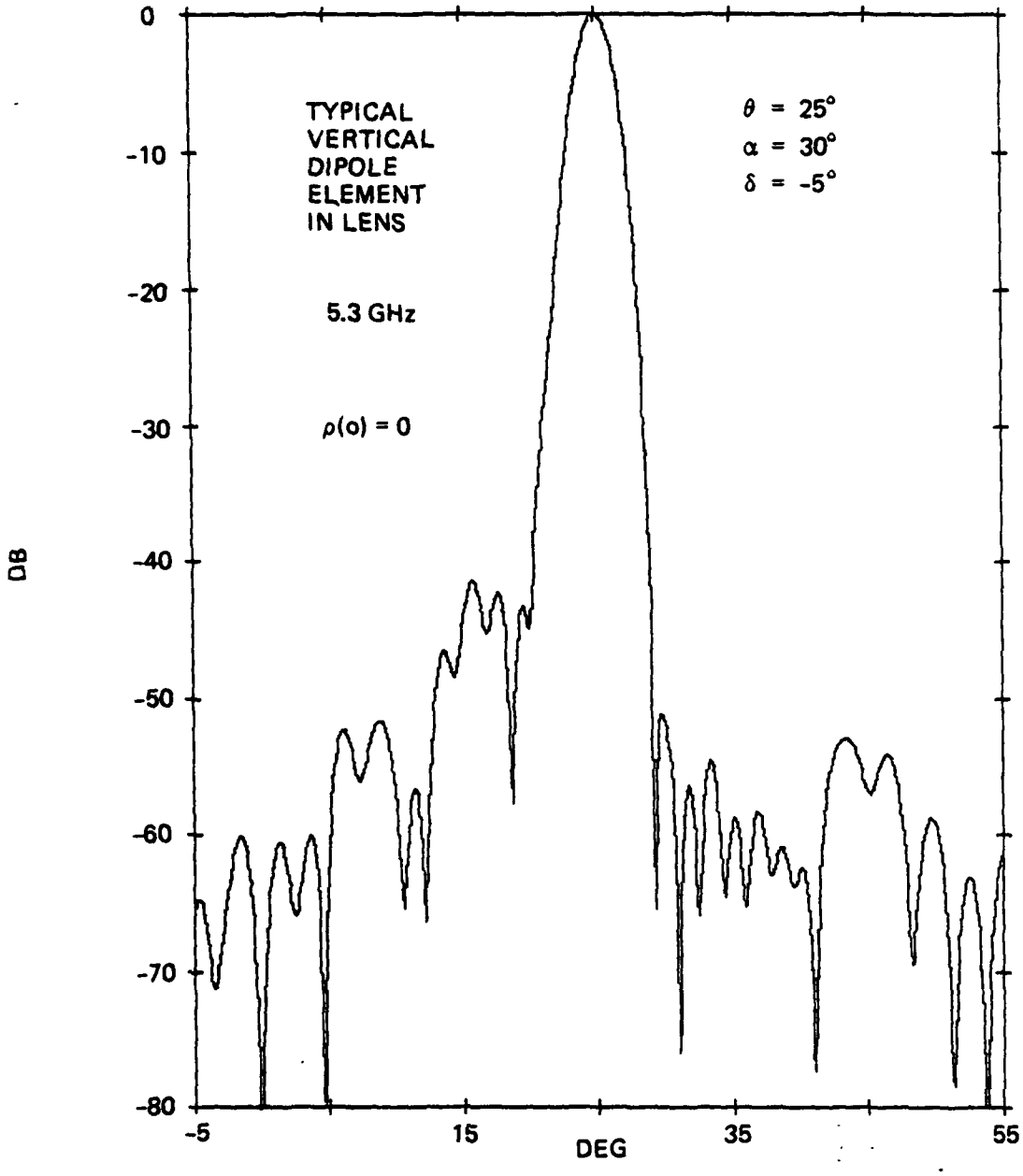

Figure 6-9. Azimuth Pattern of Antenna with Typical Vertical-Dipole Element, $\alpha = 30^{\circ}$, $\delta = -5^{\circ}$

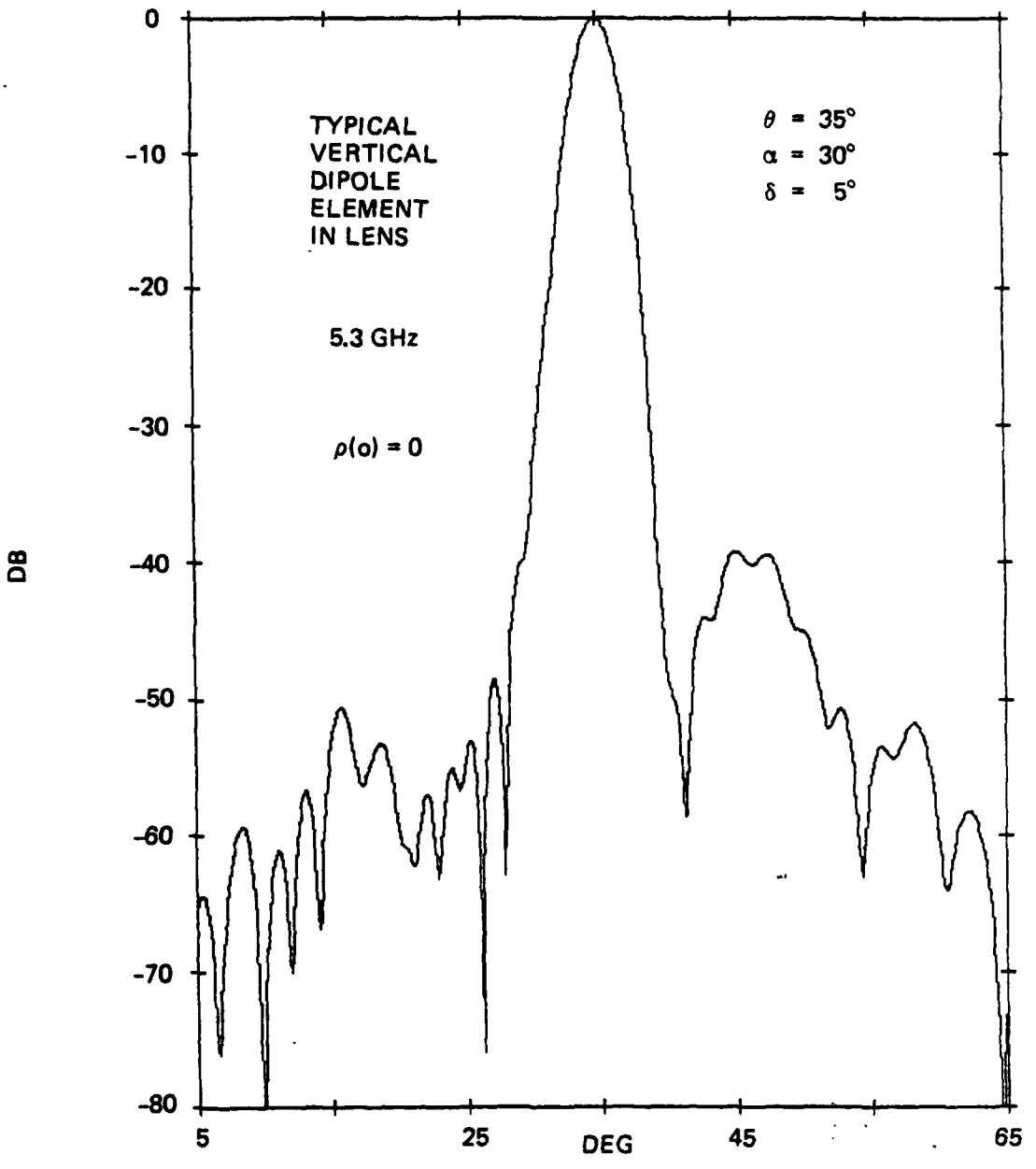

Figure 6-10. Azimuth Pattern of Antenna with Typical Vertical-Dipole Element, $\alpha = 30^{\circ}$, $\delta = 5^{\circ}$

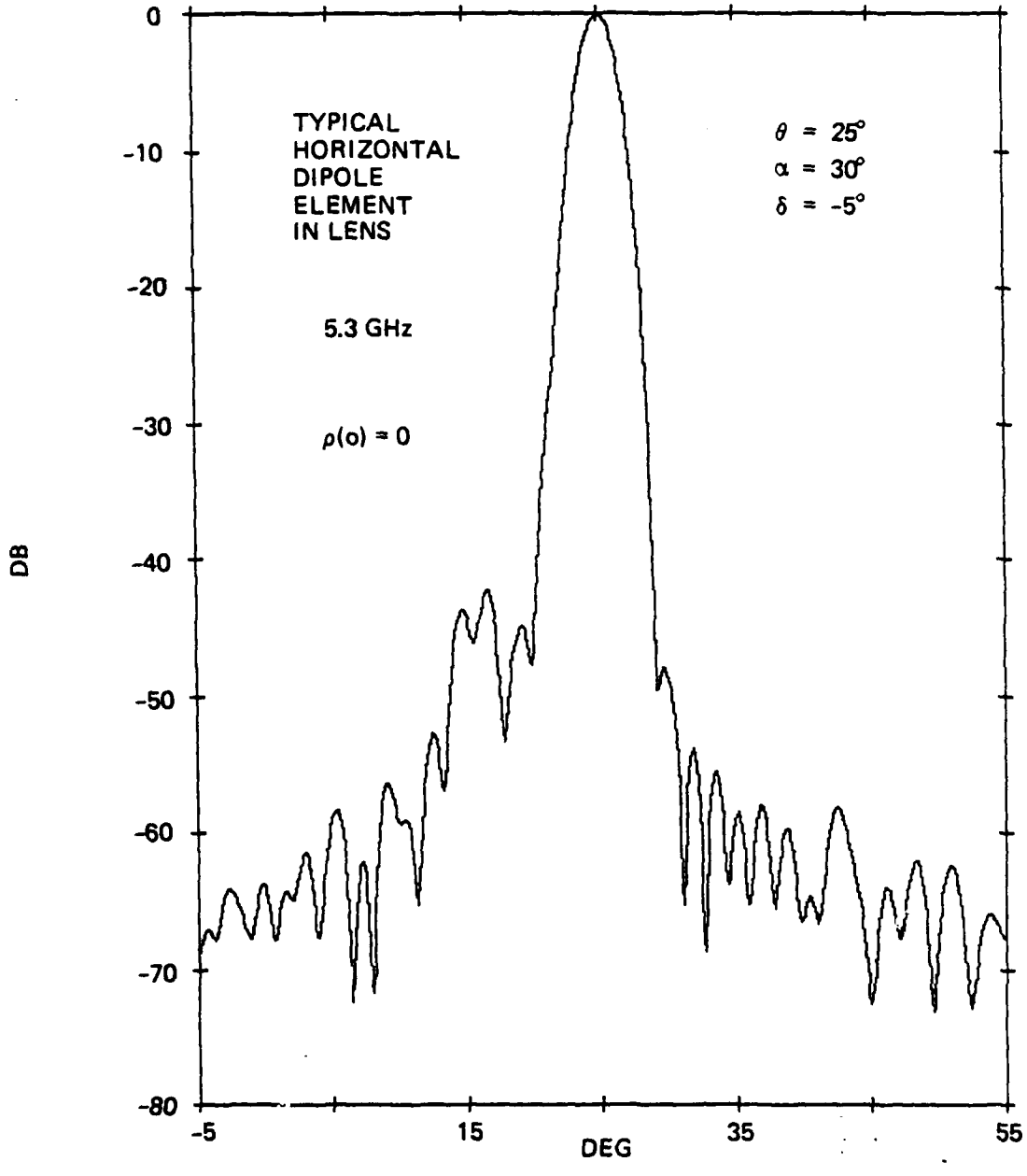

Figure 6-11. Azimuth Pattern of Antenna with Typical Horizontal-Dipole Element, $\alpha = 30^{o}$, $\delta = -5^{o}$

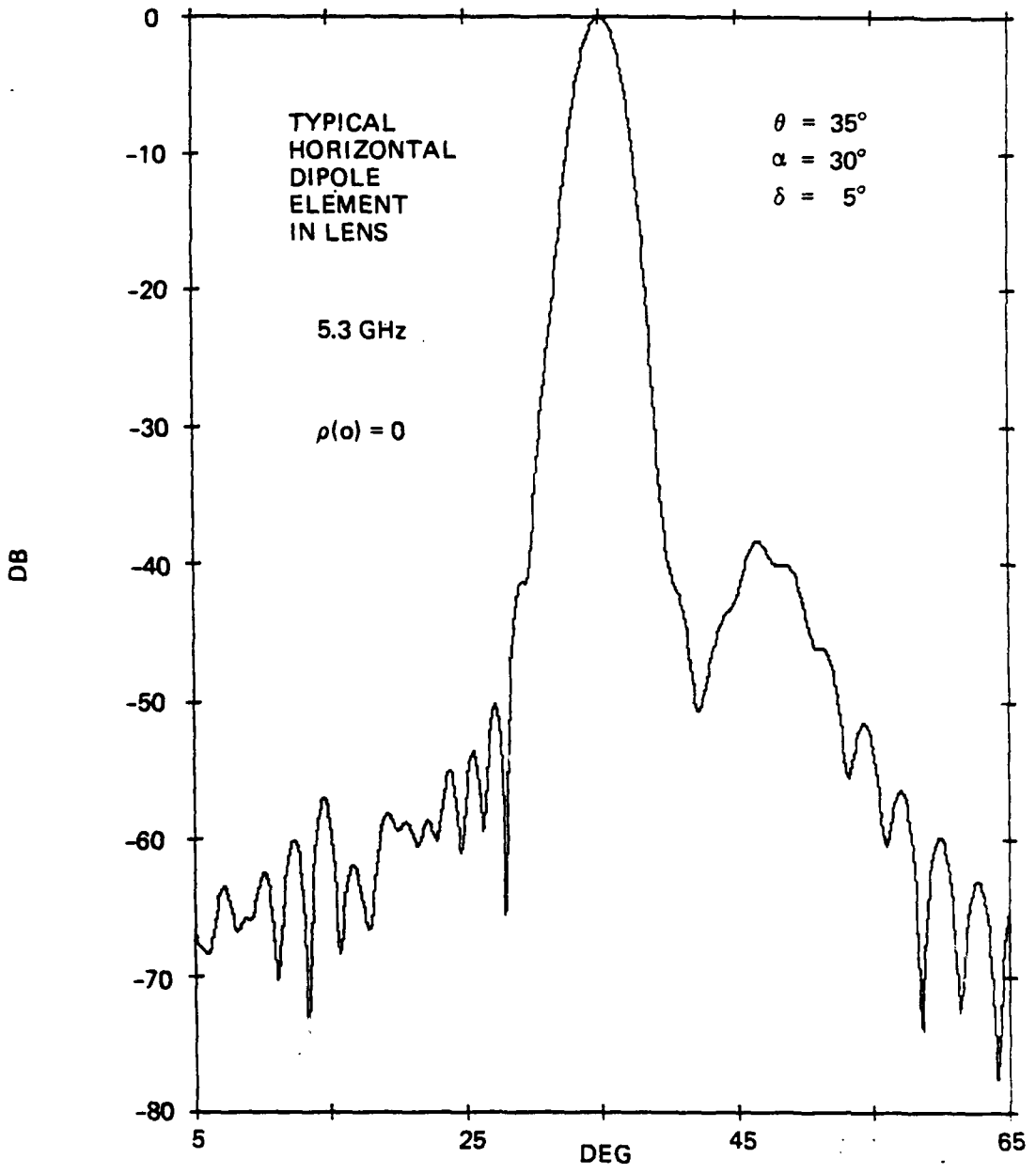

Figure 6-12. Azimuth Pattern of Antenna with Typical Horizontal-Dipole Element, $\alpha = 30^{\circ}$, $\delta = 5^{\circ}$

first-order lens internal reflection that was discussed in paragraph 6.1. Also, there can be seen in some of the patterns the much weaker second-order internal reflection radiating at an angle about 4 δ away from the main lobe.

Figures 6-13, 6-14, 6-15, and 6-16 show a similar set of azimuth patterns for a fine-steering angle (δ) of -10^{o} and $+10^{o}$. Again, a strong sidelobe is seen at about 2 δ from the main lobe. Since the strength of this sidelobe is close to that of the $\delta = \pm 5^{o}$ cases, it is evident that even when δ is large, there is not much benefit to be gained from the defocusing of the spurious beam caused by the curved lens surface.

The spurious-beam sidelobe caused by the lens internal reflection is clearly a serious problem when the antenna is fine-steered. The level of this spurious beam for the cases shown is in the -38 to -45 dB region, which is much stronger than the -50 dB level that is desired for sidelobes not near the main beam. An improvement is clearly wanted.

Effect of Feed Repositioning. Before discussing potential improvements, one question that arises is: what is the effect of the feed repositoning on the spurious-beam sidelobes? All of the azimuth patterns in figures 6-9 through 6-16 are computed for the case in which the line feed has the tilt and refocus that was discussed in paragraph 5.1. To answer this question, one azimuth pattern is computed for vertical dipoles with the line feed in its nominal position (not tilted or refocused) for $\alpha = 30^{o}$ and $\delta = 5^{o}$. Figure 6-17 gives this pattern. Comparison with the corresponding case that was given in figure 6-10 shows that a significantly lower level of the spurious beam is obtained with the repositioned feed. This is believed to be primarily the result of the reduced incidence angles encountered by the strong portion of the lens illumination when the feed is tilted. With only the 5^{o} reduction of effective incidence angles resulting from the 5^{o} feed tilt, the effective reflection coefficients of the lens surface arrays are significantly reduced.

Another question of interest is: how does the level of the spurious beam in these computed patterns compare with the level that would be obtained with the simple approximate relation of formula 36? For the vertical-dipole case with $\alpha = 30^{o}$ and $\delta = 5^{o}$, the simple formula yields a level of about -30dB for the spurious beam, based on the reflection coefficient at the center of the lens array. The -35 dB level obtained in figure 6-17 with the nominal feed position is somewhat lower, probably because the spurious beam is

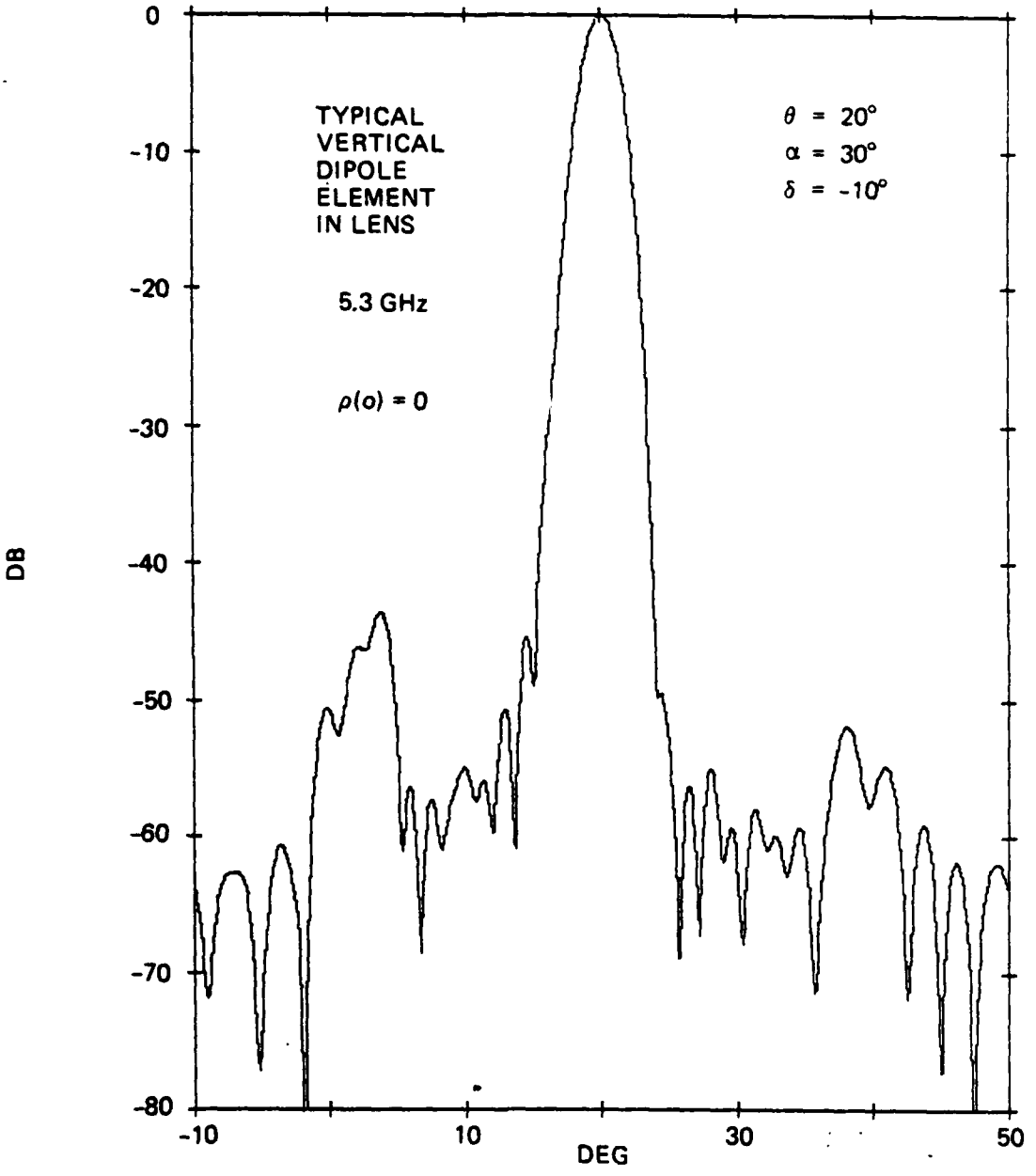

Figure 6-13. Azimuth Pattern of Antenna with Typical Vertical-Dipole Element, $\alpha = 30^{\circ}$, $\delta = -10^{\circ}$

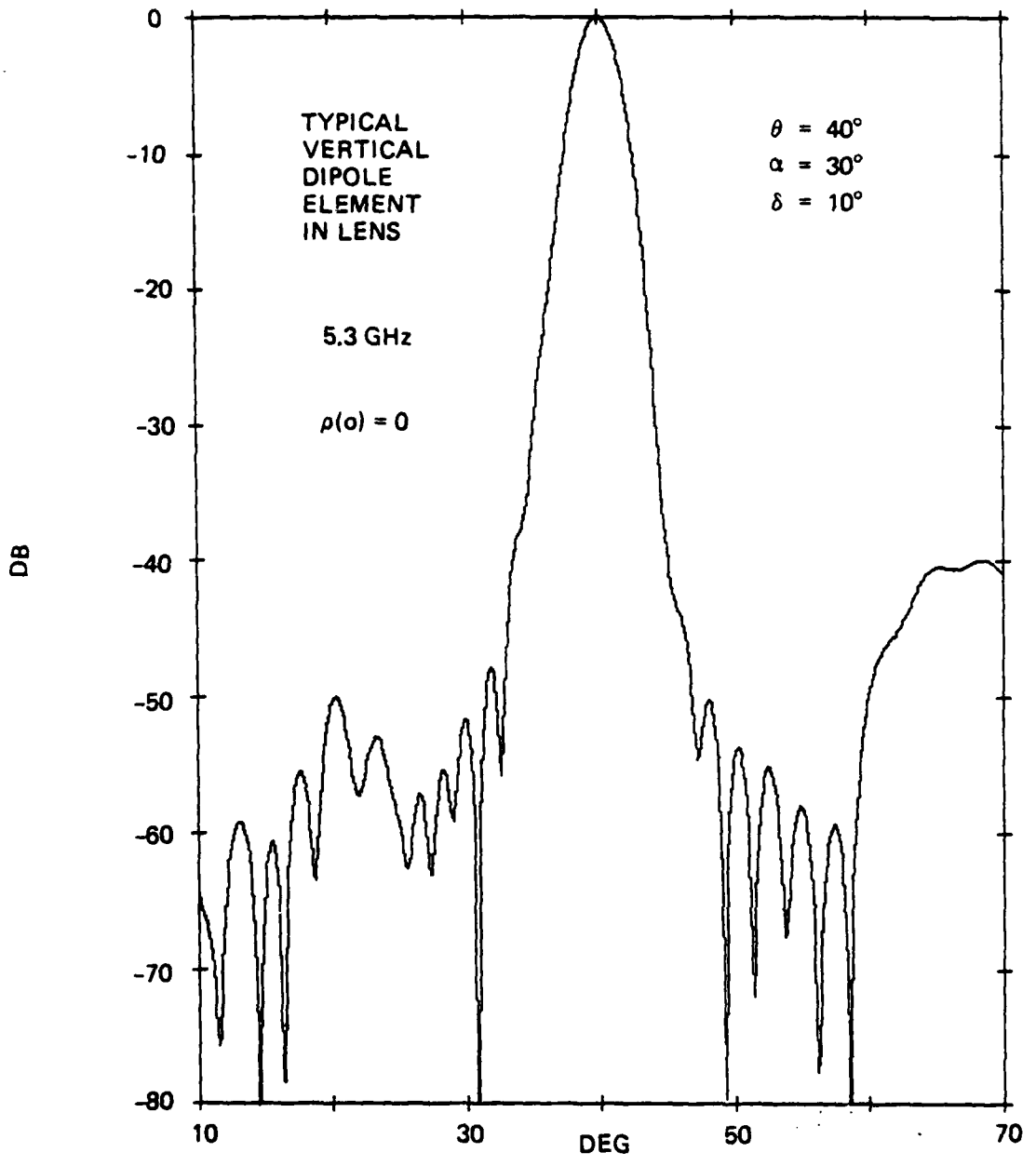

Figure 6-14. Azimuth Pattern of Antenna with Typical Vertical-Dipole Element, $\alpha = 30^{\circ}$, $\delta = 10^{\circ}$

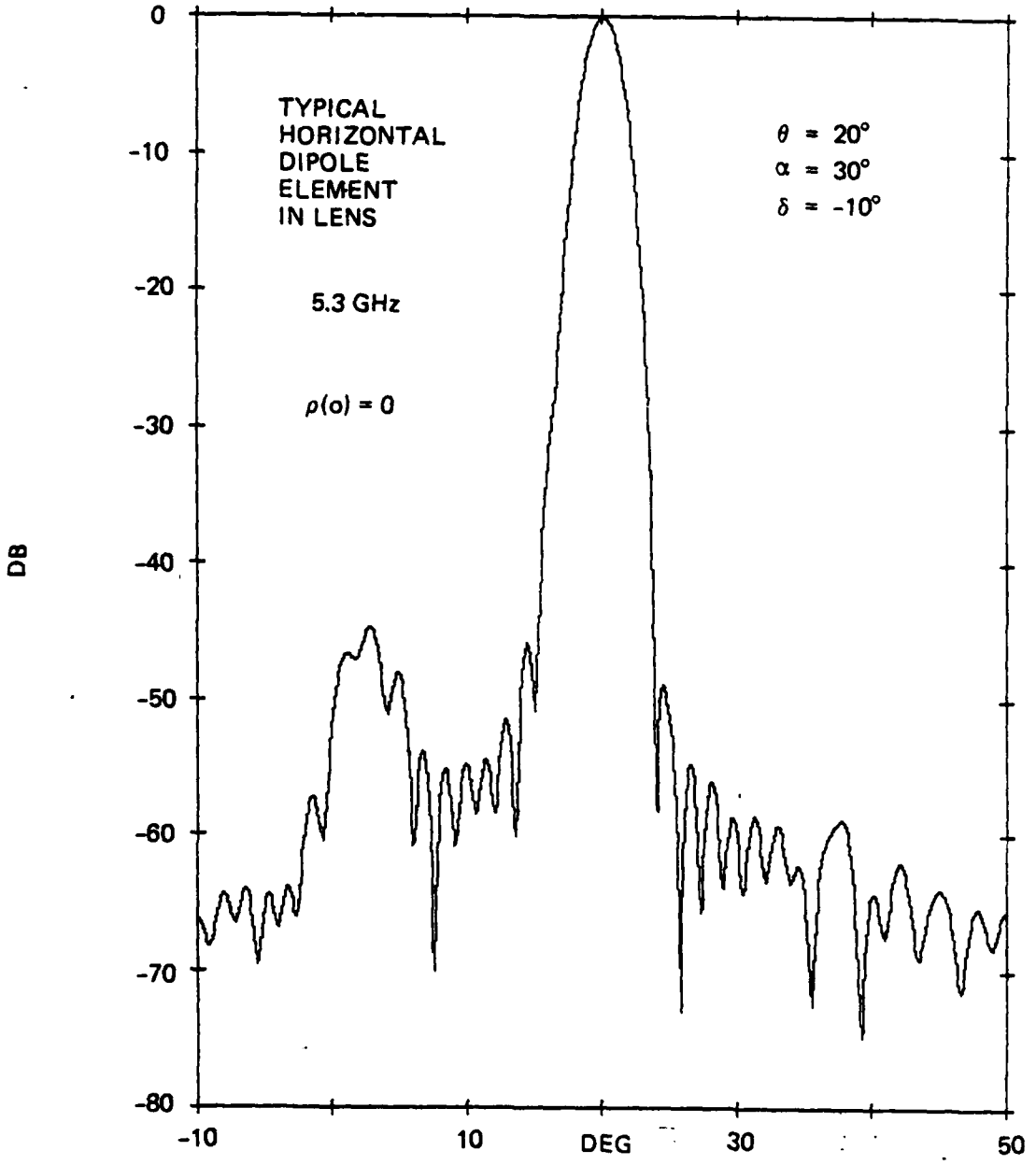

Figure 6-15. Azimuth Pattern of Antenna with Typical Horizontal-Dipole Element, $\alpha = 30^{\circ}$, $\delta = -10^{\circ}$

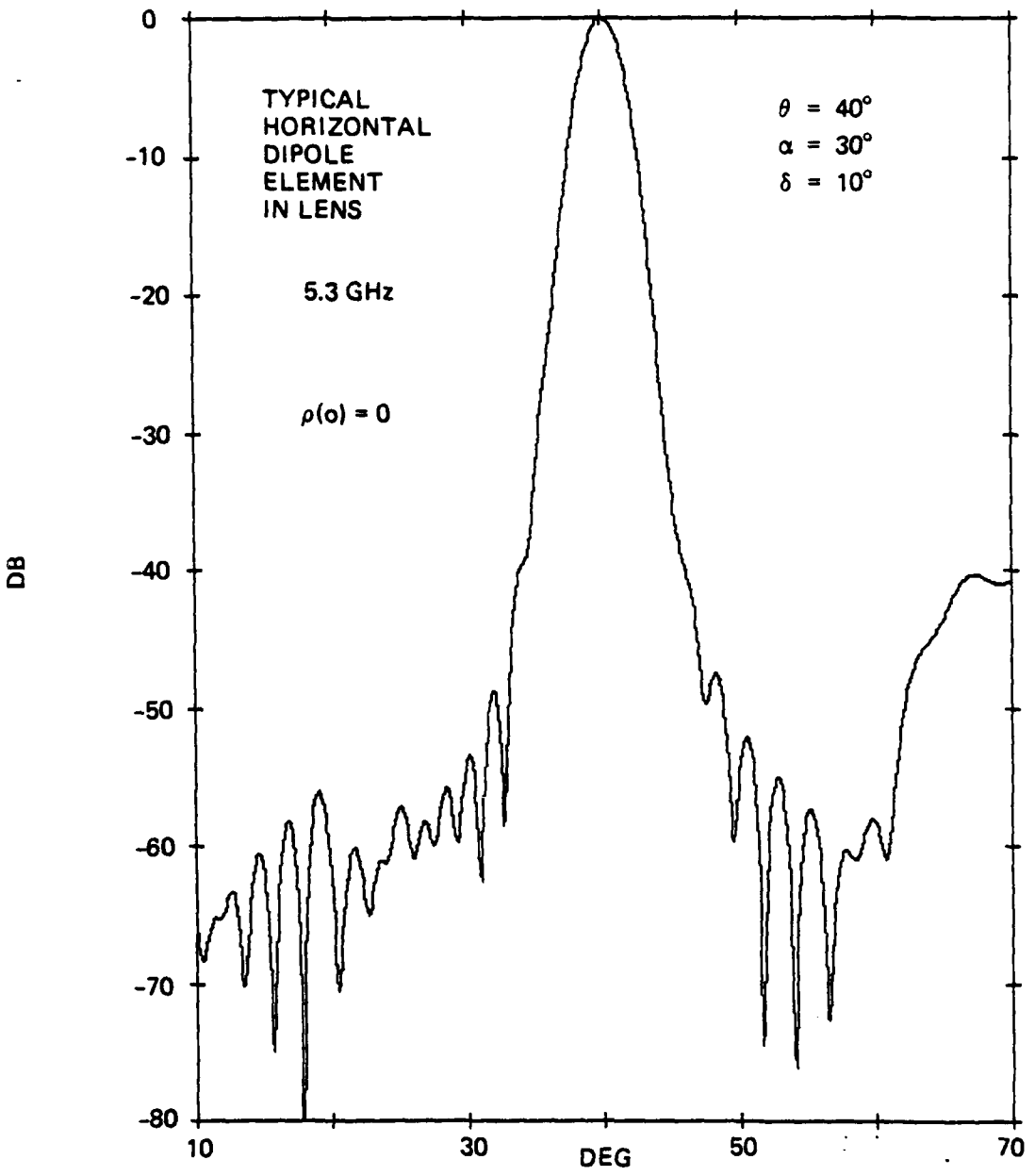

Figure 6-16. Azimuth Pattern of Antenna with Typical Horizontal-Dipole Element, $\alpha = 30^{\circ}$, $\delta = 10^{\circ}$

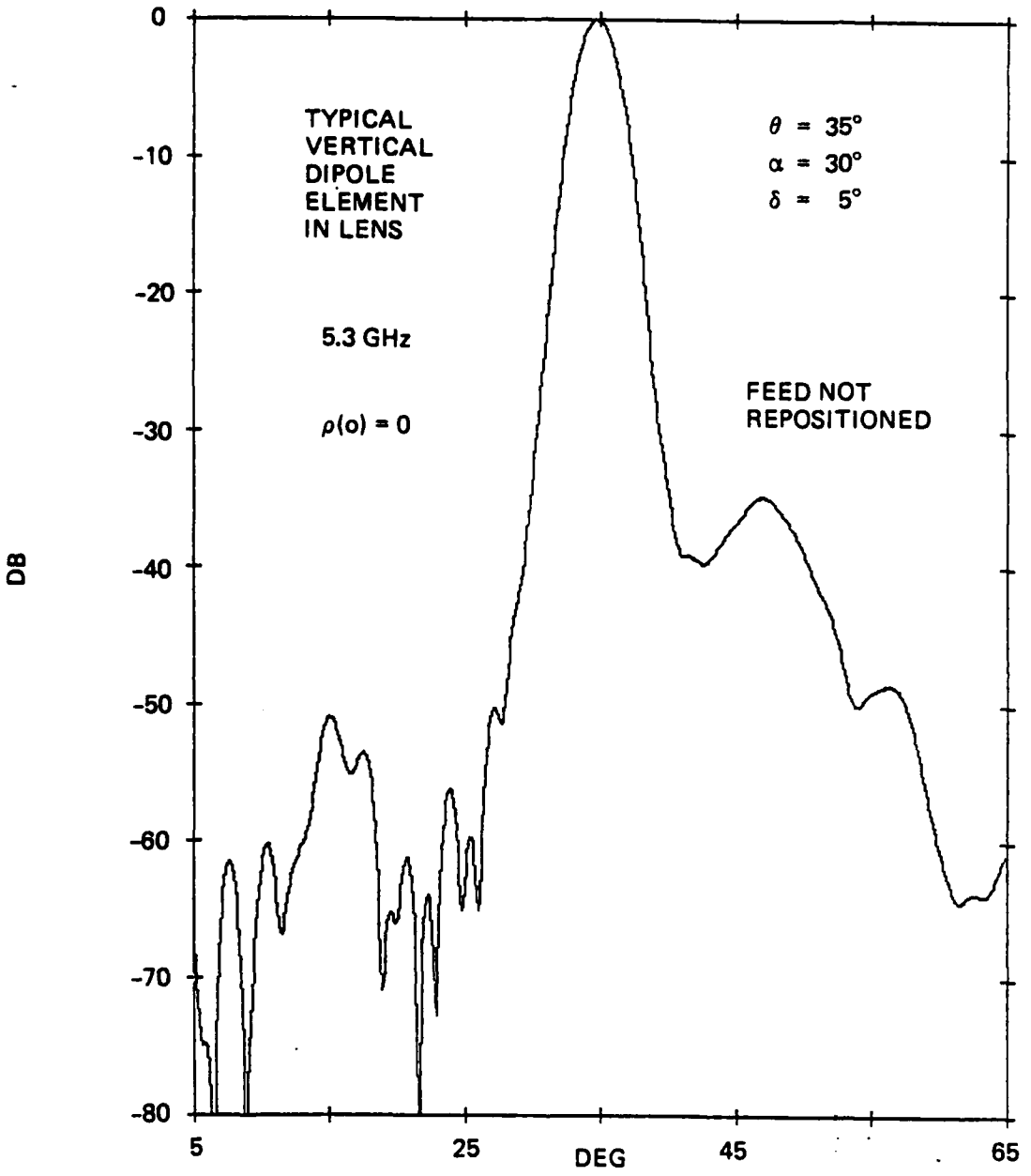

Figure 6-17. Azimuth Pattern of Antenna with Typical Vertical-Dipole Element, but with Line Feed Not Repositioned $\alpha = 30^{o}$, $\delta = 5^{o}$

broader than the main beam. However, even with the still lower levels obtained with the repositioned feed, improved performance is very much desired.

Approaches for Improvement. One possible approach for overcoming the lens internal-reflection effect is to use non-reciprocal phase shifters instead of reciprocal phase shifters for fine steering. If the non-reciprocal phase shifters provide exactly opposite phase shift for oppositely traveling waves, then fine steering would not create a separate spurious beam. The result then might be similar to the case of no fine steering, which gives a good pattern. However non-reciprocal phase shifters would require ferrite devices rather than PIN diodes, and ferrite devices would be difficult and expensive to incorporate within the closely-packed stripline cylindrical lens. Therefore this approach appears to be unattractive.

Another approach is to improve the array element impedance match. Some improvement could be obtained with the dipole elements assumed previously by matching them at a non-broadside incidence angle, but the improvement would not be sufficient to yield good patterns, and the patterns with zero coarse steering would be poorer. A better approach would be to use an array element that provides less variation of impedance with incidence angle, thereby yielding lower reflection coefficients at the lens surfaces. This approach is discussed in paragraph 6.3.

6.3 ARRAY ELEMENT FOR IMPROVED WIDE-ANGLE IMPEDANCE

As was discussed in paragraph 4.3 and shown in figure 4-14, the horizontal-plane incidence angles for both surfaces of the lens array go from 0° to about 60° for a coarse-steered beam at 30° azimuth. With electronic fine steering, the maximum incidence angle (for the outer surface) goes to about 75°. Therefore, an array element having nearly constant impedance over wide angles in the horizontal plane of incidence is wanted. In the vertical plane of incidence, the maximum incidence angle is only about 25°, corresponding to the maximum elevation scan with the cylindrical lens. Therefore, wide-angle impedance behavior is less important in the vertical plane.

The cylindrical lens medium will employ strip transmission lines connecting the inner and outer array elements. Dipole elements are well-suited for this medium, and can be printed together with the transmission lines in unitary planar layers. Therefore, dipole-type elements are appropriate for further consideration as to their wide-angle impedance behavior.

The impedance variation with horizontal incidence angle for vertical dipoles over a ground plane was shown in figures 6-3 and 6-4. While the resistance is fairly constant over a 0^{o} to 60^{o} range of angles, the reactance variation is very large. For horizontal dipoles, shown in figures 6-5 and 6-6, the opposite result occurs: the resistance variation is very large while the reactance variation is fairly small.

The grating-lobe-series viewpoint (refs 17, 18, 19) for infinite phased-array impedance analysis shows that for a closely-spaced infinite array that has no grating lobes, and which uses single-mode current elements like resonant dipoles, the variation of resistance with angle is related to the pattern of an isolated element as follows:

$$\frac{R(\psi)}{R(o)} = \frac{P_i(\psi)}{\cos\psi} \qquad (34)$$

Ref 17- L. Stark, "Radiation Impedance of a Dipole in an Infinite Planar Phased Array", Radio Science, pp. 361-377; March 1966.

Ref 18- H.A. Wheeler, "The Grating-Lobe Series for the Impedance Variation in a Planar Phased-Array Antenna", IEEE Trans. Antennas and Propagation, pp. 707-714; March 1967.

Ref 19- A.A. Oliner and R.G. Malech, "Mutual Coupling in Infinite Scanning Arrays", Chapter 3 in "Microwave Scanning Antennas", Vol. II, editor R.C.Hansen, Academic Press; 1966

where R is the infinite array resistance and P_i is the normalized power pattern of an isolated element which, in this case, includes the infinite ground plane. The resistance of the array of horizontal dipoles in figure 6-5 (E-plane scan) drops with scan off broadside because the power pattern of the isolated dipole over a ground plane drops rapidly with angle in the E plane, approaching zero well before 90°.

If the isolated element power pattern were $\cos \psi$, then the infinite-array resistance would be constant with scan. An approximation to this ideal isolated element pattern can be obtained in the E plane by bending a dipole into a V or a U in the E plane. The power pattern now has a component that does not drop to zero, permitting an optimization that yields a rather close approximation to the ideal element pattern out to 60° or more. Of course, at and near 90° the aproximation breaks down, but the lens array does not operate at those angles.

a. Resistance versus Angle for Infinitesimal Dipole/Loop Element

In order to gain some preliminary information on the scanning performance of an array of horizontal bent dipoles, a simplified approximation to the bent dipole has been made. This approximation consists of an infinitesimal straight dipole and an infinitesimal loop, colocated, copolarized, and in series with each other. A parameter "C" is defined as the ratio of loop to dipole radiation resistance for array broadside radiation without a ground plane. Thus "C" is proportional to the relative "strength" of the loop and the dipole, and is an indication of the amount of bending in the actual finite bent dipole. The parameter "C" is also equal to the ratio of power radiated at 90° to power radiated at 0° for the isolated dipole/loop element with a ground plane a quarter-wavelength away.

The variation of resistance with E-plane incidence angle (ψ) for an infinite array of closely-spaced, infinitesimal dipole/loop elements in front of a ground plane is determined from (34) to be:

$$\frac{R(\psi)}{R(o)} = \frac{1}{K}(1 - \cos 2\beta d)\cos\psi + \frac{C}{K}(1 + \cos 2\beta d)\frac{1}{\cos\psi} + \frac{2\sqrt{C}}{K}(\sin 2\beta d) \qquad (35)$$

where $\beta = \frac{2\pi\cos\psi}{\lambda}$

and d = distance from element to ground plane

and $K = 1 - \cos\frac{4\pi d}{\lambda} + C\left(1 + \cos\frac{4\pi d}{\lambda}\right) + 2\sqrt{C}\sin\frac{4\pi d}{\lambda}$

The first term is the dipole component, the second term is the loop component, and the third term is a cross product of the dipole and loop components. Note that we have normalized to the resistance at broadside, where presumably the array is matched.

Minimum Resistance Variation. Various values for the parameter "C" were tried, in order to obtain the least variation of resistance with incidence angle. Figure 6-18 shows curves of resistance variation versus E-plane incidence angle for four values of "C", with the distance (d) to the ground plane equal to a quarter wavelength. The curve for C = 0.25 yields a remarkably small variation of resistance out to at least 60^{o}.

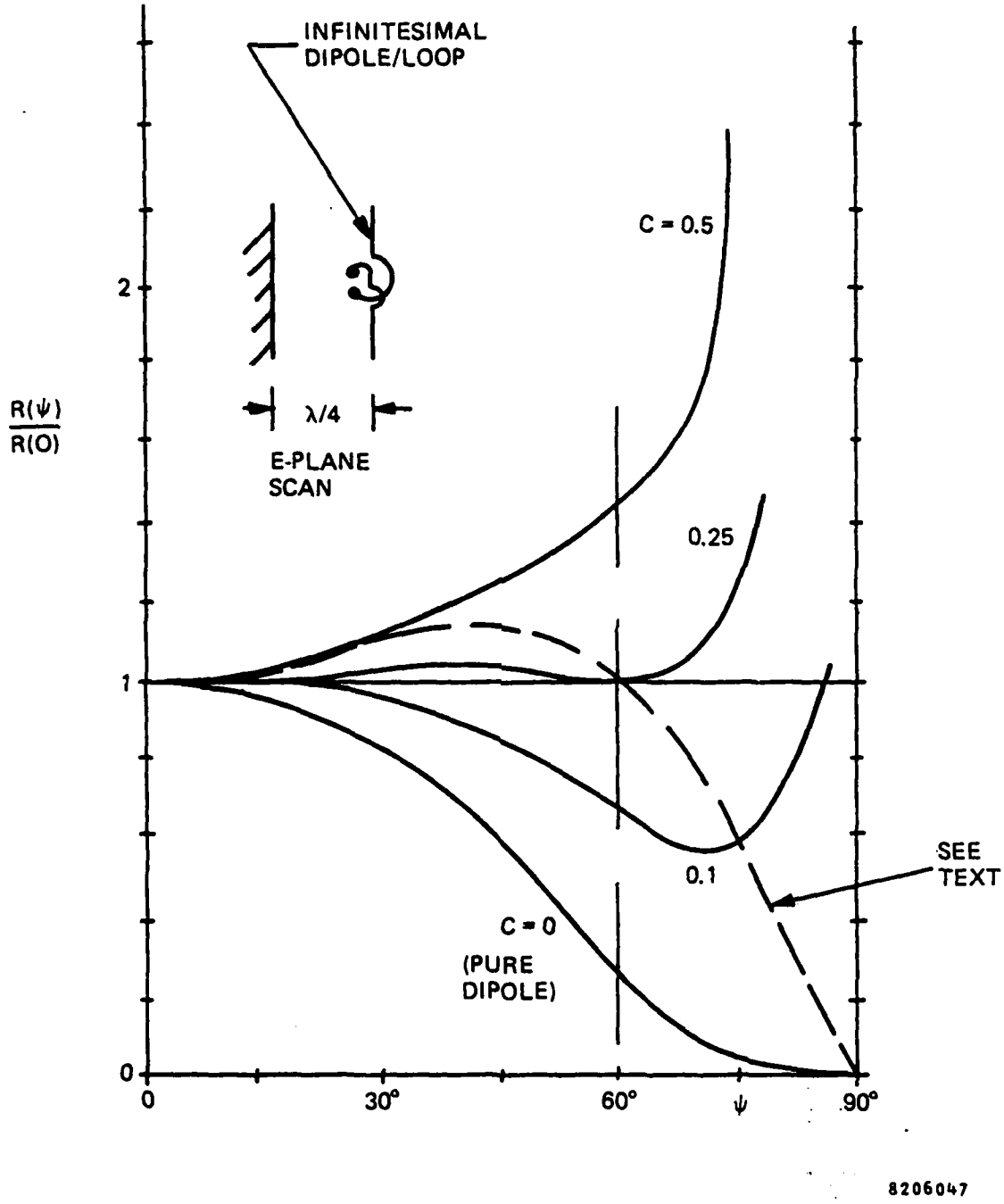

Figure 6-18. Infinitesimal Dipole/Loop Array Resistance vs Angle and "C" Parameter

For purposes of comparison, the resistance variation with H-plane incidence angle for an ordinary dipole array over a ground plane (shown earlier in figure 6-3) is indicated by a dashed curve. That case, which has a small variation of resistance out to 60°, is not nearly as good as this optimum E-plane case for the infinitesimal dipole/loop element. Even at 75° incidence angle the optimum dipole/loop element has a resistance ratio of only 1.2, compared with about 1/1.8 for the ordinary dipole.

This remarkably good performance can be explained by considering the three terms in equation 35. The first (dipole) term has a decreasing resistance with angle, while the second (loop) term has an increasing resistance with angle. These two terms provide a first-order type of compensation. However the third (cross-product) term has a resistance that first increases and then decreases with angle. It happens that this third term provides a second-order type of compensation, yielding an exceptionally small variation of resistance from 0° to over 60°.

b. Reactance versus Angle for Infinitesimal Dipole/Loop Element

The variation of reactance with incidence angle of an infinite array of infinitesimal dipole/loop elements in front of a ground plane is more difficult to compute than is the resistance variation. The grating-lobe series for reactance variation involves a two-dimensional infinite series for each of the three components (dipole, loop, and cross-product). Furthermore, the isolated element pattern in two angular coordinates must be used for the infinite series, including a polarization factor for the cross-product component. Additionally, there is a problem of convergence of the series when the elements are infinitesimal in size.

The First Term. A grating-lobe series has been formulated for the infinitesimal dipole/loop element. The first term of this infinite series is a very important term, because it contains that part of the reactance variation that is independent of the spacing between the elements. The reactance variation in this basic first term is caused by the variation of electrical distance from the element to the

ground plane. The first term can be expressed as follows for angles of incidence in the E plane:

$$\frac{X(\psi) - X(o)}{R(o)} = \frac{1}{K}(\sin 2\beta d)\cos\psi - \frac{1}{K}\sin\frac{4\pi d}{\lambda} - \frac{C}{K}(\sin 2\beta d)\frac{1}{\cos\psi} + \frac{C}{K}\sin\frac{4\pi d}{\lambda} + \frac{2\sqrt{C}}{K}(\cos 2\beta d) - \frac{2\sqrt{C}}{K}\cos\frac{4\pi d}{\lambda} \quad (36)$$

where β, d, and K are defined the same as in equation 35. Note that we have subtracted out the reactance at broadside and have normalized relative to the resistance at broadside; this corresponds to matching the array at broadside.

Curves of this first-term reactance variation with E-plane incidence angle are shown in figure 6-19 for various values of C and for d equal to a quarter wavelength. It is seen that there is not a particularly favorable value of C that minimizes the reactance variation, except for the C = 0 case which has a large variation of resistance and is therefore unacceptable. The first-term reactance variation for C = 0.25 is substantial. However, it is considerably less than the first-term reactance variation of an ordinary dipole scanned in the H plane, which is given by the dashed curve.

A range of values have been tried for d, the distance to the ground plane. Each of these have been examined for several values of C. Some cases have been found in which the first-term reactance variation is reduced, at the expense of some change in the resistance variation. Three such cases are shown in figures 6-20 and 6-21. There has not been found a case in which the first-term reactance variation is very small, while retaining a very small resistance variation.

The Complete Series. The full grating-lobe series has been applied to the reactance variation with E-plane incidence

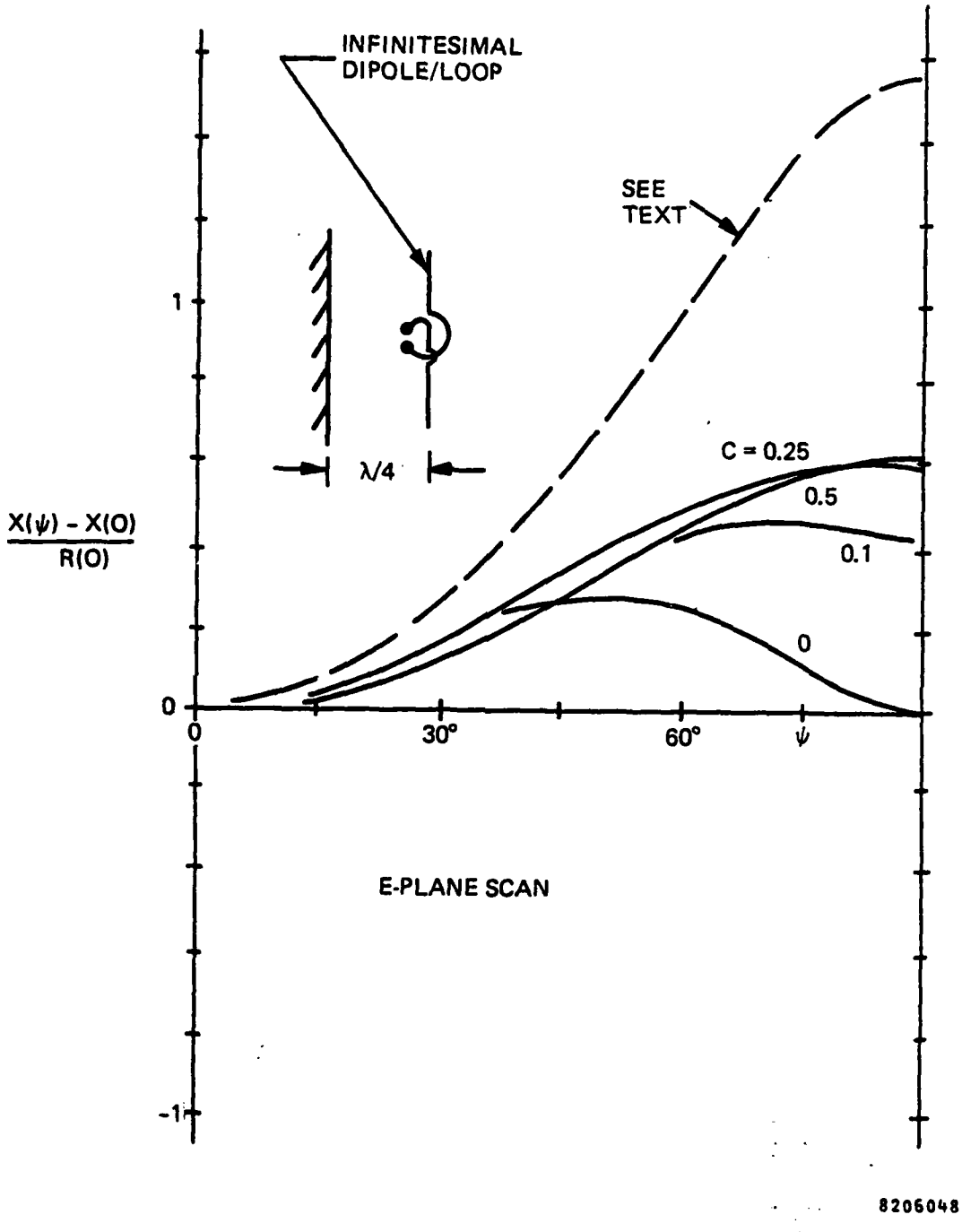

Figure 6-19. Infinitesimal Dipole/Loop Array First-Term Reactance vs Angle and "C" Parameter

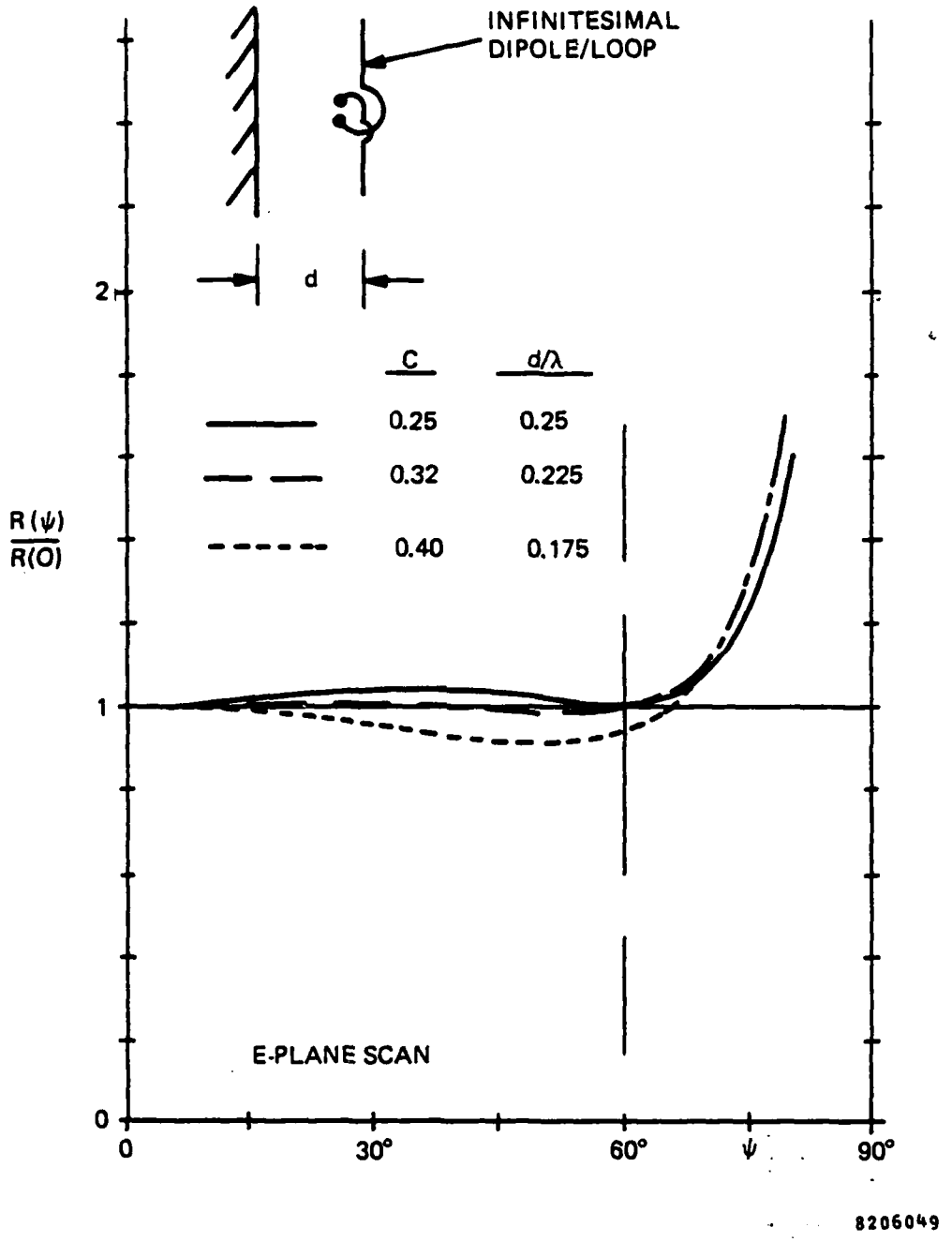

Figure 6-20. Infinitesimal Dipole/Loop Array Resistance vs Angle and Distance to Ground Plane

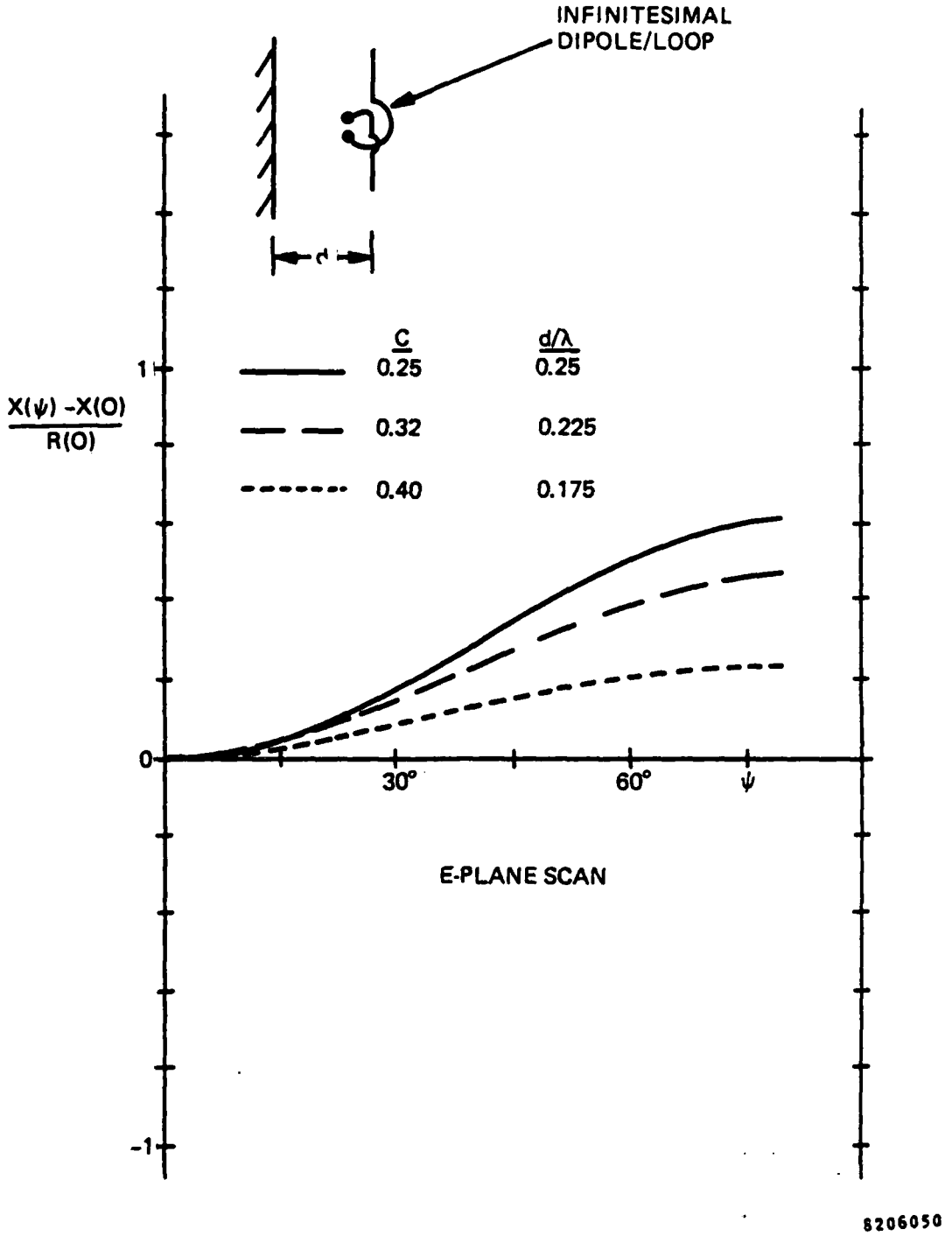

Figure 6-21. Infinitesimal Dipole/Loop Array First-Term Reactance vs Angle and Distance to Ground Plane

angle for the infinitesimal dipole/loop element. The spacing between elements now becomes significant. Figure 6-22 shows some results for C = 0.32 and d = 0.225 wavelengths, for two spacings in the E plane: 0.5 and 0.4 wavelengths. The reactance variation with 0.5 wavelength spacing is much greater, as might be expected with an element that provides radiation out to wide angles. The reactance variation with 0.4 wavelength spacing is close to that given by the first term in figure 6-21. The 0.4 wavelength spacing is clearly preferred.

Three Incidence Planes. The impedance has also been computed for the vertical plane of incidence out to 25°, representing the elevation scan requirement for the cylindrical lens antenna. In addition, the wide-angle impedance has been computed for an intermediate plane of incidence 26° from the horizontal plane, representing a combination of 25° elevation scan and 75° azimuth incidence. Figures 6-23 and 6-24 show the resistance and reactance, respectively, of these two cases together with the pure horizontal-plane-incidence case given previously. The elements are in a rectangular array with 0.4 wavelengths horizontal spacing and 0.6 wavelengths vertical spacing. The vertical-plane (H-plane) reactance variation is substantial even for the small (25°) angle encountered. This variation could be reduced somewhat by reducing the vertical spacing to 0.5 wavelengths. However the horizontal-plane (E-plane) and 26°-plane reactance variation remains as the greatest contributor to array reflection.

Infinitesimal Loop/Dipole versus Straight Dipole. Comparison of the horizontal-plane impedance variation of the infinitesimal dipole/loop array shown in figures 6-23 and 6-24 with the impedance variation of an ordinary dipole array in the H or E plane (shown earlier in figures 6-3 through 6-6) shows that the dipole/loop element gives substantially better performance. At 30° incidence the reflection coefficient for a dipole/loop array that is matched at broadside is only 0.06 as compared with approximately 0.2 for the ordinary dipole array. At 60° incidence the reflection coefficient for the dipole/loop array is only 0.20 as compared with more than 0.5 for the ordinary dipole array.

Assuming that the angular performance of the infinitesimal dipole/loop element is representative of the angular performance of a real bent-dipole element, these results indicate that horizontally-polarized bent dipoles are preferred to ordinary dipoles for the array surfaces of the cylindrical lens.

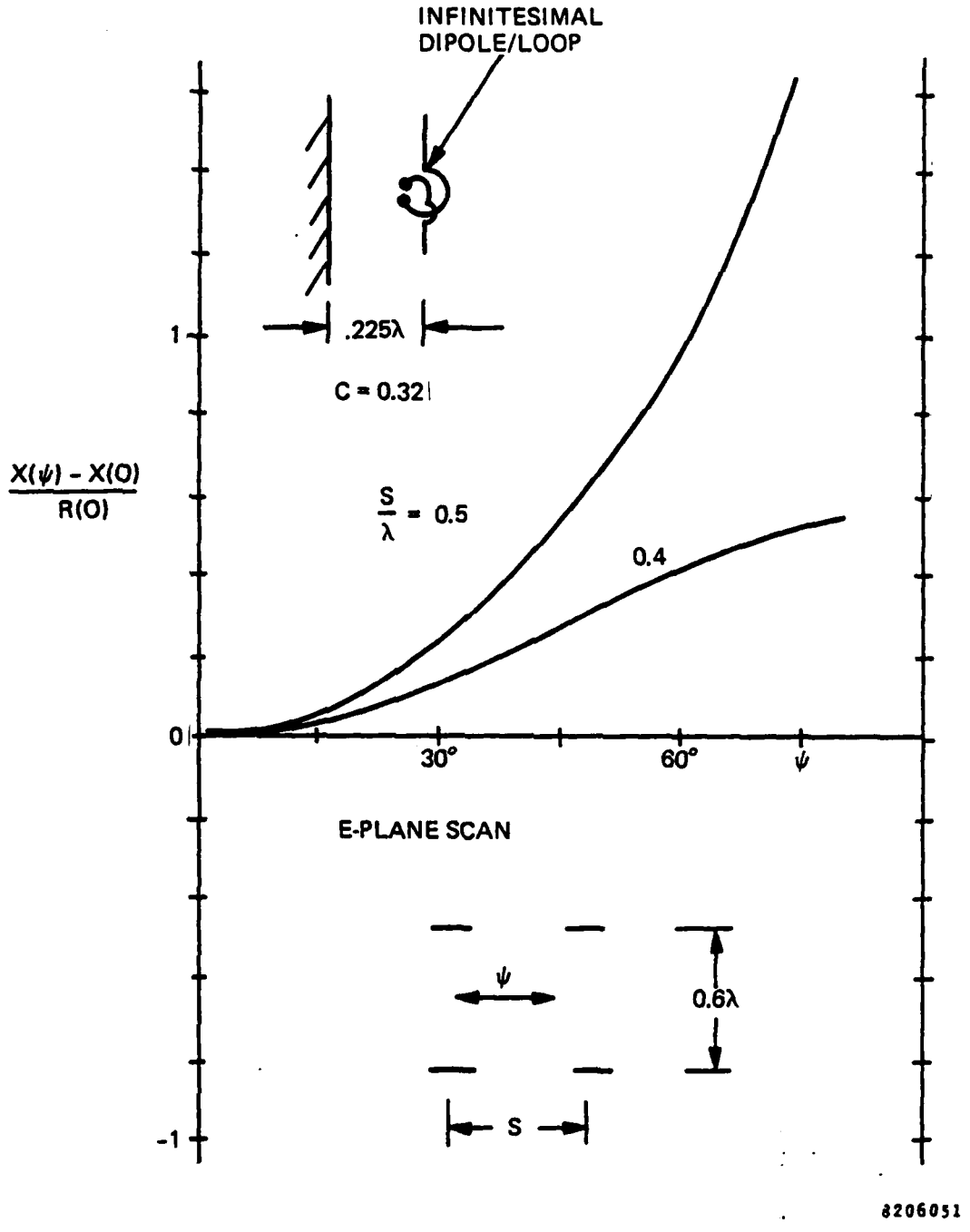

Figure 6-22. Infinitesimal Dipole/Loop Array Reactance vs Angle and Spacing Between Elements

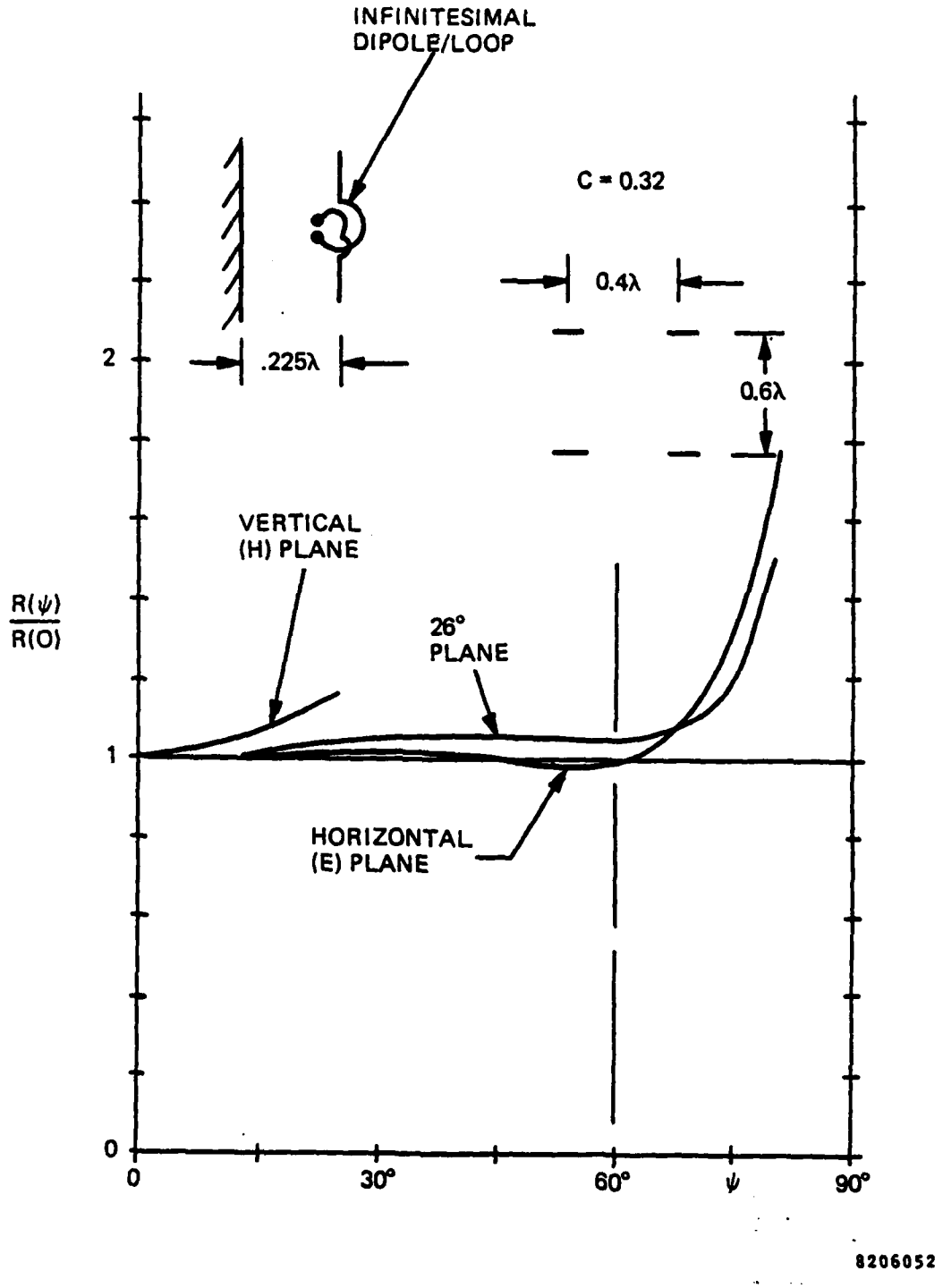

Figure 6-23. Infinitesimal Dipole/Loop Array Resistance vs Angle in Three Incidence Planes

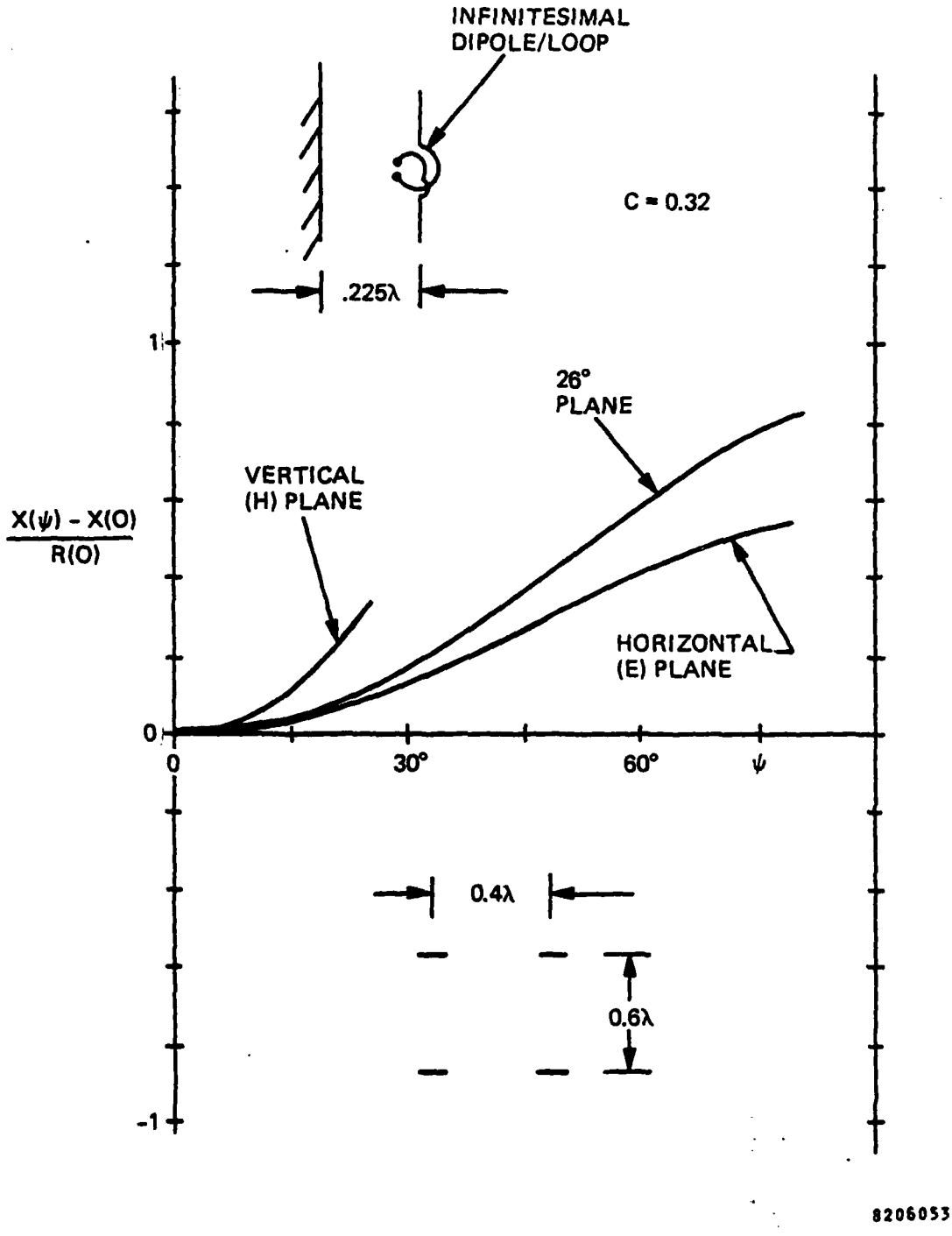

Figure 6-24. Infinitesimal Dipole/Loop Array Reactance vs Angle in Three Incidence Planes

c. Impedance versus Angle for Large Bent-Dipole Element

In order to provide a good impedance match over the operating frequency band, the dipole element should occupy most of the 0.4 wavelength horizontal space to which it is allotted in the array. An infinitesimal dipole/loop element, or even a small bent dipole, would not provide adequate wideband impedance match. Therefore a large bent dipole that comes fairly close to its neighbors is desired.

Analysis Approach. With such a bent dipole, the assumption that its variation of impedance with incidence angle can be represented by an infinitesimal dipole/loop may not be accurate, particularly for the reactance component. Therefore an analysis based on a configuration more closely resembling the actual bent dipole was desired. On the other hand, the other major objectives of the program (design and development of a cylindrical lens antenna) could not be sacrificed in order to make a complete, rigorous analysis of the bent dipole. Hence simplicity of the analysis was also a necessity.

A relatively simple, approximate analysis was suggested and defined by H.A. Wheeler. In this analysis the bent dipole is replaced by four infinitesimal dipoles suitably located, oriented, and energized to represent the natural sinusoidal-type current distribution on a thin center-fed wire. Then the mutual impedance to another such element is computed, for any relative location of the two elements, in the presence of the ground plane. This mutual impedance is then used to compute the active impedance of the center element in a finite phased array. The shape we have chosen for the bent dipole is a U rather than a V because the latter needs to have a rather small included angle to achieve the optimum impedance properties in the E plane of incidence. Figure 6-25 shows the U-shaped bent dipole and the four infinitesimal dipoles that represent it in the analysis.

Minimum Resistance Variation. Various dimensions for the several parts of the bent dipole were tried in order to minimize the variation of impedance with E-plane incidence angle. Figure 6-26 shows the resistance versus angle for three different lengths of the dipole arms. There is clearly an optimum case that yields minimum resistance variation. An effective value of "C" can be computed for this case, based on the calculated ratio of power-radiated at 90° to power at 0°. This turns out to be approximately 0.37, which is not very different from the 0.32 value that was used in figures 6-20 and 6-22.

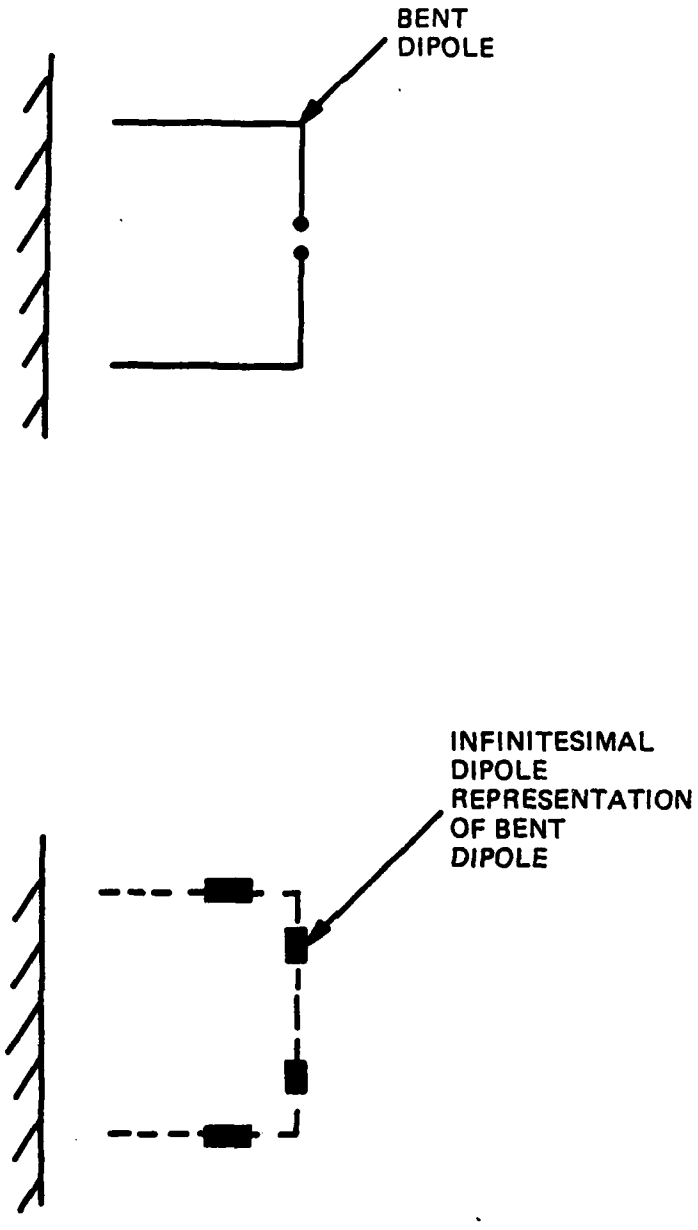

Figure 6-25. Bent Dipole and its Representation by Infinitesimal Dipoles

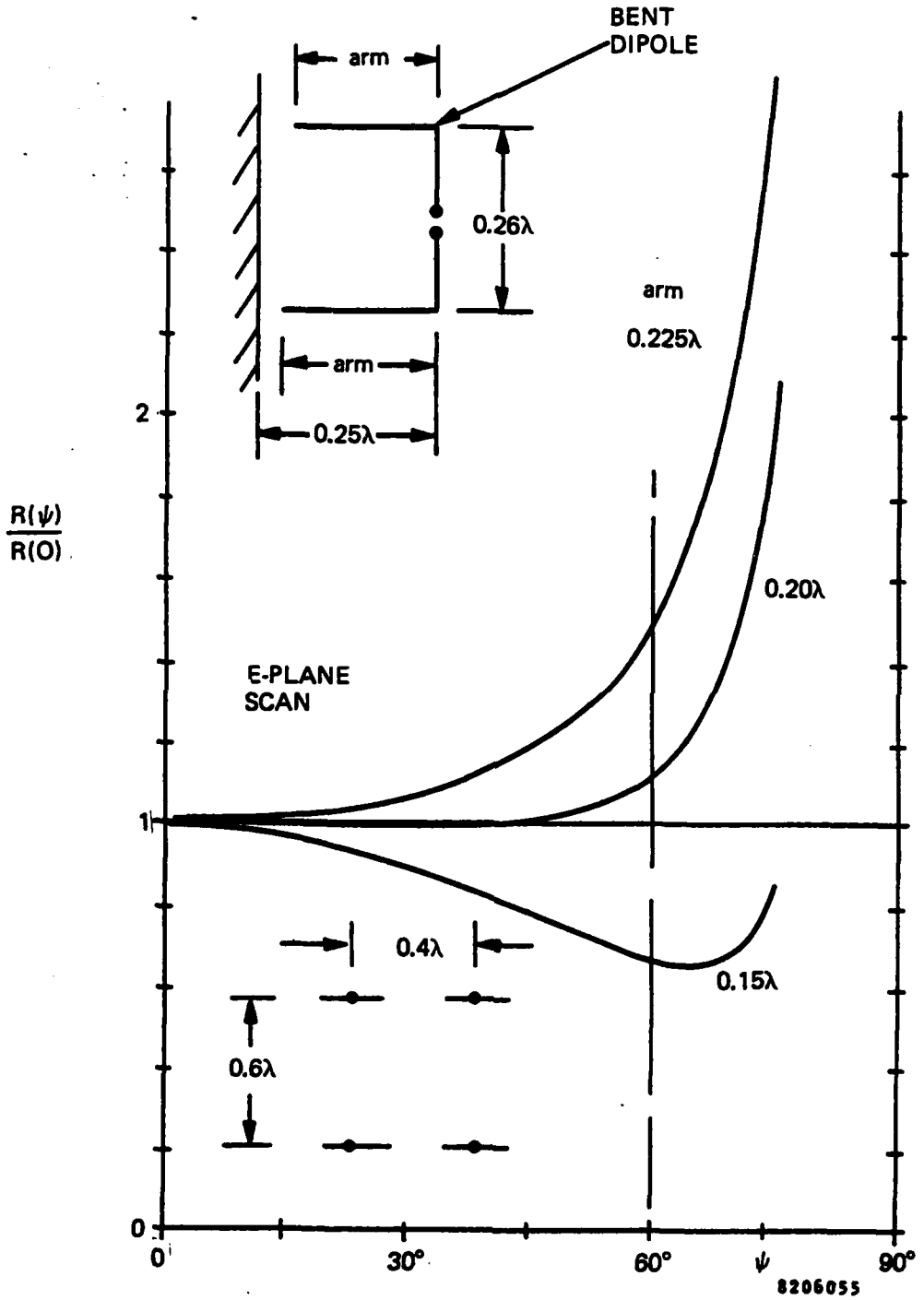

Figure 6-26. Bent Dipole Array Resistance vs Angle and Arm Length

Minimum Reactance Variation. A very interesting result was obtained for the reactance variation. Figure 6-27 shows the reactance versus E-plane angle for three different lengths of the dipole body. It is seen that when the body of the bent dipole is sufficiently long, a reactance variation that becomes negative can be obtained. Therefore the normal positive variation of reactance with angle, caused by the effect of the electrical distance to the ground plane, can be overcome. An optimum value for the body length can be found that yields a remarkably constant reactance over a range of E-plane angles from 0° to over 60°, as shown in figure 6-27.

It is speculated that the mechanism for this compensating effect is the mutual coupling between the bent arms of adjacent dipoles. For the optimum case these arms are rather close to each other (0.14 wavelengths) over their full length (0.2 wavelengths). This coupling may be acting favorably in a manner similar to the coupling of connecting circuits that are designed to provide wide-angle impedance matching (refs 20 and 21).

Effect of Frequency. To see whether this exceptionally small variation of impedance with E-plane angle would be destroyed by operation at the ends of the frequency band, the calculations are repeated using electrical dimensions appropriate to 5.0, 5.3, and 5.6 GHz. Figures 6-28 and 6-29 show the resistance and reactance variations for these three frequencies, where the dimensions have been optimized at 5.3 GHz. It is seen that there is a fairly small change of the resistance variation, as might be expected from the normal change of the sinusoidal current distribution on the bent dipole. The reactance variation changes only slightly. Therefore it appears that the wide-angle impedance in the E plane will remain excellent over the 5.0 to 5.6 GHz frequency band.

Ref 20- P.W.Hannan, D.S. Lerner, G.H. Knittel, "Impedance Matching on Phased-Array Antenna over Wide Scan Angles by Connecting Circuits", IEEE Trans. Antennas and Propagation, pp. 28-34; January 1965.

Ref 21- P.W. Hannan, "Proof that a Phased-Array Antenna Can be Impedance Matched for All Scan Angles", Radio Science, pp. 361-369; March 1967.

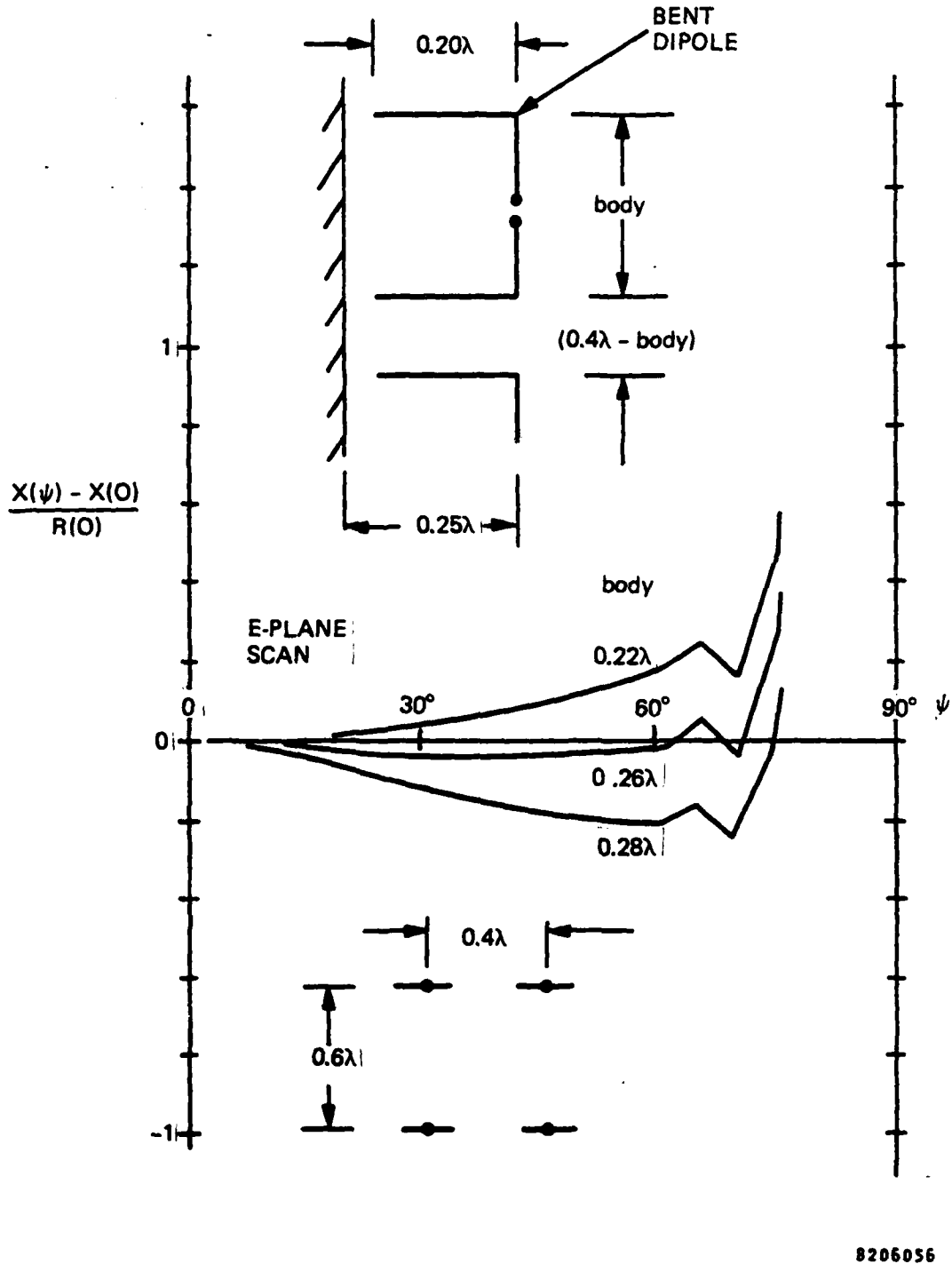

Figure 6-27. Bent Dipole Array Reactance vs Angle and Body Length

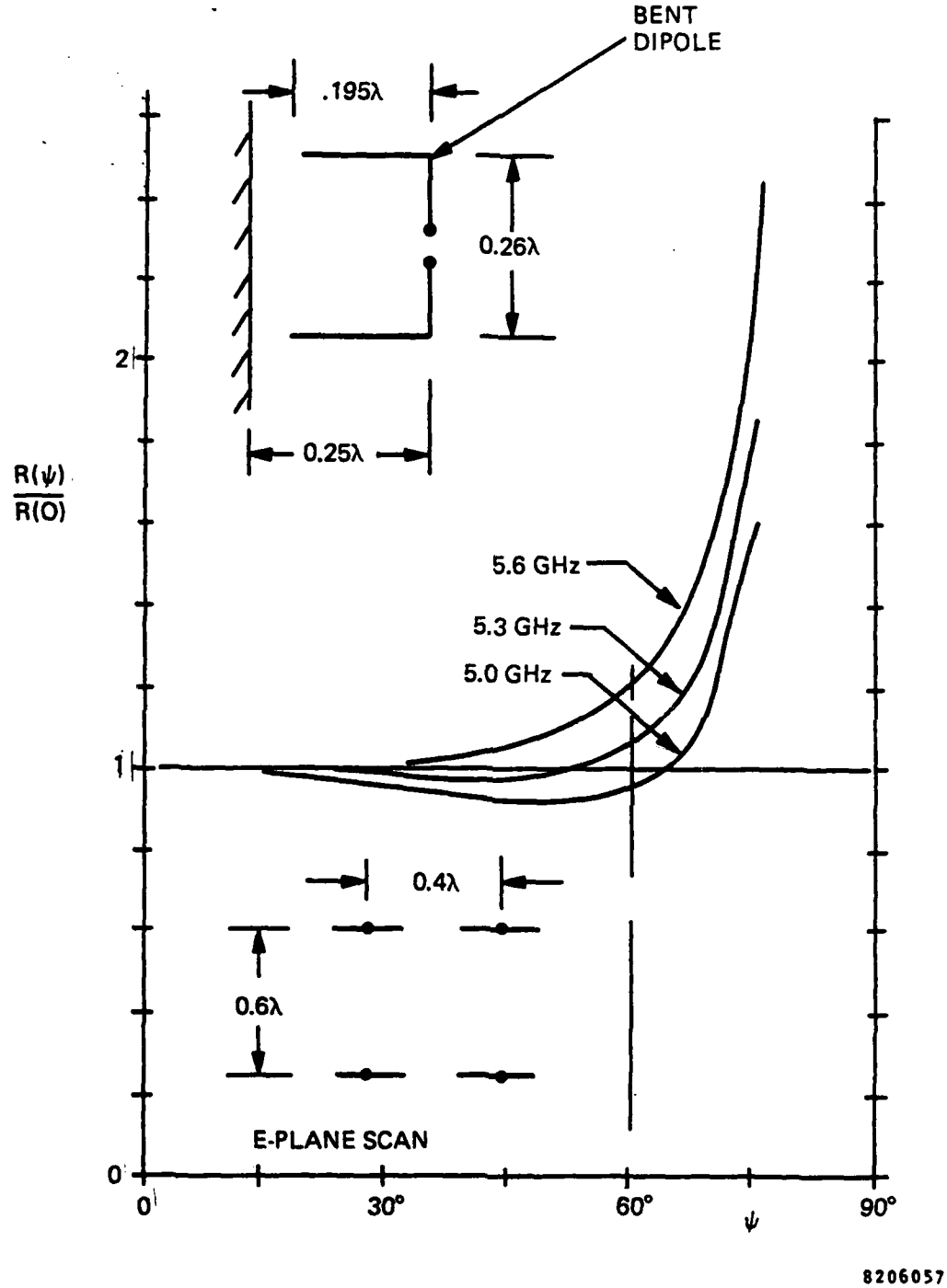

Figure 6-28. Optimum Bent Dipole Array Resistance vs Angle at Three Frequencies

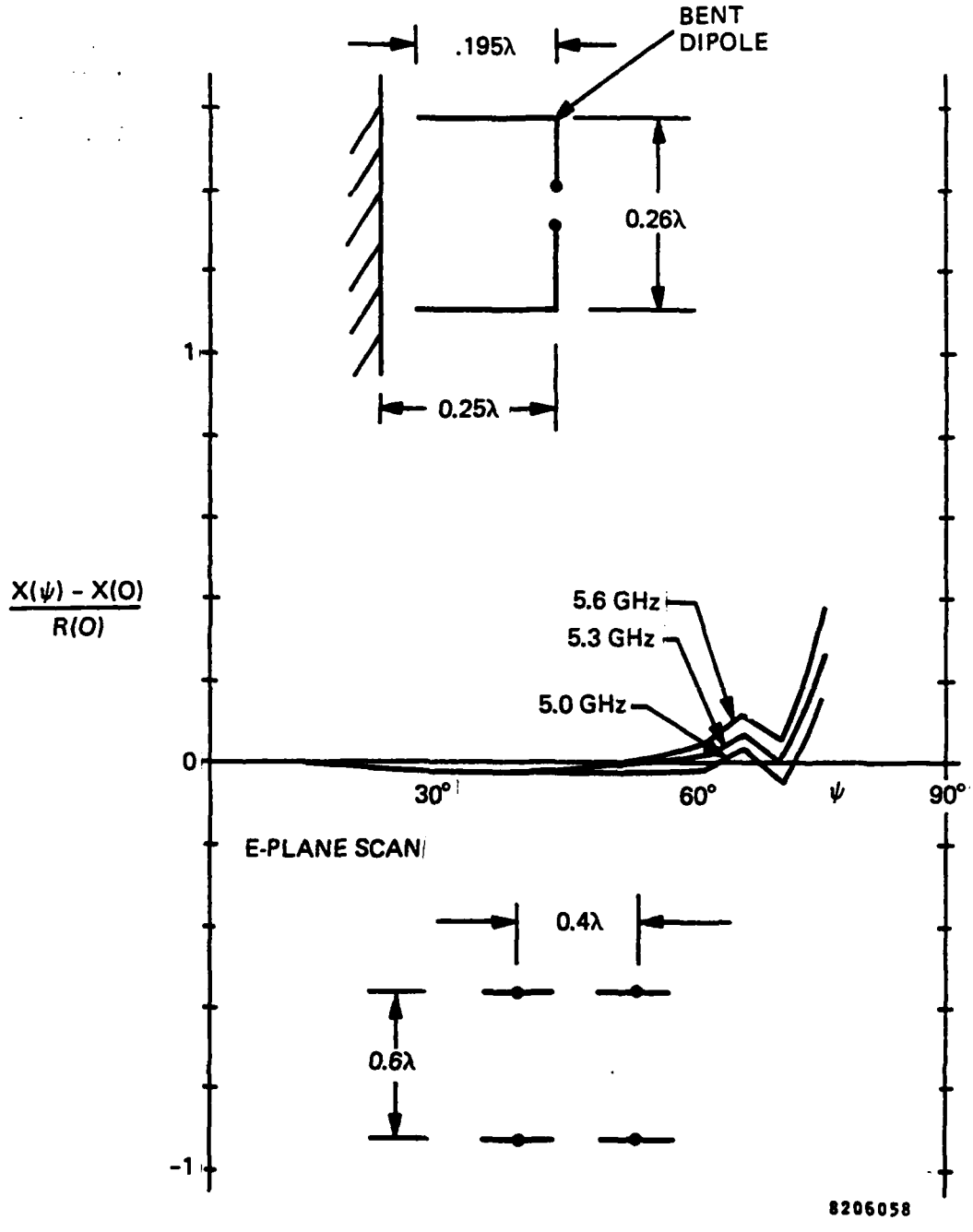

Figure 6-29. Optimum Bent Dipole Array Reactance vs Angle at Three Frequencies

Three Incidence Planes. Computations of impedance variation with angle in the vertical plane (H plane) and in the plane 26° from the horizontal plane have also been made for the large bent dipole in an array with 0.4 by 0.6 wavelengths spacing between elements. The results for all three planes are shown at 5.3 GHz in figures 6-30 and 6-31. The vertical-plane results are similar to those of an ordinary straight dipole in the H plane. It is seen that even though the maximum scan angle in the vertical plane is only 25°, the impedance variation in this plane is far greater than that in the horizontal plane out to over 60°. The 26° plane has some reactance variation from 0° to 60°, but less than the vertical-plane reactance variation from 0° to 25°.

d. Discussion of Wide-Angle Element

Bent dipoles have previously been used in wide-angle scanning arrays (ref 22). However those arrays scan to wide angles in all planes of scan, and also provide circular polarization. Therefore the opportunity to optimize the bent dipole for exceptionally good wide-angle performance in one plane of scan may not have been available. The dipoles in those arrays are bent in a V shape; whether this would affect the ability to achieve exceptional performance in one scan plane has not been studied on this program.

The impedance calculations presented in this report are based on highly simplified theoretical models of the bent dipole. The representation of the continuous current distribution on the large bent dipole by four infinitesimal dipoles is obviously an approximation. Furthermore, the assumption is made that the current distribution is a single sinusoidal mode, unaffected by the currents on adjacent dipoles. The possible effects of practical structures, such as the feeding stem or the dielectric substrate support, are also neglected. Therefore, the computed array impedance given in this report may not accurately correspond to the actual impedance of the physical bent-dipole array. However, these computed impedance results are the only ones available and will be used for this program, whose main objective is the design and development of the cylindrical lens antenna.

Ref 22- L.Stark, "Comparison of Array Element Types", Proceedings of Phased Array Antenna Symposium, edited by Oliner and Knittel, Artech House, pp. 51-66; 1972.

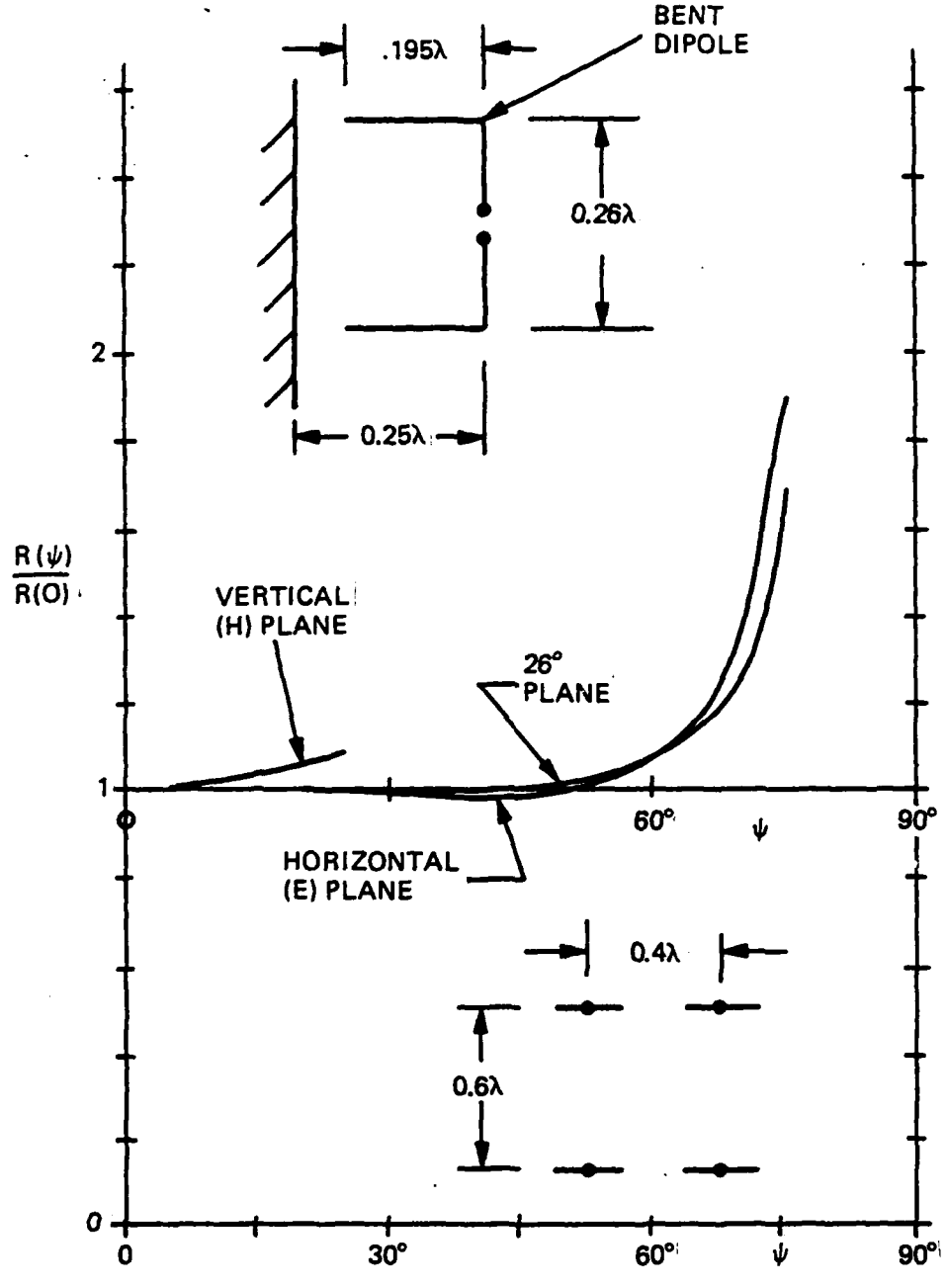

Figure 6-30. Optimum Bent Dipole Array Resistance vs Angle in Three Incidence Planes

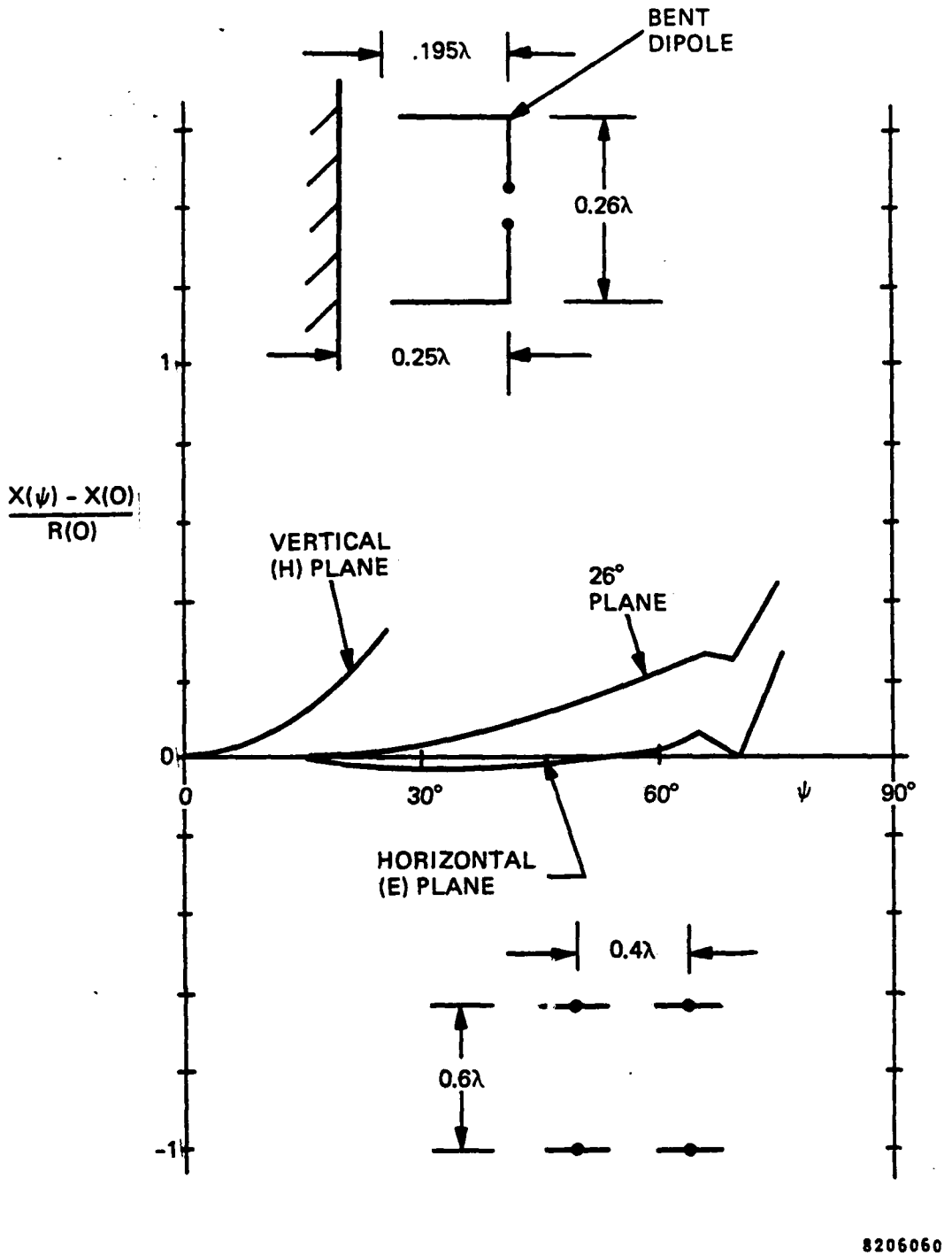

Figure 6-31. Optimum Bent Dipole Array Reactance vs Angle in Three Incidence Planes

It is our opinion that, despite the simplified theoretical model used, the impedance results given here strongly indicate that exceptionally good wide-angle performance is available from an array of bent dipoles in the E plane of incidence.

e. Computed Sidelobes with Bent Dipole

The azimuth patterns of the cylindrical lens antenna have been computed with the bent-dipole wide-angle impedance variation included. Figures 6-32 and 6-33 show the azimuth patterns for a coarse-steering angle of 30° and with fine steering of -5° and $+5^{\circ}$, respectively. These patterns show very little effect on the sidelobes that can be ascribed to the internal lens reflections. Figures 6-34 and 6-35 show azimuth patterns where the fine steering has been increased to -10° and $+10^{\circ}$. A similar result is obtained. Comparison of these results with those of figures 6-9 through 6-16 illustrate the improvement that is available with the bent dipole.

The sidelobes of the elevation patterns are also affected by the lens internal reflections when the beam is fine-steered in elevation. Although the maximum angle of incidence on the lens surface array is only 25° in the vertical plane, the impedance of the horizontal bent dipoles is approximately the same as that of ordinary straight horizontal dipoles in the vertical plane of incidence. At the extreme elevation scan angle (25°) the spurious beam caused by the lens internal reflections is estimated to be about -35dB relative to the main beam. At lesser elevation scan angles, this sidelobe becomes considerably weaker.

f. Choice of Element for Lens Surface Array

As described in the preceeding paragraphs, the horizontally-polarized bent dipole offers a major reduction in the azimuth sidelobe caused by lens internal reflections. The bent dipole is essentially as easy to print on horizontal microstrip or stripline boards as is a straight dipole. The bent dipole, however, requires extra design effort to realize in practice the improved performance that it offers.

We have selected the horizontal bent dipole for the surface arrays of the cylindrical lens. The polarization of the lens antenna is, therefore, horizontal. The spacing between elements has been chosen as 0.4 wavelengths horizontally and 0.6 wavelengths vertically for the lens surface arrays.

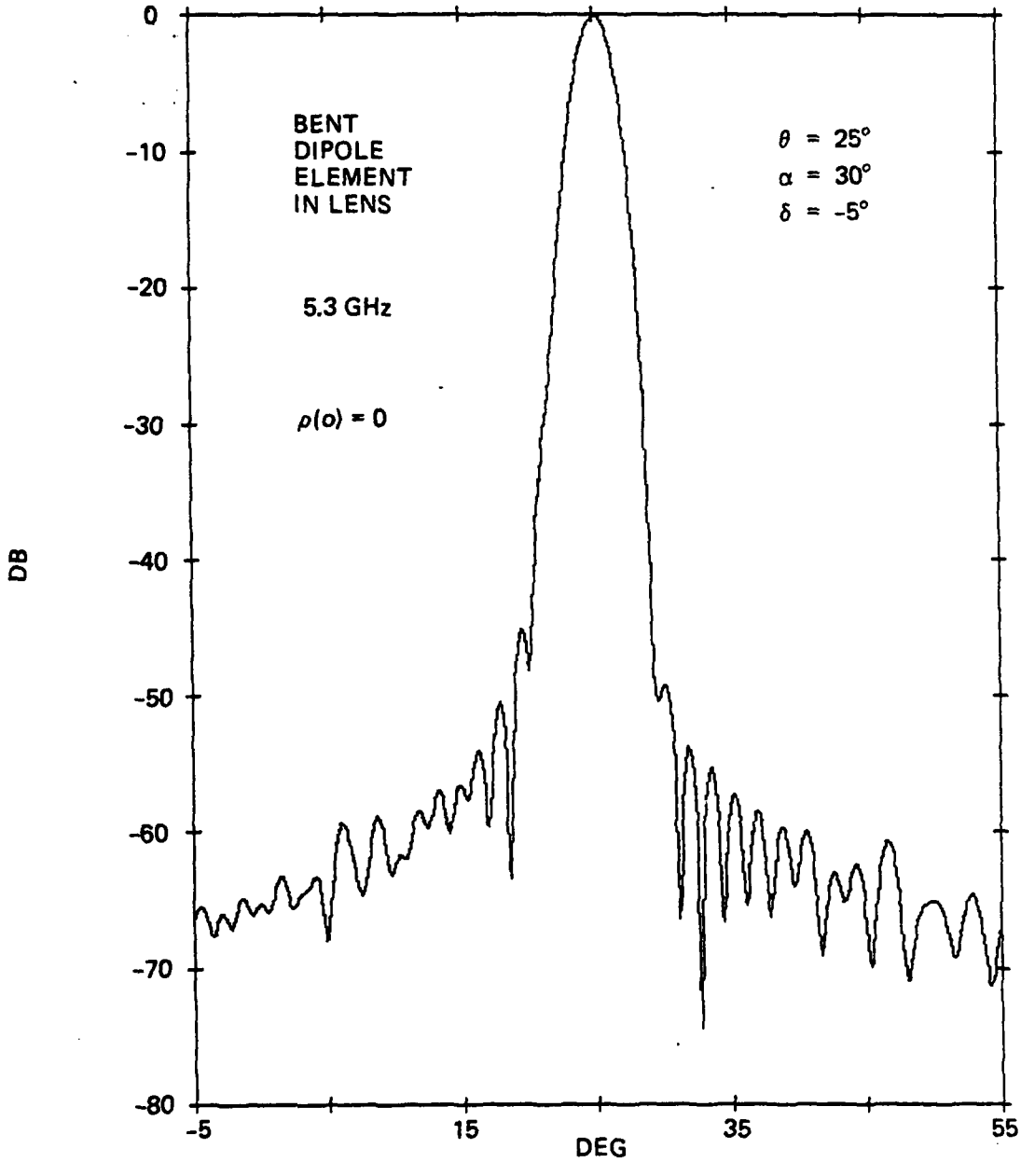

Figure 6-32. Azimuth Pattern of Antenna with Bent-Dipole Element, $\alpha = 30^{o}$, $\delta = -5^{o}$

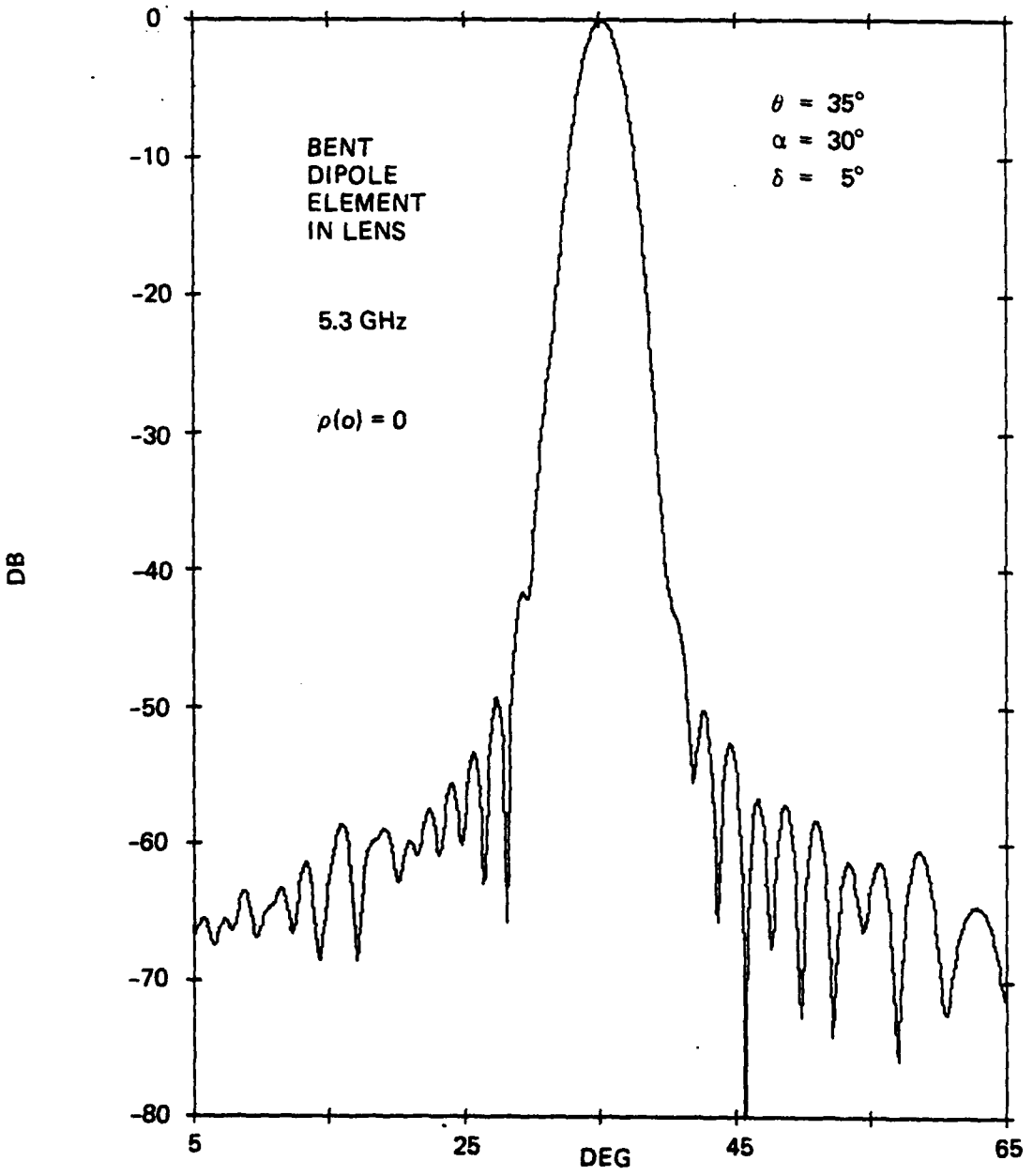

Figure 6-33. Azimuth Pattern of Antenna with Bent-Dipole Element, $\alpha = 30^{\circ}$, $\delta = 5^{\circ}$

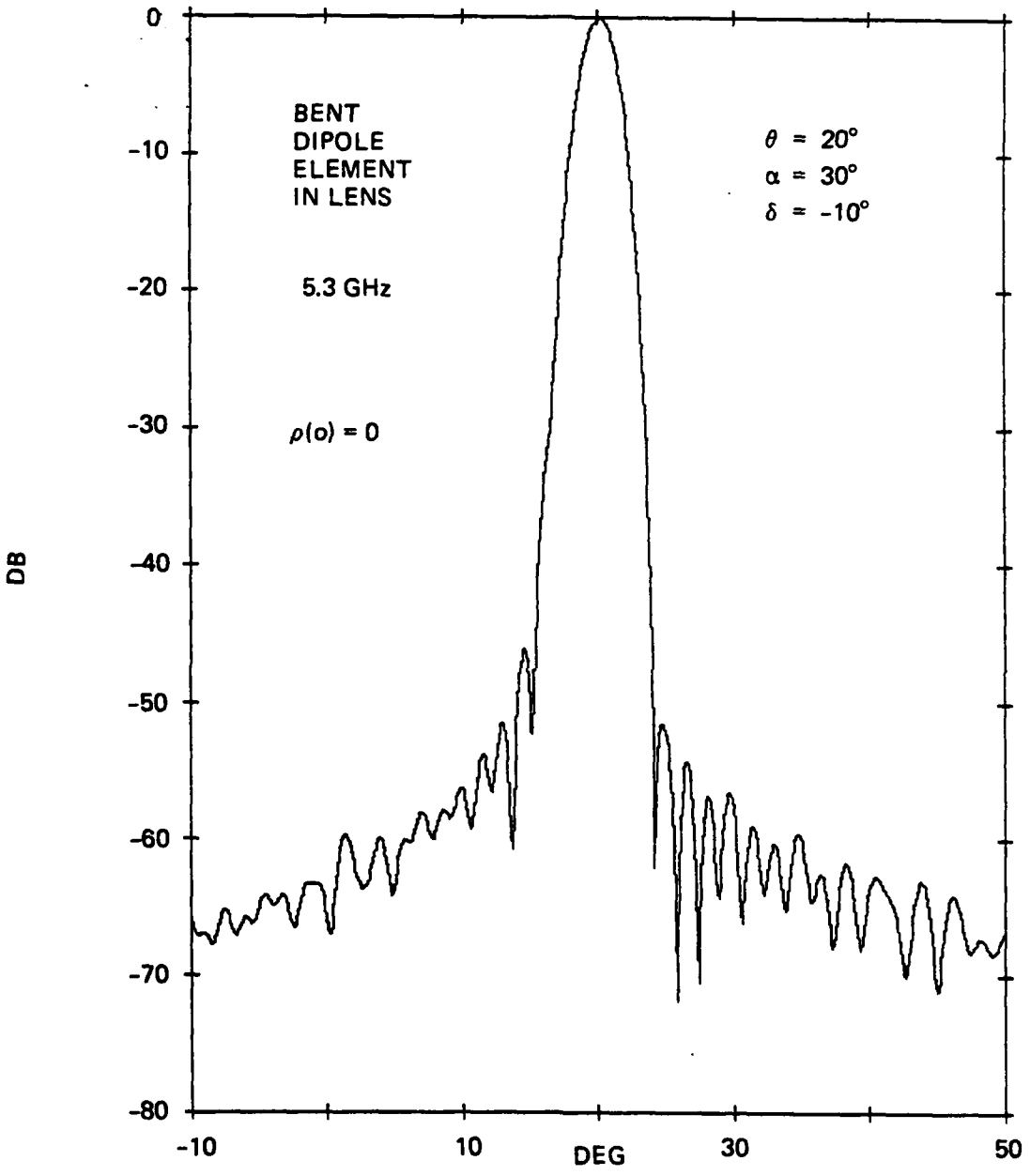

Figure 6-34. Azimuth Pattern of Antenna with Bent-Dipole Element, $\alpha = 30^{o}$, $\delta = -10^{o}$

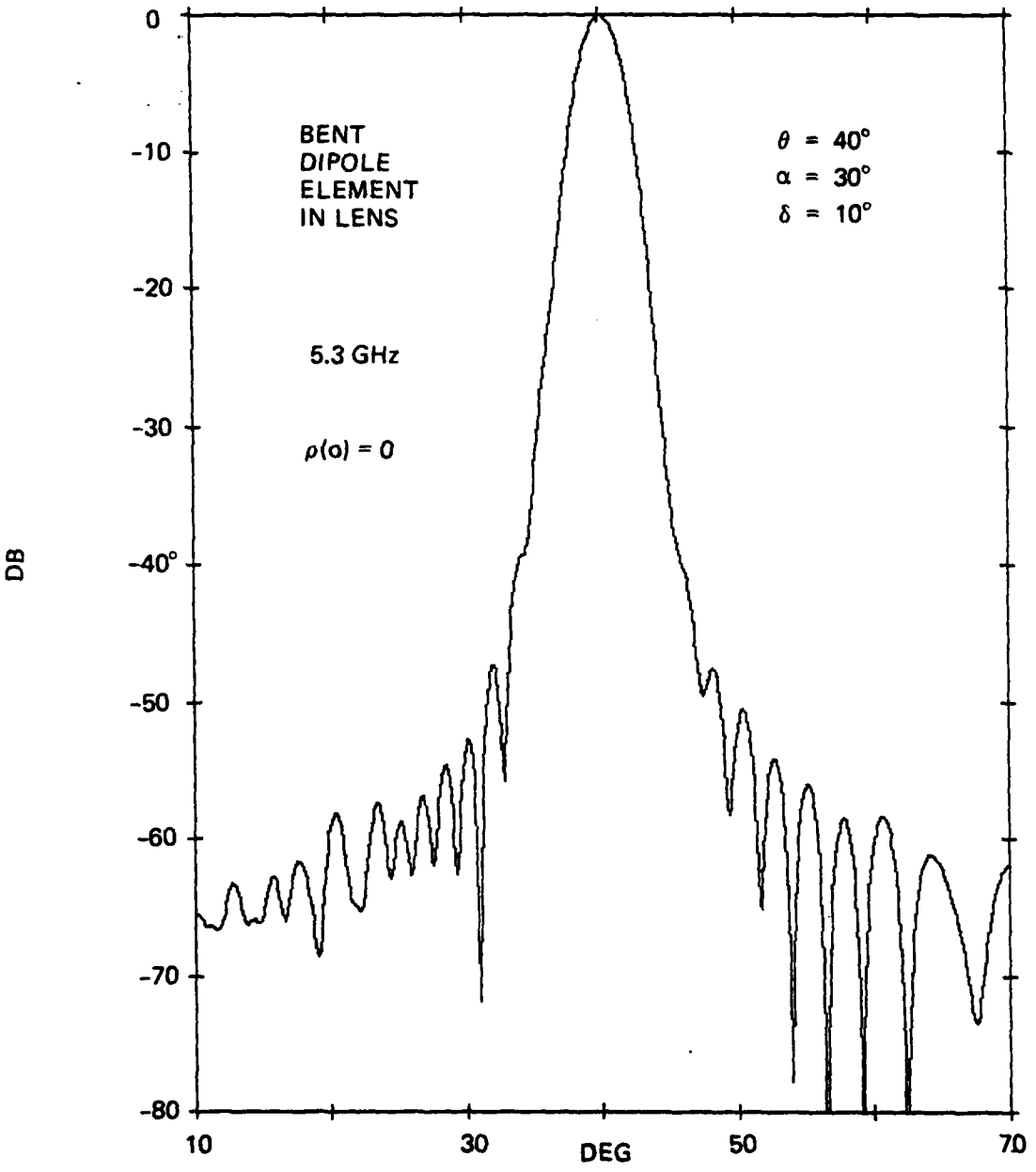

Figure 6-35. Azimuth Pattern of Antenna with Bent-Dipole Element, $\alpha = 30^{\circ}$, $\delta = 10^{\circ}$

6.4 WIDEBAND IMPEDANCE FOR ARRAY ELEMENT

It has been shown in the previous subsection that the bent dipole has the potential for exceptionally good wide angle impedance in the E plane of incidence, and that this is needed if low azimuth sidelobes are to be preserved when the antenna is fine-steered. However, good wideband impedance is also needed if the low-sidelobe performance is to be preserved over the operating frequency band from 5.0 to 5.6 GHz.

a. Design for Wideband Impedance Match

To obtain good impedance over a frequency band, the radiation Q of the array element must be low. Therefore, a large radiation resistance is desired for the element. For large radiation resistance, the element should occupy as much of the element cell as is practical. Low Q also involves as low a reactance as is practical. For low reactance the element should be as thick as is practical; with stripline construction a wide strip should be used.

The resulting bent dipole is shown in figure 6-36. This dipole occupies about three-quarters of the 0.4 wavelength space between elements in the E plane, and is estimated to have a radiation resistance of about 100 ohms in the array. The arm and body centerline dimensions of the dipole correspond to those giving the exceptionally good wideangle performance discussed previously.

The centerline length of this dipole from tip to tip is 0.65 wavelengths. Therefore, this dipole is not self-resonant. To obtain resonance, a capacitor is added across the dipole terminals at the center of the dipole. Figure 6-37 shows this capacitor, which is printed on the opposite side of the dielectric substrate from the dipole. A balanced feed line excites the dipole through stubs for double tuning; these are also printed on the opposite side from the dipole. A balun (not shown) located behind the ground plane excites the balanced feed line.

b. Measured Wideband Impedance

In order to facilitate the wideband impedance-matching process, a method is wanted for measuring the impedance versus frequency of a large array of bent dipoles near normal incidence. An excellent approach is to simulate an infinite array with a few elements in a waveguide.

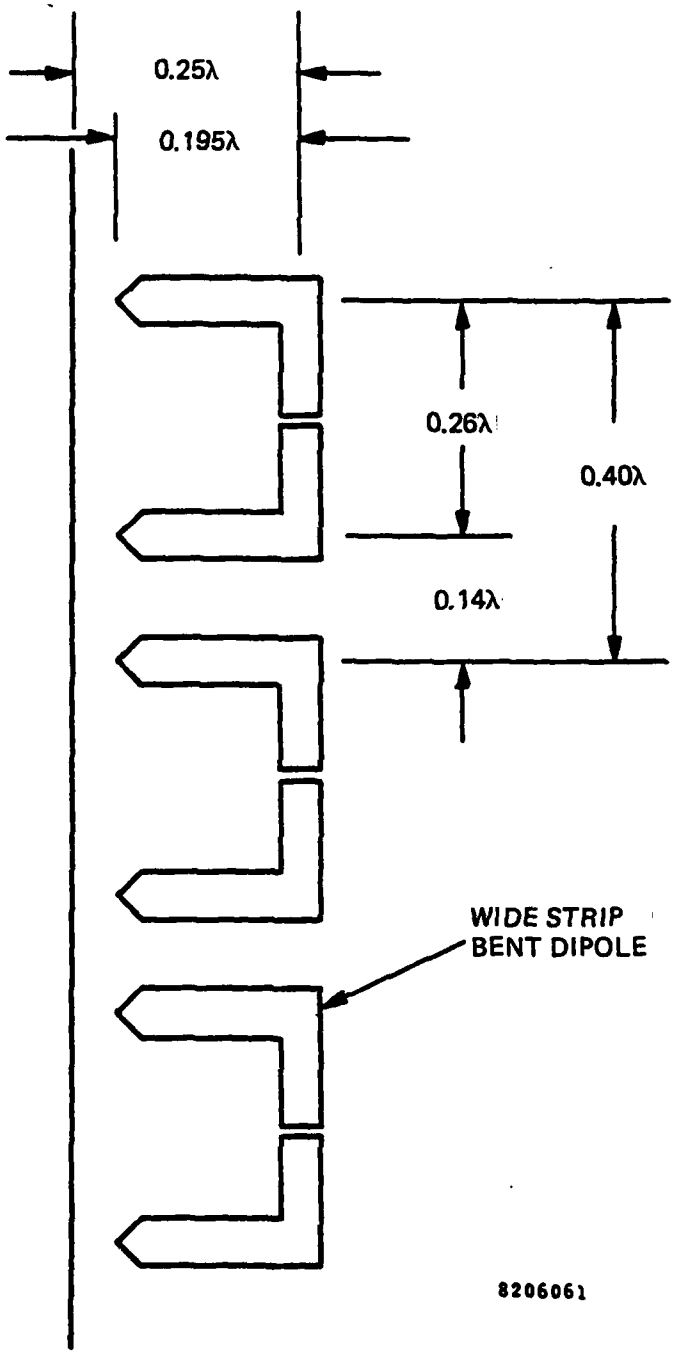

Figure 6-36. Optimum Bent Dipole in Strip Configuration

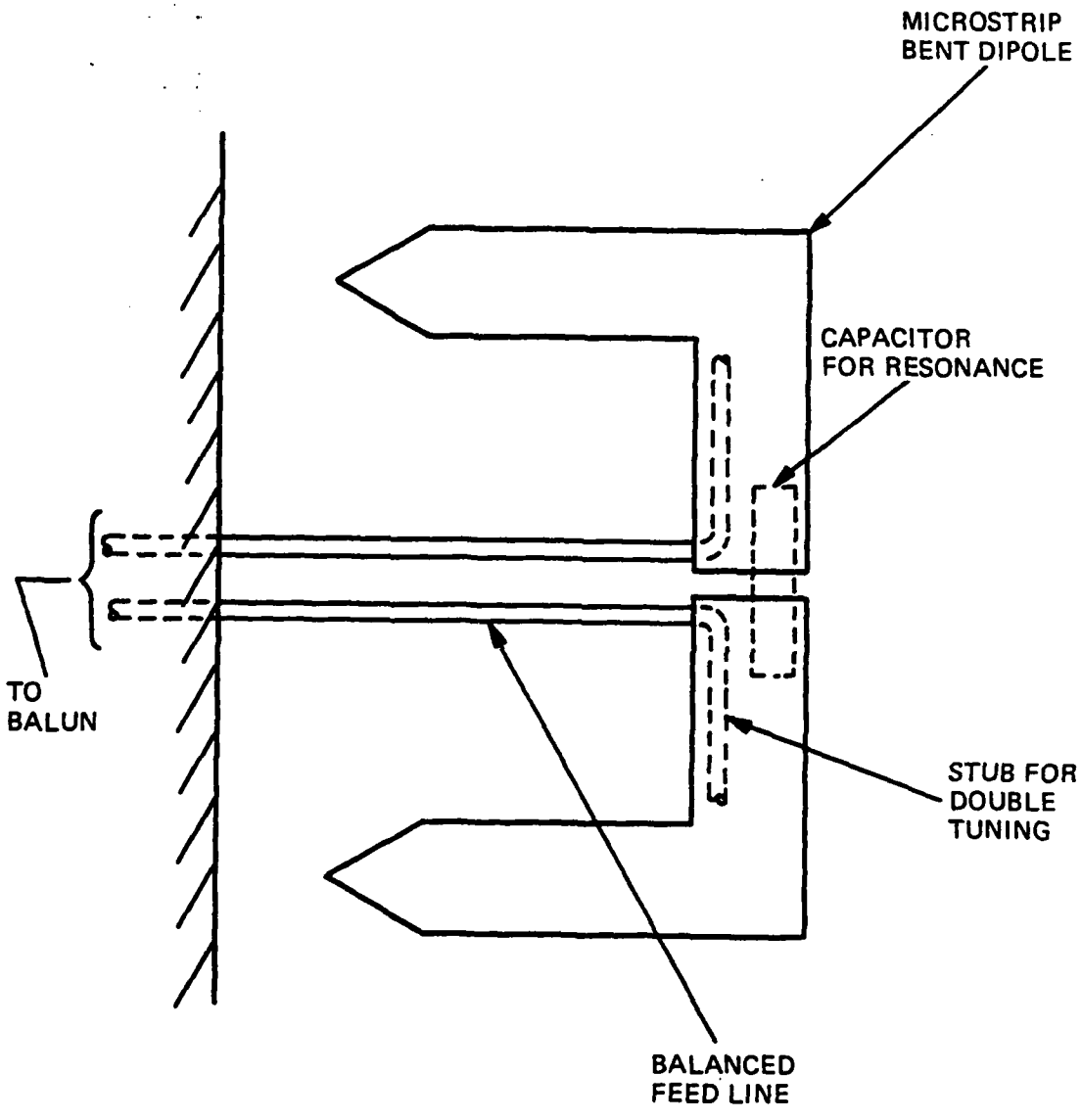

Figure 6-37. Microstrip Bent Dipole Design

Figure 6-38 shows a rectangular waveguide operating in the TE-10 mode and containing six microstrip bent dipoles. This simulator corresponds to an incidence angle of only 8^{o} in the H plane, which is sufficiently close to normal incidence to yield acceptable results.

The wideband impedance-matching process is, at the time of writing this report, only partially completed. Figure 6-39 shows the present results measured in the near-broadside simulator for the bent dipole without its balun exciter. Over about 2/3 of the frequency band, the reflection coefficient is less than approximately 0.05 (1.1 VSWR), while at the upper end of the band it is approximately 0.13 (1.3 VSWR). It seems reasonable to expect that a reflection coefficient between 0.05 and 0.10 will eventually be obtained over the 5.0 to 5.6 GHz band.

c. Wideband Computed Sidelobes with Bent Dipole

If the broadside-incidence resistance and reactance of the bent dipole at its terminals were known, they could be added to the computed wide-angle impedance of the bent dipole, and the resulting effect on antenna azimuth patterns could be exactly computed at each frequency in the band. However, the simple near-broadside simulator used does not permit the resistance and reactance to be determined at the dipole terminals; reflection coefficient magnitude is the only measured quantity that is readily available. It is possible, though, to assume a resistance and reactance that is consistent with the measured reflection coefficient, and then compute azimuth patterns that are at least representative of those that would actually be obtained.

The case of a broadside-incidence reflection coefficient assumed to be 0.05 is shown in figures 6-40 and 6-41, for a coarse-steering angle of 30^{o} and fine-steering of -5^{o} and $+5^{o}$, respectively. The case of an assumed broadside reflection coefficient of 0.10 is shown in figures 6-42 and 6-43. The 0.05 broadside reflection case is seen to give a spurious beam level that is clearly noticeable but is probably tolerable, while the 0.10 broadside reflection case gives a spurious beam level that is higher than desired for an antenna intended to have very low azimuth sidelobes.

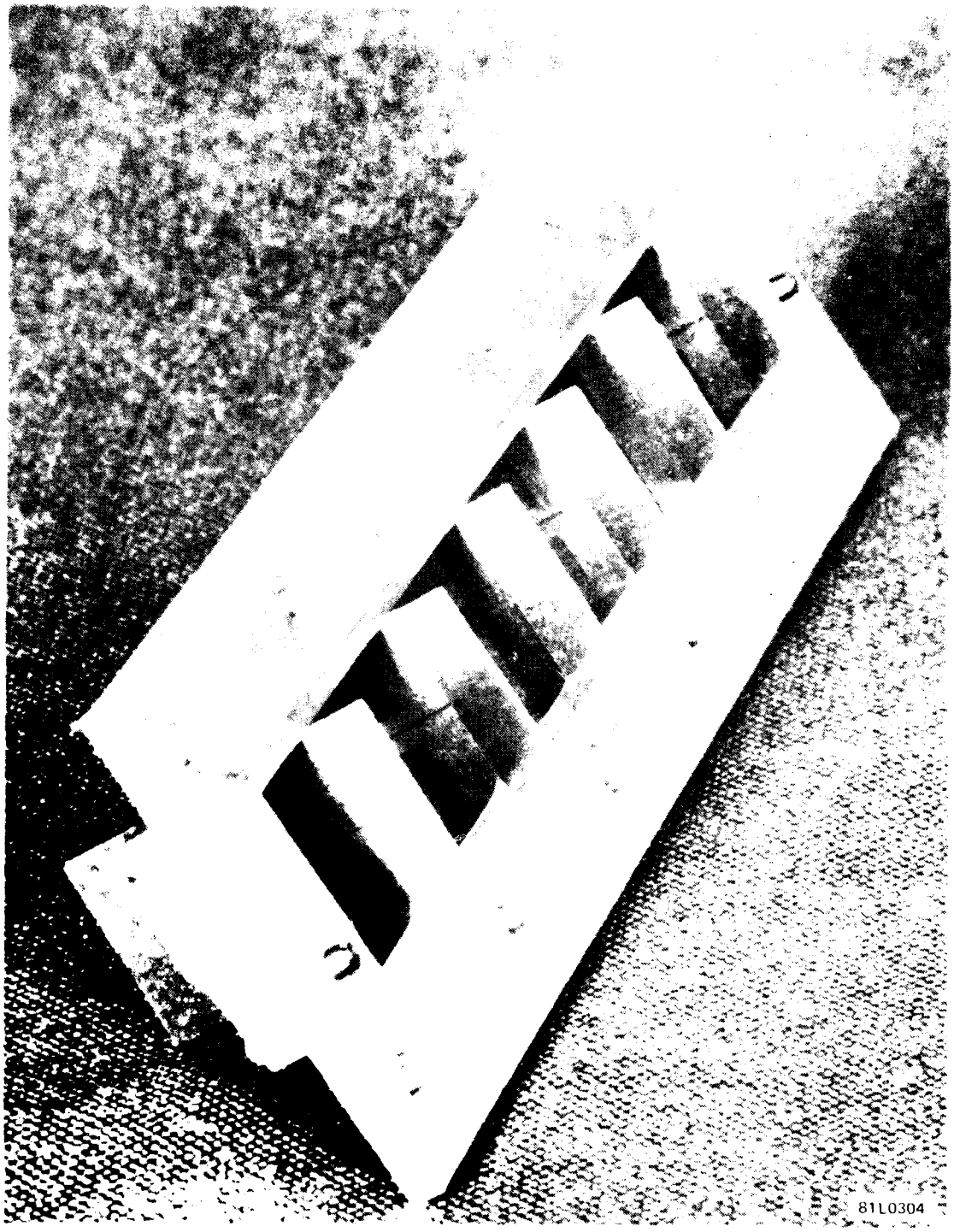

Figure 6-38. Infinite Array of Bent Dipoles Near Broadside Incidence Simulated in Waveguide

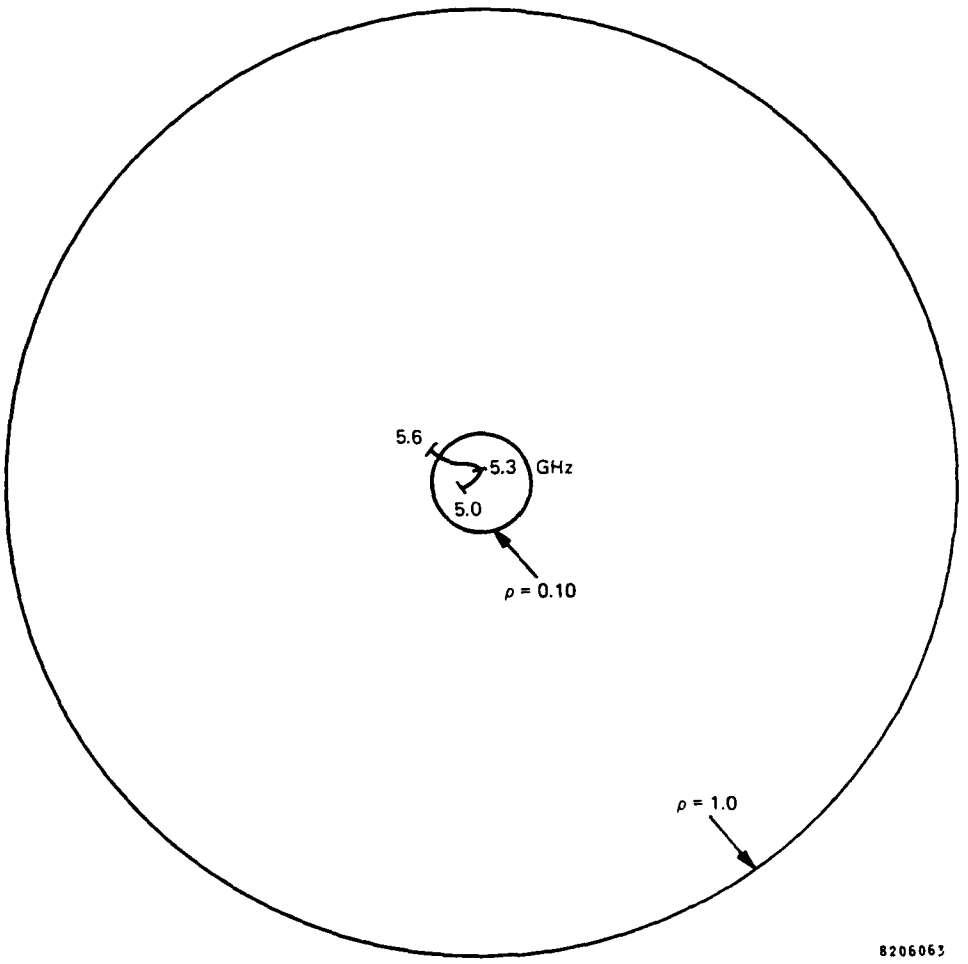

Figure 6-39. Reflection Coefficient of Preliminary Bent Dipole in Near-Broadside Simulator

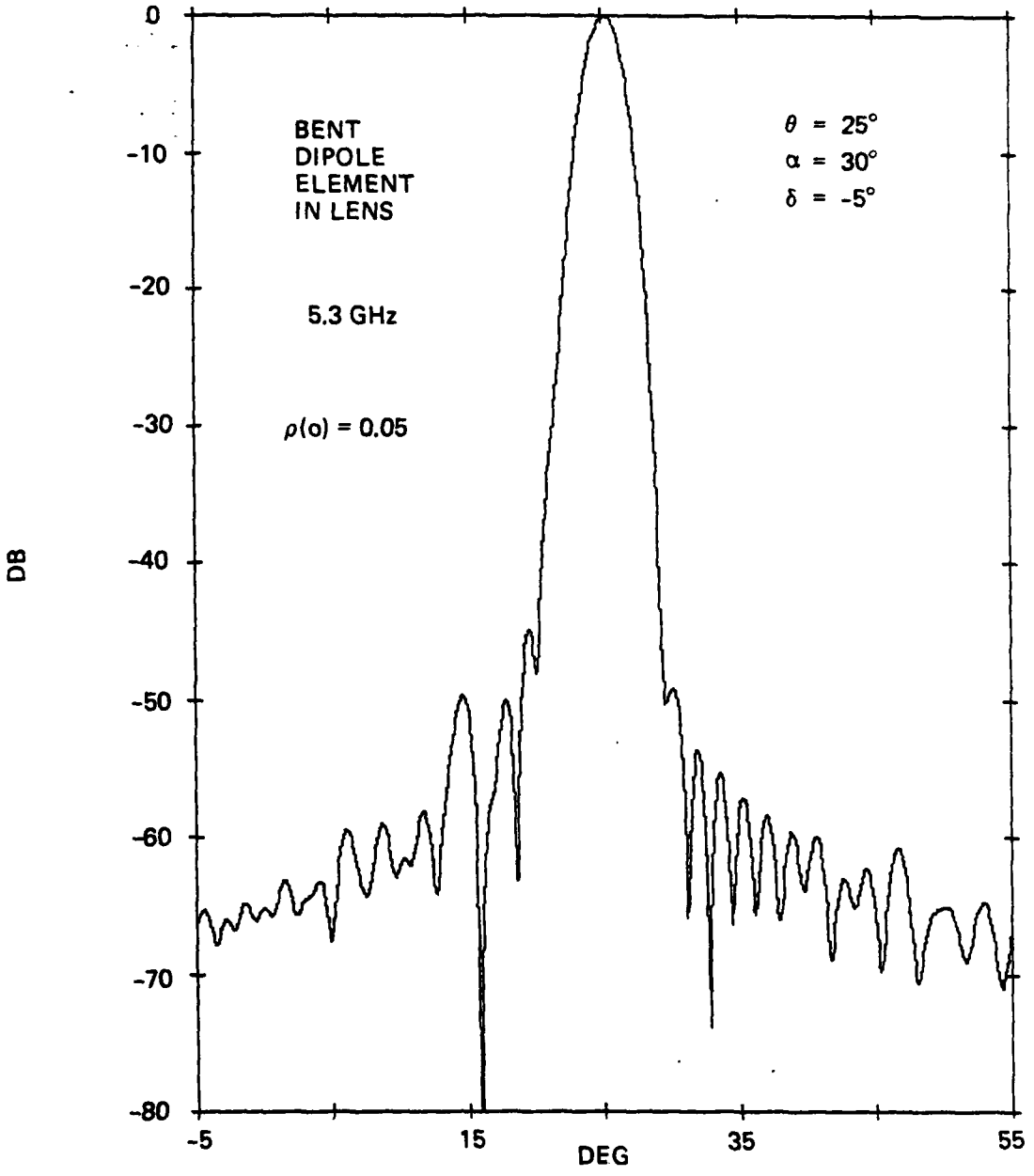

Figure 6-40. Azimuth Pattern of Antenna with Bent-Dipole Element, $\rho(o) = 0.05$, $\alpha = 30^{o}$, $\delta = -5^{o}$

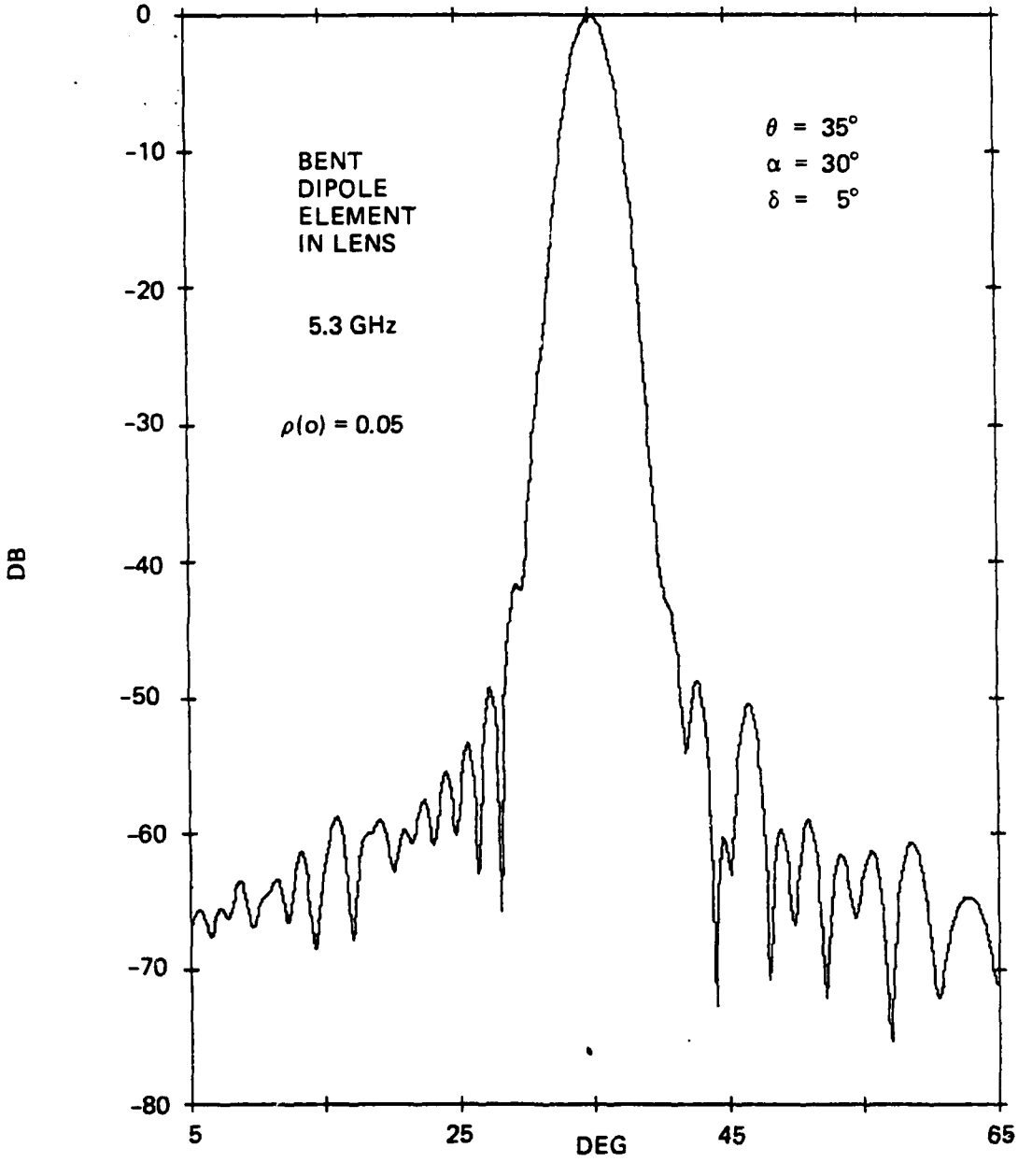

Figure 6-4i. Azimuth Pattern of Antenna with Bent-Dipole Element, $\rho(o) = 0.05$, $\alpha = 30^{o}$, $\delta = 5^{o}$

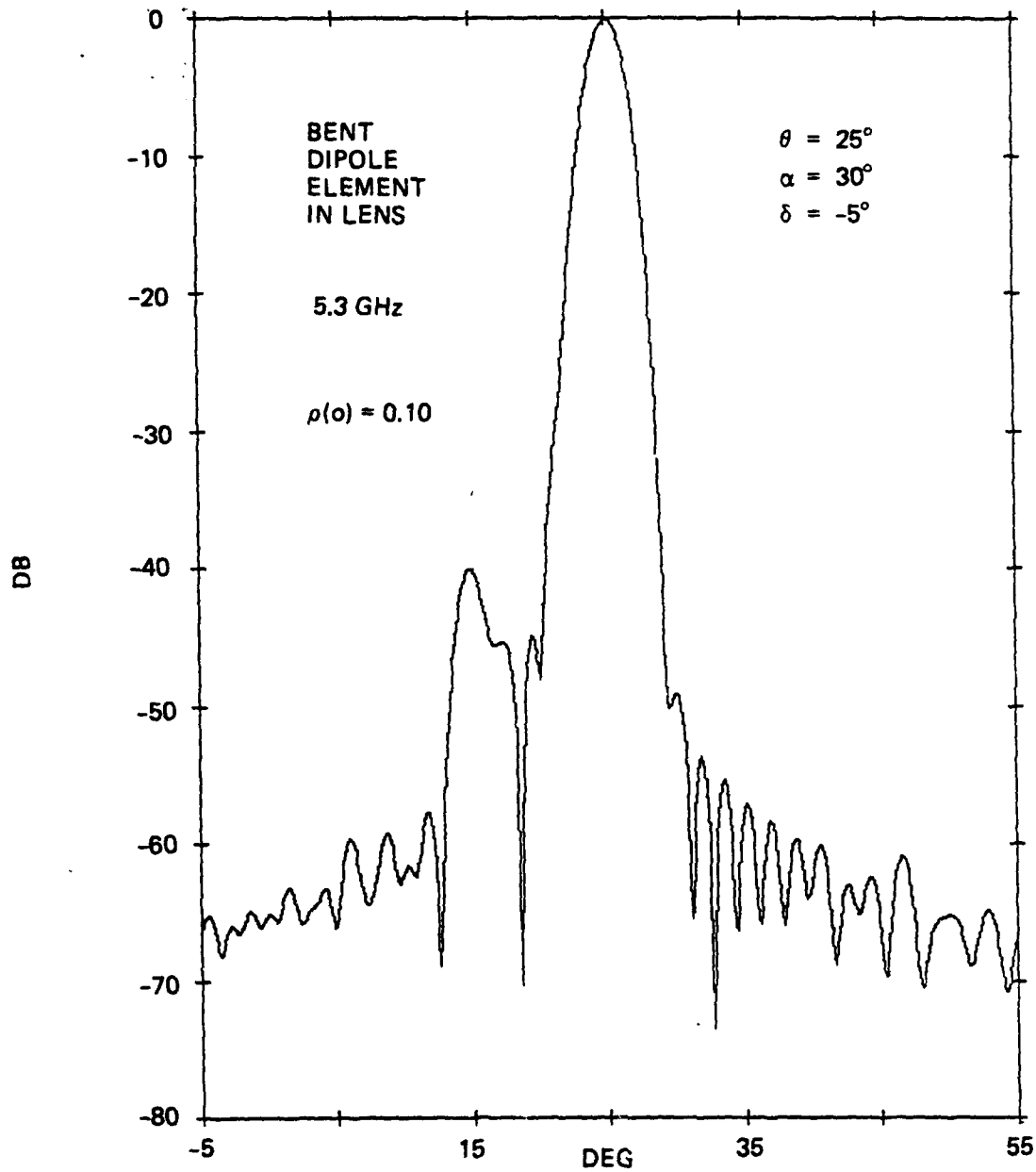

Figure 6-42. Azimuth Pattern of Antenna with Bent-Dipole Element $\rho(o) = 0.10$, $\alpha = 30^{o}$, $\delta = -5^{o}$

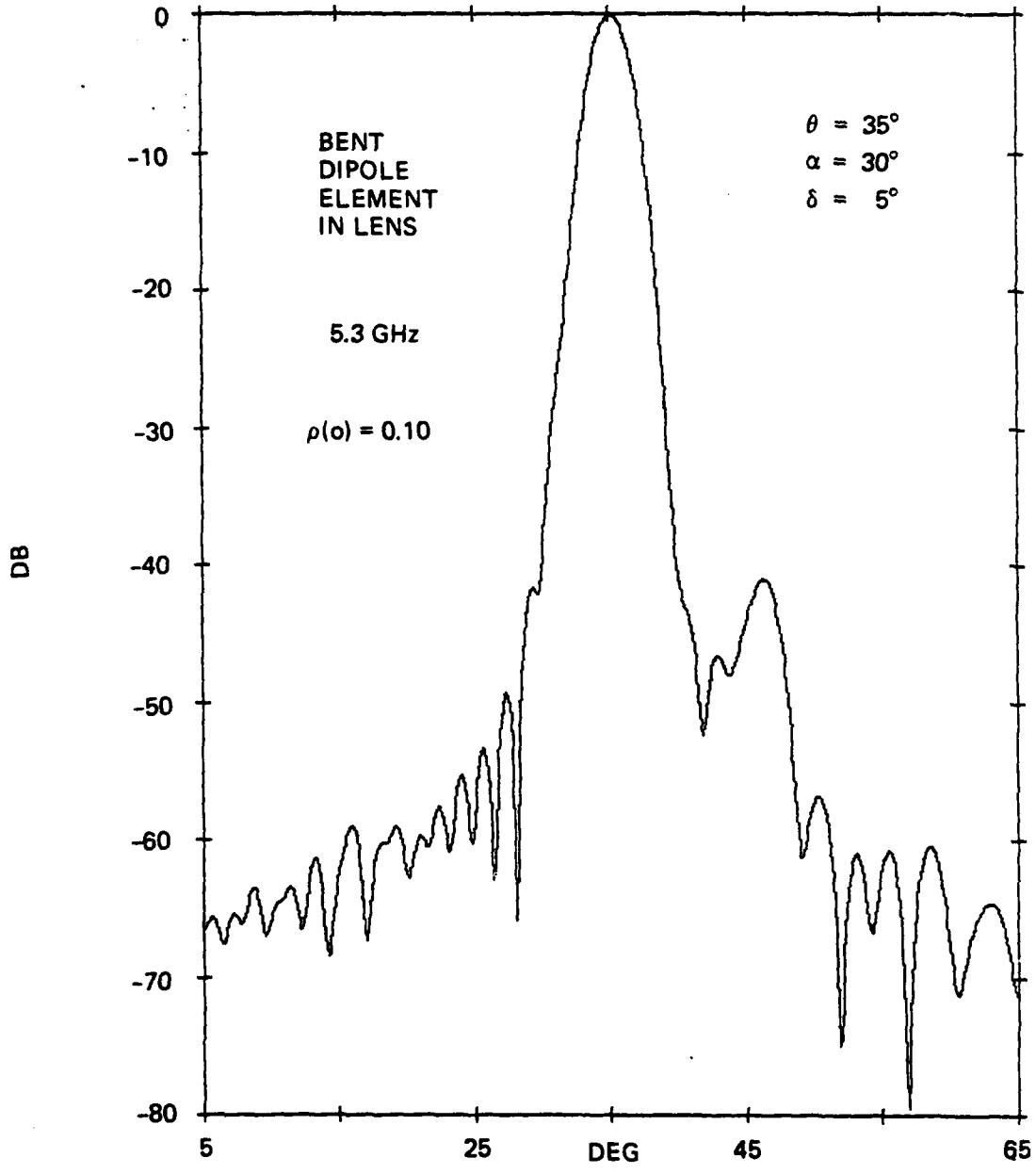

Figure 6-43. Azimuth Pattern of Antenna with Bent-Dipole Element, $\rho(o) = 0.10$, $\alpha = 30^{o}$, $\delta = 5^{o}$

6.5 DISCUSSION OF LENS INTERNAL REFLECTION EFFECTS

It has been shown that with a constant-W lens a collimated spurious beam can be created by internal reflections at the inner and outer array surfaces of the lens. When the desired beam is electronically fine-steered with reciprocal phase shifters, the spurious beam scans away from the desired beam and creates a sidelobe.

With ordinary dipole elements in the lens surface arrays, the wideangle impedance variation can cause internal reflections large enough to create a strong sidelobe. A bent dipole appears to have the capability for a remarkably small wideangle impedance variation, yielding only a weak sidelobe. The wideband impedance of the array element is also important in this respect.

An additional potential contributor to lens internal reflections is the VSWR of the phase shifters in the lens. However the location of these phase shifters can be randomized so that their reflection does not create a collimated spurious beam. No such randomization can be usefully accomplished with the surface array elements, and their impedance behavior is critically related to the sidelobe level achieved when the lens antenna is electronically fine-steered.

SECTION VII

CONCLUSIONS

This interim report has described the results of a study of a cylindrical-lens microwave antenna for achieving electronic scanning together with a wide signal bandwidth.

The particular cylindrical lens studied contains transmission lines having equal electrical lengths. This allows the beam to be scanned in elevation as well as in azimuth with no increase of phase aberration. An antenna consisting of such a lens together with a set of line feeds has the potential for providing wide-angle electronic scanning of a narrow beam with a wide signal (instantaneous) bandwidth, without needing to employ variable time-delay devices.

Lens Design. Solution of the lens equations yields two different lens contours: one with a point and the other with a dimple at the center. A special case having no central discontinuity is shown to be an R-2R lens. Phase aberrations are rather small for the general cases and are zero for the R-2R special case; the latter is selected for this program. Amplitude effects are not small, and angles of incidence at the lens surfaces can be quite large.

Azimuth Pattern Design. For the on-axis beam direction, an azimuth pattern having low sidelobes is obtainable by appropriate design of the horizontal excitation of the line-feed array. For off-axis beam directions, the curved outer surface of the cylindrical lens causes the sidelobes to increase, even though the lens has no phase aberration. This effect can be reduced by repositioning the feed or by modifying its design; the repositioning approach is simpler and is selected for this program.

Elevation Pattern Design. Feed/lens diffraction can increase the sidelobes of the elevation pattern. This effect can be made acceptably small by using a well-tapered vertical excitation of the line-feed array and by using a vertical dimension for the lens that is a little larger than that of the line feed.

Bandwidth/Scan Design. The loss caused by electronic scanning with a wide instantaneous bandwidth is reduced by increasing the number of line feeds in the antenna. For a 400 MHz wide rectangular spectrum, a set of 3 x 2 or 4 x 2 line feeds appears to be a reasonable choice. Wideband sidelobes can also be generated unless the fine steering is done with phase shifters having constant phase over the 400 MHz spectrum.

Lens Internal Reflections. With equal electrical paths in the lens, and with a large range of incidence angles at the lens surfaces, a significant multiple-reflection effect exists. When the antenna is fine steered with reciprocal phase shifters the internal reflections create a spurious-beam sidelobe that scans away from the main beam. With ordinary dipoles at the lens array surfaces, the level of this scanning sidelobe is substantially higher than is desired for this low-sidelobe antenna.

Bent Dipole Design. To reduce the lens internal reflections, a bent dipole design for the lens surface arrays is identified. Analyses based on simplifying approximations indicate that exceptionally low reflection is possible over a wide range of angles in the E plane of incidence. Preliminary measurements indicate that a good wideband impedance match should also be obtainable. Azimuth patterns computed for the bent dipole in the lens surface arrays yield a major reduction of the spurious-beam sidelobe.

Discussion. The information presented in this interim report is intended to outline the basic configuration of the cylindrical lens-array antenna, and to indicate some of its pattern and bandwidth characteristics. In the next part of this program it is expected that this antenna will be designed in detail, constructed, and tested.

The ability of the cylindrical lens-array antenna to provide wideband electronic scanning without needing variable time-delay devices relates to only one of the potential applications of this antenna, whose reflector-antenna analogue is the well-known and widely-used cylindrical-reflector antenna.

SECTION VIII

REFERENCES

Ref 1 - W. Rotman and P. Franchi, "Cylindrical Microwave Lens Antenna for Wideband Scanning Applications", Exhibit A in ESD RFP F19628-80-R-0077; November 1979.

Ref 2 - P. Franchi, N. Kernweis, W. Rotman, "Wideband Microwave Lens Antenna for Tactical Radar Applications", Proceedings of 1980 Antenna Applications Symposium, Allerton Park, Illinois; September 1980.

Ref 3 - W. Rotman et al, "Cylindrical Microwave Lens Antenna for Wideband Scanning Applications", AD-D008526; February 1981.

Ref 4 - H. B. DeVore and H. Iams, "Microwave Optics Between Parallel Conducting Sheets", RCA Review, pp. 721-732; December 1948.

Ref 5 - F. A. Jenkins and H. E. White, "Fundamentals of Optics", McGraw-Hill Book Co., pp. 120, 135; 1950.

Ref 6 - P. W. Hannan, "The Element-Gain Paradox for a Phased-Array Antenna", IEEE Trans. Antennas and Propagation, pp. 423-433; July 1964.

Ref 7 - R. L. Fante, P. R. Franchi, N. R. Kernweis, L. F. Dennett, "A Parabolic Cylinder Antenna with Very Low Sidelobes", IEEE Trans. Antennas and Propagation, pp. 53-59; January 1980.

Ref 8 - H. Jasik, "Antenna Engineering Handbook", McGraw-Hill, pp. 2.27-2.28; 1961.

Ref 9 - R. C. Hansen, "Microwave Scanning Antennas", Academic Press, Vol. 1, pp. 58-60; 1964.

Ref 10 - J. C. Sureau, A. Hessel, "On the Realized Gain of Arrays", IEEE Trans. Antennas and Propagation, pp. 122-124; January 1971.

Ref 11 - J. Frank, "Bandwidth Criteria for Phased-Array Antennas", Proceedings of the 1970 Phased Array Antenna Symposium, edited by Oliner and Knittel, Artech House, pp. 243-253; 1972.

Ref 12 - T. C. Cheston and J. Frank, Chapter 11.6 of Radar Handbook, edited by M. I. Skolnik, McGraw-Hill, pp. 11-43 to 11-50; 1970.

Ref 13 - M. S. Wheeler and D. K. Alexander, "Short Pulse Effects in Traveling-Wave Antennas", Eighth Annual Radar Symposium Record, AD-331299, pp. 293-304; June 1962.

Ref 14 - I. W. Hammer, "Frequency-Scanned Arrays", Chapter 13 in the Radar Handbook, edited by M. I. Skolnik, McGraw-Hill Book Co., pp. 13-21 to 13-23; 1970.

Ref 15 - W. B. Adams, "Phased-Array Performance with Wide-band Signals", Supplement to IEEE Trans. Aerospace and Electronic Systems, Vol. AES-3, No. 6, pp. 257-271; November 1967.

Ref 16 - M. S. Wheeler, "Pulse Excitation of a Traveling-Wave Array", IEEE Trans. Antennas and Propagation, Vol. AP-20, No. 3, pp. 239-244; May 1972.

Ref 17 - L. Stark, "Radiation Impedance of a Dipole in an Infinite Planar Phased Array", Radio Science, pp. 361-377, March 1966.

Ref 18 - H. A. Wheeler, "The Grating-Lobe Series for the Impedance Variation in a Planar Phased-Array Antenna", IEEE Trans. Antennas and Propagation, pp. 707-714; March 1967.

Ref 19 - A. A. Oliner and R. G. Malech, "Mutual Coupling in Infinite Scanning Arrays", Chapter 3 in "Microwave Scanning Antennas", Vol. II, editor R. C. Hansen, Academic Press; 1966.

Ref 20 - P. W. Hannan, D. S. Lerner, G. H. Knittel, "Impedance Matching on Phased-Array Antenna over Wide Scan Angles by Connecting Circuits", IEEE Trans. Antennas and Propagation, pp. 28-34; January 1965.

Ref 21 - P. W. Hannan, "Proof that a Phased-Array Antenna Can be Impedance Matched for All Scan Angles", Radio Science, pp. 361-369; March 1967.

Ref 22 - L. Stark, "Comparison of Array Element Types", Proceedings of Phased Array Antenna Symposium, edited by Oliner and Knittel, Artech House, pp. 51-66; 1972.

APPENDIX A

PATHS IN R-2R LENS

The remarkable R-2R lens was first described by DeVore and Iams (ref 4). Their paper clearly gives the essence of the geometrical focusing properties of the lens. In this appendix we are supplementing their derivation, for the general case of a feed located at any angle α off the lens axis.

Figure A-1 shows an R-2R lens with an off-axis feed at point s. Two rays are shown radiated by the feed, one going to the tangent point A' on the effective aperture plane, and the other going to a general point B'. It is shown that the space paths from the feed s to the points A' and B' are equal. Of course the transmission-line paths within the lens are made equal by design. Therefore, the R-2R lens provides perfect collimation for any location of the feed on the feed arc.

Also indicated in figure A-1 is the angle ψ subtended by points b and a at any feed location. It can be seen that ψ is also the angle of incidence at both the inner and outer surfaces of the lens. This geometry leads to formulas 7, 8, and 10 given earlier in this report.

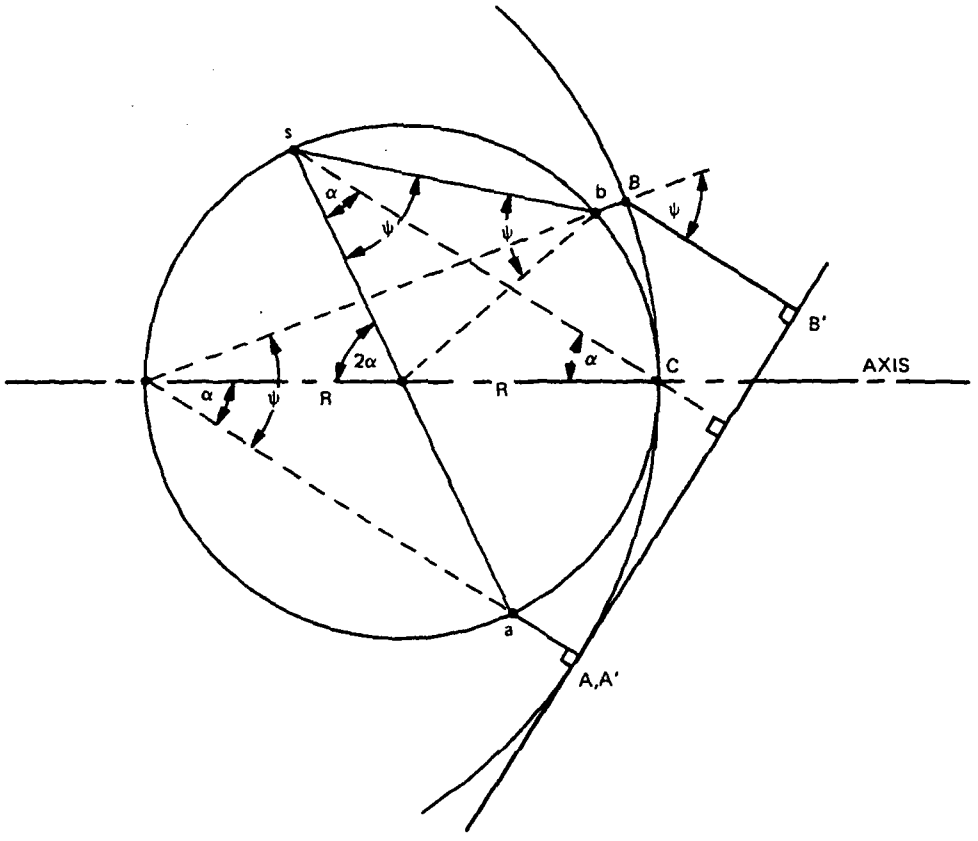

$\overline{sb} = 2R \cos\psi$ $\overline{BB'} = 2R(1 - \cos\psi)$

top path = $\overline{sb} + \overline{BB'} = 2R$

$\overline{sa} = 2R$ $\overline{AA'} = 0$

bottom path = $\overline{sa} + \overline{AA'} = 2R$

top path = bottom path = any path.

8206064

Figure A-1. Paths in R-2R Lens

MISSION
of
Rome Air Development Center

RADC plans and executes research, development, test and selected acquisition programs in support of Command, Control Communications and Intelligence (C^3I) activities. Technical and engineering support within areas of technical competence is provided to ESD Program Offices (POs) and other ESD elements. The principal technical mission areas are communications, electromagnetic guidance and control, surveillance of ground and aerospace objects, intelligence data collection and handling, information system technology, ionospheric propagation, solid state sciences, microwave physics and electronic reliability, maintainability and compatibility.

Printed by
United States Air Force
Hanscom AFB, Mass. 01731

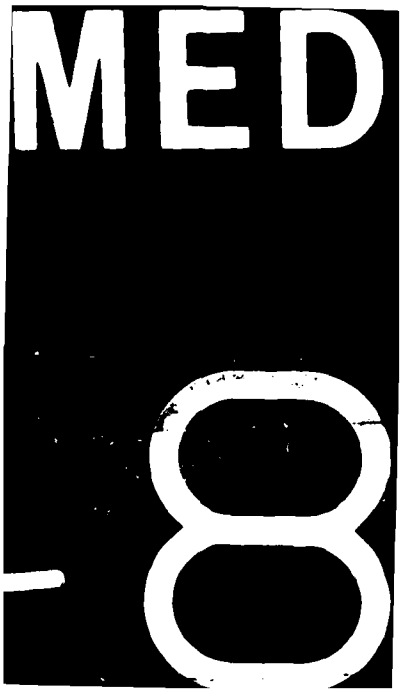
MED
8